Université de Montréal

Le système endocannabinoïde dans la rétine du singe : expression, localisation et fonctions

par
Joseph Bouskila

École d'optométrie
Programme des sciences biomédicales
Faculté de médecine

Thèse présentée à la Faculté de médecine
en vue de l'obtention du grade de doctorat
en sciences biomédicales

Décembre 2015

RÉSUMÉ

Le cannabis produit de nombreux effets psychologiques et physiologiques sur le corps humain. Les molécules contenues dans cette plante, désignées comme « phytocannabinoïdes », activent un système endogène qu'on appelle le système endocannabinoïde (eCB). Les effets de la consommation de cannabis sur la vision ont déjà été décrits sans cependant de formulation sur les mécanismes sous-jacents. Ces résultats comportementaux suggèrent, malgré tout, la présence de ce système eCB dans le système visuel, et particulièrement dans la rétine. Cette thèse vise donc à caractériser l'expression, la localisation et le rôle du système eCB dans la rétine du singe vervet, une espèce animale ayant un système visuel semblable à celui de l'humain. Nous avons mis au point un protocole expérimental d'immunohistochimie décrit dans l'article apparaissant dans l'Annexe I que nous avons utilisé pour répondre à notre objectif principal. Dans une première série de quatre articles, nous avons ainsi caractérisé l'expression et la localisation de deux récepteurs eCBs reconnus, les récepteurs cannabinoïdes de type 1 (CB1R) et de type 2 (CB2R), et d'un 3^{e} présumé récepteur aux cannabinoïdes, le récepteur GPR55. Dans l'article 1, nous avons démontré que CB1R et une enzyme clé de ce système, la *fatty acid amide hydrolase* (FAAH), sont exprimés dans les parties centrale et périphérique de la rétine, et abondamment présents dans la fovéa, une région où l'acuité visuelle est maximale. Dans l'article 2, nous avons localisé le CB2R dans des cellules gliales de la rétine : les cellules de Müller et nous avons proposé un modèle sur l'action de cette protéine dans la fonction rétinienne faisant appel à une cascade chimique impliquant les canaux potassiques. Dans l'article 3, nous avons observé le GPR55 exclusivement dans les bâtonnets qui sont responsables de la vision scotopique et nous avons soumis un deuxième modèle de fonctionnement de ce récepteur par le biais d'une modulation des canaux calciques et sodiques des bâtonnets. Vu que ces 3 récepteurs se retrouvent dans des cellules distinctes, nous avons suggéré leur rôle primordial dans l'analyse de l'information visuelle au niveau rétinien. Dans l'article 4, nous avons effectué une analyse comparative de l'expression du système eCB dans la rétine de souris, de toupayes (petits mammifères insectivores qui sont sont considérés comme l'étape intermédiaire entre les rongeurs et les primates) et de deux espèces de singe (le vervet et le rhésus). Ces résultats nous ont menés à présenter une

hypothèse évolutionniste quant à l'apparition et à la fonction précise de ces récepteurs. Dans les articles subséquents, nous avons confirmé notre hypothèse sur le rôle spécifique de ces trois récepteurs par l'utilisation de l'électrorétinographie (ERG) après injection intravitréenne d'agonistes et d'antagonistes de ces récepteurs. Nous avons conclu sur leur influence indéniable dans le processus visuel rétinien chez le primate. Dans l'article 5, nous avons établi le protocole d'enregistrement ERG normalisé sur le singe vervet, et nous avons produit un atlas d'ondes ERG spécifique à cette espèce, selon les règles de l'*International Society for Clinical Electrophysiology of Vision* (ISCEV). Les patrons électrorétinographiques se sont avérés semblables à ceux de l'humain et ont confirmé la similarité entre ces deux espèces. Dans l'article 6, nous avons démontré que le blocage de CB1R ou CB2R entraine une modification de l'électrorétinogramme, tant au niveau photopique que scotopique, ce qui supporte l'implication de ces récepteurs dans la modulation des ondes de l'ERG. Finalement, dans l'article 7, nous avons confirmé le modèle neurochimique proposé dans l'article 3 pour expliquer le rôle fonctionnel de GPR55, en montrant que l'activation ou le blocage de ce récepteur, respectivement par un agoniste (lysophosphatidylglucoside, LPG) ou un antagoniste (CID16020046), entraine soit une augmentation ou une baisse significative de l'ERG scotopique seulement. Ces données, prises ensemble, démontrent que les récepteurs CB1R, CB2R et GPR55 sont exprimés dans des types cellulaires bien distincts de la rétine du singe et ont chacun un rôle spécifique. L'importance de notre travail se manifeste aussi par des applications cliniques en permettant le développement de cibles pharmacologiques potentielles dans le traitement des maladies de la rétine.

Mots-clés : Rétine, récepteurs cannabinoïdes, immunohistochimie, singes, toupayes, rongeurs, électrorétinogramme.

ABSTRACT

Cannabis produces a range of psychological and physiological effects on the human body. Cannabinoids are the chemical compounds found in cannabis that activate an endogenous system, termed the endocannabinoid (eCB) system. Reports made in the 1970s have noted that cannabis consumption affects vision. It is therefore suggested that the eCB system is present in the visual system, particularly in the retina. This thesis aims at characterizing the expression, localization, and role of the eCB system in the vervet monkey retina. This animal model has a similar visual system as humans. Using immunohistochemistry methods presented in the article of Annexe I, we have established an experimental protocol to answer our goal. In the first series of four articles, we have characterized the expression and localization of the cannabinoid receptor 1 (CB1R), cannabinoid receptor 2 (CB2R), and the putative cannabinoid receptor GPR55. In Article 1, we have demonstrated that CB1R and a key enzyme of this system, FAAH (fatty acid amide hydrolase), are expressed in the central and peripheral retina, but heavily present in the fovea, the retinal region responsible for high acuity vision. In Article 2, we have localized CB2R in the glial Müller cells and hypothesized a possible mechanism of action of CB2R involving potassium buffering. In Article 3, we found that GPR55 is exclusively expressed in rods and have proposed its role through the modulation of calcium and sodium channels in rods. Given that these three receptors are segregated in the vervet monkey retina, we suggested that they might have distinct roles in retinal physiology. In Article 4, we reported a comparative analysis of the expression of the eCB system components in the retina of rodents, tree shrews (small mammals considered as early primates), and monkeys. This paper provides evidence that the eCB system is differently expressed in the retina of these mammals and suggests a distinctive role of eCBs in visual processing. In the subsequent series of three articles, we confirmed their suggested roles in the retina by using electroretinography (ERG) and intravitreal injections of agonist and antagonist of these receptors. We concluded that they indeed play important roles in the retina. In Article 5, we developed a standard protocol for ERG testing in our animal model and have published an ERG atlas with normalized amplitudes and latency values similar to that of humans, following the guidelines of the

International Society for Clinical Electrophysiology of Vision. In Article 6, we showed that blockade of CB1R or CB2R with specific antagonists modifies the ERG, both in photopic and scotopic conditions, which confirms the implication of these receptors in normal retinal function. Finally, in Article 7 (expression of GPR55 in rods only), we confirmed the suggest role of GPR55 in rods by showing that activation or blockade of GPR55 with a specific agonist (lysophosphatidylglucoside) or antagonist (CID16020046) increases or decreases the amplitude of the scotopic ERG waveforms. Taken together, these articles demonstrate that CB1R, CB2R, and GPR55 are differentially expressed in the vervet monkey retina and have distinct roles. This work has also clinical relevance in the way that we have discovered new pharmacological targets that can be used for treatment of many retinal diseases.

Keywords: Retina, cannabinoid receptor, immunohistochemistry, monkey, tree shrews, rodents, electroretinogram.

TABLE DES MATIÈRES

RÉSUMÉ I
ABSTRACT III
TABLE DES MATIÈRES V
LISTE DES TABLEAUX VIII
LISTE DES FIGURES IX
LISTE DES ABRÉVIATIONS X
REMERCIEMENTS XIII
I. INTRODUCTION 1
1. La rétine 3
1.1 Anatomie de la rétine 4
1.1.1 Photorécepteurs 5
1.1.2 Cellules horizontales 6
1.1.3 Cellules bipolaires 6
1.1.4 Cellules amacrines 8
1.1.5 Cellules ganglionnaires 8
1.1.6 Cellules gliales 8
1.2 Physiologie de la rétine 9
1.2.1 Voie des cônes 9
1.2.2 Voies des bâtonnets 11
1.3 Anatomie comparée de la rétine 12
1.4 Le cerveau visuel 13
2. L'électrorétinogramme 13
2.1 Onde a 16
2.2 Onde b 17
2.3 Onde i 17
2.4 Implications cliniques 18
3. Le cannabis et ses constituants naturels (phytocannabinoïdes) 18
3.1 Aperçu historique 19

3.2 THC 22
3.3 Cannabidiol 22
4. Le système endocannabinoïde 22
4.1 Les eCBs 23
4.2 Les récepteurs cannabinoïdes 23
4.3 Fonction synaptique 24
4.4 Voies de signalisation impliquées dans la diminution de la libération de neurotransmetteurs 25
5. Le cannabis et la vision 26
6. Le système endocannabinoïde et les tissus oculaires 27
6.1 Cannabinoïdes, pression intraoculaire et glaucome 28
7. Expression et localisation de CB1R dans la rétine 29
7.1 Fonction de CB1R dans la rétine 30
8. Expression et localisation de CB2R dans la rétine 31
8.1 Fonction de CB2R dans la rétine 32
9. Expression et localisation de GPR55 dans la rétine 32
9.1 Fonction de GPR55 dans la rétine 32
10. Expression et localisation des enzymes de synthèse et de dégradation dans la rétine 33
11. Le système eCB dans le thalamus visuel 34
12. Le système eCB dans le cortex visuel 35
13. Choix du modèle animal : le singe vervet de St Kitts 36
II. OBJECTIFS ET HYPOTHÈSES 38
III. CORPS DE L'OUVRAGE 40
ARTICLE 1: EXPRESSION AND LOCALIZATION OF THE CANNABINOID RECEPTOR TYPE 1 AND THE ENZYME FATTY ACID AMIDE HYDROLASE IN THE RETINA OF VERVET MONKEYS 41
ARTICLE 2: MÜLLER CELLS EXPRESS THE CANNABINOID CB2 RECEPTOR IN THE VERVET MONKEY RETINA 78
ARTICLE 3: ROD PHOTORECEPTORS EXPRESS GPR55 IN THE ADULT VERVET MONKEY RETINA 114
ARTICLE 4: COMPARATIVE ANALYSIS OF THE ENDOCANNABINOID SYSTEM IN THE RETINA OF MICE, TREE SHREWS AND MONKEYS 145
ARTICLE 5: STANDARDIZED FULL-FIELD ELECTRORETINOGRAPHY IN THE GREEN MONKEY 173

ARTICLE 6: CANNABINOID RECEPTORS CB1 AND CB2 MODULATE THE ELECTRORETINOGRAPHIC WAVES IN VERVET MONKEYS 199
ARTICLE 7: SCOTOPIC VISION IN THE MONKEY IS MODULATED BY THE G PROTEIN-COUPLED RECEPTOR 55 234
IV. DISCUSSION GÉNÉRALE 260
1. Les différences interespèces sur l'expression et le rôle des récepteurs cannabinoïdes dans la rétine 262
2. Les voies de signalisation du système eCB dans la rétine du singe 265
V. CONCLUSION ET PERSPECTIVES D'AVENIR 267
1. Rôle dans le développement 267
2. Rôle au niveau du comportement 268
2.1 Le regard préférentiel 269
2.2 Le nystagmus optocinétique 269
3. Imagerie des récepteurs cannabinoïdes 270
4. Usage du cannabis pour le traitement des maladies de la rétine 270
VI. BIBLIOGRAPHIE 272
ANNEXE I: THE GATEWAY TO THE BRAIN: DISSECTING THE PRIMATE EYE I
ANNEXE II: THE ENDOCANNABINOID SYSTEM WITHIN THE DORSAL LATERAL GENICULATE NUCLEUS OF THE VERVET MONKEY XI
ANNEXE III: LISTE DES BOURSES ET PRIX QUE CES ARTICLES ONT PERMIS DE GAGNER. XL

LISTE DES TABLEAUX

Tableau 1. Présence et localisation des composantes du système eCB dans les tissus oculaires, incluant la rétine, de plusieurs espèces. 28

LISTE DES FIGURES

Figure 1. L'œil et les différentes couches de la rétine. 4
Figure 2. Les populations neuronales principales de la rétine des mammifères. 5
Figure 3. Distribution des cônes et des bâtonnets dans la rétine..... 6
Figure 4. Schéma des différentes cellules bipolaires chez la souris, le rat et le singe. 7
Figure 5. Circuit rétinien de la voie des cônes. 10
Figure 6. Circuits rétiniens de la voie des bâtonnets..... 11
Figure 7. Montage expérimental pour l'enregistrement ERG chez le singe. 14
Figure 8. Diagramme reliant les structures de la rétine et les composantes de l'ERG. 16
Figure 9. Chronologie de la recherche sur les cannabinoïdes et le système eCB. 21
Figure 10. Schéma illustrant les composantes principales du système eCB. 23
Figure 11. Cibles cellulaires et voies de signalisation de l'AEA et du 2-AG. 24
Figure 12. Cascade biochimique survenant après l'activation de CB1R par l'AEA. 26
Figure 13. Le laboratoire situé sur l'ile de St Kitts abrite les singes vervets. 36
Figure 14. Comptage des cellules ganglionnaires dans la rétine du singe vervet normal..... 37
Figure 15. Cartographie des récepteurs CB1R, CB2R et GPR55 dans la rétine de la souris, du toupaye et du singe..... 264
Figure 16. Illustration schématique du rôle hypothétique de CB1R, CB2R et GPR55 dans la rétine du singe. 266

LISTE DES ABRÉVIATIONS

2-AG	2-arachidonoylglycérol
AC	Adénylate cyclase
AEA	Anandamide ou *N*-arachidonyléthanolamine
AMT	*Anandamide membrane transporter*
CB1R	Récepteur cannabinoïde 1
CB2R	Récepteur cannabinoïde 2
CBD	Cannabidiol
CBN	Cannabinol
DAGL	Diacylglycérol lipase
dLGN	Corps genouillé latéral dorsal
DES	*Depolarization-induced suppression of excitation*
DSI	*Depolarization-induced suppression of inhibition*
eCB	Endocannabinoïde
EEG	Électroencéphalographie
ERG	Électrorétinographie
FAAH	*Fatty acid amide hydrolase*
GABA	Acide gamma-aminobutyrique
GCL	*Ganglion cell layer*
GFAP	*Glial fibrillary acidic protein*
$G_{i/o}$	Protéine G inhibitrice
GPR55	Récepteur couplé aux protéines G 55
GS	Glutamine synthétase
iGluR	*Ionotropic glutamate receptors*
INL	*Inner nuclear layer*
IOP	*Intraocular pressure*
IPL	*Inner plexiform layer*
LPG	Lysophosphatidylglucoside
LPI	L-α-lysophosphatidylinositol
MAGL	Monoacylglycérol lipase

NAE	*N*-acyl éthanolamines
NAPE-PLD	*N*-acylphosphatidyléthanolamine phospholipase D
NDS	*Normal donkey serum*
NMDA	*N*-méthyl-D-aspartate
OAE	Virodhamine (O-arachidonoyl ethanolamine)
ONL	*Outer nuclear layer*
OPL	*Outer plexiform layer*
PBS	*Phosphate-buffered saline*
PKA	Protéine kinase A
PKC	Protéine kinase C
PIO	Pression intraoculaire
SEM	*Standard error of the mean*
SNC	Système nerveux central
THC	Tétrahydrocannabinol
TRPV1	*Transient receptor potential vanilloid type 1*
V1	Cortex visuel primaire
VEP	Potentiel évoqué visuel
VGLUT1	Transporteur glutamate vésiculaire 1

« Homo sine animale nunquam cognoscet hominem »
« L'Homme sans l'animal ne comprendra jamais l'homme »
Maurice Ptito, PhD, Dr. Med., OQ, FRSC

« Il y a l'or, et une multitude de rubis, mais les lèvres de la connaissance sont des joyaux précieux. »
Proverbes 20:15

REMERCIEMENTS

Je tiens à remercier plusieurs personnes, sans qui ce travail n'aurait pas pu se réaliser. Avant tout, c'est avec une immense gratitude que je souhaite remercier les Prs Maurice Ptito et Jean-François Bouchard d'avoir su m'encourager, par leur appui pendant toutes ces années, à mener à terme ma formation de doctorat. Je les remercie aussi pour leur incroyable et inestimable disponibilité, leur patience et toute la latitude dont ils m'ont permis de jouir au cours des multiples projets que nous avons pu réaliser. Ils ont su me motiver, m'encourager et me perfectionner dans plusieurs aspects de la recherche, mais aussi de la vie de tous les jours. Je dois préciser que chacun d'entre eux a joué un rôle majeur dans l'accomplissement de ce travail.

D'une part, le Dr Ptito m'a inculqué de très fortes valeurs éthiques, un optimisme éternel et un esprit critique. Ses sages conseils ne valent pas seulement pour le travail, mais aussi pour la vie de tous les jours. Son sens de l'humour unique en son genre a agrémenté l'ambiance de travail. Il m'a poussé à apprendre à enseigner en me permettant de le remplacer dans plusieurs de ses cours donnés aux étudiants en optométrie. Il m'a appris à ne pas devenir un « nul ».

D'autre part, je remercie Dr Bouchard pour sa grande patience et sa compréhension pour toutes mes absences au laboratoire, prévues et imprévues. Sa disponibilité continue, malgré des périodes très chargées, demandes de fonds, révisions d'articles… n'a jamais cessé de m'émerveiller. Son « œil de faucon » a pu déceler même les plus petites erreurs intercalées dans de nombreux articles et qui ont échappé à plusieurs lecteurs.

Un merci spécial à Pasha Javadi pour toutes les réalisations qu'on a pu accomplir ensemble. Toutes les discussions scientifiques, religieuses, politiques et philosophiques étaient très agréables. Tes connaissances du domaine de l'industrie pharmaceutique m'ont énormément aidé.

Un grand merci à la Dre Vanessa Harrar pour son aide précieuse sur les analyses statistiques, la préparation des figures et la rédaction des manuscrits.

Je salue toutes les personnes suivantes pour m'avoir permis de passer des heures de plaisir au laboratoire : Bruno Cécyre, Hosni Cherif, Laurent Elkrief, Alexandra Richard-Beaudry et Diana Baharova. Hocine Slimani et Léa Gagnon, je vous salue de proche et à distance.

I am very grateful to the late Dr. Frank Ervin, to Dr. Roberta Palmour and to all the staff of the Behavioural Sciences Foundation Laboratories located in St Kitts (West Indies), for their continued support on our electrophysiological and behavioural primate work.

I. INTRODUCTION

Le cannabis est une drogue dont l'usage est très répandu dans le monde. Aussi appelé marijuana, c'est un produit naturel dérivé de la plante *Cannabis sativa*. Elle est constituée de plusieurs molécules que l'on appelle phytocannabinoïdes, principalement le tétrahydrocannabinol (THC) et le cannabidiol (CBD) (Fattore, 2015). Les cannabinoïdes se lient à des récepteurs spécifiques qui se retrouvent à travers tout l'organisme, particulièrement le récepteur cannabinoïde de type 1 (CB1R) et le récepteur cannabinoïde de type 2 (CB2R) (Di Marzo, 2014). Évidemment, ces récepteurs ne sont pas présents dans le corps uniquement pour répondre à cette plante et produire des effets psychotropes. Les récepteurs cannabinoïdes répondent à des ligands endogènes qui se retrouvent naturellement dans l'organisme, les endocannabinoïdes (eCBs), notamment l'anandamide (AEA) et le 2-arachidonoyl glycérol (2-AG). L'activité au niveau de la cellule de ces eCBs est régulée par plusieurs enzymes, essentiellement la N-acylphosphatidyléthanolamine phospholipase D (NAPE-PLD), la diacylglycérol lipase (DAGL), la *fatty acid amide hydrolase* (FAAH), la monoacylglycérol lipase (MGL) et la cyclooxygénase-2 (COX-2) (Piomelli, 2003). Pris ensemble, les récepteurs cannabinoïdes, les ligands et les enzymes forment le système eCB. Ce système est présent dans tout le corps et est impliqué dans plusieurs processus physiologiques et physiopathologiques, mais son rôle principal chez l'adulte est la modulation de la neurotransmission. En effet, comme le CB1R se retrouve dans les neurones présynaptiques, il permet de réguler la transmission synaptique en modulant la relâche de plusieurs neurotransmetteurs tels que l'acide gamma-aminobutyrique (GABA), le glutamate et la dopamine (Piomelli, 2003). Par exemple, en temps normal, la stimulation d'un neurone glutamatergique va entrainer une libération de glutamate, et ainsi, induire un afflux postsynaptique du calcium par les récepteurs *N*-méthyl-D-aspartate (NMDA). Le processus de renforcement synaptique (augmentation d'amplitude de la réponse postsynaptique à la suite d'une activation intense de la synapse) est donc activé par cette augmentation du calcium dans le neurone postsynaptique. Par la suite, grâce à la stimulation des récepteurs métabotropiques du glutamate situés dans le neurone postsynaptique, les eCBs sont produits (De Petrocellis et coll., 2004). L'activation du CB1R présynaptique permet alors de diminuer la libération de

glutamate et éviter un afflux postsynaptique excessif de calcium. Certains phytocannabinoïdes contenus dans la plante *Cannabis sativa* se lient aux récepteurs cannabinoïdes et perturbent la libération de certains neurotransmetteurs normalement régulée par les eCBs (Mechoulam et coll., 2014). La plupart des études, à ce jour, se sont concentrées sur le rôle de ce système dans le SNC. Quelques évidences dans la littérature scientifique laissent présager que le système eCB est impliqué dans la fonction visuelle, particulièrement dans la fonction de la rétine. Ces études ont cependant été réalisées chez quelques espèces, notamment les rongeurs, le poisson rouge et la salamandre (Yazulla, 2008).

L'être humain est entouré de lumière. Que ce soit une lumière naturelle, comme celle du soleil ou des étoiles, ou bien une lumière artificielle, comme celle des ampoules ou des appareils électroniques, c'est au niveau de la rétine que commence le premier traitement de l'information visuelle. La lumière de notre environnement pénètre dans l'œil, passe à travers la cornée, l'humeur aqueuse, le cristallin et le vitré pour atteindre la rétine, l'organe sensoriel responsable de la conversion de la lumière en signaux électriques. Cette mince couche d'environ 0,5 mm d'épaisseur tapisse le fond d'œil. Elle est composée de plusieurs couches de neurones interconnectés par des synapses, mais ce sont principalement les photorécepteurs qui sont sensibles à la lumière. Il existe principalement deux types de photorécepteurs : les cônes et les bâtonnets (Kandel et coll., 2013). Les bâtonnets, surtout présents dans la rétine périphérique, sont impliqués dans la vision crépusculaire et ne sont pas sensibles à la couleur. Les cônes, quant à eux, sont localisés surtout dans la région centrale (fovéa) de la rétine, sont responsables de la vision diurne et sont sensibles aux différentes longueurs d'onde du spectre lumineux. Il existe aussi un troisième type de photorécepteurs beaucoup plus rare qu'on appelle les cellules ganglionnaires intrinsèquement photosensibles (Hattar et coll., 2002). Ces derniers seraient importants dans la régulation des rythmes circadiens (signaux physiologiques favorisant l'éveil et le sommeil à des moments précis de la journée). Les signaux neuronaux issus des cônes et des bâtonnets subissent ensuite un traitement par les autres composantes cellulaires de la mosaïque rétinienne. La résultante est un signal qui prend la forme de potentiels d'action dans les axones des cellules ganglionnaires qui forment le nerf optique. Ces derniers sont ensuite acheminés vers les centres supérieurs du cerveau pour le traitement nécessaire à la perception (Purves et coll., 2005). Plusieurs caractéristiques importantes de la

perception visuelle dépendent du traitement de l'information qui commence au niveau rétinien et qui dépendrait de l'action modulatrice d'un groupe de récepteurs qui font partie du système eCB dont on connait encore peu de choses.

Cette thèse se concentre donc sur l'expression, la localisation et le rôle du système eCB dans la rétine du singe. Les aspects fondamentaux de l'anatomie et la physiologie de la rétine sont d'abord présentés avec une emphase chez les primates. Par la suite, une revue de littérature est exposée sur (1) la distribution des récepteurs cannabinoïdes, des eCBs et des enzymes régulant l'activité des eCBs et (2) le rôle de ce système dans la neurotransmission, particulièrement au niveau du système visuel. Enfin, la raison pour laquelle le singe vervet a été choisi comme modèle animal dans le cadre de cette thèse sera soulignée.

1. La rétine

L'œil est l'organe de la vision, le sens qui va permettre à tous les êtres vivants de capter la lumière pour ensuite l'analyser, l'interpréter et interagir avec son environnement. C'est cette structure qui va s'occuper de décomposer les informations lumineuses en signaux électriques. La rétine est formée à partir de l'excroissance du diencéphale durant le développement du fœtus. C'est donc une extension directe du système nerveux central (SNC). Ainsi, comme la rétine fait partie intégrante du SNC, elle comporte des circuits nerveux complexes. La lumière passe à travers plusieurs structures de l'œil ainsi qu'à travers les différentes couches de la rétine, avant d'atteindre les photorécepteurs. La Figure 1 illustre comment la lumière doit traverser les six couches de la rétine afin d'intégrer le signal lumineux. Ce sont les photorécepteurs, maintenus par les nutriments de l'épithélium pigmentaire et des vaisseaux de la choroïde, qui absorbent la lumière. Ces cellules sensibles à la lumière convertissent ensuite la lumière en influx nerveux en passant par les cellules horizontales, bipolaires et amacrines. Enfin, l'influx est acheminé aux cellules ganglionnaires qui assurent la sortie de l'information par le nerf optique.

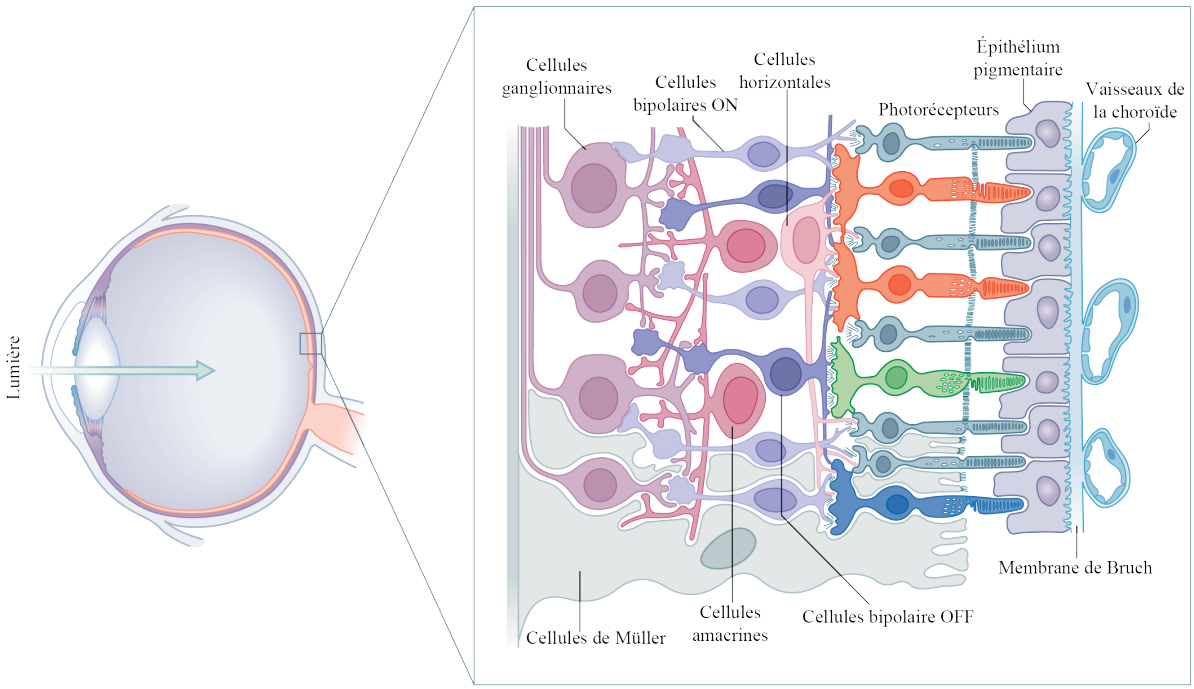

Figure 1. L'œil et les différentes couches de la rétine.
Modifiée de *Clinical Ocular Toxicology*, Fraunfelder et coll., 2008

1.1 Anatomie de la rétine

La rétine est composée de plusieurs types de cellules neuronales : les photorécepteurs, les cellules horizontales, les cellules bipolaires, les cellules amacrines et les cellules ganglionnaires. Il existe aussi 3 types de cellules gliales dans la rétine : les cellules de Müller, les astrocytes et les cellules microgliales. Toutes ces cellules neuronales et gliales sont organisées en mosaïque pour permettre d'assurer une information uniforme du champ visuel (Masland, 2001). La forme générale que peuvent prendre ces différentes cellules est illustrée dans la Figure 2 et est décrite dans les paragraphes qui suivent. De prime abord, il est important de clarifier les termes suivants : la rétine interne et la rétine externe. Dans une coupe transversale de la rétine, la rétine externe correspond au côté des photorécepteurs et la rétine interne du côté des cellules ganglionnaires.

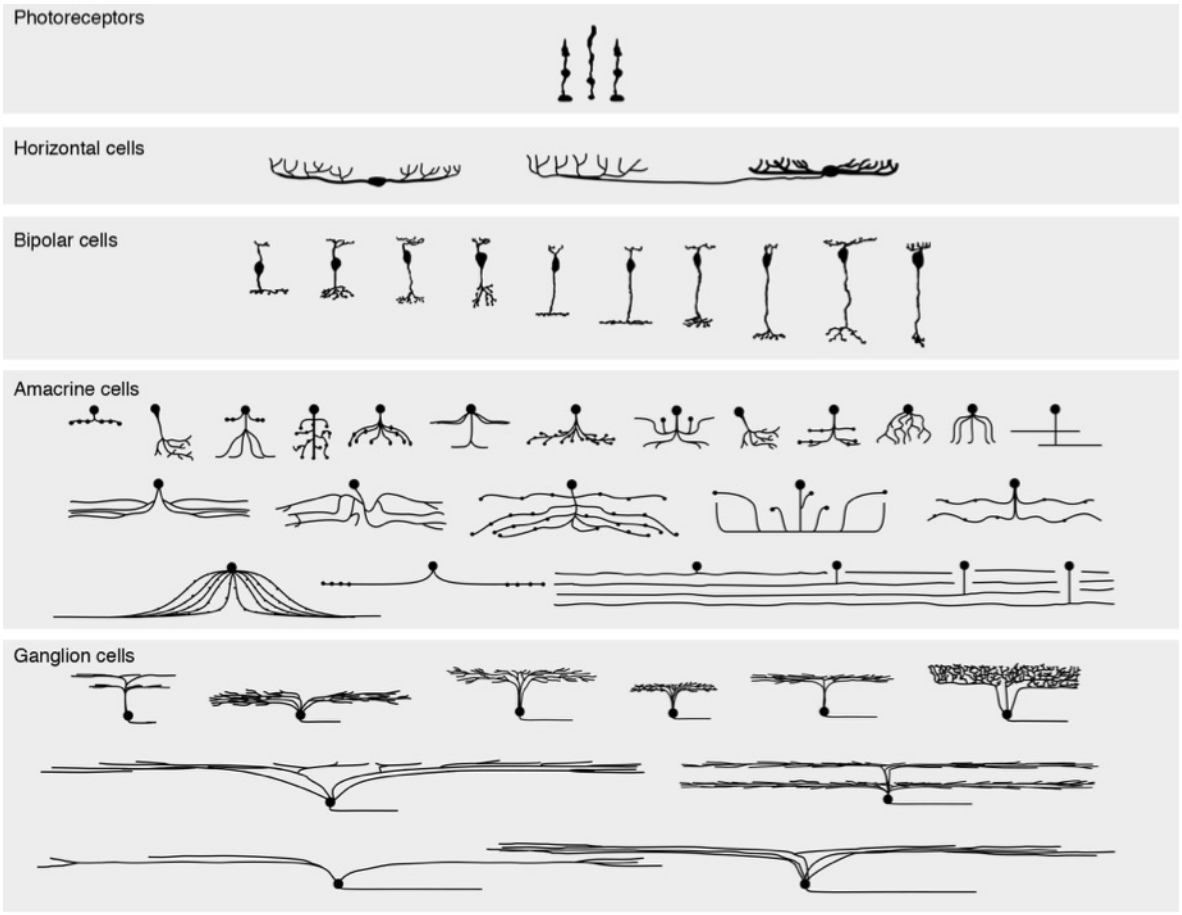

Figure 2. Les populations neuronales principales de la rétine des mammifères.
Tirée de Masland, 2001

1.1.1 Photorécepteurs

Les photorécepteurs de la rétine, les cônes et les bâtonnets, se différencient par de nombreuses caractéristiques anatomiques. Comme leurs noms l'indiquent, les cônes ont une forme conique et les bâtonnets une forme cylindrique. La rétine de la plupart des mammifères comporte 2 types de cônes, tandis que la rétine des primates humains et non humains en possède 3. Les cônes « S », responsables du traitement de l'information des longueurs d'onde courtes, les cônes « M », pour les longueurs d'onde moyennes, et les cônes « L », pour les longueurs d'onde longues. Il existe 126 millions de bâtonnets surtout en périphérie de la rétine et 6.5 millions de cônes surtout en région centrale (Osterberg, 1935). La Figure 3 illustre la distribution des cônes versus celle des bâtonnets.

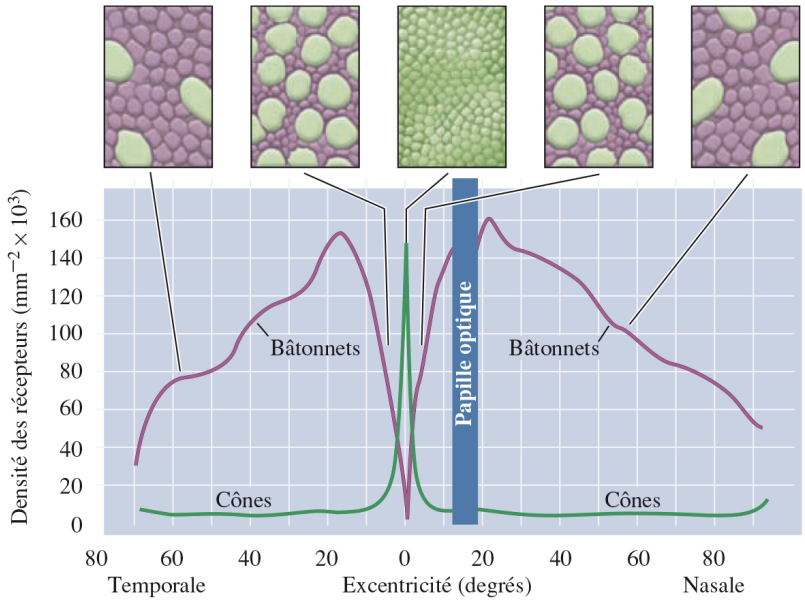

Figure 3. Distribution des cônes et des bâtonnets dans la rétine.

Tirée de *Neurosciences*, Purves et coll., 2005.

1.1.2 Cellules horizontales

Les cellules horizontales reçoivent de l'information des photorécepteurs et la transmettent à plusieurs cellules environnantes. Il existe principalement deux types de cellules horizontales, les H1 et les H2. Les cellules H1 sont liées aux cônes par leurs dendrites et aux bâtonnets par leurs branchements axonaux. La raison pour laquelle ce sous-type de cellules se lie directement aux bâtonnets est que, d'un point de vue évolutionniste, les bâtonnets sont apparus bien après les cônes (Okano et coll., 1992; Johnson et coll., 1993). Les cellules H2 sont liées aux cônes uniquement par l'intermédiaire de leur arbre dendritique et d'un petit axone. Le rôle des cellules horizontales est de réguler l'information de la rétine en émettant un signal de nature opposée à celui qui est reçu, c'est le phénomène d'inhibition latérale (Wässle, 2004).

1.1.3 Cellules bipolaires

Les cellules bipolaires reçoivent les signaux électriques des photorécepteurs et font synapse avec les cellules amacrines et ganglionnaires. Les cellules bipolaires liées aux bâtonnets ne reçoivent que l'information provenant de bâtonnets et font synapse sur les cellules amacrines AII, qui font à leur tour contact avec les cellules bipolaires liées aux cônes,

et enfin rejoindre les cellules ganglionnaires (Masland, 2001). La raison pour laquelle l'information des bâtonnets prend ce long chemin est que l'apparition des bâtonnets est survenue plus tard au cours de l'évolution (Johnson et coll., 1993; Masland, 2001; Okano et coll., 1992). En se basant sur des études sur les propriétés électrophysiologiques des cellules bipolaires, il est possible de classer ces cellules en 3 grands types : 1) les cellules bipolaires liées aux bâtonnets, 2) les cellules bipolaires liées aux cônes et 3) les cellules bipolaires mixtes (cônes/bâtonnets). Chacune de ces cellules comporte un patron de réponses à la lumière spécifique. Elles se projettent dans la rétine interne où leur axone respectif fait synapse dans différentes régions bien ségrégées (couches) de la couche plexiforme interne (IPL). Les cellules bipolaires qui se projettent dans les strates 1-2 sont des cellules bipolaires hyperpolarisantes (HBCs) et celles dans les strates 2-5 sont des cellules bipolaires dépolarisantes (DBCs) (Besharse et Bok, 2011). Comme illustrée dans la Figure 4, il existe 10 différentes cellules bipolaires ayant une morphologie bien distincte. De plus, il est possible de diviser chez plusieurs espèces l'IPL en 2 couches (une région OFF et une région ON) et seulement chez la souris, en 5 couches (Dowling, 2012).

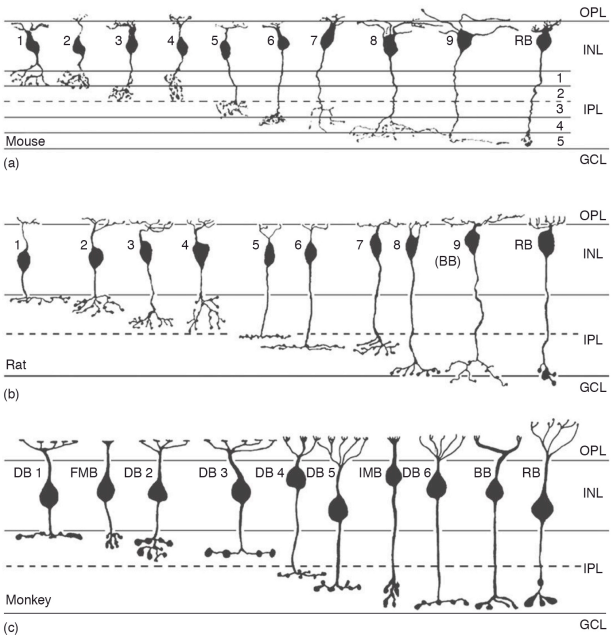

Figure 4. Schéma des différentes cellules bipolaires chez la souris, le rat et le singe. Tirée de *The Retina and its Disorders*, Besharse et Bok, 2011. Abréviations : OPL, couche plexiforme externe; INL, couche nucléaire interne; IPL, couche plexiforme interne; GCL, couche des cellules ganglionnaires; RB, cellule bipolaire liée aux bâtonnets.

1.1.4 Cellules amacrines

Les cellules amacrines sont des interneurones de la rétine. Ce sont des neurones inhibiteurs qui projettent leur arborisation dendritique dans l'IPL, et interagissent avec les cellules ganglionnaires et les cellules bipolaires (Wässle, 2004). Il existe plus de 33 différents types de cellules amacrines classées selon leur morphologie et stratification de leurs dendrites (Masland, 2001). Comme les cellules horizontales, les cellules amacrines interviennent dans l'inhibition latérale afin d'augmenter l'acuité du signal visuel (Wässle, 2004).

1.1.5 Cellules ganglionnaires

Les cellules ganglionnaires sont le dernier point du traitement de l'information neuronale rétinienne. Il existe entre 10 et 15 différents types de cellules ganglionnaires classés selon leurs morphologies (Masland, 2001). Les cellules ganglionnaires permettent de recueillir les informations du monde visuel à partir de cellules bipolaires et des interneurones (cellules horizontales et amacrines). L'information à ce niveau se présente sous la forme de messagers chimiques détectés par les photorécepteurs sur la membrane des cellules ganglionnaires.

1.1.6 Cellules gliales

Il existe trois grands types de cellules gliales dans la rétine : les cellules de Müller, les astrocytes et les cellules microgliales. Ces cellules gliales ont déjà été décrites dans la rétine il y a plus d'une centaine d'années (Sarthy et Ripps, 2006). Les cellules de Müller représentent le type de cellules gliales principales dans la rétine. Ces cellules s'étendent de façon radiale à partir des axones de cellules ganglionnaires jusqu'au niveau des photorécepteurs. Elles offrent ainsi un support structural à tous les neurones rétiniens. De plus, leurs prolongements cellulaires entourent les corps cellulaires des cellules horizontales, bipolaires et amacrines, pour maximiser le nombre de contacts entre elles (Bringmann et coll., 2006). Comme les cellules comportent l'enzyme GS (glutamine synthétase) qui transforme l'excédent de glutamate en glutamine, elles sont aussi impliquées dans la régulation de la voie verticale glutamatergique (Sarthy et Ripps, 2006).

1.2 Physiologie de la rétine

L'absorption d'un photon de lumière par le pigment photosensible situé dans les disques membranaires des photorécepteurs induit une cascade d'évènements qui est référée par le terme « mécanisme de phototransduction » (Purves et coll.., 2005). Cette cascade a été étudiée exhaustivement pour les bâtonnets dont le mécanisme est illustré ici; un mécanisme similaire est aussi en jeux dans les cônes. Dans les segments externes des bâtonnets, l'absorption de photons lumineux par la rhodopsine, le pigment protéique photosensible présent dans les bâtonnets, induit une séquence d'évènements biochimiques qui mène finalement à une baisse des niveaux intracellulaires de la guanosine monophosphate cyclique (cGMP) et la fermeture des canaux ioniques sensibles à la cGMP dans les segments externes. Cette fermeture des canaux diminue l'entrée de cations dans les segments externes, ce qui entraine une hyperpolarisation de la membrane et une baisse de la libération de glutamate dans la fente synaptique (Kandel et coll., 2013). Ces étapes se déroulent aussi dans les cônes, mais avec les photopigments propres aux cônes, l'opsine S (*short*, longueur d'onde courte, ce qui correspond au bleu), l'opsine M (*medium*, longueur d'onde moyenne, ce qui correspond au vert) ou l'opsine L (*long*, longueur d'onde longue, ce qui correspond au rouge) (Purves et coll., 2005).

1.2.1 Voie des cônes

Les cônes répondent à la lumière avec une hyperpolarisation membranaire sous forme de potentiels gradués. La voie des cônes est un circuit où chaque cône est branché sur deux cellules bipolaires au niveau de la couche plexiforme externe (OPL) et sur deux cellules ganglionnaires dans la couche plexiforme interne (IPL) (Besharse et Bok, 2011). Le jeu de synapses excitatrices et inhibitrices permet à l'hyperpolarisation (lumière transformée en signal ionique dans les photorécepteurs) initiale de stimuler de façon complémentaire deux fibres chargées de véhiculer le même message, une fibre qui décharge « ON » (voie illustrée en vert dans la Figure 5) et l'autre « OFF » qui arrête son activité spontanée (voie illustrée en rouge dans la Figure 5). Il y a donc une ségrégation de la voie des cônes dans la rétine. La libération de glutamate dans la fente synaptique (cônes/cellules bipolaires) est modulée par le changement du potentiel de membrane dans les segments externes (OS) des photorécepteurs.

Les cellules bipolaires ON produisent une entrée excitatrice aux cellules amacrines et ganglionnaires et transmettent le signal à l'aide d'une dépolarisation graduée (un potentiel est dit « gradué » lorsqu'il est proportionnel à l'intensité du stimulus détecté à l'opposé du potentiel d'action) avec changement de signe (Besharse et Bok, 2011). Les cellules bipolaires OFF produisent une entrée inhibitrice aux cellules amacrines et aux cellules ganglionnaires. Elles transmettent ainsi le signal à l'aide d'une hyperpolarisation graduée avec conservation de signe. Les cônes communiquent aussi latéralement avec d'autres cônes (et bâtonnets) via des liaisons électriques qu'on appelle jonctions GAP (GJ). La communication latérale est aussi produite par les cellules horizontales dans la couche plexiforme externe (OPL) et par les cellules amacrines dans la couche plexiforme interne (IPL).

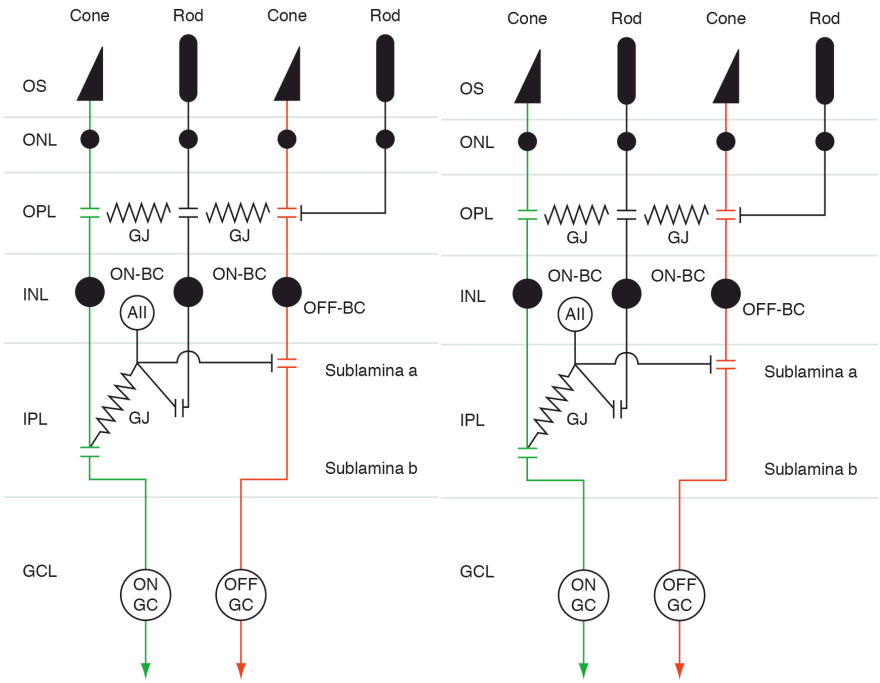

Figure 5. Circuit rétinien de la voie des cônes.

Tirée de *The Retina and its Disorders*, Besharse et Bok, 2011. Abréviations : OS, segment externe; ONL, couche nucléaire externe; OPL, couche plexiforme externe; INL, couche nucléaire interne; IPL, couche plexiforme interne; GCL, couche des cellules ganglionnaires; GJ, jonction gap.

1.2.2 Voies des bâtonnets

La voie des bâtonnets est un circuit qui comporte quatre connexions synaptiques avec deux points de forte convergence : de 20 à 50 bâtonnets convergent sur chaque cellule bipolaire de bâtonnets et de 20 à 25 cellules bipolaires de bâtonnets convergent vers chaque cellule amacrine (Masland, 2001). Au total, les signaux provenant d'au moins un millier de bâtonnets convergent sur une seule cellule ganglionnaire. Les bâtonnets peuvent répondre à la stimulation d'un seul photon alors qu'il en faut au moins une centaine pour obtenir une réponse d'un cône (Wässle, 2004). Cette organisation augmente considérablement l'amplitude du signal et assure une bonne sensibilité en faible lumière (Figure 6).

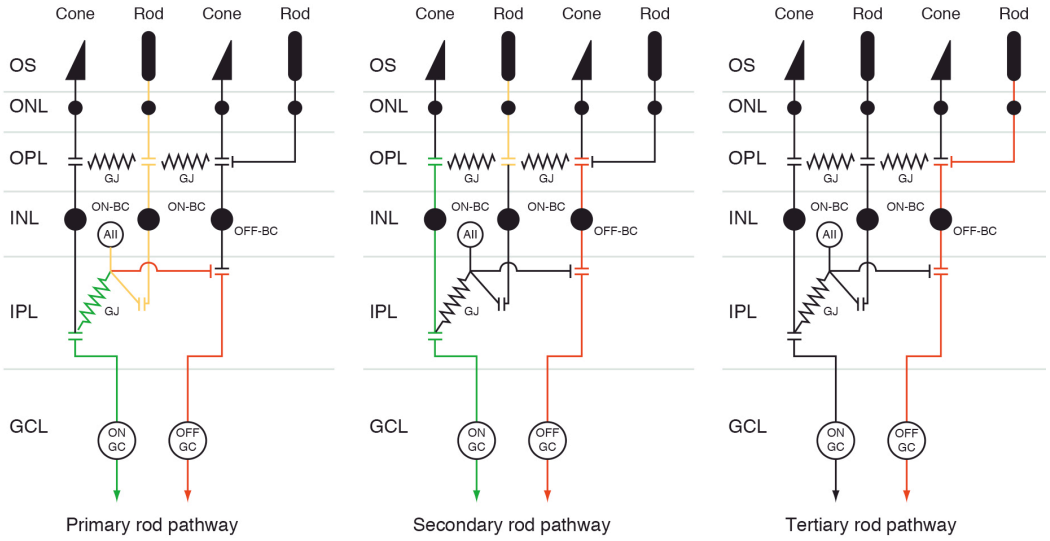

Figure 6. Circuits rétiniens de la voie des bâtonnets.

Tirée de *The Retina and its Disorders*, Besharse et Bok, 2011. Abréviations : OS, segment externe; ONL, couche nucléaire externe; OPL, couche plexiforme externe; INL, couche nucléaire interne; IPL, couche plexiforme interne; GCL, couche des cellules ganglionnaires; GJ, jonction gap.

Dans la voie primaire des bâtonnets (panneau de gauche), les bâtonnets font synapse avec des cellules bipolaires ON liées aux bâtonnets qui sont connectées à des cellules amacrines AII dans la couche plexiforme interne (voie illustrée en jaune dans le panneau de gauche de la Figure 6) (Besharse et Bok, 2011). Le signal des cellules amacrine AII s'infiltre

dans la voie des cônes en excitant les cellules bipolaires ON liées aux cônes via des jonctions électriques gap (voie illustrée en vert dans le panneau de gauche de la Figure 6) et via des synapses glycinergiques (avec changements de signe) en passant par des cellules bipolaires OFF liées aux cônes (voie illustrée en rouge dans le panneau de gauche de la Figure 6).

Dans la voie secondaire des bâtonnets (panneau du milieu), les jonctions gap se font entre bâtonnets et cônes plus précisément dans les sphérules de bâtonnets et les pédicules de cônes situés dans la couche plexiforme externe. Grâce à cette jonction gap bâtonnets/cônes, le signal des bâtonnets peut emprunter les cellules bipolaires ON et OFF liées aux cônes et donc aux cellules ganglionnaires ON et OFF (voie illustrée en vert et en rouge, respectivement).

Dans la voie des bâtonnets tertiaire (panneau de droit), le bâtonnet fait synapse directement avec une cellule bipolaire OFF liée aux cônes en « court-circuitant » la cellule bipolaire ON liées aux bâtonnets (voie illustrée en en rouge dans le panneau de droit dans la Figure 6).

1.3 Anatomie comparée de la rétine

L'œil est un système sensoriel utilisé dans l'ensemble du règne animal. Les positions relatives des liaisons entre ces couches varient entre les espèces. Certains oiseaux, comme le faucon, possèdent une meilleure acuité visuelle que celle de l'humain (Fox et coll., 1976; Reymond, 1987) et certaines autres espèces, comme les squilles et le poisson-clown, possèdent même une meilleure vision des couleurs que celle de l'humain (Marshall et Oberwinkler, 1999; Sabbah et coll., 2010. Dans cette thèse, 3 espèces animales ont été étudiées, soient la souris, le toupaye, le singe vervet et le singe macaque; les souris étant au bas de l'échelle animale; le toupaye entre les souris et les primates; et les primates se situant le plus proche de l'homme. Les souris possèdent une rétine qui est largement dominée par les bâtonnets, et de ce fait, spécialisée pour la vision scotopique (Jeon et coll., 1998) et une basse résolution spatiale (Prusky et Douglas, 2004). Les toupayes ont une rétine largement dominée par les cônes (Müller et Peichl, 1993). Tant les souris que les toupayes ne détiennent pas une fovéa responsable de la haute acuité visuelle. Ce n'est que les primates humains et non-humains qui ont une région fovéale de haute densité en cônes qui décroit en chiffres avec l'eccentricité (Osterberg, 1935; Herbin et coll., 1997).

1.4 Le cerveau visuel

Les axones des cellules ganglionnaires des primates se projettent principalement dans le corps genouillé latéral dorsal (CGLd). En effet, chez les primates, ce sont 90% des fibres qui atteignent le CGLd, tandis que chez les rongeurs ce n'est seulement que 10%, car la majorité des fibres atteignent principalement le collicule supérieur (Purves et coll., 2005). En fait, la rétine projette aussi à un vaste ensemble de structures sous-corticales dont les fonctions ne sont pas encore connues (Matteau et coll., 2003). Chez le singe, l'organisation du CGLd est semblable à l'humain, ce qui en fait un modèle de choix pour étudier la vision de l'humain (voir section *Choix du modèle animal : le singe vervet de St Kitts*). À partir du CGLd, les fibres se dirigent vers le cortex visuel primaire (Kandel et coll., 2013).

2. L'électrorétinogramme

L'électrorétinographie (ERG) est un examen d'électrophysiologie non invasif qui permet d'évaluer la fonction rétinienne (des cônes et des bâtonnets) en clinique et en laboratoire de façon objective. Il est généralement admis que l'anatomie et la physiologie de l'œil du singe sont très similaires à celles de l'homme, ce qui rend le choix de ce primate non humain comme modèle animal pour l'évaluation des effets oculaires très judicieux (Fraunfelder et coll., 2008). Comme les aspects techniques et procéduraux du protocole humain ont bien été standardisés (« *Standard for clinical electroretinography (SCE)* »), l'électrorétinogramme (ERG) peut être utilisé de routine pour étudier la toxicité rétinienne (neurotoxicité potentielle globale de drogues spécifiques chez les primates) et la fonction rétinienne. Il est ainsi possible de récolter une panoplie de données selon la méthode standard *SCE*. C'est une technique non invasive, sans douleur et sans dommages ni effets indésirables pour l'œil. Plusieurs travaux évaluant la toxicité oculaire de certaines drogues ont utilisé l'ERG chez le singe dans un laboratoire de recherche et il existe un protocole d'ERG standard pour étudier la fonction rétinienne normale et la toxicologie chez le primate non humain (Bee, 2001). Cette méthode permet aussi de séparer la fonction du système des bâtonnets de la fonction du système des cônes. Si un flash de faible intensité est envoyé vers une rétine adaptée à la noirceur, le système des bâtonnets sera activé. Si un flash est envoyé vers une rétine adaptée à la lumière, le système des cônes sera activé. Lorsque des flashs assez forts

sont envoyés vers la rétine, le tracé ERG comprend une onde a (déflexion négative initiale) suivi d'une onde b (déflexion positive). Un protocole expérimental a été mis au point et utilisé dans le cadre des expériences réalisées dans cette thèse.

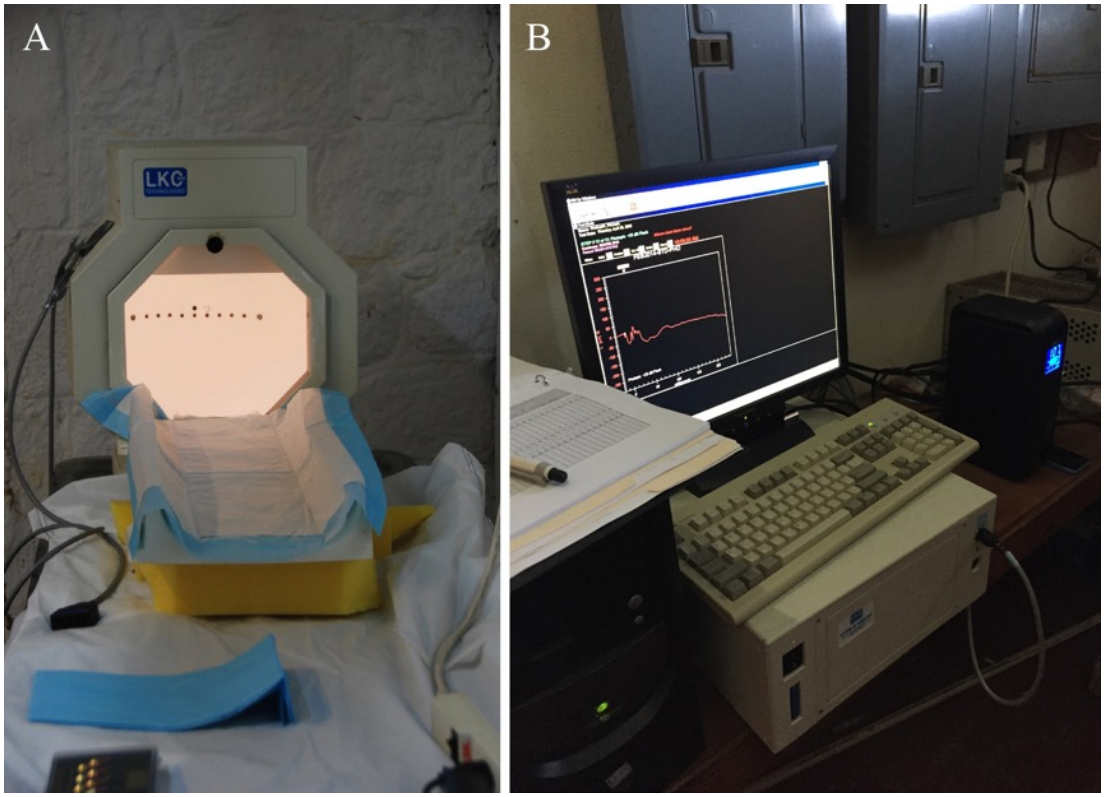

Figure 7. Montage expérimental pour l'enregistrement ERG chez le singe.
En (**A**) est illustré le ganzfeld qui permet de produire une stimulation en champ total et en (**B**) l'appareil ERG (UTAS-E3000) relié à un ordinateur.

Selon le montage expérimental utilisé dans le cadre de cette thèse, les ondes électrorétinographiques des deux yeux ont été enregistrées. La Figure 7 représente le montage expérimental mis en place dans les laboratoires du centre de recherche de l'ile de St Kitts. En ambiance obscure (condition d'adaptation à la noirceur), un flash d'intensité scotopique (de faible intensité) n'évoque que la réponse du système scotopique (voie des bâtonnets) et un flash d'intensité photopique (de haute intensité) évoque une réponse combinée des deux systèmes (voies des cônes et bâtonnets). En ambiance lumineuse (condition d'adaptation à la lumière), seul un flash d'intensité photopique (de haute intensité) produit une réponse efficace et n'évoque que la réponse du système photopique (voie des cônes) (McCulloch et coll., 2015).

La Figure 8 illustre la relation entre les structures de la rétine (partie du bas de la figure) et les composantes principales de la réponse ERG (partie du haut). L'onde a est associée à la réponse de la rétine externe (couche des photorécepteurs). L'onde b est associée à l'activité des cellules bipolaires dépolarisantes et le courant d'ions des cellules de Müller (Frishman, 2013). Les cellules amacrines sont impliquées dans la genèse des potentiels oscillatoires situés dans la portion ascendante de l'onde b. L'onde c (situé à la fin du tracé ERG de la Figure 8) est une onde lente et variable qui provient des cellules de l'épithélium pigmentaire rétinien (Marmor et Hock, 1982). L'onde c est rarement utilisée en clinique, car sa fonction est difficile à évaluer. Vu que l'ERG évalue la fonction rétinienne et qu'il est possible d'isoler la réponse de certains types cellulaires dans les ondes de l'ERG, cette technique a été choisie pour l'étude du rôle fonctionel du système eCB chez le singe.

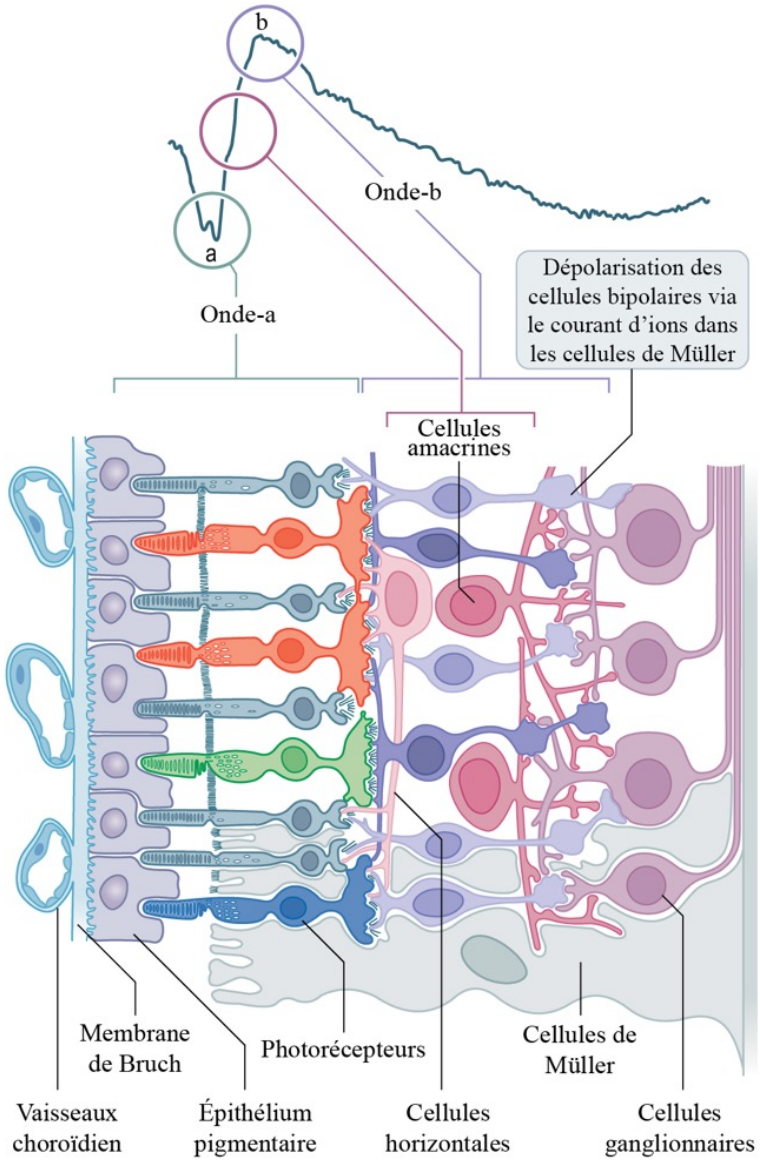

Figure 8. Diagramme reliant les structures de la rétine et les composantes de l'ERG. Modifiée de *Clinical Ocular Toxicology*, Fraunfelder et coll., 2008

2.1 Onde a

La première partie de l'onde a représente l'activité des photorécepteurs, tandis que la dernière partie de celle-ci représente l'activité de plusieurs cellules, notamment les photorécepteurs, les cellules bipolaires, les cellules amacrines et les cellules de Müller. En fait, elle est générée par les cônes, ou par l'ensemble de cônes et bâtonnets (Robson et coll., 2003). L'activation des photorécepteurs par un stimulus lumineux cause une hyperpolarisation de ces

cellules en raison de la fermeture des canaux sodiques, ce qui explique la déflexion négative de l'onde a (Barraco et coll., 2006). En condition scotopique mixte, l'onde a provient de la somme des hyperpolarisations des cônes et des bâtonnets. Le temps de latence de l'onde a diminue avec l'intensité des flashs. En condition photopique, l'onde a résulte de l'activation des cônes seulement étant donné que les bâtonnets sont saturés (Frishman, 2013).

2.2 Onde b

L'onde b est positive et beaucoup plus ample et longue que l'onde a. Elle correspond à la dépolarisation des cellules bipolaires (Stockton et Slaughter, 1989), mais les cellules de Müller sont également impliquées (Newman et Frishman, 1991). Ces dernières reflètent les courants extracellulaires de potassium produit par la dépolarisation des cellules bipolaires. En condition scotopique, l'hyperpolarisation des bâtonnets entraine une dépolarisation des cellules bipolaires ON liées aux bâtonnets et donc une onde b positive. En condition mixte (cônes et bâtonnets), c'est la dépolarisation des cellules bipolaires ON liées aux bâtonnets et celles liées aux cônes qui génère l'onde b. Les cellules de Müller contribuent aussi à l'onde b, car les besoins en glutamate et les changements en potassium des cellules bipolaires sont importants. En condition photopique, l'onde b résulte de l'action concertée de la dépolarisation des cellules bipolaires ON liées aux cônes et de l'hyperpolarisation des cellules bipolaires OFF des cônes L et M (Rigaudière et Le Gargasson, 2007). Les cellules de Müller sont également impliquées dans la genèse de cette onde, car elles servent de réservoir d'ions durant l'hyperpolarisation des photorécepteurs et reflètent les changements de concentrations de potassium lors de la dépolarisation des cellules bipolaires.

2.3 Onde i

L'onde i de l'ERG en champ total (ERG flash) est une composante positive de faible voltage qui suit l'onde b en conditions photopique (Nagata, 1963; Lachapelle, 1987; Peachy, 1989; Murayama et Sieving, 1992). L'onde i a d'abord été présentée comme un produit de la réponse OFF suite à un bref flash (Nagata, 1963), mais cette hypothèse a été débattue (Seiple et Holopigian, 1994). Plus récemment, l'onde i a été liée à l'onde P50 du p-ERG, une onde probablement issue de la réponse des cellules ganglionnaires (Rousseau et coll., 1996).

Nonobstant son origine exacte, l'onde i reste controversée. Certains prétendent qu'elle serait générée au niveau de la rétine interne (cellules ganglionnaires) (Rosolen et coll., 2004), tandis que d'autres suggèrent qu'elle provient de la rétine externe (réponse OFF des cellules bipolaires) (Rangaswamy et coll., 2004). Ce dernier point est bien mis en évidence dans des études de pathologie oculaire. Par exemple, l'onde i est éliminée lorsqu'on bloque spécifiquement la rétine externe (coté des photorécepteurs); lorsqu'on bloque la rétine interne (coté des cellules ganglionnaires), l'onde i persiste (Viswanathan et coll., 2001; Rangaswamy et coll., 2004).

2.4 Implications cliniques

L'électrorétinogramme en champ total (ERG flash) est un bon outil pour diagnostiquer plusieurs rétinopathies où la lésion est généralisée. En fait, les ondes électrorétinographiques sont modifiées dans plusieurs affections rétiniennes, particulièrement la rétinite pigmentaire, l'amaurose congénitale de Leber, la choroïdérémie, le syndrome de Goldman-Favre, la rétinoschisis juvénile liée au chromosome X et l'achromatopsie (Kolb et coll., 2011). Toutes ces maladies révèlent au niveau des tracés des anormalités marquées. Par exemple, la rétinite pigmentaire produit des ondes a et b de faibles amplitudes ou même des amplitudes supranormales (réponse du système des cônes) (Young et coll., 2012). La choroïdérémie produit des amplitudes des ondes a et b diminuées tant en condition scotopique qu'en condition photopique (Vincent et coll., 2013). De plus, les temps de latence de l'onde b scotopique et photopique sont augmentés. Plusieurs articles de revue récents font le lien entre les affectations de l'œil et les modifications de l'ERG qui en résultent (Young et coll., 2012; Vincent et coll., 2013). Pour l'instant, aucune étude ne s'est intéressée à l'état du système eCB lors des diverses maladies de la rétine.

3. Le cannabis et ses constituants naturels (phytocannabinoïdes)

Le cannabis, marijuana, hachich, joint, shit, chanvre, sont des mots qui se décrivent par eux-mêmes. L'état d'euphorie, accompagné d'une tendance au rire facile et peu motivé, accompagné d'un sentiment de relaxation, de légèreté et de flottement, est l'effet majeur du cannabis. La consommation de cannabis provoque des hallucinations et des perturbations

sensorielles augmentant les perceptions visuelles. Les personnes ayant fumé du cannabis ont une attention et une concentration diminuées, des modifications de la motricité et de la coordination, une difficulté à apprécier la situation environnante gênant la prise de décision et les actions rapides (Rafaelsen et coll., 1973). Environ 160 millions de personnes dans le monde ont consommé du cannabis au cours de l'année 2005 (United Nations Office on Drugs and Crime, 2007). La consommation de cannabis chez les adolescents est très répandue et est souvent associée à une consommation à long terme. Justement, une personne sur deux qui fume du cannabis plus de cinq fois par jour va continuer d'abuser de cette drogue 10 ans plus tard (Perkonigg et coll., 2008). Le cannabis produit donc des effets complexes sur le corps, mais le fait que son usage entraine une forte dépendance reste très controversé. D'une part, le développement de traitements pharmacologiques est souvent ralenti par l'opinion de la société et de la communauté scientifique qui admettent que le cannabis ne produit pas de dépendance. D'autre part, certaines études prétendent que le cannabis produit une forte dépendance en démontrant que le THC possède des propriétés de renforcement chez les primates non humains et que l'abstinence de la drogue cause un syndrome de retrait (Budney et coll., 2002, 2003; Tanda et Goldberg, 2003; Fattore et coll., 2008). Ce syndrome est caractérisé par l'envie, l'irritabilité, l'anxiété, l'état dépressif, le manque d'appétit et des difficultés de sommeil (Budney et coll., 2002, 2003).

3.1 Aperçu historique

L'usage médicinal et récréatif du cannabis remonte à plus de 5000 ans, mais ce n'est que depuis les années 1960 que la recherche sur les effets des molécules cannabinoïdes a commencé. Les cannabinoïdes font partie du groupe de molécules chimiques qui activent les récepteurs aux cannabinoïdes. Il existe 3 classes de cannabinoïdes : les cannabinoïdes végétaux ou phytocannabinoïdes, notamment le THC, les cannabinoïdes endogènes, principalement le AEA et 2-AG et les cannabinoïdes de synthèse comme le CP-55,940. Le cannabis était connu depuis des millénaires pour ses nombreux effets psychotropes. Cette espèce de plante annuelle, aussi connue sous le nom de chanvre (*Cannabis sativa L.*), fait partie de la famille des Cannabacées. Elle peut être subdivisée en 4 sous-espèces selon la région d'où elle provient, Sativa, Indica, Spontanea ou Kafiristanica (Clarke et Watson, 2006). Le chanvre a été longtemps utilisé pour la fabrication des tissus, des cordes, pour la

construction, l'isolation thermique et bien plus. De nos jours, le cannabis est cultivé généralement pour un usage récréatif. Certains considèrent que cette plante fait partie des drogues douces contrairement aux drogues dures comme l'héroïne qui possèdent une grande dépendance physique. Aujourd'hui, cette considération ne tient plus puisque certaines personnes font un usage dur de cette drogue, ce qui les rend fortement dépendants. De plus, il reste possible d'avoir une dépendance psychologique vis-à-vis le cannabis, ce qui signifie d'être dépendant de l'effet procuré par la consommation (Perkonigg et coll., 2008). Le chanvre peut se présenter sous plusieurs formes, notamment, de fleurs séchées femelles (marijuana), de résine de cannabis (hachich), d'huile de cannabis ou de pollen. Généralement, il est consommé avec du tabac, mais il peut aussi être mangé, inhalé ou infusé directement dans le corps (Clarke et Watson, 2006). Un article de revue sur l'histoire du cannabis et ses préparations dans le monde résume bien l'usage que plusieurs populations ont pu faire du cannabis (Russo, 2007) et ce n'est qu'un résumé qui est présenté ici. Au 10^{e} siècle, le physicien juif égyptien Isaac Israeli l'Ancien (Égypte entre 830-850 et 932-955) a noté que le cannabis pouvait traiter l'otalgie. Au 12^{e} siècle, le médecin et philosophe juif Maimonide a voyagé de son Espagne natale vers la cour royale égyptienne pour exercer la médecine. Il a lui aussi noté dans son livre médical que le cannabis pouvait traiter plusieurs maladies, en mentionnant cette plante comme une huile, et sans discuter de ses effets psychotropes. À la fin du 16^{e} siècle, Prospero Alpini (médecin et botaniste italien) a rapporté plusieurs effets psychotropes que le cannabis procurait. C'est le médecin irlandais William Brooke O'Shaughnessy qui est le premier à avoir introduit le cannabis comme traitement thérapeutique dans les années 1830 pour soulager la douleur rhumatismale et calmer les convulsions (O'Shaughnessy, 1830). Par la suite, toutes les recherches sur le cannabis se sont concentrées sur la chimie des molécules cannabinoïdes contenues dans cette plante. Les études pharmacologiques ont pour leur part fait usage de composés de synthèse pour venir à leurs conclusions. À la suite de l'isolation du cannabidiol (Mechoulam et Shvo, 1963) et de THC (Gaoni et Mechoulam, 1964), les études physiologiques ont commencé. Subséquemment, durant les années 1990s, l'identification des récepteurs cannabinoïdes, des eCBs et des antagonistes de ces récepteurs a rendu possible la recherche pharmacologique et neurobiologique. La Figure 9 illustre la chronologie de la recherche sur les cannabinoïdes et le système eCB.

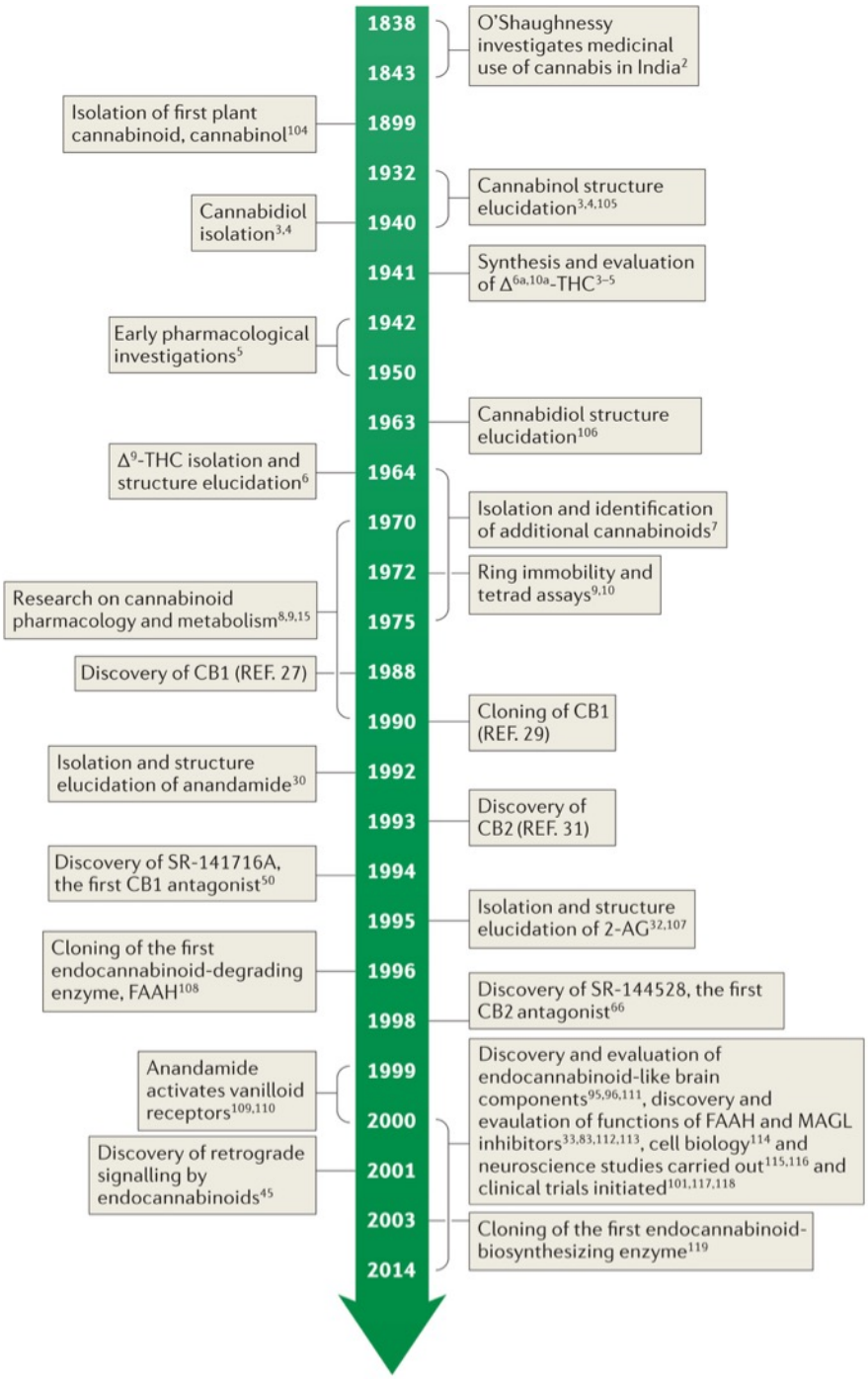

Figure 9. Chronologie de la recherche sur les cannabinoïdes et le système eCB.

Tirée de Mechoulam et coll., 2014

3.2 THC

Dans les années 1960s, Raphael Mechoulam et Yechiel Gaoni (Institut Weizmann, Rehovot, Israël) isolent le principe actif du cannabis, le Δ9-tetrahydrocannabinol (THC), responsable de la vaste majorité des effets psychotropes (Gaoni et Mechoulam, 1964; Mechoulam et Gaoni, 1965). Compte tenu de la nature lipophilique du THC, les chercheurs pensaient que cette molécule agissait de façon non spécifique en altérant la fluidité et la structure des membranes cellulaires. En démontrant plus tard que le THC n'agissait que de façon stéréosélective (ce n'est qu'une conformation spécifique qui produit les effets), cette molécule devait sans doute agir sur un récepteur ou une enzyme, mais non sur les membranes (Mechoulam et coll., 2014). Par la suite, des récepteurs possédant une affinité pour le THC ont été découverts ; puis, des ligands endogènes de ces récepteurs, les eCBs (Matsuda et coll., 1990; Munro et coll., 1993).

3.3 Cannabidiol

Le cannabidiol ne produit aucun effet psychoactif. De plus, à de fortes doses, il peut même agir contre les propriétés psychoactives du THC. Plusieurs effets bénéfiques lui sont attribués comme des effets de sédation, antiinflammatoire, antiépileptique, anxiolytique, antipsychotique et réducteur de la pression intraoculaire (voir section *Cannabinoïdes, pression intraoculaire et glaucome*). Associé au THC, il renforce les effets analgésiques de ce dernier (Russo, 2008).

4. Le système endocannabinoïde

La Figure 10 illustre les principales composantes du système eCB : les récepteurs cannabinoïdes de type 1 (CB1R) et de type 2 (CB2R), les ligands endogènes de ces récepteurs qu'on appelle les eCBs (principalement l'anandamide (AEA) et le 2-arachidonylglycérol (2-AG)) et les enzymes responsables de la synthèse (notamment la *N*-acyl phosphatidyléthanolamine phospholipase D (NAPE-PLD) et la diacylglycérol lipase (DAGL)) et de la dégradation (particulièrement la *fatty acid amide hydrolase* (FAAH) et la monoacylglycérol lipase (MAGL)) des eCBs (Hoover et coll., 2008). Tandis que la FAAH

convertit l'AEA en éthanolamine ($EtNH_2$) et en acide arachidonique (AA), la MAGL convertit le 2-AG en glycérol et en AA.

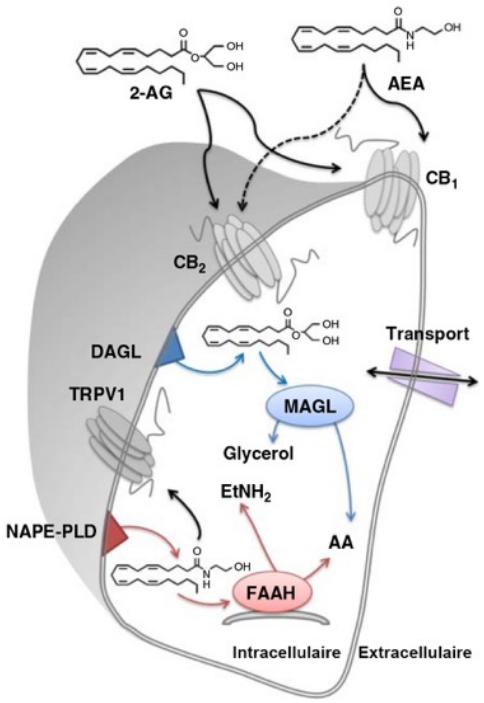

Figure 10. Schéma illustrant les composantes principales du système eCB.
Modifiée de *Cannabinoids*, Di Marzo, 2014.

4.1 Les eCBs

Les eCBs sont des dérivés d'acides gras polyinsaturés à longue chaine (amides, esters et éthers), en particulier l'acide arachidonique, retrouvés dans le système nerveux central et périphérique (De Petrocellis et coll., 2004; Bari et coll., 2006). Les eCBs les plus étudiés sont l'AEA et le 2-AG. Comme le THC se lie aux mêmes CB1R et CB2R que les eCBs, ces derniers reproduisent tous les effets centraux et périphériques du cannabis (Mechoulam et coll., 2002; Howlett et coll., 2004).

4.2 Les récepteurs cannabinoïdes

Les récepteurs cannabinoïdes sont des récepteurs à 7 passages transmembranaires et couplés aux protéines G. CB1R et CB2R sont couplés le plus souvent aux protéines G_i/G_o et inhibent ainsi l'adénylate cyclase. Ces récepteurs régulent les canaux ioniques de type

calciques et potassiques (Piomelli, 2003; Figure 11). En 1990, CB1R est identifié et cloné (Matsuda et coll., 1990). En 1993, le CB2R est découvert (Munro et coll., 1993) et, deux ans plus tard, cloné (Facci et coll., 1995). Récemment, plusieurs études démontrent qu'il existerait possiblement d'autres récepteurs aux cannabinoïdes, comme le *G protein-coupled receptor 55* (GPR55), le récepteur ionotropique *transient receptor potential vanilloide 1* (TRPV1) et les récepteurs nucléaires *peroxisome proliferator-activated receptor* (PPAR) (voir chapitre 3 de *Cannabinoids*, Di Marzo, 2014). La Figure 11 montre les voies de signalisations principales pour CB1R, CB2R, GPR55, TRPV1 et PPAR.

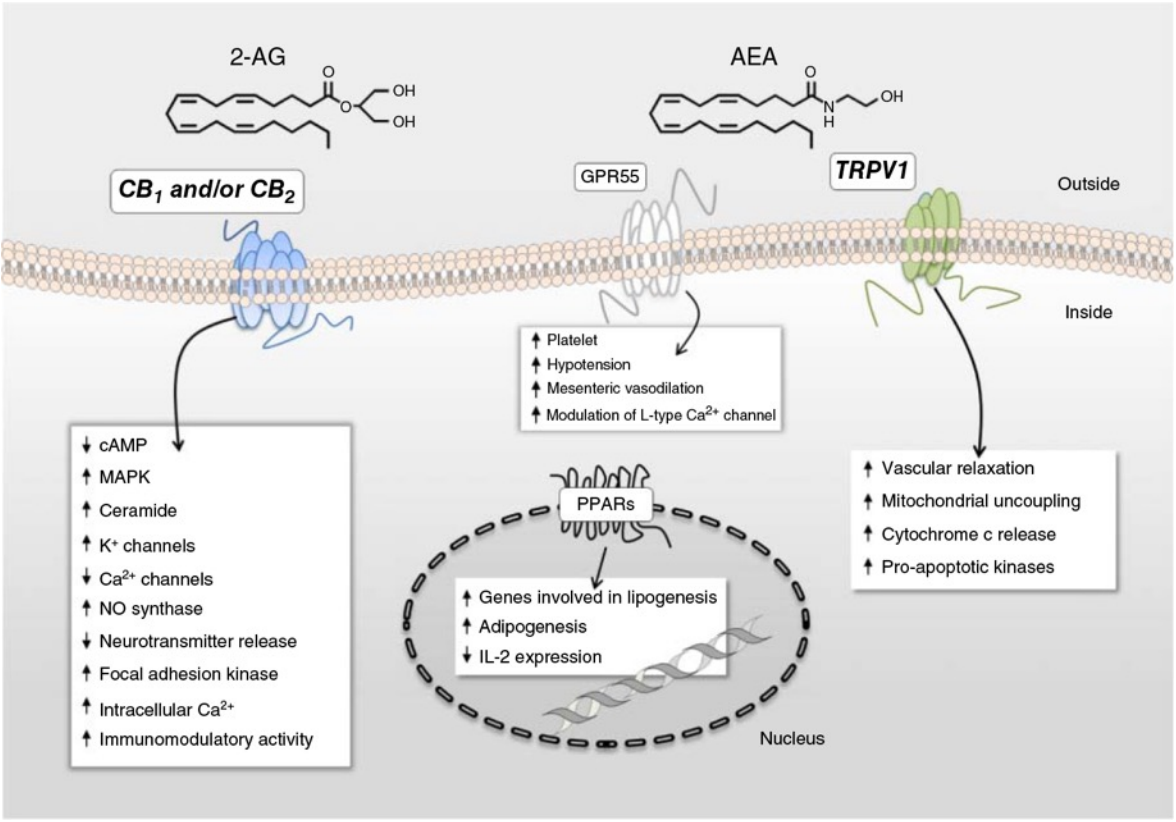

Figure 11. Cibles cellulaires et voies de signalisation de l'AEA et du 2-AG.
Modifiée de *Cannabinoids*, Di Marzo, 2014

4.3 Fonction synaptique

La synthèse des eCBs se fait sur demande suite à la dépolarisation d'une cellule ou suite à la stimulation de récepteurs postsynaptiques (Gomez-Ruiz et coll., 2007). Ils agissent ensuite comme signal rétrograde sur la membrane présynaptique où ils activent les récepteurs

cannabinoïdes. Les eCBs sont ainsi considérés comme des médiateurs lipidiques locaux (Bisogno, 2008). Dans le SNC, la localisation des éléments du système des eCBs dans les synapses glutamatergiques et GABAergiques suggèrent un rôle important dans la transmission synaptique. L'inhibition de l'adénylate cyclase engendre l'activation des canaux potassiques et l'inhibition des canaux calciques dans les cellules, et, conséquemment, l'effet net de l'activation du CB1R est une hyperpolarisation locale menant à la baisse de neurotransmetteurs (De Petrocellis et coll., 2001). Si les eCBs agissent de façon postsynaptique, ils vont contrecarrer les entrées activatrices des cellules postsynaptiques. Ce mécanisme a justement été proposé pour les interactions avec la transmission postsynaptique de la dopamine (Felder et coll., 1998; Rodríguez de Fonseca et coll., 1998; Giuffrida et coll., 1999). Cependant, cet effet est secondaire à l'importante action présynaptique puisque (1) la concentration de CB1R est plus élevée dans les terminaisons présynaptiques et (2) les agonistes de CB1R ont un effet inhibiteur sur la libération de plusieurs neurotransmetteurs et neuropeptides (Rodríguez de Fonseca et coll., 1997; Beinfeld et Connolly, 2001; Schlicker et Kathmann, 2001; Piomelli, 2003). L'inhibition de la libération de neurotransmetteurs au niveau du neurone présynaptique est associée à l'action inhibitrice des eCBs sur les canaux calciques principalement via CB1R (Bisogno, 2008). Toutefois, la raison pour laquelle le système endocannabinoïde agit de façon rétrograde n'est pas encore complètement élucidée.

4.4 Voies de signalisation impliquées dans la diminution de la libération de neurotransmetteurs

L'entrée massive d'ions Ca^{++} dans le neurone postsynaptique active la phospholipase D (PLD) qui agit sur la *N*-arachidonoyl phosphatidyléthanolamine (NAPE) pour produire l'anandamide (Figure 12). L'anandamide quitte le neurone postsynaptique à l'aide d'un transporteur (*anandamide membrane transporter* (AMT), en violet dans la Figure 12) et active le CB1R présynaptique. Par le biais d'une protéine $G_{i/o}$, CB1R inhibe l'adénylate cyclase (AC en blanc dans la Figure 12), ouvre les canaux potassiques présynaptiques, inhibe l'entrée d'ions Ca^{++} présynaptique et diminue la libération de neurotransmetteurs (principalement le glutamate ou le GABA). L'anandamide est finalement retourné dans le neurone postsynaptique à l'aide de l'AMT et est dégradé en acide arachidonique et éthanolamine.

L'internalisation de l'anandamide dans le neurone est rapide, dépendante de la température, indépendante de l'hydrolyse de l'anandamide et sensible à l'inhibition pharmacologique (Beltramo et coll., 1997; Piomelli et coll., 1999; Kathuria et coll., 2003; Fegley et coll., 2004).

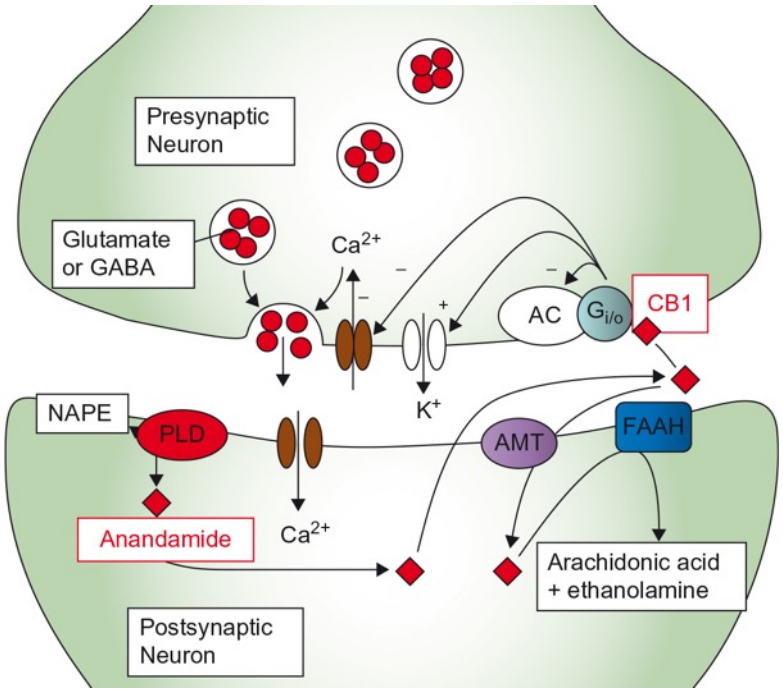

Figure 12. Cascade biochimique survenant après l'activation de CB1R par l'AEA. Modifiée de *Cannabinoids in Neurologic and Mental Disease*, Fattore, 2015.

5. Le cannabis et la vision

La consommation de cannabis affecte plusieurs fonctions biologiques comme l'appétit, la mémoire et la coordination motrice (Tsou et coll., 1998). Il n'est donc pas étonnant de retrouver les composantes du système eCB, particulièrement CB1R, dans toutes les structures cérébrales régulant ces fonctions. Les effets psychophysiques que peut procurer une consommation de cannabis sur la vision sont pourtant très peu étudiés, et ce, pour les raisons qui suivent. Tout d'abord, la dose réelle qui atteint les récepteurs cannabinoïdes dépend de sa voie d'administration (orale, inhalation, intraveineuse, etc). De plus, un groupe placebo est difficile à obtenir vu que le cannabis a un goût et une odeur bien distincte. L'intoxication peut être affectée par l'environnement et les attentes du sujet. Il y a aussi la polytoxicologie qui peut intervenir. Les gens peuvent prendre de l'alcool et d'autres drogues en plus de la

marijuana au moment de l'étude. Enfin, les effets sur l'attention compliquent l'identification des seuils de détection (voir Yazulla, 2008 pour un article de revue). Depuis longtemps, des études ont démontré qu'une prise de cannabis peut diminuer la pression intraoculaire et améliorer la vision nocturne (Adams et coll., 1978; Green, 1979). D'autres tests ont été menés sur 5 conducteurs, dont trois consommateurs occasionnels de cannabis. Sachant que l'œil joue un rôle primordial dans la conduite (par lui transitent 90% des informations nécessaires à l'anticipation des gestes du pilote), ils ont testé l'acuité visuelle, la vision des reliefs, des couleurs, des contrastes, la vision de nuit, la vision périphérique, le temps de récupération après éblouissement. Les fumeurs de cannabis font tous des erreurs dans la vision des couleurs. Le temps de récupération après éblouissement augmente en moyenne de 63% et deux sur cinq ont des difficultés à stabiliser un point fixe et à apprécier les distances (Adams et coll., 1978). Ces évidences démontrent que le cannabis peut produire des effets importants sur la vision.

6. Le système endocannabinoïde et les tissus oculaires

Il est bien connu que la consommation de marijuana induit une vasodilatation des vaisseaux de la sclérotique (les « yeux rouges ») et une réduction de la pression oculaire (Adams et coll., 1978). Initialement, on croyait que la marijuana produisait ces effets en agissant de façon non spécifique sur les membranes des cellules nerveuses (Mechoulam et coll., 2014). Nous savons maintenant hors de tout doute que les cannabinoïdes se lient aux récepteurs cannabinoïdes qui sont présents dans plusieurs types cellulaires de l'œil (voir Yazulla, 2008; Bouchard et coll., 2015; Schwitzer et coll., 2015 pour des articles de revue). Plusieurs études de physiologie et biochimie ont démontré la présence du système eCB dans diverses régions des tissus oculaires. L'ARNm du CB1R est retrouvé dans le corps ciliaire et le trabéculum, un tissu de fibres collagènes situé dans l'angle iridocornéen, de plusieurs espèces, dont le bovin et l'humain (Porcella et coll., 1998; Stamer et coll., 2001; Lograno et Romano, 2004; Chen et coll., 2005). La protéine CB1R est aussi détectée dans l'épithélium ciliaire et conjonctival (Stamer et coll., 2001; Straiker et coll., 1999b). L'épithélium cornéen du bovin exprime l'ARNm du CB1R, MAGL, ABHD6, ABHD12 et NAPE-PLD (Murataeva et coll., 2015). L'AEA, le 2-AG et le PEA sont présents dans plusieurs tissues oculaires

humain, excepté le cristallin (Chen et coll., 2005; Matias et coll., 2006). La présence de plusieurs composantes du système eCB dans les tissus oculaires, incluant la rétine, est rapportée dans le Tableau 1 suivant (Cairns et coll., 2015).

Table 1: Presence and localization of endocannabinoids in the mammalian eye.

	Retina	Iris	TM	SC	CB	Choroid	Species	References
AEA	+	+	+		+	+	Cow, human, pig, rat	Matsuda et al. [7]; Bisogno et al. [9]; Stamer et al. [15]; Chen et al. [17], but see Straiker et al. [10]
2-AG	+	+			+	+	Cow, human, rat	Bisogno et al. [9]; Straiker et al. [10]; Chen et al. [17]
PEA	+	+			+	+	Cow, human, rat	Bisogno et al. [9]; Straiker et al. [10]; Chen et al. [17]

+, Endocannabinoid is present in tissue; TM, trabecular meshwork; SC, Schlemm's canal; CB, ciliary body.

Table 2: Presence and localization of endocannabinoid synthesizing and degrading enzymes in the mammalian eye.

	Retina	Iris	TM	SC	CB	Choroid	Species	References
DGLα/β	+[a]						Mouse, rat	Hu et al. [24]; Zabouri et al. [26]
NAPE-PLD	+						Mouse, rat	Zabouri et al. [26]; Cécyre et al. [33]
FAAH	+		+				Cow, monkey, mouse, rat	[b]Bisogno et al. [9]; Yazulla [3]; Yazulla et al. [12]; Njie et al. [22]; Hu et al. [24]; Bouskila et al. [27]
MGL	+		+				Mouse, rat	Njie et al. [21]; Yazulla [3]; Hu et al. [24]
ABHD6	+						Rat	Hu et al. [24]

+, Protein expression (immunohistochemistry, Western blotting); TM, trabecular meshwork; SC, Schlemm's canal; CB, ciliary body. [a]DGLβ was associated only with blood vessels in the retina [24]. [b]Pharmacological evidence only.

Table 3: Presence and localization of classical and non-classical cannabinoid-binding receptors in the mammalian eye.

	Retina	Iris	TM	SC	CB	Choroid	Species	References
CB1	+, ‡	+, ‡	+, ‡	+	+, ‡	‡	Guinea pig, human, mouse, monkey, pig, rat	Porcella et al. [8, 14]; Straiker et al. [10, 11]; Yazulla et al. [12]; Stamer et al. [15]
CB2	+, ‡		+				Monkey, pig, rat	Lu et al. [13]; Zhong et al. [18]; [a]He et al. [19]; Lopez et al. [25]; Cécyre et al. [33], but see Porcella et al. [8], and Bouskila et al. [30]
GPR18	+, ‡	+	+		+	+	Mouse, rat	Caldwell et al. [32]; MacIntyre et al. [34]
GPR55	+[b]		+				Monkey, pig	Kumar et al. [28]; Bouskila et al. [31]
TRPV1	+, ‡						Cat, monkey, rat	Yazulla and Studholme [16]; Nucci et al. [20]; Sappington et al. [23]
PPARα	‡						Cow, pig	Kumar et al. [28]; [c]Romano and Lograno [29]

+, Protein expression (immunohistochemistry, Western blotting); ‡, mRNA expression (RT-PCR). TM, Trabecular meshwork; SC, Schlemm's canal; CB, ciliary body. [a]Pharmacological evidence only. [b]Staining exclusive to rods. [c]Pharmacological data from ophthalmic artery only.

Tableau 1. Présence et localisation des composantes du système eCB dans les tissus oculaires, incluant la rétine, de plusieurs espèces.

Tirée de Cairns et coll., 2015

6.1 Cannabinoïdes, pression intraoculaire et glaucome

La découverte que l'inhalation de marijuana peut diminuer la pression intraoculaire (PIO) remonte en début des années 1970 (Hepler et Frank, 1971). Dès lors, plusieurs

molécules agissant sur le système eCB ont été synthétisées dans le but de traiter les pathologies où la PIO est élevée (Green, 1979; Jarvinen et coll., 2002; Nucci et coll., 2008; Pinar-Sueiro et coll., 2011), un important facteur de risque du glaucome hypertensif (Heijl et coll., 2002). Le glaucome, 2^{e} cause de cécité au niveau mondial, cause une atteinte progressive du nerf optique, caractérisé par la perte des cellules ganglionnaires de la rétine (King et coll., 2013). Pourtant, le mécanisme précis menant à la perte des cellules ganglionnaires dans le glaucome demeure obscur et la normalisation de la PIO reste l'approche thérapeutique actuelle (Zhang et coll., 2012; Tamm et coll., 2013; Schmidl et coll., 2015). L'utilisation de molécules cannabinoïdes dans le traitement de l'hypertension oculaire en clinique est très limitée, probablement due à leur efficacité très variable, et ce, pour plusieurs raisons : la réduction de la PIO est de courte durée seulement, il peut survenir une désensibilisation des récepteurs et plusieurs effets indésirables comportementaux peuvent se manifester (Pinar-Sueiro et coll., 2011).

7. Expression et localisation de CB1R dans la rétine

Il est maintenant bien établi qu'il existe un système eCB rétinien qui est responsable, du moins en partie, des effets visuels après consommation de cannabis. En effet, la photosensibilité, le contraste et l'acuité visuelle sont affectés après l'ingestion de THC et prennent place au niveau rétinien. Dès la fin des années 1990, CB1R a été exhaustivement étudié au niveau de la rétine de plusieurs espèces en usant des techniques telles que l'hybridation *in situ*, la réaction en chaine par polymérase (PCR), l'immunobuvardage ou l'immunohistochimie. Utilisant l'hybridation *in situ*, CB1R a d'abord été localisé dans la couche des cellules ganglionnaires (GCL) et la couche nucléaire interne (INL), de la rétine du rat (Buckley et coll., 1998). Par la suite, l'expression de CB1R, en usant de l'immunohistochimie, a été détectée dans la rétine de l'humain, du singe, de la souris, du rat, du poussin, de la salamandre et du poisson rouge; toutes ces espèces possédant une expression de CB1R similaire dans la couche plexiforme externe (OPL), la couche plexiforme interne (IPL) et la GCL. (Straiker et coll., 1999a; Straiker et coll., 1999b). Plusieurs études subséquentes se sont concentrées sur la distribution cellulaire de la protéine CB1R en ayant recours au double marquage immunohistochimique (un anticorps dirigé contre CB1R et un

autre dirigé contre un marqueur cellulaire spécifique de la rétine). Au niveau des photorécepteurs, CB1R est exprimé dans les segments internes (Straiker et coll., 1999a; Zabouri et coll., 2011a) de plusieurs espèces et externes chez l'homme (Straiker et coll., 1999b). Une très forte expression est retrouvée dans les pédicules des cônes (Straiker et coll., 1999a; Yazulla et coll., 1999; Yazulla et coll., 2000; Zabouri et coll., 2011a). Au niveau des cellules horizontales, l'expression se situe dans leurs corps cellulaires et non dans leurs dendrites (Straiker et coll., 1999a; Zabouri et coll., 2011a; Yazulla et coll., 1999). Cette expression est moins forte comparée à l'expression des cellules de la voie verticale glutamatergique. Au niveau des cellules bipolaires, l'expression est localisée préférentiellement dans les dendrites, les corps cellulaires et les axones des cellules bipolaires liées aux bâtonnets que dans les cellules bipolaires liées aux cônes (Straiker et coll., 1999a; Yazulla et coll., 1999). Au niveau des cellules amacrines, plusieurs études ont identifié une expression notamment au niveau des celles utilisant le GABA (Straiker et coll., 1999a; Yazulla et coll., 1999; Warrier et Wilson, 2007; Zabouri et coll., 2011a). Dans la couche plexiforme interne, une expression diffuse de CB1R a été notée (Straiker et coll., 1999a; Straiker et coll., 1999b). L'expression est retrouvée au niveau des synapses des cellules bipolaires liées aux bâtonnets (Yazulla et coll., 1999). Il y a une expression plus forte dans les synapses ON que OFF des cellules bipolaires liées aux cônes (Yazulla et coll., 2000). Au niveau des cellules ganglionnaires, l'expression de CB1R est retrouvée dans leurs corps cellulaires ainsi que dans leurs fibres (Straiker et coll., 1999a; Straiker et coll., 1999b; Lalonde et coll., 2006; Zabouri et coll., 2011a). Quant aux cellules de Müller, l'expression de CB1R n'a pas été détectée dans la rétine de plusieurs espèces (Straiker et coll., 1999a; Zabouri et coll., 2011a), sauf dans la rétine du poisson rouge (Yazulla et coll., 2000).

7.1 Fonction de CB1R dans la rétine

L'activation de CB1R au niveau des photorécepteurs, des cellules bipolaires, des cellules horizontales, des cellules amacrines et des cellules ganglionnaires mène à une inhibition de la libération de neurotransmetteurs. Les agonistes de CB1R diminue la relâche de [^{3}H]-noradrénaline et de [^{3}H]-dopamine chez le cochon d'Inde (Schlicker et coll., 1996) via une protéine $G_{i/o}$ (Weber et Shlicker, 2001; Savinainen et Laitinen, 2004). De façon générale, comme l'expression de CB1R est abondante dans la voie verticale, comprenant les

photorécepteurs, les cellules bipolaires et les cellules ganglionnaires, ce récepteur joue un rôle majeur dans la relâche de glutamate (Yazulla, 2008). Le rôle de CB1R dans la rétine a été étudié chez la souris, en comparant les ondes électrorétinographiques de souris CB1R KO et leur souche sauvage (Cécyre et coll., 2013). Les résultats de cette dernière étude démontrent que les valeurs d'amplitudes et de latences sont normales et même comparables à celles obtenues chez la souris sauvage.

8. Expression et localisation de CB2R dans la rétine

La distribution du CB2R dans la rétine a beaucoup moins été étudiée comparativement au CB1R. Ceci peut être expliqué par le fait qu'il n'existe que très peu d'anticorps spécifiques au CB2R (Cécyre et coll., 2014b) et qu'initialement, on pensait que CB2R était exclusivement présent dans les cellules immunitaires. Au début, on présumait que CB2R n'était pas présent dans la rétine adulte (Porcella et coll., 1998; Buckley et coll., 1998). Par contre, pas très longtemps après, l'ARNm du CB2R est retrouvé dans la rétine du rat (Lu et coll., 2000). L'ARNm CB2R a aussi été détecté dans la rétine du poisson rouge (Cottone et coll., 2013). La localisation de la protéine CB2R est maintenant bien déterminée dans la rétine du rat et se retrouve dans l'épithélium pigmentaire, les segments internes des photorécepteurs, et dans les cellules horizontales et amacrines (Lopez et coll., 2011). Plus précisément, CB2R est retrouvé dans les cônes et bâtonnets, dans les cellules horizontales, dans quelques cellules amacrines, cellules bipolaires et cellules ganglionnaires dans la rétine de souris (Cécyre et coll., 2013). La distribution cellulaire de la protéine CB2R a bien été déterminée en faisant appel à la méthode de double marquage immunohistochimique. Au niveau des photorécepteurs, l'expression est retrouvée dans les segments internes et externes des cônes et bâtonnets (Cécyre et coll., 2013). Pourtant, CB2R n'est pas présent dans les pédicules des cônes (Cécyre et coll., 2013). Au niveau des cellules horizontales, l'expression est dans la membrane du soma et au niveau des dendrites (Lopez et coll., 2011; Cécyre et coll., 2013). Au niveau des cellules bipolaires, l'expression est concentrée dans la membrane du soma et au niveau des axones des cellules bipolaires liées aux bâtonnets (Cécyre et coll., 2013). L'expression est aussi retrouvée dans la membrane du soma des cellules bipolaires liées aux cônes (Cécyre et coll., 2013). Dans les cellules amacrines, l'expression est retrouvée seulement dans quelques types spécifiques de

cellules amacrines (Lopez et coll., 2011; Cécyre et coll., 2013). Au niveau des cellules ganglionnaires, l'expression est retrouvée dans leurs somas (Lopez et coll., 2011; Cécyre et coll., 2013). Pour ce qui est des cellules de Müller, aucune expression n'a été retrouvée dans leurs membranes, leurs somas, et leurs fibres internes et externes, s'étendant de la membrane limitante interne et externe (Cécyre et coll., 2013). L'expression de CB2R dans la rétine des primates n'est pas connue.

8.1 Fonction de CB2R dans la rétine

Une seule étude s'est concentrée sur le rôle de CB2R dans la rétine de souris en utilisant l'ERG. Cécyre et coll. (2013) ont démontré que la fonction rétinienne de la souris CB2R KO est changée. En condition scotopique, l'amplitude de l'onde a est augmentée et en condition photopique, le temps d'adaptation à la lumière est changé (Cécyre et coll., 2013). Ce résultat suggère que CB2R semble être impliqué dans les mécanismes rétiniens sous-tendant les processus d'adaptation à la lumière chez la souris.

9. Expression et localisation de GPR55 dans la rétine

Le récepteur GPR55 a été suggéré comme un 3^{e} récepteur cannabinoïde étant donné qu'il peut se lier à l'anandamide et au THC (Ryberg et coll., 2007). Vu que rares sont les anticorps spécifiques dirigés contre GPR55, peu d'études ont démontré son expression au niveau de la rétine. L'ARNm et la protéine GPR55 ont été détectés dans les rétines de hamster et de la souris, utilisant respectivement l'hybridation *in situ* et l'immunohistochimie (Cherif et coll., 2015). L'expression protéique de GPR55 dans la rétine des primates n'est pas connue.

9.1 Fonction de GPR55 dans la rétine

Il n'existe aucune étude à ce jour concernant le rôle de GPR55 dans la rétine adulte. Comparant la souris GPR55 KO et sa souche sauvage correspondante, Cherif et coll. (2015) ont démontré que GPR55 est important pour le développement normal de la rétine. Les axones de cellules ganglionnaires en développement doivent atteindre leurs cibles dans le thalamus visuel. Ce développement se fait grâce aux molécules de guidage qui permettent aux cônes de croissance de naviguer dans leur environnement. Cette étude a démontré que GPR55 est

exprimé dans la voie rétino-thalamo-corticale au cours du développement. De plus, ils ont démontré que GPR55 peut réguler la morphologie du cône de croissance et la croissance axonale. D'une part, l'ajout de LPI ou O1602 (des agonistes de GPR55) dans des explants de rétine en culture a induit une chimioattraction du cône de croissance et une augmentation du nombre de filopodes. D'autre part, le cannabidiol (un antagoniste de GPR55) a induit une chimiorépulsion du cône de croissance et diminué la longueur et le nombre des projections des explants rétiniens.

10. Expression et localisation des enzymes de synthèse et de dégradation dans la rétine

Les premières études voulant caractériser l'expression des enzymes responsables du contrôle des niveaux d'eCBs, se sont d'abord concentrées sur les enzymes de dégradations, probablement dues à l'absence dans le marché d'anticorps spécifiques. L'enzyme responsable de la dégradation de l'AEA, la FAAH, est présente dans la rétine de souris (Hu et coll., 2010), de rats (Yazulla et coll., 1999; Zabouri et coll., 2011b), et du singe (Straiker et coll., 1999). L'expression de cette enzyme a été la première à être bien caractérisée. La FAAH se retrouve donc dans les cellules horizontales, les cellules amacrines dopaminergiques, les dendrites des cellules amacrines cholinestérase-positives et dans les cellules ganglionnaires de la rétine du rat (Yazulla et coll., 1999). Une étude subséquente plus poussée a démontré que l'expression de FAAH se trouve dans les cônes, les cellules bipolaires liées aux bâtonnets, et dans une portion de cellules ganglionnaires dans la rétine du rat (Zabouri et coll., 2011b). Dans la rétine de souris, cette enzyme est exprimée dans les segments internes des photorécepteurs, dans l'ONL, la GCL, dans une sous-population de cellules amacrines et cellules bipolaires liées aux cônes, et enfin dans les terminaisons synaptiques des bâtonnets (Hu et coll., 2010). L'enzyme de dégradation MAGL est exprimée dans la rétine des souris et rats. Cette dernière est détectée dans l'OPL, l'IPL et la GCL (Hu et coll., 2010). Dans l'IPL, MAGL est présente sous la forme de 2 lignes : une au centre de l'IPL et l'autre dans la partie distale de l'IPL (proche de l'INL). Dans l'OPL, MAGL est retrouvé dans les sphérules de bâtonnets et dans les pédicules de cônes. En fait, MAGL est exprimée dans les cellules amacrines et de Müller, ainsi que les cellules bipolaires liées aux cônes de type 2 (Cécyre et coll., 2014a). Ce n'est que récemment

que la localisation de l'enzyme responsable de la synthèse du 2-AG a été décrite. La DAGLα (diacylglycérol lipase alpha) se retrouve dans les 2 couches synaptiques de la rétine de souris, dans l'OPL et l'INL (Hu et coll., 2010). En fait, DAGLα est présente dans les terminaisons synaptiques des cellules bipolaires OFF liées aux cônes, ainsi que dans les dendrites de certaines cellules bipolaires. Dans la rétine de rats, cette enzyme est localisée dans les cônes et bâtonnets, les prolongements des cellules horizontales, quelques cellules bipolaires liées aux cônes, cellules amacrines et cellules ganglionnaires (Cécyre et coll., 2014a). La DAGLβ est exclusivement retrouvée dans les vaisseaux de la choroïde (Hu et coll., 2010). En outre, l'enzyme de synthèse NAPE-PLD, responsable de la production de AEA et de OEA entre autres, est présente dans la rétine de rat (Zabouri et coll., 2011a).

11. Le système eCB dans le thalamus visuel

Vu que CB1R est un récepteur ubiquitaire et fortement exprimé à travers le SNC, il n'est pas étonnant de retrouver le système eCB dans le cerveau visuel. CB1R est retrouvé dans le corps genouillé latéral de la même espèce, avec une expression abondante dans les couches magnocellulaires (Javadi et coll., 2015). L'enzyme de dégradation de l'anandamide, le FAAH suit le même patron d'expression tandis que l'enzyme de synthèse NAPE-PLD est exprimée de façon homogène à travers les couches magnocellulaires et parvocellulaires du CGLd (Javadi et coll., 2015). Les couches koniocellulaires, quant à elles, expriment peu CB1R, FAAH et NAPE-PLD (Javadi et coll., 2015).

À ce jour, peu d'études se sont concentrées sur le rôle du système eCB dans le traitement de l'information visuelle au-delà de la rétine. Au niveau du dLGN du rat, l'activation de CB1R modifie la réponse visuelle (Dasilva et coll., 2012; Dasilva et coll., 2014). Dans ces études, utilisant des enregistrements unitaires extracellulaires, les auteurs ont noté que 28% des cellules du dLGN augmentent leur réponse suite de la stimulation visuelle lorsque des agonistes (AEA, 2-AG ou O2545, un cannabinoïde synthétique soluble dans l'eau) sont injectés. Les 72% restants montrent une diminution de la réponse visuelle lorsque ces même agonistes ont été injectés. De plus, tous ces effets sont bloqués lorsque l'AM251, un antagoniste de CB1R est injecté préalablement aux agonistes. Ces deux études suggèrent que

CB1R au niveau du thalamus module l'information visuelle envoyée à V1. Aucune étude n'a établit le rôle précis de CB2R ou de GPR55 dans le thalamus visuel du primate.

12. Le système eCB dans le cortex visuel

CB1R est retrouvé dans les différentes couches de l'aire visuelle primaire (V1) du singe vervet (données non publiées). Une étude portant sur l'expression de CB1R dans le cortex du singe macaque a noté que ce récepteur est présent au niveau de V1, avec une forte densité dans les couches V-VI, mais avec une absence de signal dans la couche IV (Eggan et Lewis, 2007). Chez la souris, CB1R se trouve abondamment dans les couches II/III et VI du cortex strié et dans les terminaisons nerveuses inhibitrices (colocalisation de VGAT et CB1R) (Yoneda et coll., 2013). Le système eCB semble également être d'une importance capitale durant le développement de V1 vu que la protéine CB1R est augmentée tout au long de son développement, avec un patron d'expression spécifique à P20 (20^{e} jour postnatal) jusqu'à l'âge adulte (Yoneda et coll., 2013). Dans les couches II et III de V1, les eCBs jouent un rôle important dans la maturation des cellules GABAergiques. En effet, la maturation de ces cellules GABAergiques lors du développement de l'œil est affectée chez des souris élevées dans le noir. Ce même effet est aussi retrouvé lorsque des agonistes de CB1R sont appliqués directement dans V1 (Jiang et coll., 2010a; Jiang et coll., 2010b). Ces mêmes études ont aussi noté que les synapses GABAergiques des couches II, III et V de V1 ne viennent pas à maturation normale chez la souris CB1R KO. Ces résultats suggèrent qu'une vision normale est nécessaire pour stimuler le système eCB et mener à une transmission GABAergique normale dans les cellules du cortex visuel de la souris (Sun et coll., 2015). Une autre étude a montré que le blocage pharmacologique des récepteurs cannabinoïdes perturbe le développement des colonnes de dominance oculaires dans les couches II et III, et pas IV des souriceaux (Liu et coll., 2008). En outre, les agonistes des récepteurs cannabinoïdes augmentent l'amplitude et la fréquence des courants inhibiteurs postsynaptiques dans V1 de la souris (Garkun et coll., 2014). Chez le singe macaque, l'ajout d'agonistes de récepteurs cannabinoïdes modifie le traitement du signal visuel, en affectant les temps de réponse des neurones de V1 et V2 (Ohiorhenuan et coll., 2014). Récemment, il a été démontré que chez les souris CB1R KO, l'organisation fonctionnelle du cortex visuel primaire et la sélectivité des

neurones sont modifiées (Abbas Farishta et coll., 2015). Plusieurs études sont toutefois nécessaires pour évaluer l'impact de CB2R dans V1. Comme CB2R est présent au niveau de la rétine, il est fort probable que CB2R ait aussi un rôle important au niveau de V1.

13. Choix du modèle animal : le singe vervet de St Kitts

Malgré le progrès des techniques non invasives pour étudier le cerveau humain *in vivo*, les études animales sont toujours nécessaires pour étudier le système nerveux. Même si la plupart des réactions biochimiques et physiologiques des neurones représentent des fonctions communes et fondamentales des systèmes nerveux, il existe des disparités notables qui se traduisent par des capacités sensorielles, motrices et cognitives différentes (Buckner et Krienen, 2013) et le système visuel est justement un bon exemple. Le système visuel humain est sophistiqué et unique aux primates, incluant les singes. La haute acuité visuelle, la vision des couleurs, le détail tridimensionnel, ainsi que reconnaitre, différencier et se souvenir de certains objets dans des situations complexes sont des fonctions communes aux primates.

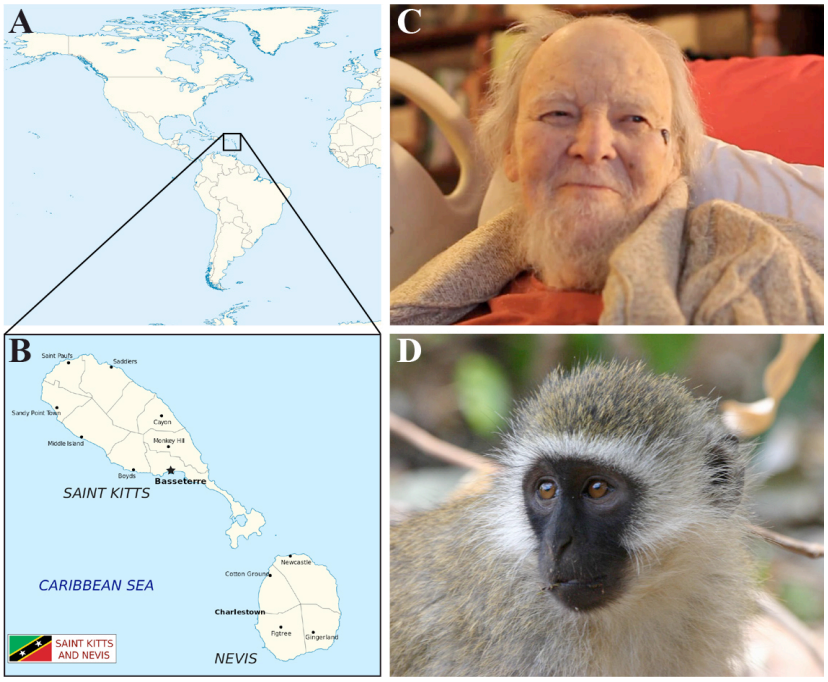

Figure 13. Le laboratoire situé sur l'ile de St Kitts abrite les singes vervets.
La BSF (*Behavioural Science Foundation*) située dans les Caraïbes (**A**-**B**) a été fondé par le Dr Frank Ervin décédé le 24 avril 2015 (**C**). Le singe vervet (**D**) est le primate non humain le plus utilisé en recherche après le macaque.

Le singe vervet est devenu un modèle animal important pour la recherche en neurosciences de la vision (Figure 13). Le génome de cette espèce est 90% similaire à celui de l'homme, ce qui fait un excellent modèle pour l'étude des pathologies humaines comportementales ou physiologiques (Palmour et coll., 1997; Jasinska et coll., 2007). Depuis plusieurs années, le vervet est utilisé pour l'étude du système visuel, ce qui a mené à une description anatomique exhaustive de ces structures visuelles, particulièrement la rétine (Herbin et coll., 1997), et à la publication d'atlas d'anatomie du cerveau (Mikula et coll., 2007; Mikula et coll., 2008; Woods et coll., 2011). La taille du cerveau par rapport à leur poids corporel d'environ 3,5 kg chez l'adulte rend très avantageuse l'étude électrophysiologique des déficiences visuelles émergeant de la rétine ou du nerf optique. L'organisation de la rétine chez cette espèce est similaire aux singes de l'Ancien Monde, notamment le macaque. La rétine contient plusieurs couches et différentes cellules : des photorécepteurs, cellules bipolaires, cellules ganglionnaires, cellules horizontales et amacrines. La densité de cônes décroit de la *fovéa centralis* jusqu'à la périphérie rétinienne contenant une forte densité de bâtonnets (Osterberg, 1935; Herbin et coll., 1997). La présence d'une fovéa lui procure une excellente acuité visuelle, une vision des couleurs et une sensibilité à la lumière, tandis la périphérie rétinienne est responsable de la vision scotopique (vision de nuit) (Jacobs, 2008). Le nombre de cellules ganglionnaires est aussi comparable à ceux rapportés pour le macaque (Herbin et coll., 1997; Finlay et coll., 2008). La Figure 14 qui suit rapporte le comptage des cellules ganglionnaires dans la rétine du singe vervet normal.

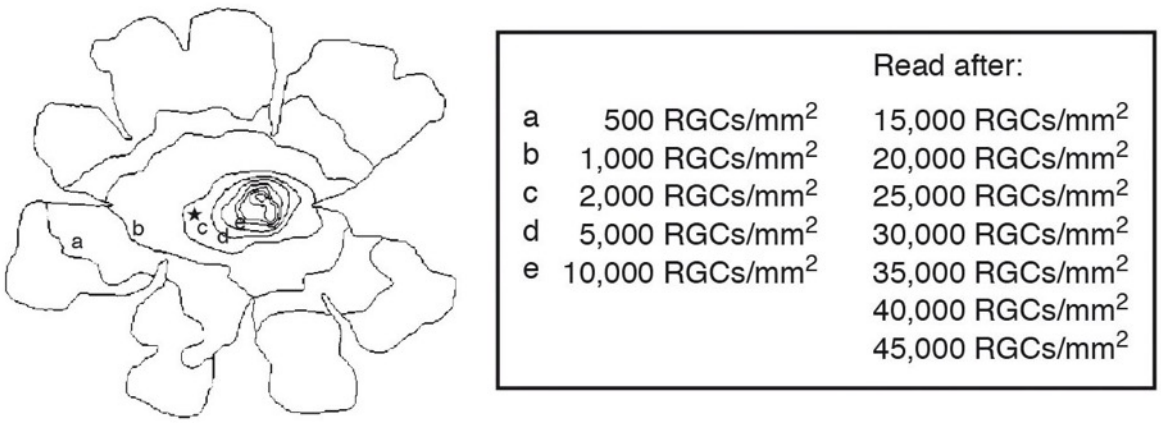

Figure 14. Comptage des cellules ganglionnaires dans la rétine du singe vervet normal. Tirée de Herbin et coll., 1997.

De plus, les réponses ERG obtenues chez le singe macaque, une espèce similaire au singe vervet, correspondent aussi très bien à celles obtenues chez l'homme (Bee, 2001). Toutes ces évidences valident le singe vervet comme un excellent modèle animal pour l'étude de la fonction rétinienne.

II. OBJECTIFS ET HYPOTHÈSES

Le but principal de cette thèse est de caractériser l'expression et le rôle du système endocannabinoïde dans la rétine du singe. Quelques études des années 1970 ont noté des effets visuels après consommation de marijuana, notamment la photosensibilité, la vision des couleurs et le recouvrement après éblouissement. Toutes ces dernières fonctions prennent place au niveau de la rétine. Même à ce jour, il n'existe que très peu d'études sur les fonctions perceptives du système eCB. Comme l'organisation anatomique de la rétine du singe vervet est similaire à celle de l'homme (présence d'une fovéa), il devient plus aisé d'extrapoler nos résultats à la fonction rétinienne humaine. Les sept chapitres du corps de cet ouvrage démontrent comment les différents récepteurs eCBs sont non seulement exprimés et localisés dans des endroits bien spécifiques de la mosaïque rétinienne, mais encore ont des fonctions visuelles spécifiques. Nous avons proposé les hypothèses suivantes :

1. CB1R devrait être abondamment exprimé dans la rétine centrale (cônes).
2. CB2R devrait être exprimé exclusivement dans la glie rétinienne (cellules de Müller).
3. GPR55 devrait surtout se retrouver dans les bâtonnets de la rétine périphérique.
4. L'expression du système eCB devrait être différente d'une espèce animale à l'autre (souris, toupayes et singes).
5. Le singe vervet devrait possèder un patron électrorétinographique semblable à celui de l'homme.
6. Le blocage par des antagonistes spécifiques de CB1R (principalement dans les cônes) ou CB2R (exclusivement dans les cellules de Müller) devrait modifier les ondes électrorétinographiques en condition photopique seulement.

7. GPR55 devrait être un modulateur de la fonction rétinienne scotopique vu sa localisation exclusive sur les bâtonnets.

III. CORPS DE L'OUVRAGE

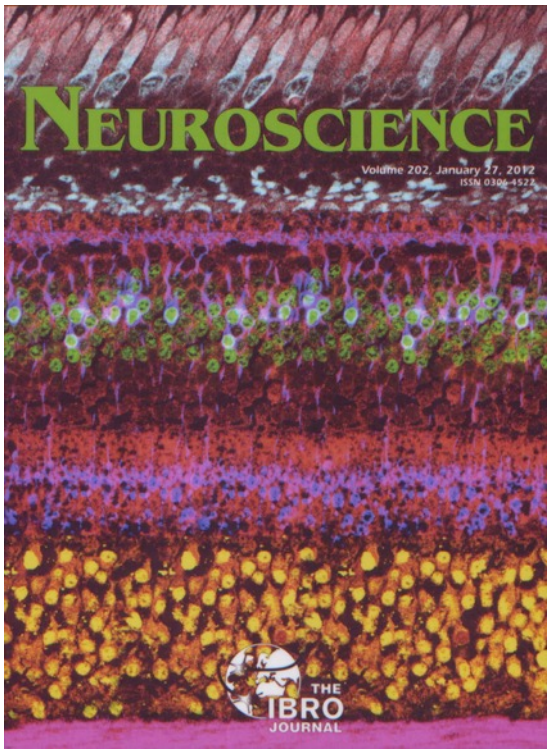

ARTICLE 1: EXPRESSION AND LOCALIZATION OF THE CANNABINOID RECEPTOR TYPE 1 AND THE ENZYME FATTY ACID AMIDE HYDROLASE IN THE RETINA OF VERVET MONKEYS

Publié dans :

Bouskila J, Burke MW, Zabouri N, Casanova C, Ptito M, Bouchard JF (2012) Expression and localization of the cannabinoid receptor type 1 and the enzyme fatty acid amide hydrolase in the retina of vervet monkeys. Neuroscience 202:117-130. (cover page)

Expression and Localization of the Cannabinoid Receptor Type 1 and the Enzyme Fatty Acid Amide Hydrolase in the Retina of Vervet Monkeys

Joseph Bouskila[1], Mark W Burke[2], Nawal Zabouri[1], Christian Casanova[1], Maurice Ptito[1] & Jean-François Bouchard[1]

[1]School of Optometry, University of Montreal, Montreal, QC, Canada

[2]Department of Physiology & Biophysics, College of Medicine, Howard University, Washington D.C.

Correspondence should be addressed to:

Jean-François Bouchard, BPharm, PhD

School of Optometry, room 260-7

3744 Jean-Brillant,

University of Montreal,

Abstract

The presence of a widespread endocannabinoid (eCB) system within the nervous system, including the retina, has been demonstrated in recent years. Expression patterns of the cannabinoid receptor type 1 (CB1R) and enzyme fatty acid amide hydrolase (FAAH) are available for rodents, but data for humans and monkeys are scarce. We therefore thoroughly examined the distribution pattern of CB1R and FAAH throughout the retina of the vervet monkey (*Chlorocebus sabeus*) using confocal microscopy. Our results demonstrate that CB1R and FAAH are expressed throughout the retina, from the foveal pit to the far periphery. CB1R and FAAH are present in the photoreceptor, outer plexiform, inner nuclear, inner plexiform, and retinal ganglion cell layers (PRL, OPL, INL, IPL and RGCL, respectively). More specifically, in PRL, CB1R and FAAH are preferentially expressed in cones of the central retina. In OPL, these two components of the eCB system are concentrated not only in the cone pedicles but also in rod spherules with, however, a less intense staining pattern. Triple-labeling immunofluorescence revealed that both cone and rod bipolar cells express CB1R and FAAH. Heavy staining is detected in RGC somas and axons. Neither CB1R nor FAAH are found in the retinal glia, the Müller cells. These data indicate that the eCB system is present throughout the primate retina and is ideally positioned to modulate central and peripheral retinal functions.

Keywords: endocannabinoids, cannabinoid receptor CB1, fatty acid amide hydrolase, monkey retina, immunohistochemistry, confocal microscopy.

Introduction

The *Cannabis sativa* plant contains a group of substances termed cannabinoids that modulate neuronal activity by activating two G protein-coupled receptors, the cannabinoid receptors CB1 (CB1R) and CB2 (CB2R) (Piomelli, 2003; Atwood and Mackie, 2010). These receptors exert their action through distinct signal transduction mechanisms and are activated physiologically by endogenous ligands called endocannabinoids (eCBs), such as anandamide (AEA) and 2-arachidonoylglycerol (2-AG) (Gómez-Ruiz et al., 2007). The activation of the CB1R inhibits the transmembrane enzyme adenylyl cyclase and modulates calcium and potassium ion channels through $G_{i/O}$ (Freund et al., 2003; Rodríguez de Fonseca, et al., 2005; Turu and Hunyady, 2010). Anatomically, CB1R is prominently present on GABAergic and glutamatergic terminals (Tsou et al, 1998; Katona et al., 1999; Monory et al., 2006) and is widely expressed in central (hippocampus, cortex, basal ganglia and cerebellum) and peripheral nervous systems (Herkenham et al., 1991a, 1991b; Egertová and Elphick, 2000). The presynaptic location of CB1R plays a key role in synaptic transmission allowing the eCB system to act as a modulatory system that regulates learning, memory, motor coordination, neuroprotection (Di Marzo et al., 1998) and visual processing (Straiker et al., 1999a; Straiker et al, 1999b).

Fatty acid amide hydrolase (FAAH), an intracellular enzyme that is attached to the membrane by the N-terminal domain, is mainly responsible for degrading AEA, one of the two chief eCBs, into arachidonic acid and ethanolamine (Deutsch and Chin, 1993; Elphick and Egertová, 2001 for review). FAAH has already been localized in selected areas of the human central nervous system but not in human visual structures (Romero et al, 2002). The CB1R ligand AEA is also considered as a candidate endogenous TRPV1 receptor ligand that co-localizes with some FAAH positive amacrine cells (Zimov and Yazulla, 2007). Other lipids that are not CB1R ligands are also broken down by FAAH, such as oleamide (Cravatt et al, 1996). The expression pattern of FAAH in the retina has been demonstrated in photoreceptors, cone bipolar cells, ganglion cells and some amacrine cells of rodents (Yazulla et al., 1999; Hu et al., 2010), but data are not available for the primate retina.

The organization of the retinal mosaic has an incidence on visual functions, the center being mainly involved in visual acuity, color coding and photopic sensitivity (cone vision), whereas the periphery is more concerned with scotopic functions (rod vision) (Jacobs, 2008; Wässle et al., 1995). If eCBs and cannabinoid receptors are mainly expressed in cones of the central retina, then visual functions associated with the foveal cones should be affected by cannabis consumption. Indeed, several case reports in the 1970's mentioned some visual effects after cannabis consumption, such as an increase in glare recovery at low contrast (Adams et al., 1978), a reduction in Vernier and Snellen acuities (Adams et al., 1975; Kiplinger et al., 1971), blurred vision (Noyes et al., 1975), change in color discrimination and increased photosensitivity (Dawson et al., 1977). There has also been evidence for central effects of cannabinoid use in vision by binocular depth inversion technique and EEG recordings of the occipital cortex (Semple et al., 2003; Skosnik et al., 2006).

The presence of CB1R in the retina of many species suggested that eCB signaling system is phylogenetically preserved and could play an important role in retinal functions (Straiker et al., 1999a). Studies have reported the presence of the eCB system in various retinal cell types (cones, bipolar, ganglion, horizontal and amacrine cells) (see Yazulla 2008 for review). The modulatory effects of cannabinoids at all stages of retinal processing have also been described (Yazulla, 2008). Moreover, critical proteins defining cannabinoid circuitry like diacylglycerol lipase α and β, monoacylglycerol lipase, α/β-hydrolase domain 6, cannabinoid receptor-interacting protein 1a, FAAH and N-acylethanolamine-hydrolizing acid amidase, have been localized in the adult mouse retina (Hu et al., 2010). CB1R and FAAH are expressed in cones, amacrine cells and ganglion cells and have been both localized in the rat retina essentially in horizontal and rod bipolar cells (Yazulla et al., 1999).

The distribution of receptors and the organization of the retina in humans and primates vary from the center to the periphery. Indeed, there is a monotonous decrease in the number of cones from the *fovea centralis* (that exclusively contains cones) to the far periphery that contains mainly rods (Osterberg, 1935). Moreover, the density of ganglion cells is much

higher in the fovea compared to the periphery (Herbin et al, 1997). Therefore, the expression of the eCB system should be different from the center of the retina to the far periphery, a difference that would also be evident in central retinal targets such as the dorsal lateral geniculate nucleus and the superior colliculus and their cortical recipient areas, the striate and extra-striate cortices.

To our knowledge, there has been only one comparative study that showed the presence of CB1R in the monkey retina (Straiker et al., 1999a). However, in that study the authors do not mention where in the retina the sample was taken and the complete specific retinal cell types expressing CB1R have not been entirely described. The present study therefore aims to extend previous data on the monkey retina by thoroughly characterizing the expression and cellular localization of CB1R and FAAH.

Experimental Procedures

Animal Preparation. One female and two male vervet monkeys (Chlorocebus sabaeus) at 42 months of age were used for this study. The animals were born and raised in enriched environments in the laboratories of the Behavioral Sciences Foundation (St-Kitts, West Indies). The animals were fed with primate chow (Harlan Teklad High Protein Monkey Diet; Harlan Teklad, Madison, WI) and fresh local fruits, with water available ad libitum. The monkey eyes were kindly provided by Professor Roberta Palmour. The monkeys were part of a developmental study approved by the McGill University Animal Care and Use Committee.

Antibody characterization. All the primary antibodies used in this work, their sources, and working dilutions, are summarized in Table 1. These antibodies were successfully used in previous studies and are well characterized by us and other authors in regards to the specific primate retinal cell type immunostaining, as described below for each antibody.

Table 1. Primary antibodies used in this study.

Antibody[1]	Immunogen	Source[2]	Working dilution
CB	Purified bovine Kidney calbindin-D28K	Sigma-Aldrich, St. Louis, MO, C9848, Mouse monoclonal, Clone CB-955	1:500
CHX10	Peptide containing the aa 44-61 of human CHX10	Santa Cruz Biotechnology, Santa Cruz, CA, sc-21690, Goat polyclonal	1:100
PKCα	Peptide mapping the aa 296-317 of human PKCα	Santa Cruz Biotechnology, Santa Cruz, CA, sc-8393, Mouse monoclonal, Clone H-7	1:500
Brn-3a	Fusion protein containing aa 186-224 of Brn3a protein	Chemicon, Temecula, CA, MAB1585, Mouse monoclonal	1:100
Syntaxin	Synaptosomal plasma fraction of rat hippocampus (Barnstable et al., 1985)	Sigma-Aldrich, St. Louis, MO, S0664, Mouse monoclonal, Clone HPC-1	1:500
GS	Full protein purified from sheep brain	Chemicon, Temecula, CA, MAB302, Mouse monoclonal, Clone GS-6	1:500
CB1R	Fusion protein containing aa 1-77 of rat CB1R	Sigma-Aldrich, St. Louis, MO, C1233, Rabbit polyclonal	1:150
FAAH	Synthetic peptide aa 561-579 of rat FAAH	Cayman Chemical, Ann Arbor, MI, 101600, Rabbit polyclonal	1:100

[1]Abbreviations: CB, Calbindin; PKCα, Protein Kinase C (α isoform); GS, Glutamine Synthetase; CB1R, Cannabinoid Receptor type 1; FAAH, Fatty Acid Amide Hydrolase; aa, amino acids.

[2]The source column indicates the commercial company, catalog reference and origin. The clone designation is given for monoclonal antibodies.

Calbindin. The mouse monoclonal (IgG1) to calbindin (CB) (Sigma, St. Louis, MO) was obtained by using as an immunogen purified bovine kidney Calbindin-D-28K. This antibody recognizes a 28kDa band on Western Blots. Immunostaining against calbindin is known to label cones outside the foveal region, cone bipolar cells and a subset of horizontal cells on human and monkey retinal sections (Chiquet et al., 2002; Fischer et al., 2001; Kolb et al., 2002; Martínez-Navarrete et al., 2007; Martínez-Navarrete et al., 2008).

CHX10. The goat polyclonal (IgG) to CHX10 from Santa Cruz Biotechnology (Santa Cruz, CA) was raised by using as an immunogen a peptide containing the amino acids 44–61 of human CHX10 (sequence PPSSHPRAALDGLAPGHL). According to the manufacturer, this antibody gives a single band of 46kDa on Western blots of mouse eye extracts. This transcription factor targets the nuclei of all bipolar cells in mammals, including monkeys (Martínez-Navarrete et al., 2008).

PKC. The mouse monoclonal (IgG2a) to protein kinase C (PKC) was developed by Santa Cruz Biotechnology by using as an immunogen purified bovine PKC, and its epitope mapped to its hinge region (amino acids 296–317). It detects the PKCα isoform, a well-known specific marker for rod bipolar retinal cells (Mills and Massey, 1999). As stated by the manufacturer, this antibody gives a single band of 80kDa on Western blots of human cell lines, and has been previously used for immunohistochemistry on rodent (Zabouri et al., 2011a) and monkey (Cuenca et al., 2005; Martínez-Navarrete et al., 2008) retinas.

Brn3a. The mouse monoclonal to Brn3a was developed by Chemicon International by using as an immunogen amino acids 186-224 of Brn3a fused to the T7 gene 10 protein. We used the POU-domain transcription factor Brn3a to label the nuclei of retinal ganglion cells. The Brn3a antibody shows no reactivity to Brn3b or Brn3c by western blot and no reactivity to Brn3a knock-out mice (manufacturer's technical information). Its specificity for monkey (Xiang et al., 1995) and rodent (Nadal-Nicolás et al., 2009) retinal ganglion cells has been documented.

Syntaxin. The mouse anti-syntaxin monoclonal clone HPC-1 was used to target retinal amacrine and horizontal cells and retinal ganglion cell axons. It was developed by Barnstable et al. (1985) and is produced by Sigma (St. Louis, MO). The syntaxin antibody recognizes syntaxin-1, a 35kDa protein, from hippocampal, retinal and cortical neurons (Inoue et al.,

1992). This antibody labels interneurons, horizontal and amacrine cells, in the developing and adult human retina (Nag and Wadhwa, 2001). We have successfully used this antibody to label monkey retinal amacrine and horizontal cells. The staining pattern obtained in the current study was similar to that found in human retina (Nag and Wadhwa, 2001).

GS. The mouse anti-glutamine synthetase (GS) monoclonal antibody was obtained from Chemicon International by using as an immunogen the GS purified from sheep brain. This antibody generates a single 45kDa protein in adult retinal tissue (Chang et al, 2007). It labels Müller cells in rat retina (Riepe and Norenburg, 1977) and across the monkey retina (Nishikawa and Tamai, 2001).

CB1R. The rabbit anti-CB1R recognizes a major band of 60kDa and less intense bands of 23, 72 and 180kDa (manufacturer's data sheet). This antibody targets the rat CB1R but specifically recognizes the CB1R (60kDa) from many species, including monkey tissue (technical sheet).

FAAH. The anti-FAAH was developed by Cayman Chemical by using a synthetic peptide corresponding to 561–579 amino acid fragment of rat fatty acid amine hydrolase conjugated to KLH as an immunogen (manufacturer's data sheet). The rabbit anti-FAAH yields a dense band at about 66kDa and a very light one below 37kDa, and its specificity for rat FAAH positive cells has been demonstrated (Suárez et al., 2008; Zabouri et al., 2011a).

Tissue preparation. The retina was dissected free from the eyecup in a PBS bath. The retina was laid flat so that the vitreous body could be removed by blotting with filter paper and gentle brushing (Burke et al., 2009). Samples of retina (4 mm2) were taken at 2, 6 and 10 mm from the center of the optic disc in the temporal, nasal, dorsal and ventral eccentricities along with the fovea. Each sample was then cryoprotected in 30% sucrose overnight and embedded in Shandon embedding media at −65°C. Retinal samples were then sectioned in a cryostat (16 μm) and mounted onto gelatinized glass microscope slides, air-dried and stored at −20°C for further processing.

Western blotting. A fresh dissected sample of retina was homogenized by hand using a sterile pestle in RIPA buffer (150 mM NaCl, 20 mM Tris, pH 8.0, 1%, NP-40 (USB Corp., Cleveland, OH), 0.1% SDS, 1 mM EDTA), supplemented with a protease inhibitor mixture

(aprotinin (1:1000), leupeptin (1:1000), pepstatin (1:1000) and phenylmethylsulfonyl fluoride (0.2 mg/ml); Roche Applied Science, Laval, QC). Samples were then centrifuged at 4°C for 10 minutes, and the supernatant was extracted and stored at -20°C until further processing. Protein content was equalized using a Thermo Scientific Pierce BCA Protein Assay Kit (Fischer Scientific, Ottawa, ON, Canada). Thirty micrograms of protein/sample of the homogenate was resolved with 10% sodium dodecyl sulfate (SDS)-polyacrylamide gel electrophoresis, transferred onto a nitrocellulose membrane filter (BioTrace NT, Life Sciences, Pall, Pensacola, FL), blocked for 1 hour in 5% skim milk (Carnation, Markham, ON) in TBST (0.15 M NaCl, 25 mM Tris-HCl, 25 mM Tris, 0.5% Tween- 20), and incubated overnight with primary antibodies, namely rabbit anti-CB1R (1:1000) and rabbit anti-FAAH (1:500), in blocking solution. The following day, the blot was exposed to a secondary antibody conjugated to horseradish peroxidase (1:5000; Jackson ImmunoResearch, West Grove, PA) in blocking solution for 2 hours. Detection was carried out by using home-made ECL Western blotting detection reagents. The membrane was then stripped, reblocked, and exposed to a second primary antibody, until all proteins of interest were tested. Densitometric analysis was performed using Scion Image software (version 4.03) (Frederick, MD).

Immunohistochemistry. Single-, double- and triple-labelings of the retina were performed according to previously published methods (Zabouri et al., 2011a). Briefly, sections were postfixed for 5 minutes in 70% ethanol, rinsed 3 x 5 minutes in Tris 0.1 M buffer, pH 7.4/Triton 0.03%, and blocked for 90 minutes in 10% normal goat serum (NDS) in Tris 0.1 M buffer/0.5% Triton. Sections were incubated overnight at room temperature with primary antibody in blocking solution. The CB1R or FAAH antibody was used conjointly with a known retinal cell type marker: calbindin, CHX10, PKCα, syntaxin, Brn-3a or glutamine synthetase (Table 1). The next day, sections were washed for 10 minutes and 2 x 5 minutes in Tris 0.1 M/Triton 0.03%, blocked in 10% NDS, Tris 0.1 M/0.5% Triton for 30 minutes and incubated with a secondary antibody for 1 hour: Alexa 488 donkey anti-mouse, Alexa 488 donkey anti-goat, Alexa 555 donkey anti-rabbit or Alexa 647 donkey anti-mouse, (1:200) all in blocking solution as described above. Sections were washed again in Tris buffer, counterstained with bisbenzimide (Hoechst 33258, Sigma Aldrich, 2.5 µg/mL), a fluorescent nuclear marker, and coverslipped with GelTol Mounting Medium (Thermo Electron

Corporation). In order to test the specificity of our antibodies directed either against CB1R or FAAH, immunolabelings were performed on mice retinal tissue, one where the cnr1 gene has been deleted (generously provided by Dr Beat Lutz) (*cnr1*-/-, Marsicano et al., 2002) and the other where the FAAH gene has been deleted (generously provided by Dr Gabriella Gobbi, McGill University) (*faah*-/-, Cravatt et al, 2001).

Sequential labeling of CB1R and FAAH. The CB1R and FAAH antibodies that we selected came from the same host, making the use of simultaneous double-labeling protocol not adequate. To circumvent this problem, we used a sequential protocol previously described by our research group (Zabouri et al., 2011a; Zabouri et al., 2011b). Briefly, the sections were labeled in a serial manner. The exposition to the first primary antibody was conducted as described above, followed by incubation of a goat anti-Fab fragment solution (Jackson ImmunoResearch Laboratories; Brandon, 1985). This allowed for the tagging of the first primary antibody as goat rather than rabbit. The sections were revealed with a secondary Alexa donkey anti-goat 488. Thereafter, they were exposed to a second primary antibody overnight and revealed the following day with an Alexa donkey anti-rabbit 647. The validity of the sequential staining was then verified for FAAH/CB1R co-labeling with the following two controls: (1) omission of the second primary antibody resulted in a strong staining with the goat secondary 488 but no staining with rabbit secondary 647; (2) omission of the first secondary and second primary antibodies revealed no signal for the goat secondary 488 and faint signal for the rabbit secondary 647.

Confocal microscopy. Fluorescence was detected with a Leica TCS SP2 confocal laser-scanning microscope (Leica Microsystems, Exton, PA), using a 40X or a 100X objective. Images were obtained sequentially from the green, red and far-red channels on optical slices of less than 0.9 μm of thickness. Throughout the results section, images taken from the green channel correspond to the retinal cell markers, and those from the red channel to the CB1R or the FAAH; for the triple labeling, the far-red channel relates to an additional cell marker.

Results

Single-label immunocytochemistry

Single-labeling immunohistochemistry was performed to test the specificity of the CB1R or FAAH antibodies in cnr1 or faah knockout mouse retinas and no staining was found (Figure 1A-1D). Immunoblot analysis of vervet monkey retinal tissue for anti-CB1R and anti-FAAH was very similar to that previously reported for rodent retinas (Yazulla et al., 1999; Zabouri et al., 2011a). For CB1R-immunoreactivty (IR) (Figure 1E), a single band was detected at 60kDa and for FAAH-IR (Figure 1F), a single band was observed at 66kDa. Even though the CB1R and FAAH antibodies were targeting rat protein sequences, they generated robust and specific staining in the vervet monkey retina. Control sections in which primary antibodies were omitted were also processed in parallel and did not show any specific immunoreactivity. CB1R and FAAH were found throughout the retinal layers (photoreceptor layer, outer plexiform layer, inner nuclear layer, inner plexiform layer and ganglion cell layer) and at all eccentricities studied from the fovea centralis to the far periphery. However, the intensity of the immunoreactivity decreases with retinal eccentricity (Figures 2 and 3).

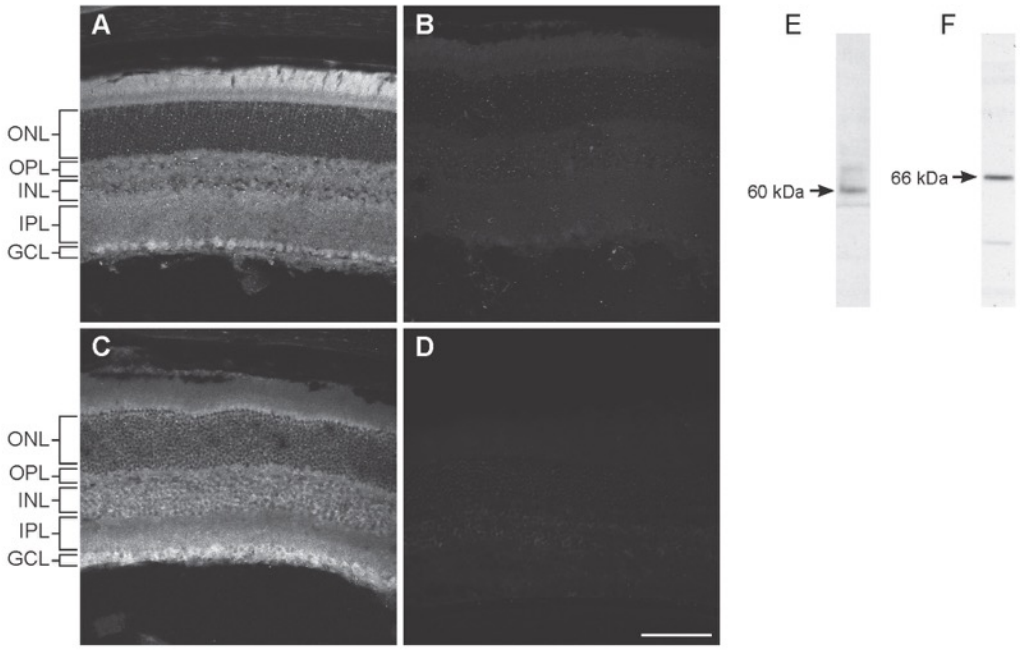

Figure 1. Single-label immunofluorescence showing the specificity of the antibodies targeting the endocannabinoid receptor CB1 (CB1R) and fatty acid amide hydrolase (FAAH). CB1R

immunoreactivity in a wild type mouse retina (A). CB1R labeling is not evident in the cnr1-/- mouse (B). FAAH enzyme immunoreactivity in a wild type mouse retina (C). Lack of FAAH immunofluorescence in the faah knockout mouse (D). ONL, outer nuclear layer; OPL, outer plexiform layer; INL, inner nuclear layer; IPL, inner plexiform layer; GCL, ganglion cell layer. Scale bar = 75 µm. Immunoblots of CB1R-IR and FAAH-IR in the monkey retina (E-F). Specific recognition of CB1R was seen at 60kDa (E) and of FAAH at 66kDa (F).

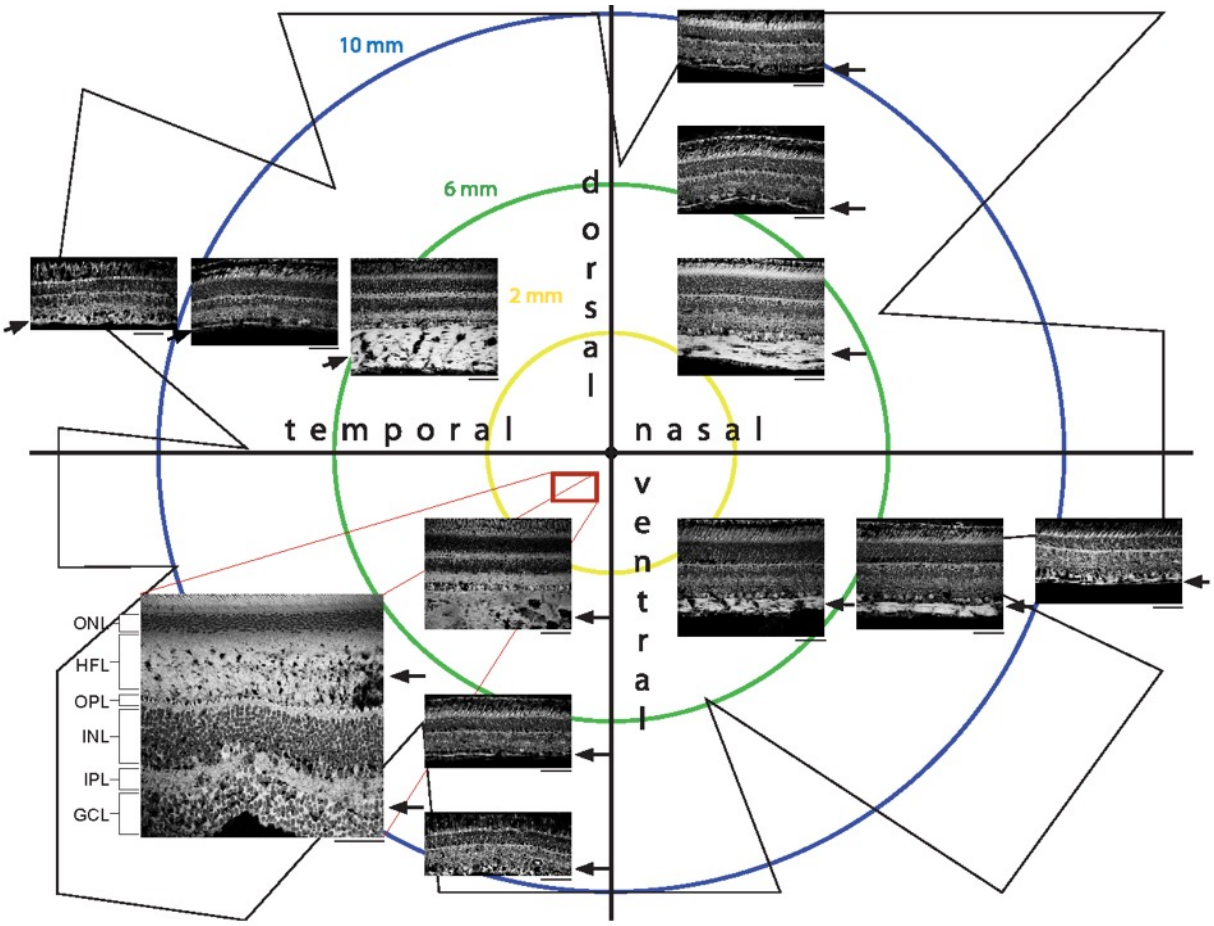

Figure 2. Schematic illustration of the labeling pattern of CB1R-IR throughout the monkey retina. Note that the most prominent staining of CB1R is located in the nerve fiber layer and central retinal ganglion cell layer (indicated by the arrows). ONL, outer nuclear layer; NFL, nerve fiber layer; OPL, outer plexiform layer; INL, inner nuclear layer; IPL, inner plexiform layer; GCL, ganglion cell layer. Scale bar = 75 µm.

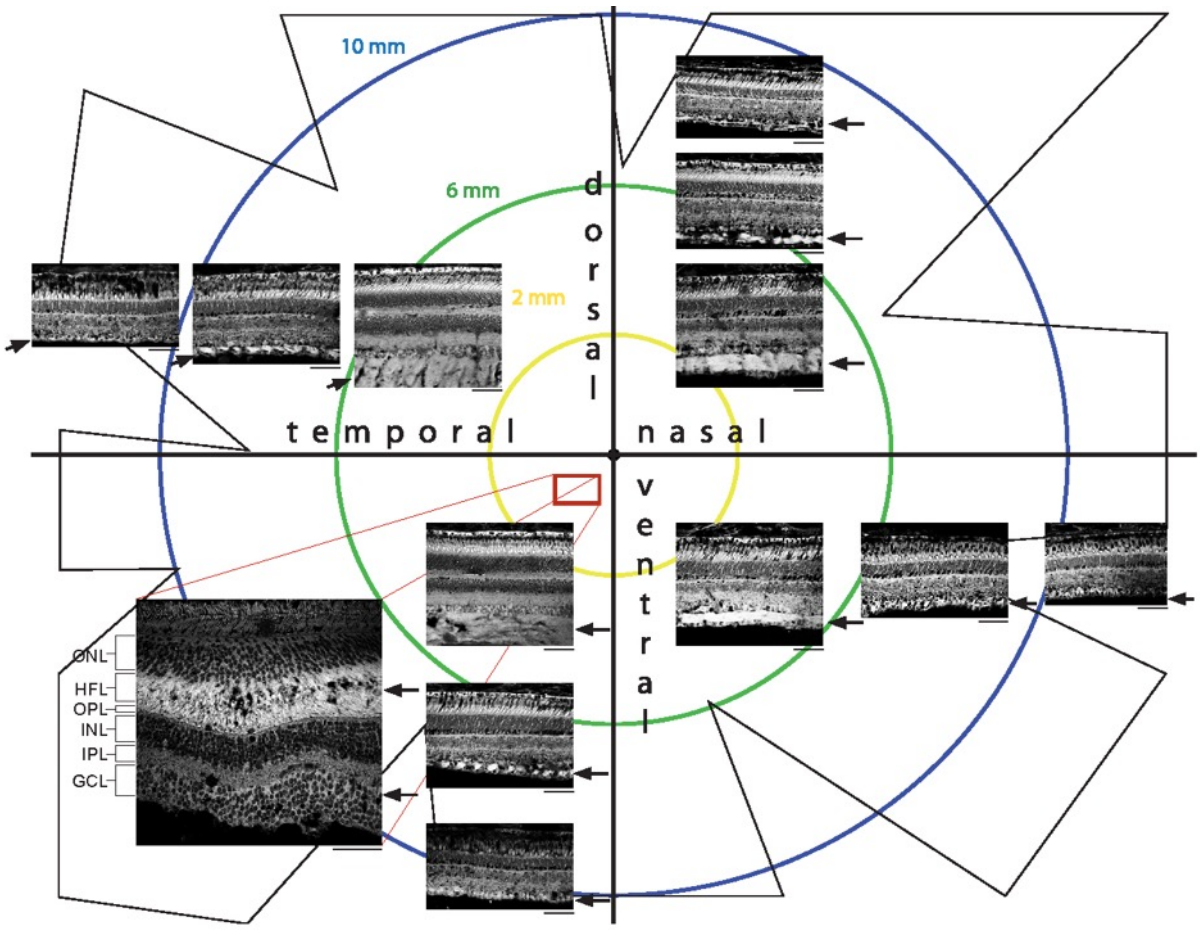

Figure 3. Schematic illustration of the labeling pattern of FAAH-IR throughout the monkey retina. Note that the most prominent staining of FAAH is located in the nerve fiber layer and retinal ganglion cell layer of the central retina (indicated by the arrows). ONL, outer nuclear layer; NFL, nerve fiber layer; OPL, outer plexiform layer; INL, inner nuclear layer; IPL, inner plexiform layer; GCL, ganglion cell layer. Scale bar = 75 μm.

Cellular Distribution of CB1R and FAAH

In order to verify the retinal cell type expression, double immunostaining was carried out for CB1R or FAAH and a specific molecular marker for primate retinal cells. A consistent staining pattern across all three monkey retinas was found for each double staining. Although labeling was located in all layers of the retina, from the photoreceptor to the ganglion cell layers, CB1R immunoreactivity was most prominent in the plexiform layers and the retinal

ganglion cell layer within the central retina (Figure 2). FAAH distribution was similar to the CB1R distribution and densely expressed in the photoreceptor and ganglion cell layers (Figure 3). The CB1R and FAAH distribution profile showed a consistent expression pattern across the retina, as illustrated in the low magnification (40x) views of immunostained retinal sections shown in Figures 2 and 3.

CB1R immunoreactivity in the photoreceptor layer was found throughout the cones, with positive staining in the membrane and cytosol (Figure 4). CB1R is present in the outer and inner segments, in the cell body and in the pedicles. It is preferentially expressed in cones with little evidence of staining in the inner segments and spherules of rods. FAAH, on the other hand, was more prominent in the Henle fiber layer and cone pedicles (Figure 5). CB1R and FAAH are expressed in cones both in the central and peripheral retina (Figure 4 and Figure 5).

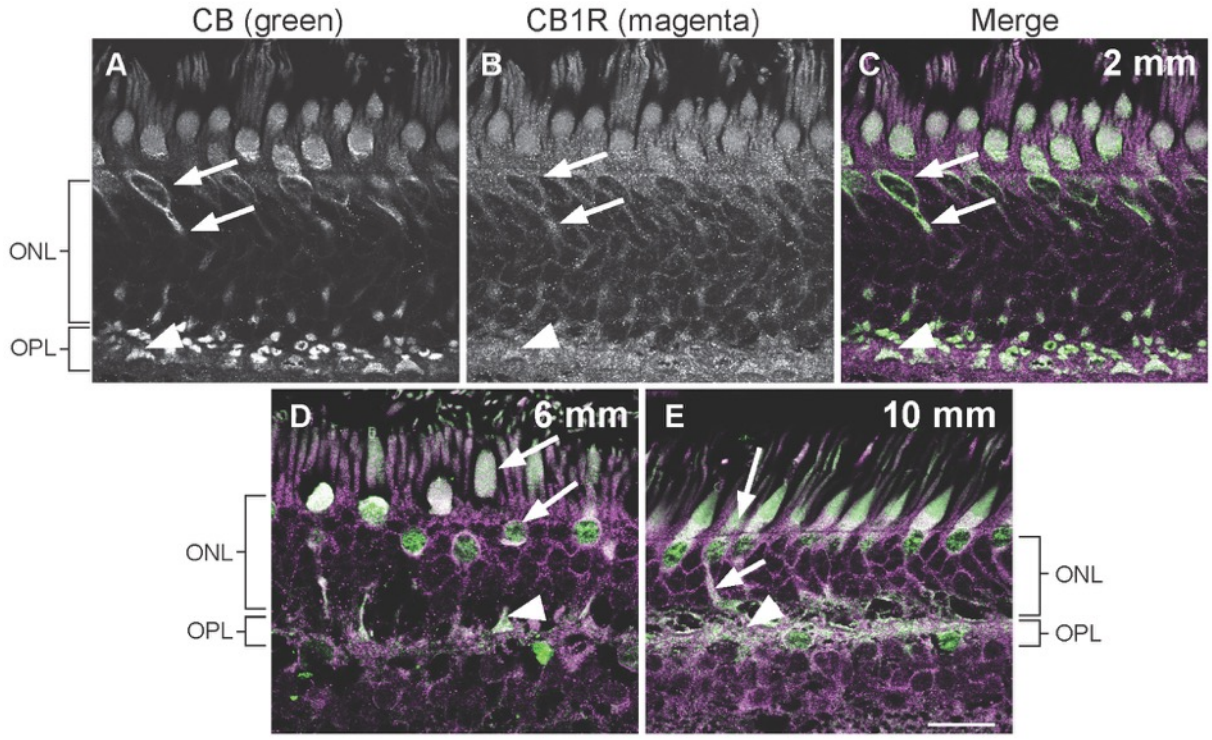

Figure 4. Double-label immunofluorescence illustrating co-localization of CB1R-IR with calbindin-IR. Confocal micrographs of retinas co-immunolabeled for CB1R (magenta) and calbindin (green), a specific marker for cones in the primate, at different retinal eccentricities (A-C: 2 mm; D: 6 mm; E: 10 mm). Arrows indicate CB1R positive cones and arrowheads

positive cone pedicles. ONL, outer nuclear layer; OPL, outer plexiform layer. Scale bar = 25 µm.

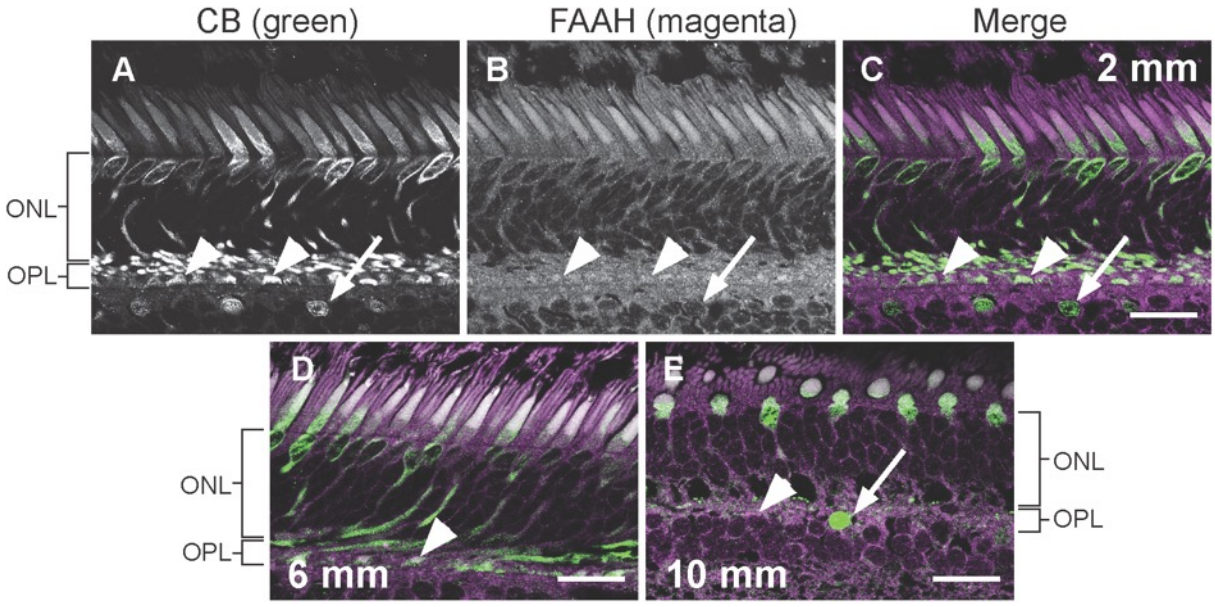

Figure 5. Double-label immunofluorescence illustrating co-localization of FAAH-IR with calbindin. Confocal micrographs of retinas co-immunolabeled for FAAH (magenta) and calbindin (green), a specific marker for cones in the primate, at different retinal eccentricities (A-C: 2 mm; D: 6 mm; E: 10 mm). Arrowheads indicate FAAH positive cone pedicles. Arrows point at calbindin positive horizontal cells that express FAAH. ONL, outer nuclear layer; OPL, outer plexiform layer. Scale bar = 18.75 µm for A-D and and 25 µm for E.

The inner nuclear layer comprises bipolar, horizontal, amacrine and Müller cells. To distinguish the cone and rod bipolar cells from the other cell types, a triple immunolabeling was performed. The antibodies targeting the homeobox transcription factor CHX10 present in all bipolar cells nuclei, and the protein kinase c (PKC) present in rod bipolar cells and a subset of amacrine cells, were used to identify the cell type localization of the eCB components. Both cone and rod bipolar cells were CB1R and FAAH immunoreactive (Figure 6 and Figure 7). No differences in staining were observed between central versus peripheral retina.

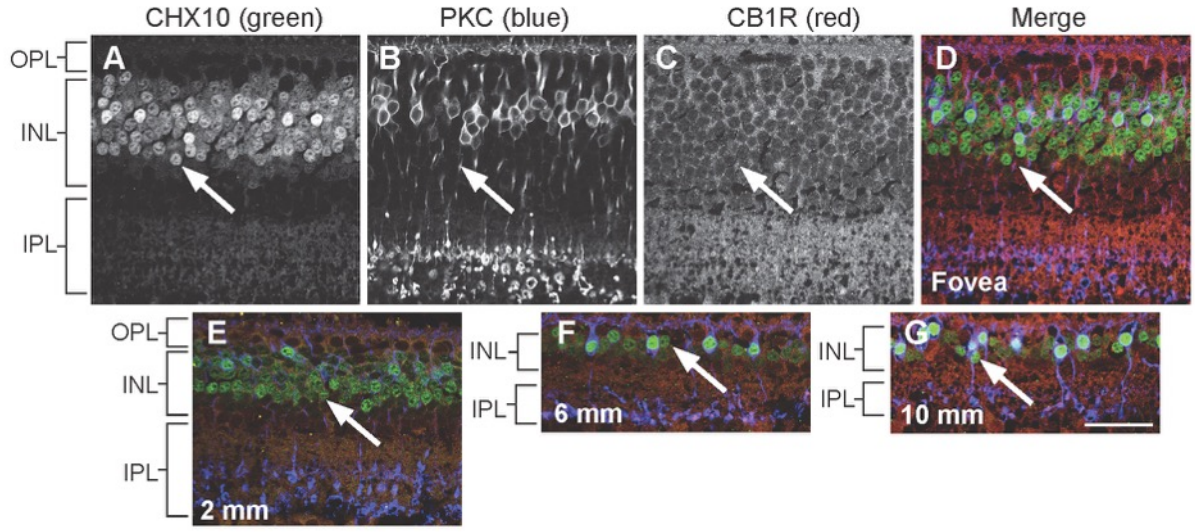

Figure 6. CB1R is present in all bipolar cells (CHX10 positive), but is preferentially expressed in rod bipolar cells (CHX10 and PKC positive). Confocal micrographs illustrating single or triple labeling in the foveal region (A-D), at 2 mm (E), at 6 mm (F) and at 10 mm (G) of eccentricity. Arrows indicate, in each panel, one of the rod bipolar cells that are CB1R immunoreactive. OPL: outer plexiform layer; INL: inner nuclear layer; IPL: inner plexiform layer. Scale bar = 25 μm.

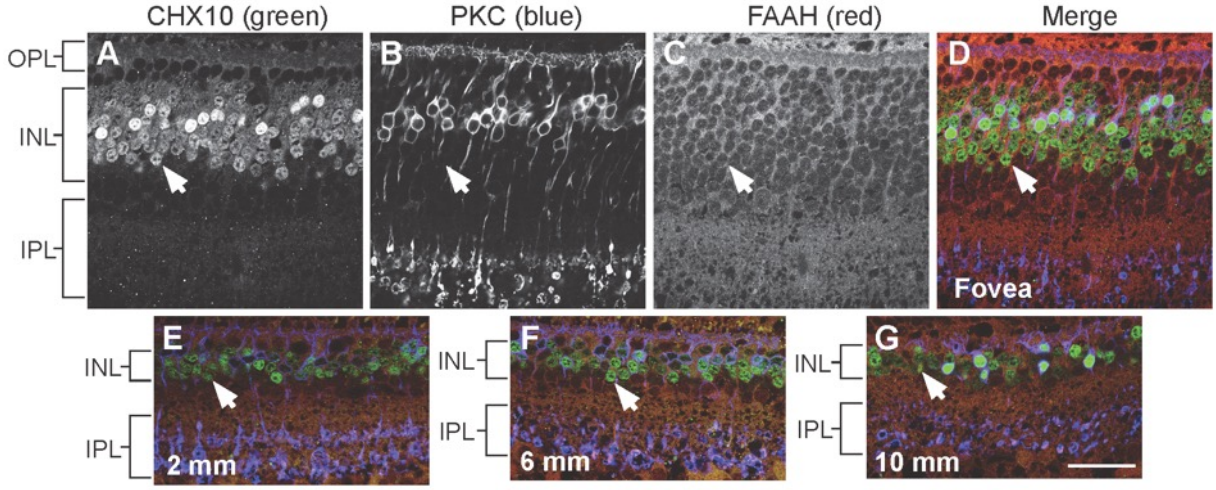

Figure 7. FAAH is present in all bipolar cells (CHX10 positive). Confocal micrographs illustrating single or triple labeling in the foveal region (A-D), at 2 mm (E), at 6 mm (F) and at 10 mm (G) of eccentricity. Arrows indicate, in each panel, an example of the rod bipolar cells

that are FAAH immunoreactive. OPL: outer plexiform layer; INL: inner nuclear layer; IPL: inner plexiform layer. Scale bar = 25 μm.

For targeting the retinal ganglion cell population, we used the Brn3a immunoreactivity that specifically labels retinal ganglion cell nuclei. CB1R staining was detected in the ganglion cell layer, present in the RGC soma (Figure 8) and axons (Figure 10). Axon fiber staining was obtained with syntaxin (Wiedenmann and Franke, 1985; Nag and Wadhwa, 2001). Double labeling Brn3a/CB1R and syntaxin/CB1R indicated that CB1R is expressed throughout the ganglion cells including their axons. This distribution pattern is similar for FAAH (Figure 9 and Figure 10). Non-Brn3a positive cells that are CB1R or FAAH immunoreactive were found and are presumably displaced amacrine cells (Figure 8 and Figure 9).

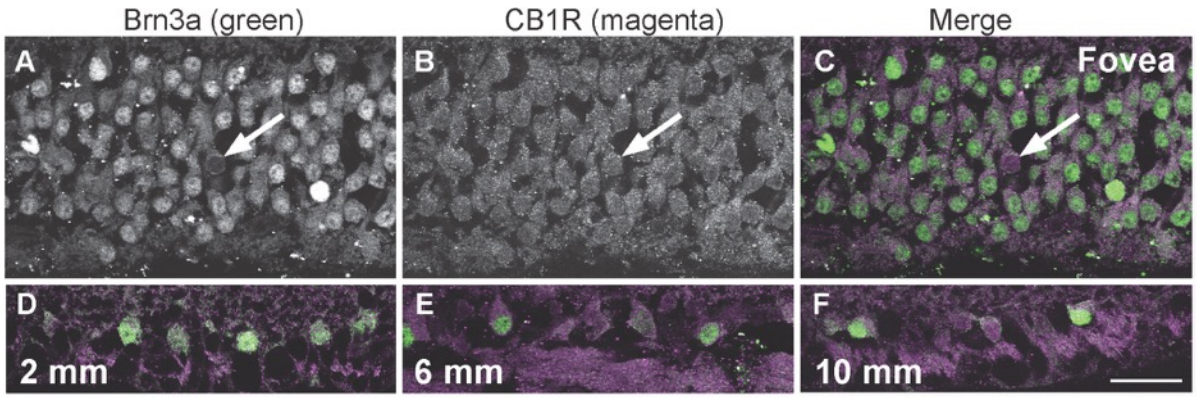

Figure 8. Double-label immunofluorescence illustrating co-localization of CB1R-IR (magenta) with Brn3a-IR (green) at different eccentricities (A-C: fovea; D: 2 mm; E: 6 mm; F: 10 mm). The antibody against Brn3a labels the nucleus of ganglion cells in the monkey retina and these cells were also all CB1R immunoreactive. The intense labeling of CB1R in the ganglion cells was localized in the ganglion cells cytosol. Arrows point at non-Brn3a positive cells that are CB1R immunoreactive. Scale bar = 30 μm.

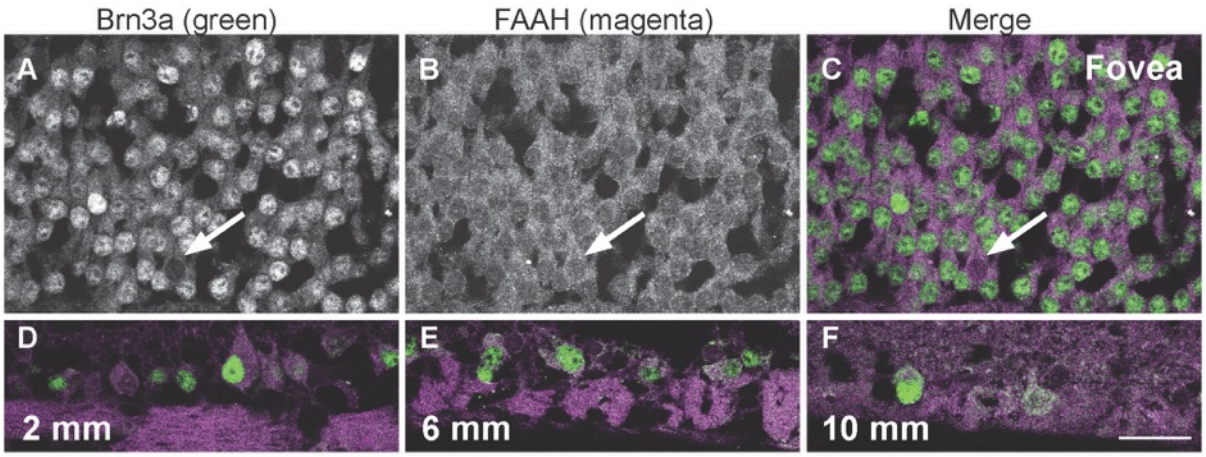

Figure 9. Double-label immunofluorescence illustrating co-localization of FAAH (magenta) with Brn3a-IR (green) at different eccentricities (A-C: fovea; D: 2 mm; E: 6 mm; F: 10 mm). All Brn3a positive ganglion cells in the monkey retina were also FAAH immunoreactive. The intense labeling of FAAH in the ganglion cells was localized in the ganglion cells cytosol. Arrows point at non-Brn3a positive cells that are FAAH immunoreactive. Scale bar = 30 µm.

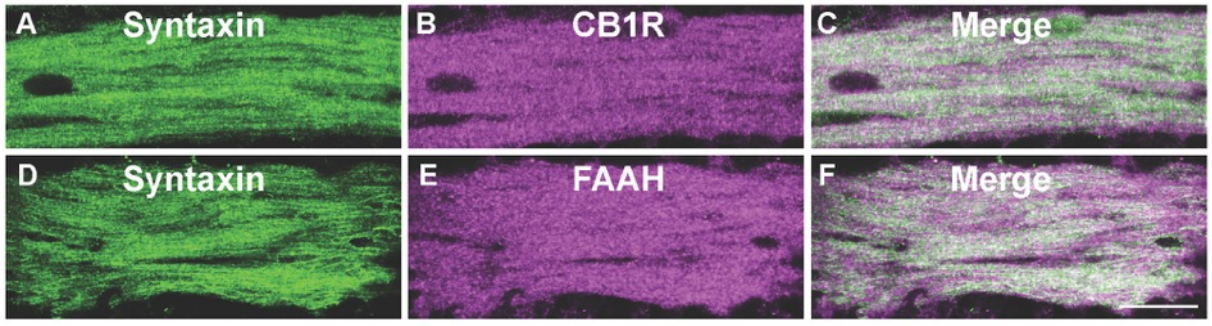

Figure 10. Double-label immunofluorescence illustrating co-localization of CB1R-IR (A-C) and FAAH-IR (D-F) with syntaxin-IR in a paraveal region taken at 2 mm of eccentricity where the retinal ganglion cell axons are dense. High magnification confocal micrographs of retinas co-immunolabeled for CB1R or FAAH (magenta) and syntaxin (green), a marker of RGC axons. Scale bar = 18.75 µm.

The monoclonal antibody HPC-1 that recognizes syntaxin was also used to label the retinal interneurons, horizontal and amacrine cells. Those lateral projecting neurons show little

expression of CB1R and FAAH. Their staining in horizontal and amacrine cells was limited to the membrane of the soma as well as the cytosol. Large amacrine cell bodies were slightly more labeled than others. No notable differences were found in relation to eccentricity (Figure 11 and Figure 12).

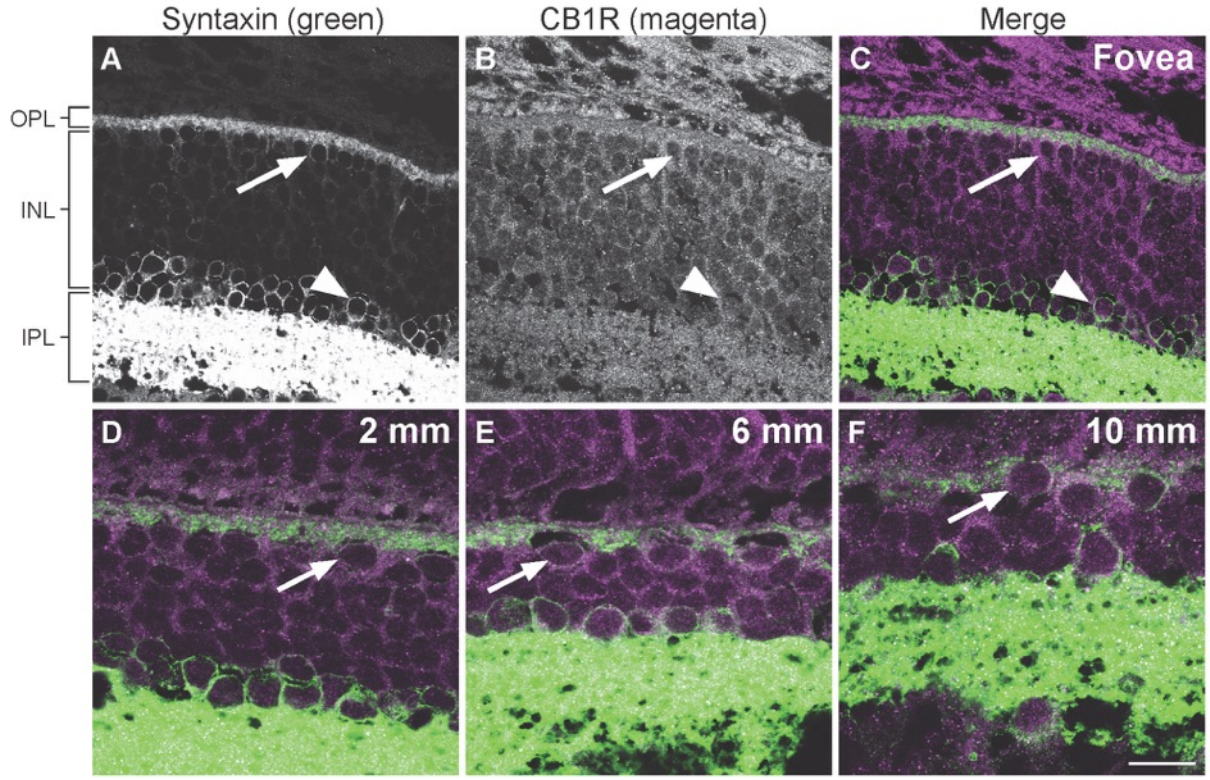

Figure 11. Double-label immunofluorescence illustrating co-localization of CB1R-IR (magenta) with syntaxin-IR (green) near the fovea centralis (fovea) (A-C) and at 2 mm (D), 6 mm (E) and 10 mm (F) of eccentricity. Syntaxin-immunoreactive horizontal (arrows) and amacrine cells (arrowheads) were double labeled for CB1R. Syntaxin-IR labeled heavily the membrane of horizontal cells and OPL but lightly their cytosol. Syntaxin-IR labeled heavily the membrane of amacrine cells and IPL but lightly their cytosol. ONL, outer nuclear layer; OPL, outer plexiform layer; INL, inner nuclear layer; IPL, inner plexiform layer. Scale bar = 18.75 µm for A-D and 15 µm for E-F.

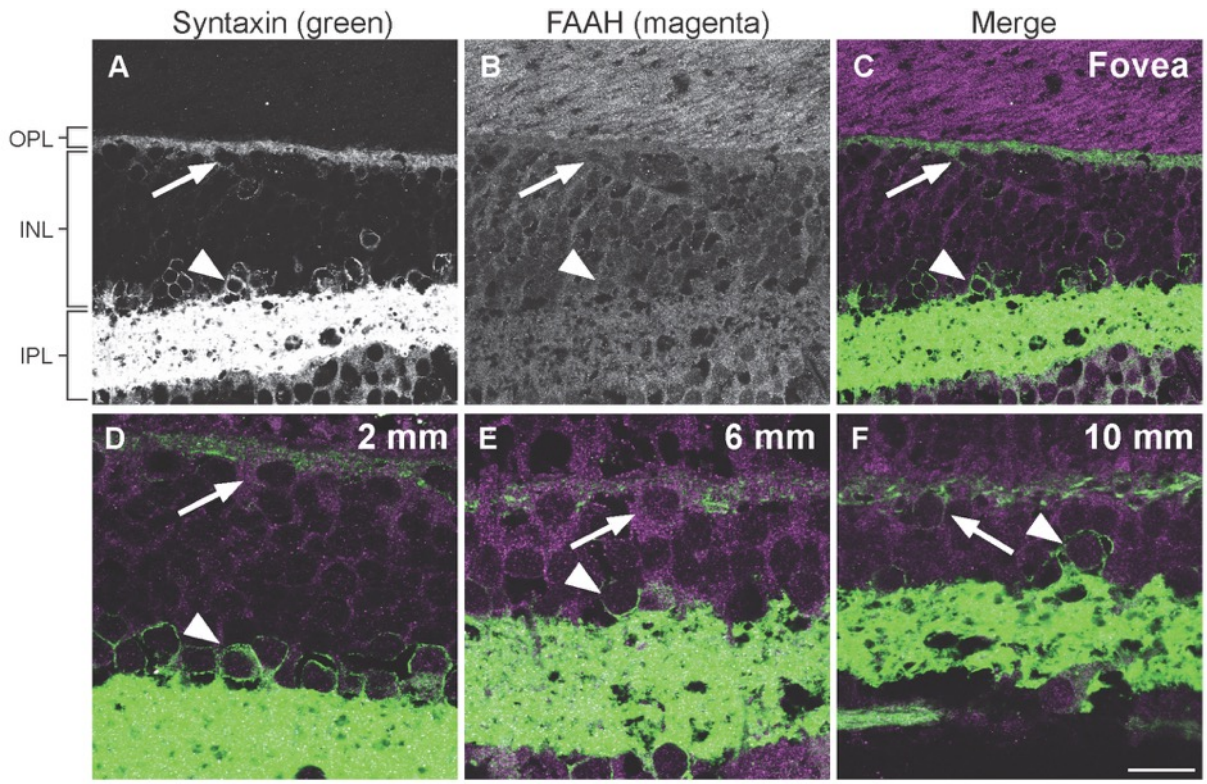

Figure 12. Double-label immunofluorescence illustrating co-localization of FAAH-IR (magenta) with syntaxin-IR (green) near the fovea centralis (fovea) (A-C) and at 2 mm (D), 6 mm (E) and 10 mm (F) of eccentricity. Syntaxin-immunoreactive horizontal (arrows) and amacrine cells (arrowheads) were double labeled for FAAH. ONL, outer nuclear layer; OPL, outer plexiform layer; INL, inner nuclear layer; IPL, inner plexiform layer. Scale bar = 30 µm for A-C and 15 µm for D-F.

In order to assess if retinal glia express the eCB components, the antibody against glutamine synthetase (GS) was used to identify Müller cells throughout the retina. Müller cells did not show any expression of CB1R or FAAH (Figures 13 and 14 respectively). In all three pairs of retinas, we found the same staining pattern. No differences in the expression of CB1R and FAAH with regard to eccentricity were observed.

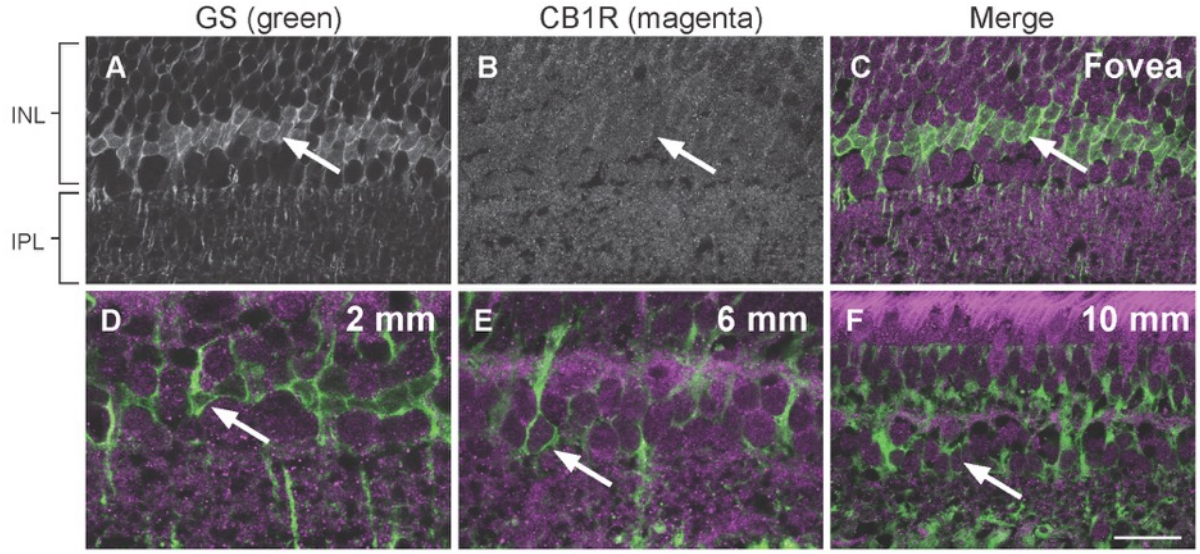

Figure 13. CB1R immunoreactivity in Müller cells. A-F: Vertical sections taken near the fovea (A-C) and at 2 mm (D), 6 mm (E) and 10 mm (F) of eccentricity. Confocal micrographs of retinas co-immunolabeled for CB1R and a cell type specific marker for Müller cells, glutamine synthetase (GS). Each protein is presented alone in gray scale in the first columns. The merge image is presented in the last column (CB1R in magenta and GS in green). Arrows point at Müller cells that do not express CB1R. INL, inner nuclear layer; IPL, inner plexiform layer. Scale bar = 30 µm for A-C, F and 18.75 µm for D-E.

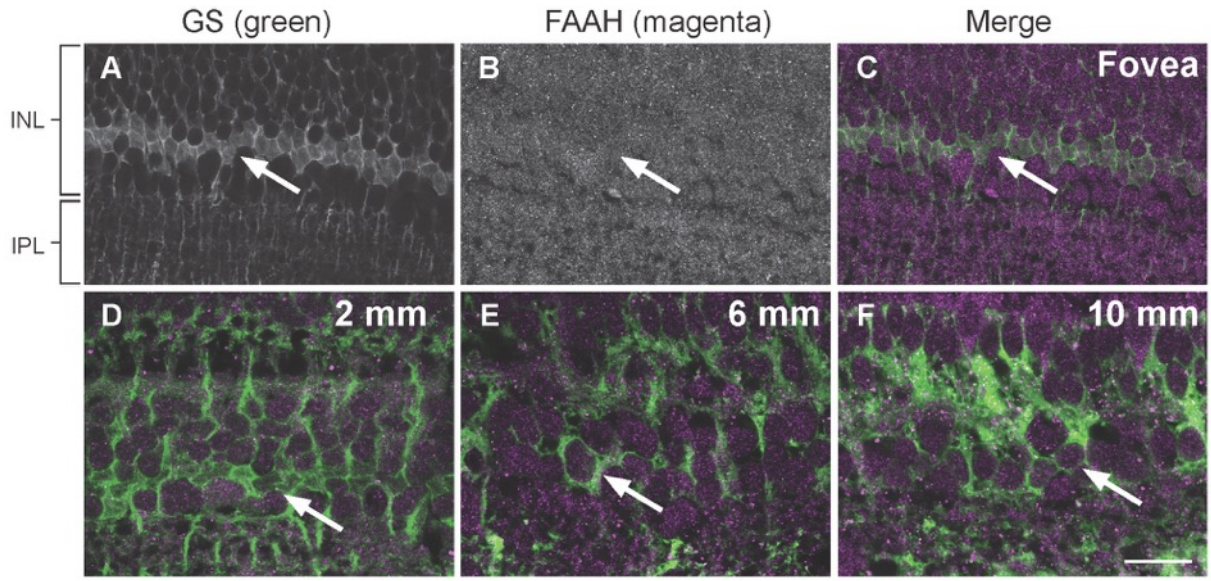

Figure 14. FAAH immunoreactivity in Müller cells. A-F: Vertical sections taken near the fovea (A-C) and at 2 mm (D), 6 mm (E) and 10 mm (F) of eccentricity. Confocal micrographs of retinas co-immunolabeled for FAAH and glutamine synthetase (GS). Each protein is presented alone in gray scale in the first columns. The merge image is presented in the last column (FAAH in magenta and GS in green). Arrows point at Müller cells that do not express FAAH. INL, inner nuclear layer; IPL, inner plexiform layer. Scale bar = 30 μm for A-C and 18.75 μm for D-F.

Co-expression of FAAH and CB1R in all retinal cells is presented in Figure 15A-C. There is a large overlap in the expression of these two proteins in the outer plexiform layer, inner nuclear layer, inner plexiform layer, ganglion cell layer and nerve fiber layer. Detailed analysis of the expression of both proteins for each cell type is found throughout Figures 4 to 14. These data are summarized in Figure 15J for all retinal cell types. Note that for the most part, CB1R and FAAH expression overlap at different eccentricities and in all neuronal cell types with the exception of the rod outer segments and somas, and Müller cells. In the fovea, however, the signal intensity is higher as expected from the cone (Osterberg, 1935) and ganglion cells distributions (Herbin et al., 1997).

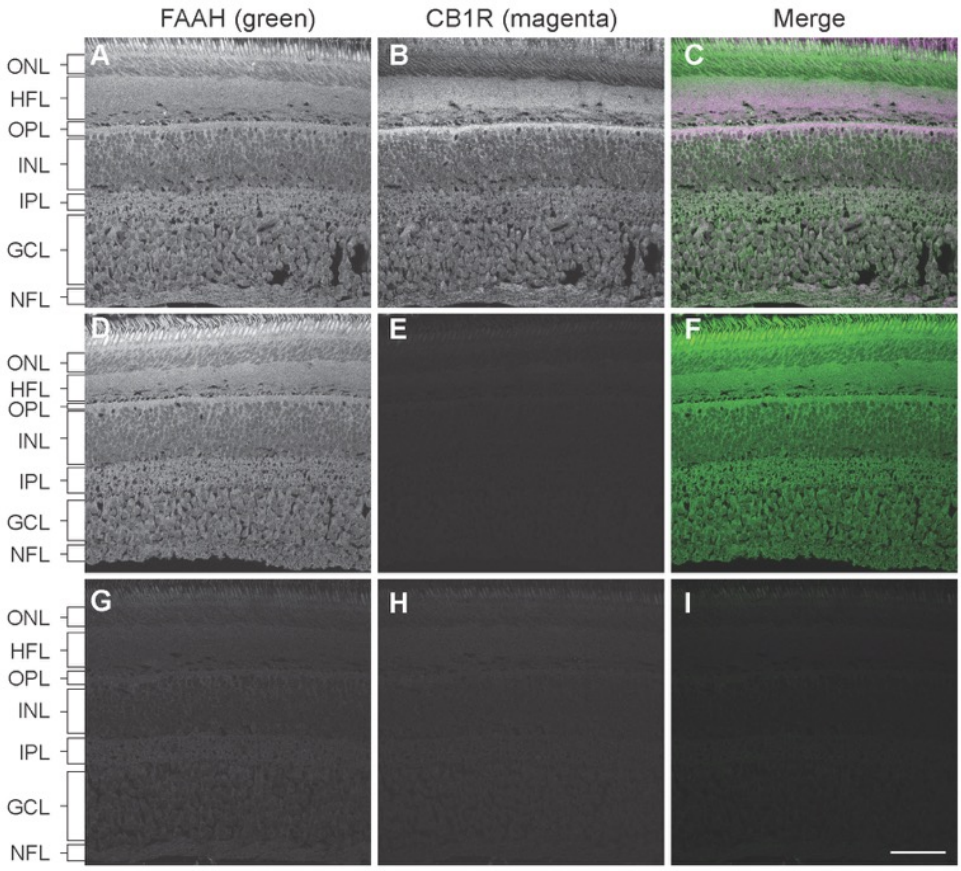

J

Cell type \ Retinal location	Fovea	2 mm	6 mm	10 mm
Cone outer segments	+++ +	+++ +	++ +	++ +
Cone somas	+++ +++	++ +++	++ +++	++ +++
Cone pedicles	+++ +++	+++ +++	+++ +++	+++ +++
Rod outer segments	- -	- -	- -	- -
Rod somas	- -	- -	- -	- -
Rod spherules	- -	+ +	+ +	+ +
Horizontal cells	+ +	+ +	+ +	+ +
Cone bipolar cells	+ +	+ +	+ +	+ +
Rod bipolar cells	++ ++	++ ++	++ ++	++ ++
Amacrine cells	+ +	+ +	+ +	+ +
Ganglion cells	+++ +++	+++ +++	+++ +++	+++ +++
Müller cells	- -	- -	- -	- -

Figure 15. Comparison of CB1R and FAAH expression. Confocal micrographs of retinas co-immunolabeled for CB1R (green) and FAAH (magenta). FAAH (A, D, G) and CB1R (B, E,

H) signals, and their overlay (C, F, I) for the complete sequential protocol (A-C) in the monkey central retina. (D–F): the second primary antibody was omitted; (G–I): the first secondary and second primary antibodies were lacking. Scale bar = 75 um. (J) Table summarizing CB1R (green) and FAAH (magenta) distribution at different retinal eccentricities. The staining intensity was scored as - (no signal), + (weak), ++ (medium), +++ (high).

Discussion

The present study reports that the distribution of CB1R and FAAH is widespread throughout the vervet monkey retina. These eCB components are present in different retinal cell types, namely cones, bipolar, ganglion, horizontal and amacrine cells and is consistent with that found in the rodent retina (Yazulla et al., 1999; Yazulla 2008, for review; Zabouri et al., 2011a). The cellular expression pattern of CB1R labeling in the vervet monkey retina resembles that found in other vertebrates, particularly rhesus monkeys (Straiker et al., 1999a) and humans (Straiker et al., 1999b). We provide here a comprehensive set of results that further extends the data obtained by Straiker et al (1999a) by showing the retinal specific cell types expressing CB1R at various eccentricities. We also demonstrate the expression and cellular localization of FAAH. Although CB1R is clearly present in cones, their pedicles revealed a more prominent labeling. CB1R immunoreactivity was not detected in rod inner segments. Heavy CB1R staining was observed in the cone pedicles, not only in the foveal pit but also throughout the retina. However, FAAH was present throughout the cone with a more intense staining in the inner segments including the pedicles. Globally, the expression of CB1R and FAAH throughout the retina relates to cell density.

Like the photoreceptors, the bipolar cells within the inner nuclear layer (cone and rod bipolar cells) express both CB1R and FAAH. This suggests that eCBs might modulate cone (photopic) and rod (scotopic) vision. Indeed, there is evidence that marijuana use alters color discrimination (Dawson et al., 1977) and increases the glare recovery at low contrast (Adams et al., 1978). Our results are consistent with the suggestion that the vertical cone-bipolar-RGC pathway that prominently expresses CB1R and FAAH plays an important role in glutamate release in each one of the retinal cell types (Wässle, 2004; Yazulla 2008). However, the low expression of both CB1R and FAAH in horizontal and amacrine cells (the lateral pathway) in this study and in lower mammals (Yazulla et al., 1999) reinforces the pivotal role exerted by the vertical retinal pathway. The presence of the eCB system within the plexiform layers suggests an autoregulatory mechanism in horizontal and amacrine inhibitory neurons. The different expression of the eCB components within the vertical and lateral retinal pathways could result in a modulation of the synaptic gain in the plexiform layers by the inhibition of neurotransmitter release in cone pedicles (Yazulla et al., 1999).

Our understanding of the role of the eCB system in visual processing stems primarily from studies conducted in lower mammals and vertebrates, namely mouse, rat, goldfish and the tiger salamander (Yazulla et al, 1999; Straiker et al, 1999a; Yazulla 2008 for review). As such, some retinal circuits have a species-specific function that could be acted upon by the eCB system. For example, the rod pathway is highly preserved across mammals, whereas trichromatic color processing is found primarily in humans and most old world monkeys (Ptito et al., 1973; Rosenberg and Talebi, 2009). Indeed, in these species, the fovea centralis made exclusively of cones, is responsible for color vision and optimal visual acuity (Osterberg, 1935). This biological adaptation optimizes the visual information available in the environment (Herbin et al., 1997). The eCB signaling system may be restricted in its phylogenetic distribution, because to date its existence has only been firmly established in vertebrate species (Elphick and Egertová, 2001).

In the central nervous system (CNS), the activation of CB1R modulates the neuronal membrane permeability to Ca2+ and K+ ions and the activity of adenylyl cyclase, thereby affecting neurotransmitter release and action (Di Marzo, 1998). Electrophysiological research carried out in the mammalian retina to find a specific eCB neuromodulatory action has not been conclusive (Straiker et al., 1999a; Yazulla 2008 for review). For example, recordings in goldfish cones following the application of WIN 55,212-2 (a CB1R agonist) showed that the photocurrent recovered to baseline more quickly than in controls. It was therefore concluded that the functional consequence of this effect was to increase the photosensitivity to bright flashes (Yazulla, 2008). On the contrary, Adam et al., (1978) reported an increase time in the glare recovery in photopic conditions under the influence of marijuana in humans. These two results appear contradictory, but given that the expression of CB1R is more widely expressed throughout the monkey cones than the goldfish ones (Yazulla et al., 2000), it would be plausible that the sites of action of tetrahydrocannabinol (THC, the active compound in marijuana) are broader in primates.

The most prominent CB1R and FAAH expression was found in cone synaptic terminals and in the ganglion cell layer. This suggests that cannabinoids act not only on photoreceptors as previously reported (Yazulla 2008 for review) but also directly on ganglion cells. Indeed, at the level of RGCs, CB1R and FAAH are strongly expressed in the cell body

and axons. This appears to be unusual because in the mammalian CNS it has been thought that CB1R is not present in large neurons, like pyramidal and Purkinje cells, but instead in smaller pre-synaptic neurons (Elphick and Egertová, 2001). However, recent research suggests that the eCB system is also found in large caliber axons (Marsicano and Lutz, 1999; Hill et al., 2007). RGCs do not have large caliber axons, yet they strongly express CB1R and FAAH providing anatomical evidence that eCBs serve an autoregulatory function to modulate the output of ganglion cells as proposed by Yazulla (2008).

Our results also showed that Müller cells in monkeys do not express CB1R or FAAH, which is in agreement with some studies conducted on the retina of other adult mammals (Yazulla, 2008; Zabouri et al., 2011a). CB1R is transiently expressed in rat Müller cells between postnatal day 3 and day 9 (Zabouri et al., 2011a). However, only one study (Yazulla et al., 2000) reported the presence of CB1R in Müller cells of the goldfish retina. The existence of the eCB system within the retinal glia is largely unexplored and further research is needed to establish its presence across species and its specific functions.

Although the literature on the distribution of the molecular components of the eCB system in the rodent retina has evolved, little is still known about the expression of this signaling system in the retina of species more closely related to humans. In the rodent retina, CB1R has been reported in photoreceptors, bipolar cells, gabaergic amacrine cells, horizontal cells, and the inner plexiform layer (Yazulla et al., 1999; Hu et al., 2010; Zabouri et al., 2011a). Similarly, in the human retina, the eCB system is expressed in the outer segments of photoreceptors, the inner and outer plexiform layers, the inner nuclear layer and the ganglion cell layer (Straiker et al., 1999b). This overall pattern of CB1R distribution is also found in the rhesus monkey, indicating that the eCB system is similarly expressed in the retina across species (Yazulla et al., 1999; Hu et al., 2010). Our results support and extend this notion by showing that the eCB system is not only present in the monkey retina, but it is more salient in the foveal region compared to the periphery. This different center-periphery distribution of the eCB system suggests an additional role of this system in central retinal functions.

The eCB system has also been observed in the central nervous system. The patterns of expression of CB1R and FAAH have been assigned to different types of distributions: complementary, overlapping or unrelated (Egertová et al., 2003; Yazulla, 2008). In the

complementary pattern, in brain regions like the cerebellar cortex, hippocampus and neocortex, FAAH positive neurons are post-synaptic to processes expressing CB1R. This expression pattern proposes a retrograde pre-synaptic regulation of transmitter release by eCBs (Tsou et al., 1998; Egertová et al., 1998; Egertová et al., 2003). In the overlapping pattern, neurons express both CB1R and FAAH (Marsicano and Lutz, 1999; Hill et al., 2007) with FAAH located in neurons that are proximal to CB1R expressing axon fibers. Here, FAAH may influence eCB signaling but more remotely (Egertová et al., 2003). Finally, in the unrelated pattern, neurons express only one of these two components, suggesting that the spatial impact and/or duration of eCB signaling may be less restricted than in regions enriched with FAAH (Egertová et al., 2003). In the present study, CB1R and FAAH in the retina are generally expressed in an overlapping pattern (Figure 15) suggesting that the eCB system might be responsible for an auto-feedback control of neurotransmitter release. We also show that FAAH is targeted to the axonal and somato-dendritic compartments of the retinal ganglions cells, therefore supporting the notion that FAAH is located both presynaptically (at the photoreceptor level) and postsynaptically (at the bipolar and ganglion cell level). This result is consistent with what has been previously shown in the mouse olfactory bulb, where FAAH is also expressed pre- (olfactory-receptor neuron terminals) and post-synaptically (mitral cells) (Egertová et al., 2003). Not surprisingly and in agreement with our previous assumption, eCBs are also expressed in the visual cortex of the developing rodent brain (Jiang et al, 2010), indicating that the whole visual pathway from retina to cortex is influenced by the eCB system.

Conclusion

To our knowledge, this is the first report that CB1R and FAAH have been localized in specific cell types in the old-world monkey retina at all eccentricities of tissue sampling. The distribution of the eCB system throughout the retina might explain the deleterious effects of marijuana consumption on visual functions. Since CB1R and FAAH are highly expressed in central cones, the administration of exogenous cannabinoids may alter several retinal functions, such as visual acuity, color discrimination and photosensitivity.

Acknowledgements

This work was supported in part by the Natural Science and Engineering Research Council of Canada (M.P. and C.C.) and the Canadian Institutes of Health Research (MOP-86495, J.-F.B.). J.B. was supported by a CIHR studentship and J.-F.B. by a Chercheur-Boursier Junior 2 from the Fonds de la recherche en santé du Québec. We thank Sophie Charron, Florence Dotigny and Ikiel Ptito for excellent technical assistance. We are grateful to Dr Frank Ervin and Dr Roberta Palmour of the Behavioral Sciences Foundation Laboratories of St Kitts, West Indies, for supplying the eyes and the fresh retinas.

References

Adams AJ, Brown B, Flom MC, Jones RT, Jampolsky A (1975) Alcohol and marijuana effects on static visual acuity. Am J Optom Physiol Opt 52:729-735.

Adams AJ, Brown B, Haegerstrom-Portnoy G, Flom MC, Jones RT (1978) Marijuana, alcohol, and combined drug effects on the time course of glare recovery. Psychopharmacology (Berl) 56:81-86.

Aguado T, Monory K, Palazuelos J, Stella N, Cravatt B, Lutz B, Marsicano G, Kokaia Z, Guzman M, Galve-Roperh I (2005) The endocannabinoid system drives neural progenitor proliferation. FASEB J 19:1704-1706.

Argaw A, Duff G, Zabouri N, Cécyre B, Chaine N, Cherif H, Tea N, Lutz B, Ptito M, Bouchard JF (2011) Concerted action of CB1 cannabinoid receptor and deleted in colorectal cancer in axon guidance. J Neurosci 31:1489-1499.

Atwood BK, Mackie K (2010) CB2: a cannabinoid receptor with an identity crisis. Br J Pharmacol 160:467-479.

Barnstable CJ, Hofstein R, Akagawa K (1985) A marker of early amacrine cell development in rat retina. Brain Res 352:286-290.

Burke M, Zangenehpour S, Bouskila J, Boire D, Ptito M (2009) The Gateway to the Brain: Dissecting the Primate Eye. J Vis Exp e1261.

Chang ML, Wu CH, Jiang-Shieh YF, Shieh JY, Wen CY (2007) Reactive changes of retinal astrocytes and Muller glial cells in kainate-induced neuroexcitotoxicity. J Anat 210:54-65.

Chiquet C, Dkhissi-Benyahya O, Chounlamountri N, Szel A, Degrip WJ, Cooper HM (2002) Characterization of calbindin-positive cones in primates. Neuroscience 115:1323-1333.

Cravatt BF, Demarest K, Patricelli MP, Bracey MH, Giang DK, Martin BR, Lichtman AH (2001) Supersensitivity to anandamide and enhanced endogenous cannabinoid signaling in mice lacking fatty acid amide hydrolase. Proc Natl Acad Sci U S A 98:9371-9376.

Cravatt BF, Giang DK, Mayfield SP, Boger DL, Lerner RA, Gilula NB (1996) Molecular characterization of an enzyme that degrades neuromodulatory fatty-acid amides. Nature 384:83-87.

Cuenca N, Herrero MT, Angulo A, de Juan E, Martinez-Navarrete GC, Lopez S, Barcia C, Martin-Nieto J (2005) Morphological impairments in retinal neurons of the scotopic visual pathway in a monkey model of Parkinson's disease. J Comp Neurol 493:261-273.

Dawson WW, Jimenez-Antillon CF, Perez JM, Zeskind JA (1977) Marijuana and vision--after ten years' use in Costa Rica. Invest Ophthalmol Vis Sci 16:689-699.

Deutsch DG, Chin SA (1993) Enzymatic synthesis and degradation of anandamide, a cannabinoid receptor agonist. Biochem Pharmacol 46:791-796.

Di Marzo V, Melck D, Bisogno T, De Petrocellis L (1998) Endocannabinoids: endogenous cannabinoid receptor ligands with neuromodulatory action. Trends Neurosci 21:521-528.

Egertová M, Cravatt BF, Elphick MR (2003) Comparative analysis of fatty acid amide hydrolase and cb(1) cannabinoid receptor expression in the mouse brain: evidence of a widespread role for fatty acid amide hydrolase in regulation of endocannabinoid signaling. Neuroscience 119:481-496.

Egertová M, Elphick MR (2000) Localisation of cannabinoid receptors in the rat brain using antibodies to the intracellular C-terminal tail of CB. J Comp Neurol 422:159-171.

Egertová M, Giang DK, Cravatt BF, Elphick MR (1998) A new perspective on cannabinoid signalling: complementary localization of fatty acid amide hydrolase and the CB1 receptor in rat brain. Proc Biol Sci 265:2081-2085.

Elphick MR, Egertova M (2001) The neurobiology and evolution of cannabinoid signalling. Philos Trans R Soc Lond B Biol Sci 356:381-408.

Fischer AJ, Hendrickson A, Reh TA (2001) Immunocytochemical characterization of cysts in the peripheral retina and pars plana of the adult primate. Invest Ophthalmol Vis Sci 42:3256-3263.

Freund TF, Katona I, Piomelli D (2003) Role of endogenous cannabinoids in synaptic signaling. Physiol Rev 83:1017-1066.

Gómez-Ruiz M, Hernández M, de Miguel R, Ramos JA (2007) An overview on the biochemistry of the cannabinoid system. Mol Neurobiol 36:3-14.

Herbin M, Boire D, Ptito M (1997) Size and distribution of retinal ganglion cells in the St. Kitts green monkey (Cercopithecus aethiops sabeus). J Comp Neurol 383:459-472.

Herkenham M, Lynn AB, de Costa BR, Richfield EK (1991a) Neuronal localization of cannabinoid receptors in the basal ganglia of the rat. Brain Res 547:267-274.

Herkenham M, Lynn AB, Johnson MR, Melvin LS, de Costa BR, Rice KC (1991b) Characterization and localization of cannabinoid receptors in rat brain: a quantitative in vitro autoradiographic study. J Neurosci 11:563-583.

Hill EL, Gallopin T, Ferezou I, Cauli B, Rossier J, Schweitzer P, Lambolez B (2007) Functional CB1 receptors are broadly expressed in neocortical GABAergic and glutamatergic neurons. J Neurophysiol 97:2580-2589.

Hu SS, Arnold A, Hutchens JM, Radicke J, Cravatt BF, Wager-Miller J, Mackie K, Straiker A (2010) Architecture of cannabinoid signaling in mouse retina. J Comp Neurol 518:3848-3866.

Inoue A, Obata K, Akagawa K (1992) Cloning and sequence analysis of cDNA for a neuronal cell membrane antigen, HPC-1. J Biol Chem 267:10613-10619.

Jacobs GH (2008) Primate color vision: A comparative perspective. Vis Neurosci 25:619-633.

Jiang B, Huang S, de Pasquale R, Millman D, Song L, Lee H-K, Tsumoto T, Kirkwood A (2010) The Maturation of GABAergic Transmission in Visual Cortex Requires Endocannabinoid-Mediated LTD of Inhibitory Inputs during a Critical Period. Neuron 66:248-259.

Katona I, Sperlagh B, Sik A, Kafalvi A, Vizi ES, Mackie K, Freund TF (1999) Presynaptically located CB1 cannabinoid receptors regulate GABA release from axon terminals of specific hippocampal interneurons. J Neurosci 19:4544-4558.

Kiplinger GF, Manno JE, Rodda BE, Forney RB (1971) Dose-response analysis of the effects of tetrahydrocannabinol in man. Clin Pharmacol Ther 12:650-657.

Kolb H, Zhang L, Dekorver L, Cuenca N (2002) A new look at calretinin-immunoreactive amacrine cell types in the monkey retina. J Comp Neurol 453:168-184.

Leonelli M, Britto LR, Chaves GP, Torrao AS (2005) Developmental expression of cannabinoid receptors in the chick retinotectal system. Brain Res Dev Brain Res 156:176-182.

Marsicano G, Lutz B (1999) Expression of the cannabinoid receptor CB1 in distinct neuronal subpopulations in the adult mouse forebrain. Eur J Neurosci 11:4213-4225.

Marsicano G, Wotjak CT, Azad SC, Bisogno T, Rammes G, Cascio MG, Hermann H, Tang J, Hofmann C, Zieglgansberger W, Di Marzo V, Lutz B (2002) The endogenous cannabinoid system controls extinction of aversive memories. Nature 418:530-534.

Martinez-Navarrete GC, Angulo A, Martin-Nieto J, Cuenca N (2008) Gradual morphogenesis of retinal neurons in the peripheral retinal margin of adult monkeys and humans. J Comp Neurol 511:557-580.

Martinez-Navarrete GC, Martin-Nieto J, Esteve-Rudd J, Angulo A, Cuenca N (2007) Alpha synuclein gene expression profile in the retina of vertebrates. Mol Vis 13:949-961.

Mills SL, Massey SC (1999) AII amacrine cells limit scotopic acuity in central macaque retina: A confocal analysis of calretinin labeling. J Comp Neurol 411:19-34.

Monory K, Massa F, Egertova M, Eder M, Blaudzun H, Westenbroek R, Kelsch W, Jacob W, Marsch R, Ekker M, Long J, Rubenstein JL, Goebbels S, Nave KA, During M, Klugmann M, Wolfel B, Dodt HU, Zieglgansberger W, Wotjak CT, Mackie K, Elphick MR, Marsicano G, Lutz B (2006) The endocannabinoid system controls key epileptogenic circuits in the hippocampus. Neuron 51:455-466.

Nadal-Nicolas FM, Jimenez-Lopez M, Sobrado-Calvo P, Nieto-Lopez L, Canovas-Martinez I, Salinas-Navarro M, Vidal-Sanz M, Agudo M (2009) Brn3a as a marker of retinal ganglion cells: qualitative and quantitative time course studies in naive and optic nerve-injured retinas. Invest Ophthalmol Vis Sci 50:3860-3868.

Nag TC, Wadhwa S (2001) Differential expression of syntaxin-1 and synaptophysin in the developing and adult human retina. J Biosci 26:179-191.

Nishikawa S, Tamai M (2001) Muller cells in the human foveal region. Curr Eye Res 22:34-41.

Noyes R, Jr., Brunk SF, Avery DA, Canter AC (1975) The analgesic properties of delta-9-tetrahydrocannabinol and codeine. Clin Pharmacol Ther 18:84-89.

Osterberg G (1935) Topography of the layer of rods and cones in the human retina. Acta Ophtal suppl 6:11-97.

Piomelli D (2003) The molecular logic of endocannabinoid signalling. Nat Rev Neurosci 4:873-884.

Ptito M, Cardu B, Lepore F (1973) Spectral sensitivity in primates: a comparative study. Percept Mot Skills 36:1239-1247.

Riepe RE, Norenburg MD (1977) Müller cell localisation of glutamine synthetase in rat retina. Nature 268:654-655.

Rodríguez de Fonseca F, Del Arco I, Bermudez-Silva FJ, Bilbao A, Cippitelli A, Navarro M (2005) The endocannabinoid system: physiology and pharmacology. Alcohol Alcohol 40:2-14.

Romero J, Hillard CJ, Calero M, Rabano A (2002) Fatty acid amide hydrolase localization in the human central nervous system: an immunohistochemical study. Brain Res Mol Brain Res 100:85-93.

Rosenberg A, Talebi V (2009) The primate retina contains distinct types of Y-like ganglion cells. J Neurosci 29:5048-5050.

Semple DM, Ramsden F, McIntosh AM (2003) Reduced binocular depth inversion in regular cannabis users. Pharmacol Biochem Behav 75:789-793.

Skosnik PD, Krishnan GP, Vohs JL, O'Donnell BF (2006) The effect of cannabis use and gender on the visual steady state evoked potential. Clin Neurophysiol 117:144-156.

Straiker A, Stella N, Piomelli D, Mackie K, Karten HJ, Maguire G (1999a) Cannabinoid CB1 receptors and ligands in vertebrate retina: localization and function of an endogenous signaling system. Proc Natl Acad Sci U S A 96:14565-14570.

Straiker AJ, Maguire G, Mackie K, Lindsey J (1999b) Localization of cannabinoid CB1 receptors in the human anterior eye and retina. Invest Ophthalmol Vis Sci 40:2442-2448.

Suárez J, Bermudez-Silva FJ, Mackie K, Ledent C, Zimmer A, Cravatt BF, de Fonseca FR (2008) Immunohistochemical description of the endogenous cannabinoid system in the rat cerebellum and functionally related nuclei. J Comp Neurol 509:400-421.

Tsou K, Brown S, Sanudo-Pena MC, Mackie K, Walker JM (1998) Immunohistochemical distribution of cannabinoid CB1 receptors in the rat central nervous system. Neuroscience 83:393-411.

Turu G, Hunyady L (2010) Signal transduction of the CB1 cannabinoid receptor. J Mol Endocrinol 44:75-85.

Vitalis T, Laine J, Simon A, Roland A, Leterrier C, Lenkei Z (2008) The type 1 cannabinoid receptor is highly expressed in embryonic cortical projection neurons and negatively regulates neurite growth in vitro. Eur J Neurosci 28:1705-1718.

Wässle H (2004) Parallel processing in the mammalian retina. Nat Rev Neurosci 5:747-757.

Wässle H, Grüunert U, Chun M-N, Boycott BB (1995) The rod pathway of the macaque monkey retina: Identification of AII-amacrine cells with antibodies against calretinin. J Comp Neurol 361:537-551.

Wiedenmann B, Franke WW (1985) Identification and localization of synaptophysin, an integral membrane glycoprotein of Mr 38,000 characteristic of presynaptic vesicles. Cell 41:1017-1028.

Xiang M, Zhou L, Macke JP, Yoshioka T, Hendry SH, Eddy RL, Shows TB, Nathans J (1995) The Brn-3 family of POU-domain factors: primary structure, binding specificity, and expression in subsets of retinal ganglion cells and somatosensory neurons. J Neurosci 15:4762-4785.

Yazulla S (2008) Endocannabinoids in the retina: from marijuana to neuroprotection. Prog Retin Eye Res 27:501-526.

Yazulla S, Studholme KM, McIntosh HH, Deutsch DG (1999) Immunocytochemical localization of cannabinoid CB1 receptor and fatty acid amide hydrolase in rat retina. J Comp Neurol 415:80-90.

Yazulla S, Studholme KM, McIntosh HH, Fan SF (2000) Cannabinoid receptors on goldfish retinal bipolar cells: electron-microscope immunocytochemistry and whole-cell recordings. Vis Neurosci 17:391-401.

Zabouri N, Bouchard JF, Casanova C (2011a) Cannabinoid receptor type 1 expression during postnatal development of the rat retina. J Comp Neurol 519:1258-1280.

Zabouri N, Ptito M, Casanova C, Bouchard JF (2011b) Fatty acid amide hydrolase expression during retinal postnatal development in rats. Neuroscience 195:145-165.

Zimov S, Yazulla S (2007) Vanilloid receptor 1 (TRPV1/VR1) co-localizes with fatty acid amide hydrolase (FAAH) in retinal amacrine cells. Vis Neurosci 24:581-591.

ARTICLE 2: MÜLLER CELLS EXPRESS THE CANNABINOID CB2 RECEPTOR IN THE VERVET MONKEY RETINA

Publié dans :

Bouskila J, Javadi P, Casanova C, Ptito M, Bouchard JF (2013) Muller cells express the cannabinoid CB2 receptor in the vervet monkey retina. J Comp Neurol 521:2399-2415. (cover page)

Müller cells express the cannabinoid CB2 receptor in the vervet monkey retina

Joseph Bouskila[1, 2], Pasha Javadi[1], Christian Casanova[1], Maurice Ptito[1, 3], and Jean-François Bouchard[1]

[1]School of Optometry, University of Montreal, Montreal, QC, Canada
[2]Biomedical Sciences, Faculty of Medicine, University of Montreal, Montreal, QC, Canada
[3]BRAINlab, Department of Neuroscience and Pharmacology, University of Copenhagen, Copenhagen, Denmark

Abbreviated title: CB2R expression in Müller cells

Associate Editor: Ian A. Meinertzhagen

Keywords: Endocannabinoids, CB1R, CB2R, Retinal Glia, Immunofluorescence, Confocal Microscopy

Correspondence should be addressed to:
Jean-François Bouchard, BPharm, PhD
School of Optometry, room 260-7
3744 Jean-Brillant,
University of Montreal,
Montreal, Quebec, Canada, H3T 1P1

Financial Support: The Natural Science and Engineering Research Council of Canada (311892-2010, JFB; 6362-2012, MP; 194670-2009, CC) and the Canadian Institutes of Health Research (MOP-86495, JFB) supported this work. JB holds a scholarship from "Fonds de recherche du Québec - Santé (FRQS)". MP is Harland Sanders Chair professor in Visual Science. JFB is supported by a "Chercheur-Boursier Junior 2" from FRQS.

Abstract

The presence of the cannabinoid receptor type 1 (CB1R) has been largely documented in the rodent and primate retinas in recent years. There is however some controversy concerning the presence of the CB2 receptor (CB2R) within the central nervous system. Only recently, CB2R has been found in the rodent retina, but its presence in the primate retina has not yet been demonstrated. The aim of this study was twofold: 1) to characterize the distribution patterns of CB2R in the monkey retina and compare this distribution to that previously reported for CB1R and 2) to resolve the controversy on the presence of CB2R in the neural component of the retina. We therefore thoroughly examined the cellular localization of CB2R in the vervet monkey (*Chlorocebus sabeus*) retina, using confocal microscopy. Our results demonstrate that CB2R, like CB1R, is present throughout the retinal layers with however striking dissimilarities. Double labeling of CB2R and glutamine synthetase shows that CB2R is restricted to Müller cell processes, extending from the internal limiting membrane with very low staining, to the external limiting membrane with heavy labeling. We conclude that CB2R is indeed present in the retina but exclusively in the retinal glia whereas CB1R is only expressed in the neuro-retina. These results extend our knowledge on the expression and distribution of cannabinoid receptors in the monkey retina, although further experiments are still needed in order to clarify their role in retinal functions.

Introduction

Anandamide (AEA) and 2-arachidonoylglycerol (2-AG) are endocannabinoids (eCBs) that bind to cannabinoid receptors (CB1R and CB2R) to exert their physiological effects (Devane et al., 1992; Mechoulam et al., 1995; Sugiura et al., 1995; Piomelli, 2003). The eCBs are endogenous lipid messengers that are involved in the regulation of many physiological processes in mammals (Di Marzo et al., 2007). They are synthetized on demand and rapidly degraded by enzymes, particularly fatty acid amide hydrolase (FAAH), monoglycerol lipase (MGL) and cyclooxygenase-2 (COX-2) (Cravatt et al., 1996; Dinh et al., 2002; Kozak et al., 2000). The activation of cannabinoid receptors by eCBs leads to cannabis-like effects and CB1R is considered to be the main element responsible of those properties. The eCB system present in the retina likely plays a role in the visual effects of cannabis (Yazulla, 2008 for review). The distribution of CB1R has been well characterized in the retina of rodents and primates (Yazulla et al., 1999; Straiker et al., 1999; Bouskila et al., 2012). It is present in cone pedicles and rod spherules, bipolar cells, amacrine cells, horizontal cells, and ganglion cells. This pattern is also observed in the central and peripheral parts of the monkey retina (Bouskila et al., 2012).

Concerning CB2R, its mRNA was first detected by reverse transcription polymerase chain reaction (RT-PCR) in the adult mouse retina and by *in situ* hybridization in the adult rat retina (Lu et al., 2000) but not in rat embryos (Buckley et al., 1998). Interestingly, using different transcripts, CB2 mRNA was not detected in rat and human retinas (Porcella et al., 1998, 2000). In agreement with Lu et al. (2000), using immunohistochemistry, CB2R protein was localized in rat retinal pigment epithelium, inner photoreceptor segments, horizontal and amacrine cells, cells localized in the ganglion cell layer, and in fibres of inner plexiform layer (López et al., 2011). However, this study did not proceed by double labeling with specific retinal cell markers. Instead, cell types were identified based on the position in the retinal layer and on the morphology of the cells. CB2R expression was found in the trabecular meshwork of the porcine eye, in which an injection of a CB2R agonist increased aqueous humour outflow (Zhong et al., 2005). The presence of both CB1R and CB2R has been reported in human retinal pigment epithelial cells in primary cultures and ARPE-19 cells (Wei et al., 2009). Recently, CB2R expression was found at mRNA levels by RT-PCR and protein by

Western blot analysis in *in vitro* retinal explants and primary cultures of human Müller glia (Krishnan and Chatterjee, 2012).

The human CB2R was cloned first (Munro et al., 1993). Subsequent studies on CB2R expression patterns focused on the presence of CB2R in peripheral tissues of the immune system (Galiègue et al., 1995). Later on, CB2R was cloned in the mouse (Shire et al., 1996) and rat (Griffin et al., 2000). Unlike CB1R, which is highly conserved across mammalian species, sequences of the murine and human CB2R are divergent, raising the possibility of species-specific amino acid sequences. Indeed, CB2R has evolved far more rapidly (McPartland et al., 2007), such that there is only an 81% sequence homology at the amino acid level between the rat and human CB2R, increasing to 87% identity in the critical trans-membrane regions (Griffin et al., 2000). As a result, rodent models may not reliably predict the performance of a CB2R agonist for human CB2 receptors (Mackie, 2008). Consequently, accurate comparisons between human and rodent receptors are crucial considering that cannabinoids vary in their affinity to CB2R depending upon the species (Mukherjee et al., 2004). Our study will fill an important gap in the knowledge of the expression patterns of CB2R in the retina.

The presence of CB2R in neurons has raised an important debate in the scientific community (Atwood and Mackie, 2010). While some are convinced that CB2R is not present in neurons, or at least at very low levels (Atwood and Mackie, 2010), others suggest otherwise (Onaivi et al., 2012). Nevertheless, all agree that CB2R is present in the CNS and could be expressed in its glial elements. Despite the extensive knowledge of the distribution of CB2R in the rodent brain, there are no published reports regarding its expression and localization in the human and monkey retinas. Given that endocannabinoids are present in human ocular tissues especially the retina (Chen et al., 2005), it is reasonable to assume the presence of cannabinoid receptors therein. Therefore, the main objective of this study is to characterize the expression and localization patterns of CB2R throughout the *in vivo* monkey retina.

Materials and Methods

Choice of species. Monkey tissue, the experimental model for the current study, was chosen for several reasons. First monkey tissue allows us to generalize more easily to humans. The anatomical similarity between the monkey and human retina is remarkable. Primates are mammals that have a macular/foveal region and multiple cone types, which offers them high visual acuity and color vision. Finally, the high cross-reactivity between human and monkey antigens increases chances of success for targeting CB2R in monkeys using an anti-human CB2R antibody.

Animal Preparation. Three adult vervet monkeys (*Chlorocebus sabaeus*) were used for this study. Monkey tissues were kindly provided by Professor Roberta Palmour from McGill University, Montreal, Canada. The monkeys were part of Dr. Palmour's and Dr. Ptito's research project that was approved by the McGill University Animal Care and Use Committee. The animals were born and raised in enriched environments in the laboratories of the Behavioural Sciences Foundation (St-Kitts, West Indies) that is recognized by the Canadian Council on Animal Care (CCAC). The animals were fed with primate chow (Harlan Teklad High Protein Monkey Diet; Harlan Teklad, Madison, WI) and fresh local fruits, with water available *ad libitum*. The experimental protocol was reviewed and approved by the local Animal Care and Use Committee and the Institutional Review Board of the Behavioural Science Foundation. Each animal was sedated with ketamine (10 mg/kg, i.m.), deeply anaesthetized with sodium pentobarbital (25 mg/kg, i.v.) and perfused transcardially with phosphate buffer saline (PBS pH 7.4), followed by 4% paraformaldehyde.

Antibody characterization. All the primary antibodies used in this work, their sources and working dilutions, are summarized in Table 1. These antibodies were successfully used in previous studies and are well characterized in regards to the specific primate retinal cell type immunostaining, as described below for each antibody.

Table 1. Primary Antibodies Used in this Study

Antibody[1]	Immunogen	Source[2]	Working dilution
GS	Full protein purified from sheep brain	Chemicon, Temecula, CA, MAB302, Mouse monoclonal, Clone GS-6	H: 1:500
CB	Purified bovine Kidney calbindin-D28K	Sigma-Aldrich, St. Louis, MO, C9848, Mouse monoclonal, Clone CB-955	H: 1:250
PKCα	Peptide mapping the aa 296-317 of human PKCα	Santa Cruz Biotechnology, Santa Cruz, CA, sc-8393, Mouse monoclonal, Clone H-7	H: 1:500
PV	Full protein purified from frog muscle	Sigma-Aldrich, St. Louis, MO, P3088, Mouse monoclonal, Clone PARV-19	H: 1:250
Syntaxin	Synaptosomal plasma fraction of rat hippocampus (Barnstable et al., 1985)	Sigma-Aldrich, St. Louis, MO, S0664, Mouse monoclonal, Clone HPC-1	H: 1:500
Brn-3a	Fusion protein containing aa 186-224 of Brn3a protein	Chemicon, Temecula, CA, MAB1585, Mouse monoclonal	H: 1:100
CB1R	Fusion protein containing aa 1-77 of rat CB1R	Sigma-Aldrich, St. Louis, MO, C1233, Rabbit polyclonal	H: 1:150
CB2R	Synthetic peptide from aa 20-33 of human CB2R	Cayman Chemical, Ann Arbor, MI, 101550, Rabbit polyclonal	H: 1:150 W: 1:500
Kir4.1	Synthetic peptide from the c-terminal region of human Kir4.1	Osenses, Keswick, South Australia, OSP00134W, Goat polyclonal	H: 1:500
GAPDH	The full-length rabbit muscle GAPDH protein	Sigma-Aldrich, St. Louis, MO, G8795, Mouse polyclonal	W: 1:20000

[1]Abbreviations: GS, Glutamine Synthetase; CB, Calbindin; PKCα, Protein Kinase C (α isoform); PV, parvalbumin; CB1R, Cannabinoid Receptor type 1; CB2R, Cannabinoid Receptor type 2; GAPDH, Glyceraldehyde-3-Phosphate Dehydrogenase; aa, amino acids; H, immunohistochemistry; W, Western blot.

[2]The source column indicates the commercial company, catalog reference and origin. The clone designation is given for monoclonal antibodies.

GS. The mouse monoclonal (IgG2a) to glutamine synthetase (GS) was obtained from Chemicon International (Temecula, CA) and directed against GS purified from sheep brain. This antibody generates a single 45 kDa band in immunoblots of adult mammalian brain tissue (manufacturer's data sheet). This antibody labels Müller cells in rat (Riepe and Norenburg, 1977) and monkey retinas (Nishikawa and Tamai, 2001; Bouskila et al., 2012).

Calbindin. The mouse monoclonal (IgG1) to calbindin (CB) was obtained from Sigma (St. Louis, MO) and directed against purified bovine kidney Calbindin-D-28K. This antibody recognizes a 28 kDa band on Western Blots (manufacturer's data sheet). The calbindin antibody labels cones outside the foveal region, cone bipolar cells and a subset of horizontal

cells in human and monkey retinas (Chiquet et al., 2002; Fischer et al., 2001; Kolb et al., 2002; Martínez-Navarrete et al., 2007; Martínez-Navarrete et al., 2008; Bouskila et al., 2012).

PKC. The mouse monoclonal (IgG2a) to protein kinase C (PKC) was developed by Santa Cruz Biotechnology (Santa Cruz, CA) by using as immunogen purified bovine PKC and its epitope is mapped to its hinge region (amino acids 296–317). It detects the PKCα isoform, a well-known specific marker for rod bipolar cells (Mills and Massey, 1999). As stated by the manufacturer, this antibody gives a single band of 80 kDa on Western blots of human cell lines, and has been previously used for immunohistochemistry on rodent (Zabouri et al., 2011a; Zabouri et al., 2011b) and monkey (Cuenca et al., 2005; Martínez-Navarrete et al., 2008; Bouskila et al., 2012) retinas.

PV. The mouse monoclonal (IgG1) to parvalbumin (PV) was obtained from Sigma (St. Louis, MO) by using as immunogen purified frog muscle PV. It recognizes a 12 kDa band from human, bovine, pig, canine, feline, rabbit, rat, and fish tissues (manufacturer's technical information). The pattern of labeling with this antibody was the same as reported previously (Kolb et al., 2002; Bordt et al., 2006). This small calcium-binding protein is expressed in the primate retina by horizontal cells (Wässle et al., 2000) and the antiserum has been used to visualize monkey thalamic nuclei (Qi et al., 2011).

Syntaxin. The mouse monoclonal (IgG1) to syntaxin (clone HPC-1) was developed by Barnstable et al. (1985) and is distributed by Sigma (St. Louis, MO). This antibody recognizes syntaxin-1, a 35 kDa protein, from hippocampal, retinal and cortical neurons (Inoue et al., 1992). This antibody labels horizontal cells and amacrine cells, in the developing and adult human retina (Nag and Wadhwa, 2001). The staining pattern obtained in the current study was similar to that found in human retina (Nag and Wadhwa, 2001). We have used this antibody to label monkey retinal amacrine and horizontal cells (Bouskila et al., 2012).

Brn3a. The mouse monoclonal (IgG1) to Brn3a was obtained from Chemicon International (Temecula, CA) and made against amino acids 186-224 of Brn3a fused to the T7 gene 10 protein. The Brn3a antibody shows no reactivity to Brn3b or Brn3c by western blot and no reactivity to Brn3a knockout mice (manufacturer's technical information). Its specificity for

rodent (Nadal-Nicolás et al., 2009) and monkey (Xiang et al., 1995) retinal ganglion cells has been documented. We used the POU-domain transcription factor Brn3a to label the nuclei of retinal ganglion cells (Bouskila et al., 2012).

CB1R. The rabbit anti-CB1R was obtained from Sigma (St. Louis, MO). It was developed by using a highly purified fusion protein containing the first 77 amino acid residues of the rat CB1R as the immunogen. It recognizes a major band of 60 kDa and less intense bands of 23, 72, and 180 kDa (manufacturer's data sheet, C1233). This antibody targets the rat CB1R (Zabouri et al., 2011a) but specifically recognizes the CB1R (60 kDa) from many species (manufacturer's data sheet), including vervet monkey retinal tissue (Bouskila et al., 2012).

CB2R. The rabbit anti-CB2R was obtained from Cayman Chemical (Ann Arbor, MI). It was developed by using a synthetic peptide corresponding to the amino acids 20-33 (NPMKDYMILSGPQK) of the human CB2R sequence conjugated to KLH as immunogen. This antibody recognizes a band at 45 kDa and a band at 39-40 kDa (manufacturer's data sheet, 101550). This antibody was used in human nervous tissues (Ellert-Miklaszewska et al., 2007; Zurolo et al., 2010). Its specificity to CB2R was recently validated in CB2R knockout mice retinal tissue. CB2R immunohistochemistry signal present in CB2R wild-type mice was completely absent in their knockout littermates (Argaw et al., 2011).

GAPDH. The mouse monoclonal (IgM) to GAPDH (GlycerAldehyde-3-Phosphate DeHydrogenase, clone GAPDH-71.1) was obtained from Sigma (St. Louis, MO) by using as immunogen purified rabbit muscle GAPDH (whole molecule). As stated by the manufacturer, this antibody recognizes monkey GAPDH and gives a single band at about 37 kDa.

Kir4.1. The goat polyclonal anti-Kir4.1 antibody was purchased from Osenses (Keswick, South Australia). This antibody was raised against a synthetic peptide corresponding to amino acids 352-368 (PEKLKLEESLREQAEKE) of human KCNJ10 (Kir4.1) conjugated to an immunogenic carrier protein and gives a single band at about 37 kDa in Western Blot. The peptide is homologous in mouse and rat and was predicted to react in rat, mouse and human tissues (manufacturer's technical information, cat. #OSP00134W). It has been characterized

by immunoblot and immunostaining of HEK cells transfected with Kir4.1 and used to target the Kir4.1 in mouse cortical astrocytes (Li et al., 2001).

CB2R blocking peptide. The CB2R blocking peptide containing the human CB2R amino acid sequence 20-33 (NPMKDYMILSGPQK; Cayman Chemical; catalog number 301550) was used in the present study for immunohistochemistry and western blot analysis. The specificity of the CB2R antibody was also tested by preincubation with the corresponding blocking peptide. For preadsorption, the primary antibody was diluted in PBS and incubated with a ratio 1:1 for 2 hours at room temperature with occasional inversion. Thereafter, the antibody-blocking peptide solution was added to the slices and subsequent immunohistochemistry followed the protocol as described further.

Tissue preparation. The eyes were extracted and the retina was dissected free from the eyecup in a PBS bath. The retina was laid flat so that the vitreous body could be removed by blotting with filter paper and gentle brushing (Burke et al., 2009). Samples of retina (4 mm^2) were taken from the center (radius of 4 mm around the fovea), middle (radius of 10 mm around the fovea) and periphery (radius of 20 mm around the fovea), along with the fovea. Each sample was cryoprotected in 30% sucrose overnight and embedded in Shandon embedding media at -65°C. Retinal samples were sectioned in a cryostat (18 µm) and mounted onto gelatinized glass microscope slides, air-dried and stored at -20°C.

Western blotting. In order to test the specificity of the CB2R antisera, Western blots were performed on monkey tissue. A fresh dissected sample of retina, visual cortex or cerebellum was homogenized by hand by using a sterile pestle in RIPA buffer (150 mM NaCl, 20 mM Tris, pH 8.0, 1%, NP-40 (USB Corp., Cleveland, OH, USA), 0.1% SDS, 1 mM EDTA), supplemented with a protease-inhibitor mixture (aprotinin (1:1,000), leupeptin (1:1,000), pepstatin (1:1,000) and phenylmethylsulfonyl fluoride (0.2 mg/ml); Roche Applied Science, Laval, QC, Canada). Samples were centrifuged at 4°C for 10 minutes, and the supernatant was extracted and stored at -20°C until further processing. Protein content was equalized by using a Thermo Scientific Pierce BCA Protein Assay Kit (Fisher Scientific, Ottawa, ON, Canada). Thirty micrograms of protein/sample of the homogenate was resolved with 10% sodium

dodecyl sulfate (SDS)-polyacrylamide gel electrophoresis, transferred onto a nitrocellulose membrane filter (BioTrace NT, Life Sciences, Pall, Pensacola, FL), blocked for 1 hour in 5% skim milk (Carnation, Markham, ON, Canada) in TBST (0.15 M NaCl, 25 mM Tris-HCl, 25 mM Tris, 0.5% Tween- 20), and incubated overnight with the primary antibody, namely, rabbit anti-CB2R (1:500) in blocking solution. The following day, the blot was exposed to a secondary antibody conjugated to horseradish peroxidase (1:5,000; Jackson ImmunoResearch, West Grove, PA) in blocking solution for 2 hours. Detection was carried out by using homemade ECL Western blotting detection reagents (final concentrations: 2.50 mM luminol, 0.4 mM p-coumaric acid, 0.1 M Tris-HCl pH 8.5, 0.018% H_2O_2). The membrane was then air-stripped, reblocked, and exposed to a second primary antibody, namely mouse anti-GAPDH (1:20,000), until all proteins of interest were tested. Densitometric analysis was performed by using ImageJ software (Version 1.45; http://rsb.info.nih.gov/ij/) on scanned films.

Immunohistochemistry. Single, double and triple labeling of the retina were performed according to previously published methods (Bouskila et al., 2012). Briefly, sections were postfixed for 5 minutes in 70% ethanol, rinsed 3 x 5 minutes in 0.1 M Tris buffer, pH 7.4/0.03% Triton and blocked for 90 minutes in 10% normal goat serum (NDS) in 0.1 M Tris buffer/0.5% Triton. Sections were incubated overnight at room temperature with primary antibody in blocking solution. The CB2R antibody was used conjointly with a known retinal cell type marker: calbindin, PKCα, syntaxin, Brn3a, or glutamine synthetase (Table 1). The next day, sections were washed for 10 minutes and 2 x 5 minutes in 0.1 M Tris /0.03% Triton, blocked in 10% NDS, 0.1 M Tris /0.5% Triton for 30 minutes and incubated with secondary antibody for 1 hour: Alexa 488 donkey anti-mouse, Alexa 488 donkey anti-goat, Alexa 555 donkey anti-mouse or biotinylated donkey anti-rabbit followed by the addition of streptavidin-Alexa 647 (1:200), all in a blocking solution as described above. Sections were washed again in Tris buffer, counterstained with bisbenzimide (Hoechst 33258, Sigma, 2.5 μg/mL), a fluorescent nuclear marker, and coverslipped with Fluoromount-G™ Mounting Medium (SouthernBiotech, Birmingham, AL).

Sequential labeling of CB1R and CB2R. The CB1R and CB2R antibodies that we selected came from the same host, making the use of simultaneous double-labeling protocol not

adequate. To circumvent this problem, we used a sequential protocol previously described by our research group (Zabouri et al., 2011a; Zabouri et al., 2011b; Bouskila et al., 2012). Briefly, the sections were labeled in a serial manner. The exposition to the first primary antibody was conducted as described above, followed by incubation of a goat anti-Fab fragment solution (Jackson ImmunoResearch Laboratories, West Grove, PA); Brandon, 1985). This allowed for the tagging of the first primary antibody as goat rather than rabbit. The sections were revealed with a secondary Alexa donkey anti-goat 488. Thereafter, they were exposed to a second primary antibody overnight and revealed the following day with an Alexa donkey anti-rabbit 647. The validity of the sequential staining was then verified for CB1R/CB2R co-labeling with the following two controls: (1) omission of the second primary antibody resulted in a strong staining with the goat secondary 488 but no staining with rabbit secondary 647; (2) omission of the first secondary and second primary antibodies revealed faint signal for the goat secondary 488 and no signal for the rabbit secondary 647.

Confocal microscopy. Fluorescence was detected with a Leica TCS SP2 confocal laser-scanning microscope (Leica Microsystems, Exton, PA), using a 40X (n.a.: 1.25 – 0.75) or a 100X (n.a.: 1.40 – 0.7) objective. Images were obtained sequentially from the green and far-red channels on optical slices of less than 0.9 µm of thickness. Throughout the *Results* section, images taken from the green channel correspond to the retinal cell markers and from the far-red channel to CB2R. When co-expression of CB2R and retinal cell markers was ambiguous in some retinal layers, co-labeling or its absence was demonstrated by taking z-stacks with optimized steps. This allowed for visualization of the cells in the X-Y, X-Z and Y-Z axes, thereby confirming the presence or absence of CB2R in the cells. All photomicrograph adjustments, including size, color, brightness, and contrast were done with Adobe Photoshop (CS5, Adobe Systems, San Jose, CA) and then exported to Adobe InDesign (CS5, Adobe Systems, San Jose, CA), where the final figure layout was completed. The schematic panels of Figure 9 were created using Adobe Illustrator (CS5, Adobe Systems, San Jose, CA).

Results

CB2R antibody specificity. Immunoblots of CB2R antisera in homogenates of fresh vervet monkey retina, visual cortex, and cerebellum (Figure 1A) showed one intense band at 45 kDa for each homogenate. Pre-incubation with CB2R blocking peptide completely abolished antibody signal (Figure 1B). The same blot was reprobed using the GAPDH antibody (37 kDa) to ensure the proper equalization and loading of all samples (Figure 1A and 1B, lower panels). As an added control, the CB2R antibody was preadsorbed with its blocking peptide prior to incubation with retinal sections, resulting in an absence of staining signal in the section (Figure 1D, see CB2R blocking peptide paragraph in the Materials and Methods section). Furthermore, the CB2R knock out mice validated the specificity of anti-CB2R by elimination of the immunolabeling (Argaw et al., 2011). CB2R-immunoreactivity (IR) was present throughout the monkey retina, extending from the fovea centralis to the periphery and from the external limiting membrane to some cell bodies of the inner nuclear layer (Figure 1C). CB2R was densely expressed in the Henle Fiber layer (Figure 1C), comprising the cone photoreceptor oblique axons with accompanying Müller glial cell processes and forming a pale-staining fibrous-looking area not seen in the peripheral retina (Figure 3H).

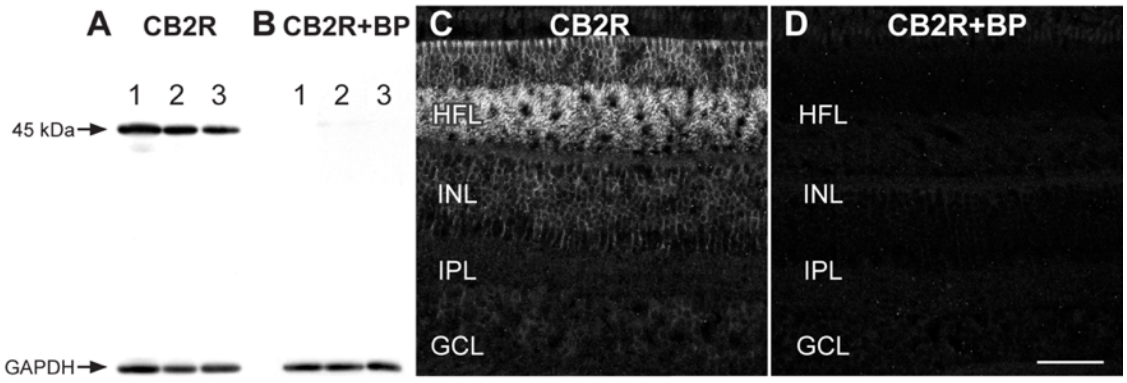

Figure 1. Characterization of CB2R antibody in the vervet monkey. Western blot analysis of total protein samples from retina (**A – lane 1**), visual cortex (**A – lane 2**) and cerebellum (**A – lane 3**) showing detection of one heavy protein band at 45 kDa. The band was not detected when the antibody was pre-incubated with the corresponding CB2R blocking peptide (BP) (**B – lanes 1-3**). All lanes contained 10 μg of total protein. The lower blots for CB2R and CB2R-BP show the expression of the protein GAPDH and demonstrates loading in all lanes. Immunohistochemistry on vervet retinal tissue with the anti-CB2R antibody revealed a unique

staining profile (**C**). When the CB2R antibody was pre-incubated with its BP, it revealed an absence of staining (**D**). HFL, Henle fiber layer; INL, inner nuclear layer; IPL, inner plexiform layer; GCL, ganglion cell layer. Scale bar = 75 μm.

CB2R immunoreactivity throughout the monkey retina. The expression pattern of CB2R near the fovea and in the peripheral retina seems different on visual examination, but this is misleading, because Müller cells have different morphological characteristics in the central and peripheral retina (Distler and Dreher, 1996). If one looks at the pattern of Müller cell processes, CB2R distributions are rather similar. The strongest CB2R signal is localized in the Henle fiber layer with generally weaker signals in the inner retina (Figure 2).

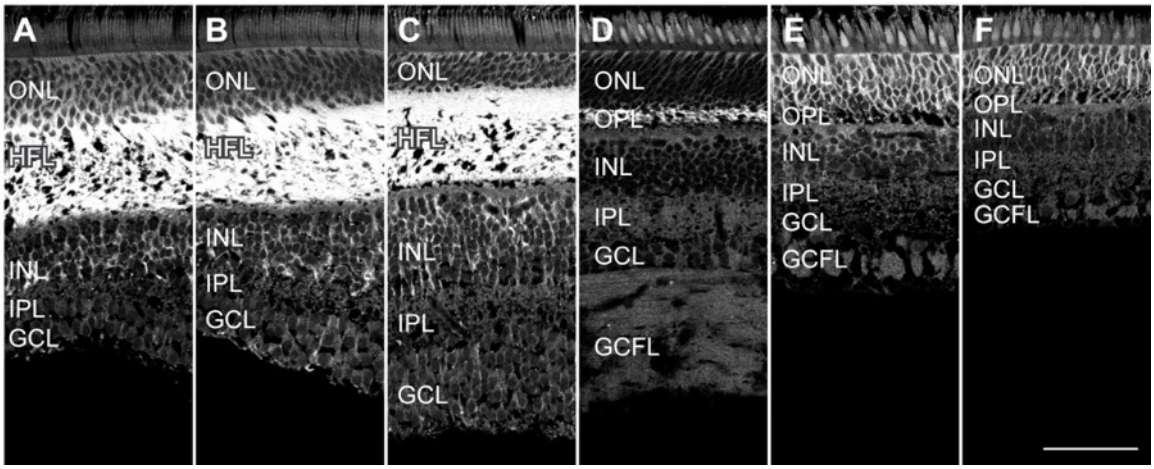

Figure 2. Labeling pattern of CB2R-IR throughout the monkey retina. Confocal micrographs taken from the fovea (**A**), and from 1 mm (**B**), 2 mm (**C**), 5 mm (**D**), 10 mm (**E**), 20 mm (**F**) of the fovea. Note that the most prominent staining of CB2R is located in the Henle fiber layer present in samples of central retina. ONL, outer nuclear layer; HFL, Henle fiber layer; OPL, outer plexiform layer; INL, inner nuclear layer; IPL, inner plexiform layer; GCL, ganglion cell layer; GCFL, ganglion cell fiber layer. Scale bar = 75 μm.

Double-label immunohistochemistry. In order to verify the retinal cell type expression, double immunostaining was carried out for CB2R and a specific molecular marker for primate retinal cells. A consistent staining pattern across all three monkey retinas was found for each double staining. Although labeling was located in all distal layers of the retina, from the photoreceptor to the inner nuclear layers, CB2R-IR was most prominent in the Henle Fiber layer within the central retina (Figures 3, 5, 6, 9).

Cellular distribution of CB2R

CB2R is present in Müller cells. The extensive CB2R-immunoreactive fibers along the external limiting membrane were suggestive of Müller cells (Figure 3A-C). This hypothesis was tested by double-labeling CB2R-IR with GS-IR, which labels Müller cells in the mammalian retina, including vervet monkey retina (Riepe and Norenburg, 1977; Bouskila et al., 2012). All fibers that were GS-immunoreactive were also double labeled for CB2R-IR in the central retina (Figure 3D-F) and in the middle retina (Figure 3G-I). This included all the Müller cell fibers but not Müller cell bodies (Figure 3A-C). Most prominent staining was found in the distal retina with only faint staining in the proximal retina. On occasion, some GS-immunoreactive proximal fibers were not CB2R-immunoreactive. Villous processes extending beyond the external limiting membrane (arrows) did not co-localize with CB2R-IR.

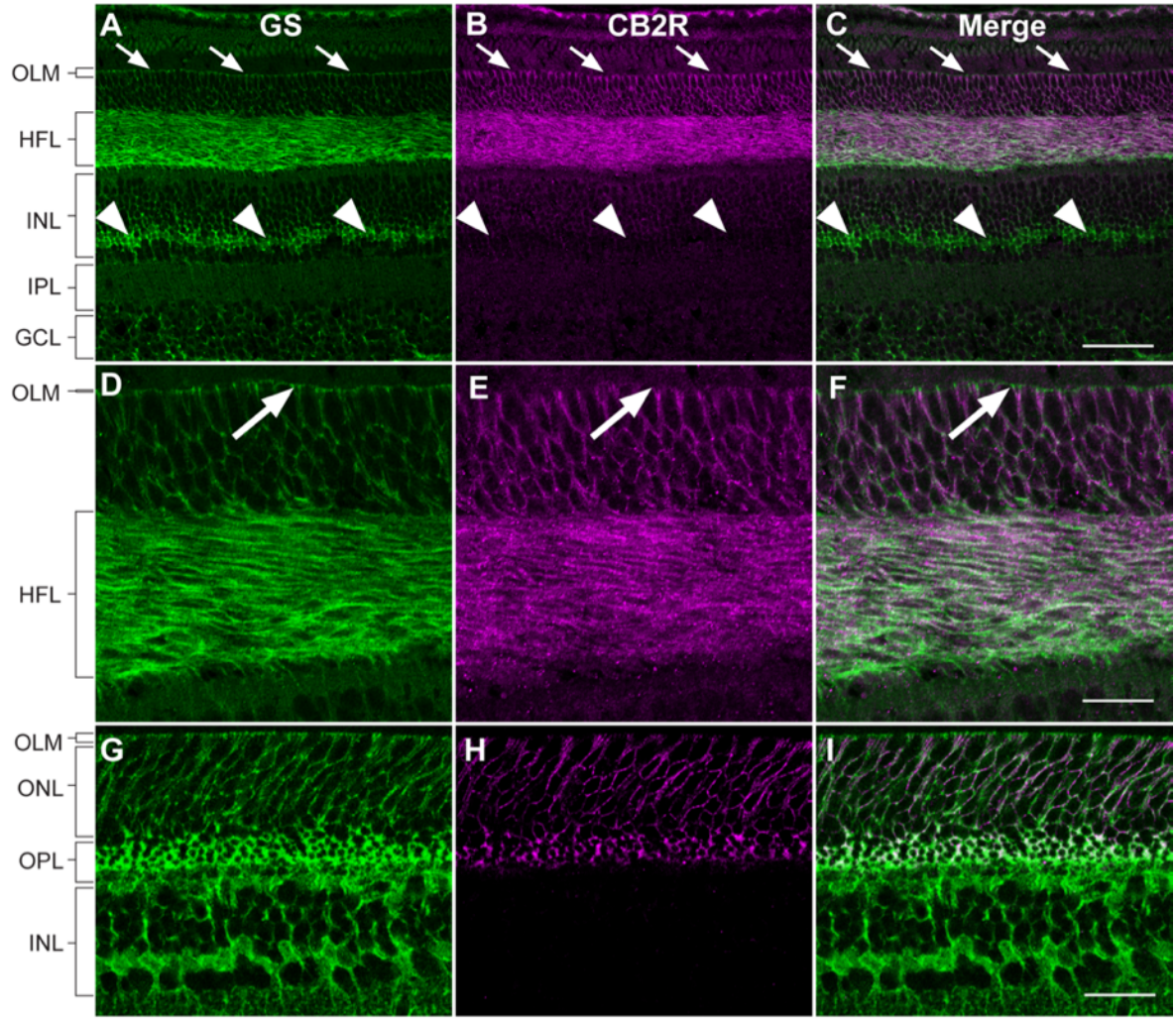

Figure 3. CB2R co-localizes extensively with glutamine synthetase-labeled Müller cells in the monkey retina. **A-I**: Vertical sections taken near the fovea (**A-F**) and in the middle retina (**G-I**). Confocal micrographs of retinas co-immunolabeled for CB2R and glutamine synthetase (GS), a cell type specific marker for Müller cells. Each protein is presented alone in gray scale in the first columns. The merge image is presented in the last column (GS in green and CB2R in magenta). Arrows indicate the projections of the Müller cell membrane in the apical margin known as apical villi that lack CB2R. Arrowheads point at Müller cell bodies that do not express CB2R. **D-F**: Higher magnification views of the outer limiting membrane (OLM) demonstrate the absence CB2R/GS double labeling in the Müller cell villi. OLM, outer limiting membrane; HFL, Henle fiber layer; INL, inner nuclear layer; IPL, inner plexiform layer; GCL, ganglion cell layer. Scale bar = 75 μm for **A-C**, and 30 μm for **D-I**.

No expression of CB2R in cones. Because the Henle fiber layer comprises densely packed oblique cone photoreceptor axons with accompanying Müller cell processes, CB2R and calbindin co-localization was needed to rule out the possibility that CB2R was present in cones. Given that CB labels cones outside the foveola, a central (Figure 4A-C) and middle (Figure 4D-F) retinal samples were taken to perform co-localization with CB2R and CB. Although the patterns of CB2R-IR throughout the ONL and OPL appeared very similar to those of GS-IR, it was not clear from an overlay projection presented in Figure 4 that CB2R-IR is truly adjacent to cone axons. A flattened Z-series indicated that CB2R-IR in the ONL was due exclusively to fibers of the Müller cells and do not include cone axons (Figure 4G). In order to further corroborate the localization of CB2R in GS-positive fibers, but not in CB-positive axons, confocal optical sections, were investigated in the X-Z and Y-Z projections. The X-Z and Y-Z images were drawn through the point of double-labeling between CB-IR and CB2R-IR, and the two orthogonal views clearly show no overlap (Figure 4H).

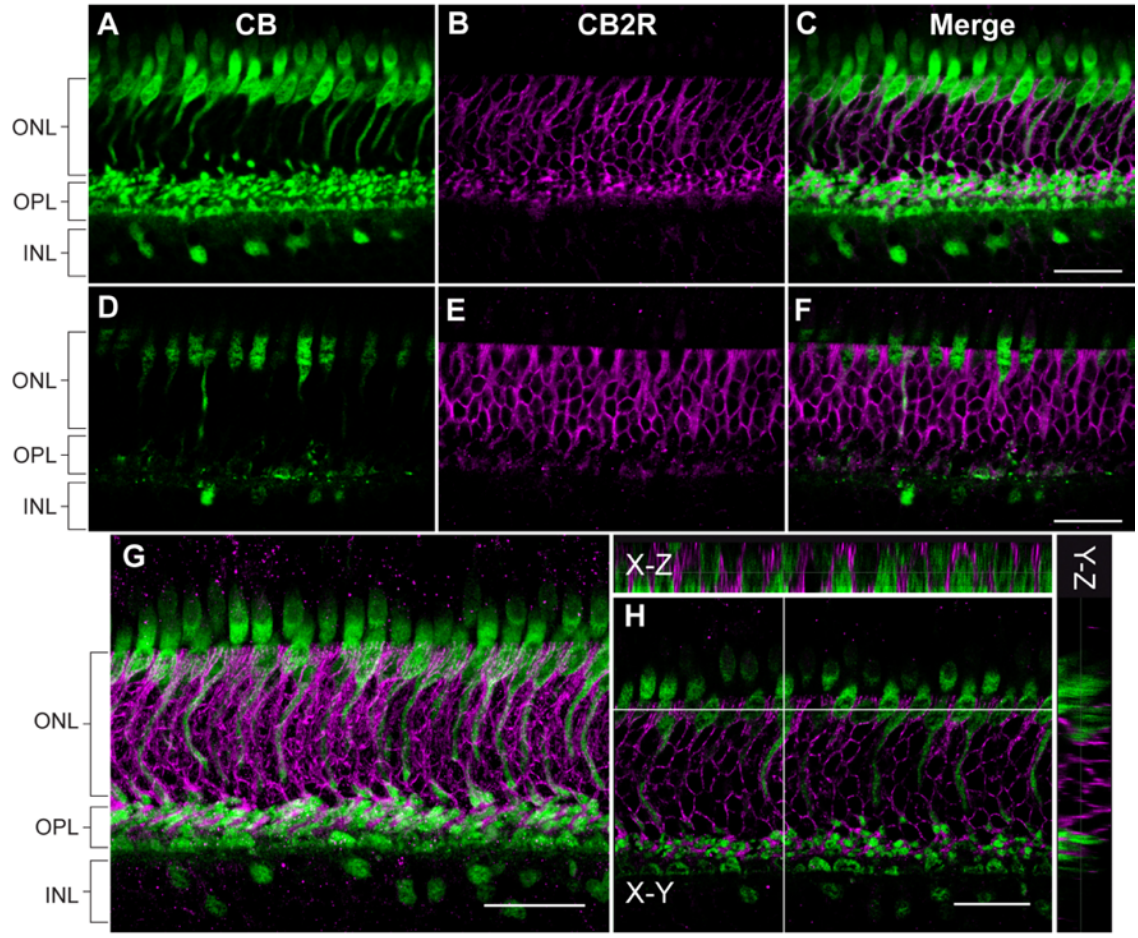

Figure 4. Double-label immunofluorescence illustrating localization of calbindin (CB) and CB2R. **A-C**: Calbindin-IR labeled cone photoreceptors in the monkey central retina, and these were not CB2R immunoreactive. Note that CB2R-IR appears co-localized in the ONL, but a flattened Z-series (**G**) and a 3D reconstruction in the X-Z and Y-Z axes showed no co-localization (**H**). CB2R-IR was not present throughout cones outside of the central region, as illustrated in the overlay of the two micrographs (**D-F**). This overlay clearly shows that the CB2R-immunoreactive outer processes were neighboring to the CB-immunoreactive cone photoreceptors. ONL, outer nuclear layer; OPL, outer plexiform layer; INL, inner nuclear layer. Scale bar = 75 μm.

CB2R is not present in rod bipolar cells. Occasionally, there were CB2R-immunoreactive cell fibers in the proximal INL that looked like PKC-immunoreactive rod bipolar cell axons in the central retina (Figure 5A-C) and peripheral retina (Figure 5D-F). No PKC-immunoreactive

rod bipolar cell, including its cell body, axon and axon terminal, was co-localized with CB2R-IR, confirming that CB2R-IR was not present in rod bipolar cells.

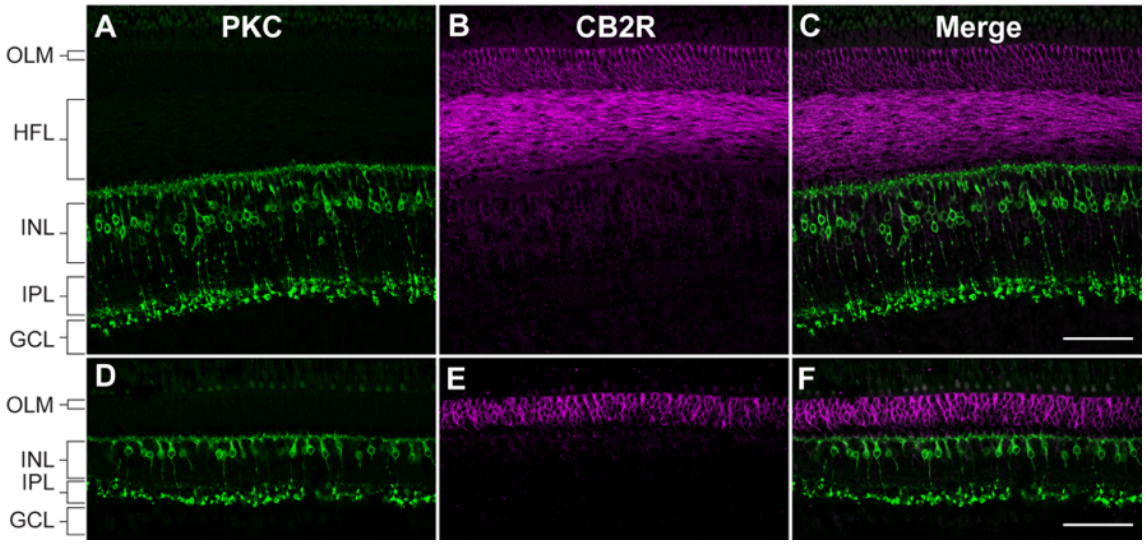

Figure 5. Double-label immunofluorescence illustrating the localization of PKC and CB2R. **A-F**: Vertical sections showing PKC-positive fibers representing rod bipolar cell axons that appear co-localized near the fovea (**A-B**) and in the middle retina (**D-F**). CB2R-IR followed the Müller cell processes insinuating themselves between cell bodies of the neurons in the inner nuclear layer. No PKC-immunoreactive cell was CB2R-immunoreactive. OLM, outer limiting membrane; HFL, Henle fiber layer; INL, inner nuclear layer; IPL, inner plexiform layer; GCL, ganglion cell layer. Scale bar = 75 μm.

Horizontal cells do not express CB2R. CB2R-IR did not co-localize with PV-IR in the central retina (Figure 6A-C) and peripheral retina (Figure 6D-F) indicating that horizontal cells were not CB2R-immunoreactive. The PV-IR is classically associated with equal staining of 2 morphological types of horizontal cells in the primate retina (arrows), H1 and H2 horizontal cells (Röhrenbeck et al., 1987), and no clear co-localization was found in any horizontal cells of the vervet monkey retina (Figure 6A-F).

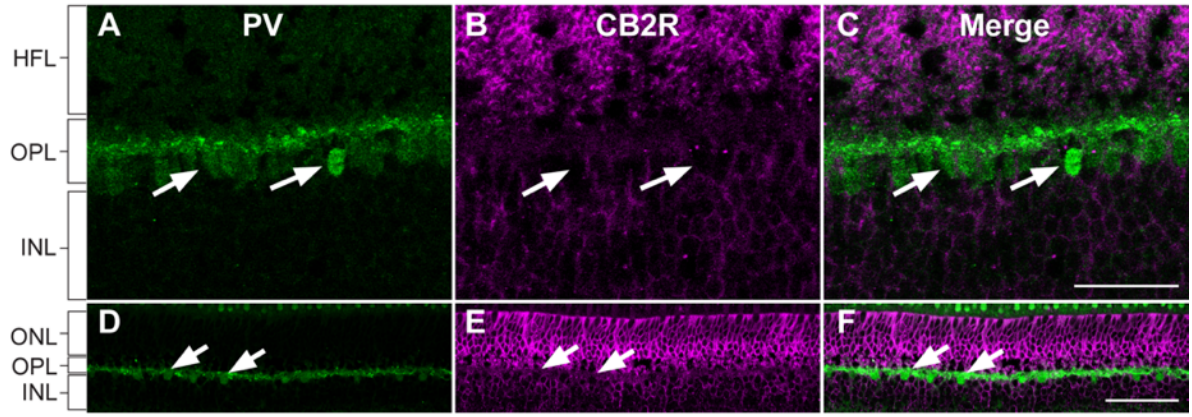

Figure 6. Localization of parvalbumin (PV) and CB2R within the central and peripheral retina. Note that the CB2R labeling (magenta) is not located within PV-immunoreactive horizontal cell somata and processes (green). High-magnification images of PV, CB2R, and merged views, respectively in the central retina (**A-C**) and in the middle retina (**D-F**). Occasional CB2R-immunoreactive fibers in the OPL surround the horizontal cell somata (arrows). HFL, Henle fiber layer; ONL, outer nuclear layer; OPL, outer plexiform layer; INL, inner nuclear layer. Scale bar = 37.5 μm for **A-C** and 75 μm for **D-F**.

CB2R is not present in amacrine cells. The monoclonal antibody HPC-1 that recognizes syntaxin in horitzontal and amacrine cells was used to evaluate CB2R-IR expression in amacrine cells (Figure 7A-C). Despite variations in intensity of immunolabeling, virtually no amacrine cells showed expression of CB2R-IR in the central retina (Figure 7D-F) or the middle retina (Figure 7G-I). Although there was no visible expression of CB2R in horizontal cells (arrows) and amacrine cells (arrowheads), the staining found in the layers of horizontal and amacrine cells was limited to the Müller cell processes (Figure 7B and 7E).

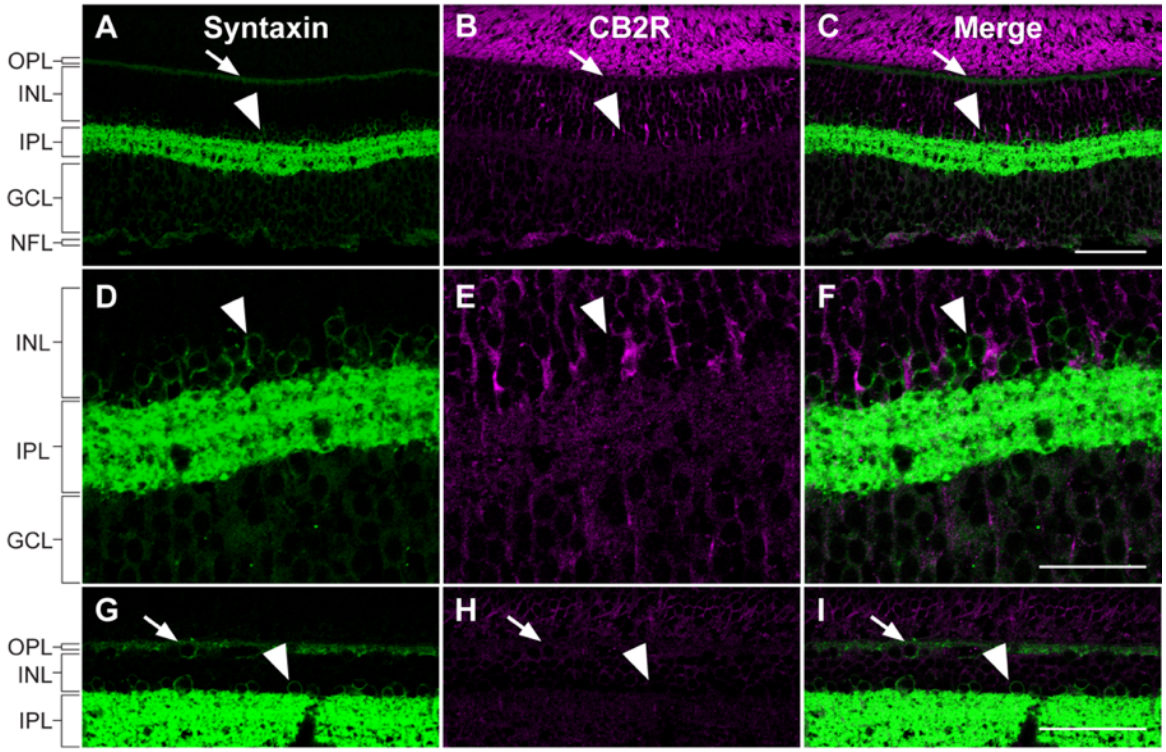

Figure 7. Double-label immunofluorescence illustrating the localization of syntaxin (green) and CB2R (magenta) in the monkey retina. **A-C**: Syntaxin-immunoreactive horizontal (arrows) and amacrine cells (arrowheads) were clearly not labeled with CB2R in the central retina. **D-F**: Higher magnification of syntaxin-IR and CB2R-IR in the central retina. **G-I**: Syntaxin-IR and CB2R-IR in the middle retina. Syntaxin-IR labeled heavily the membrane of horizontal cells in the OPL but lightly their cytosol, and also labeled heavily the membrane of amacrine cells and IPL but lightly their cytosol. OPL, outer plexiform layer; INL, inner nuclear layer; IPL, inner plexiform layer; GCL, ganglion cell layer; NFL, nerve fiber layer. Scale bar = 75 μm for **A-C** and **G-I**, and 37.5 μm for **D-F**.

CB2R is absent in ganglion cells. Brn3a immunoreactivity specifically labels retinal ganglion cell nuclei. CB2R-IR was not detected in ganglion cell bodies (arrowheads) either in the central (Figure 8A-C) or middle retina (Figure 8D-F). Displaced Brn3a-positive cells located in the IPL were not CB2R-immunoreactive (arrows). Double-labeling Brn3a/CB2R showed that CB2R was not expressed in ganglion cells.

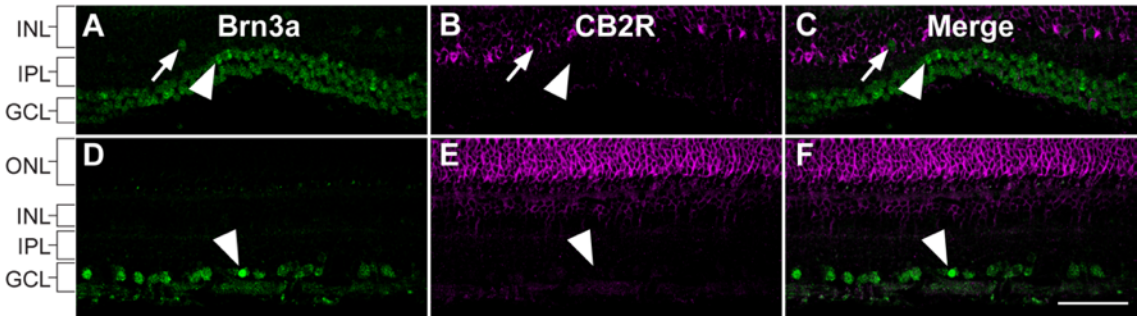

Figure 8. Double-label immunofluorescence illustrating localization of CB2R (magenta) and Brn3a (green) in the central retina (**A-C**) and in the middle retina (**D-F**). The antibody against Brn3a labels the nucleus of ganglion cells in the monkey retina and these cells were not CB2R immunoreactive. The occasional labeling of CB2R in the ganglion cell layer was localized in the Müller cells inner processes. Arrows point at Brn3a positive cell that is not localized in the GCL and arrowheads indicate Brn3a positive ganglion cells that are not CB2R-immunoreactive. ONL, outer nuclear layer; INL, inner nuclear layer; IPL, inner plexiform layer; GCL, ganglion cell layer. Scale bar = 75 µm.

Differential CB1R and CB2R labeling. Double-labeling of CB1R-IR and CB2R-IR was performed in a retinal sample of 2 mm eccentricity from the fovea (Figure 9A-C) and of 6 mm eccentricity from the fovea (Figure 9J-L) to differentiate the localization of these cannabinoid receptors. There was no large overlap in the expression of these two receptors in the ONL, INL, IPL, and GCL, but apparent overlap in the HFL. Detailed analysis of the expression of CB1R for each cell type has been previously characterized (Bouskila et al., 2012) and precise expression of CB2R is presented in Figures 3-8. Note that for the most part, CB1R expression is found throughout the retinal neurons of the monkey retina and CB2R in the retinal Müller cells. In order to distinguish CB1R-IR from CB2R-IR in the HFL, a 6 mm eccentricity sample of the monkey retina was taken, as the HFL is only present in the central retina close to the fovea. Figure 9A-C shows immunostaining for the complete protocol where strong signals for both CB1R (Figure 9A) and CB2R (Figure 9B) can be seen. Figure 9D-F illustrates the first control in which the second primary antibody was omitted: a clear signal for CB1R (Figure 9D) whereas no staining for CB2R (Figure 9E). Figure 9G-I presents the results for the second control where the first secondary and second primary antibodies were omitted: no staining for

CB1R (Figure 9G) and CB2R (Figure 9H). Figure 9J-L clearly shows no co-localization of CB1R (Figure 9J) and CB2R (Figure 9K) in the outer retina. Arrowheads follow a CB1R-positive cone cell body and axon; note that CB2R-positive Müller cell processes envelop this cone. These data are summarized in Figure 10A for all retinal cell types.

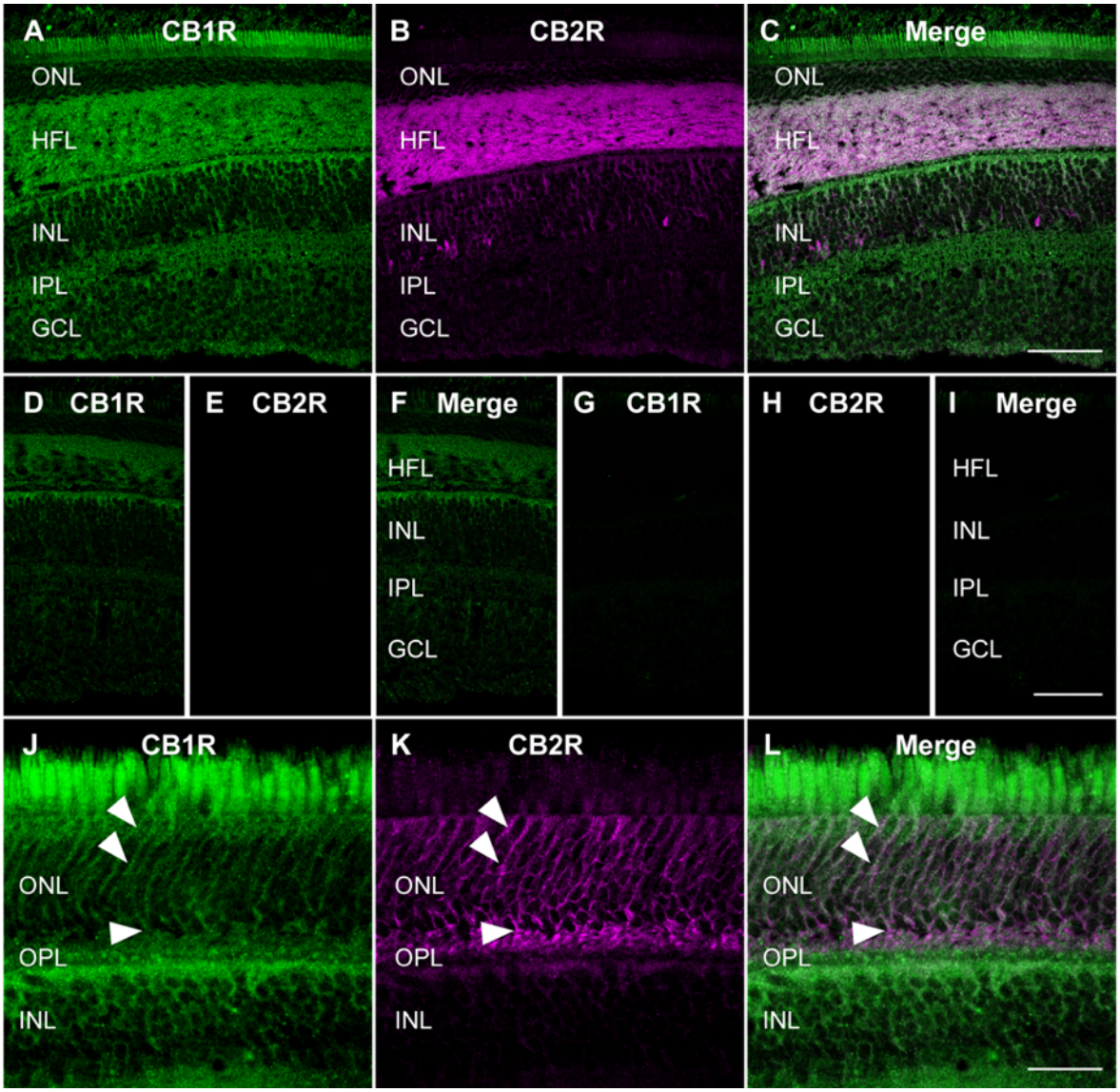

Figure 9. Comparison of CB1R and CB2R retinal expressions. Confocal micrographs of retinas co-immunolabeled for CB1R (green) and CB2R (magenta). CB1R (**A, D, G, J**), CB2R (**B, E, H, K**) signals, and their overlay (**C, F, I, L**). **A-C**: Complete sequential protocol in the central retina. **D–F**: The second primary antibody was omitted. **G–I**: The first secondary and second primary antibodies were lacking. **J-L**: Localization of CB1R and CB2R in the outer retina. Arrowheads follow a CB1R-positive cone cell body and axon, and CB2R-positive

Müller cells processes that enroll this cone. ONL, outer nuclear layer; HFL, Henle fiber layer; INL, inner nuclear layer; IPL, inner plexiform layer; GCL, ganglion cell layer. Scale bar = 75 µm.

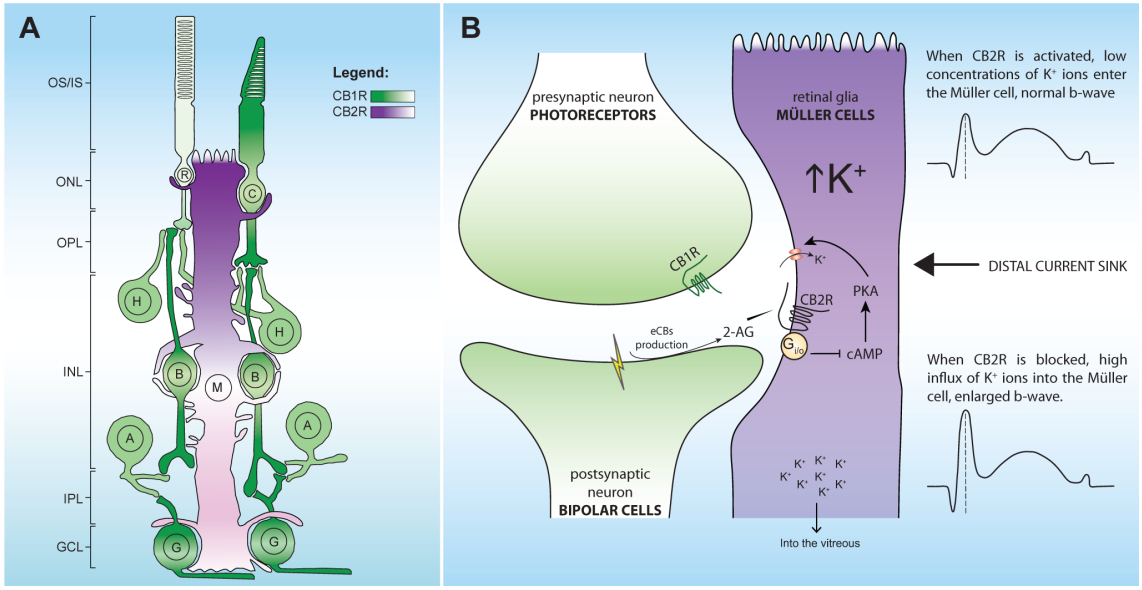

Figure 10. Schematic illustration representing the localization of the principal cannabinoid receptors (**A**) and a hypothetical function for CB2R (**B**) in the monkey retina. CB1R is localized in neural components and CB2R in glial components (Müller cells). Color bars in the legend indicate the intensity of CB1R (green) and CB2R (magenta) expressions. OS/IS, outer and inner segments of rods and cones; ONL, outer nuclear layer; OPL, outer plexiform layer; INL, inner nuclear layer; IPL, inner plexiform layer; GCL, ganglion cell layer; C, cones; R, rods; H, horizontal cells; B, bipolar cells; A, amacrine cells; G, retinal ganglion cells; M, Müller cells.

Triple labeling of CB2R, GS, and Kir4.1. Triple immunofluorescent labeling was performed in order to verify if potassium channels co-localize with CB2R in Müller cells. Expression of Kir4.1 was found in CB2R positive and GS positive Müller cells of the central retina. Co-expression of CB2R and Kir4.1 was found in the HFL but scarcely in the proximal parts of Müller cells (Figure 11A-D). There was a large overlap in the expression of GS and Kir4.1 in the INL, IPL, and GCL (Figure 11E-L).

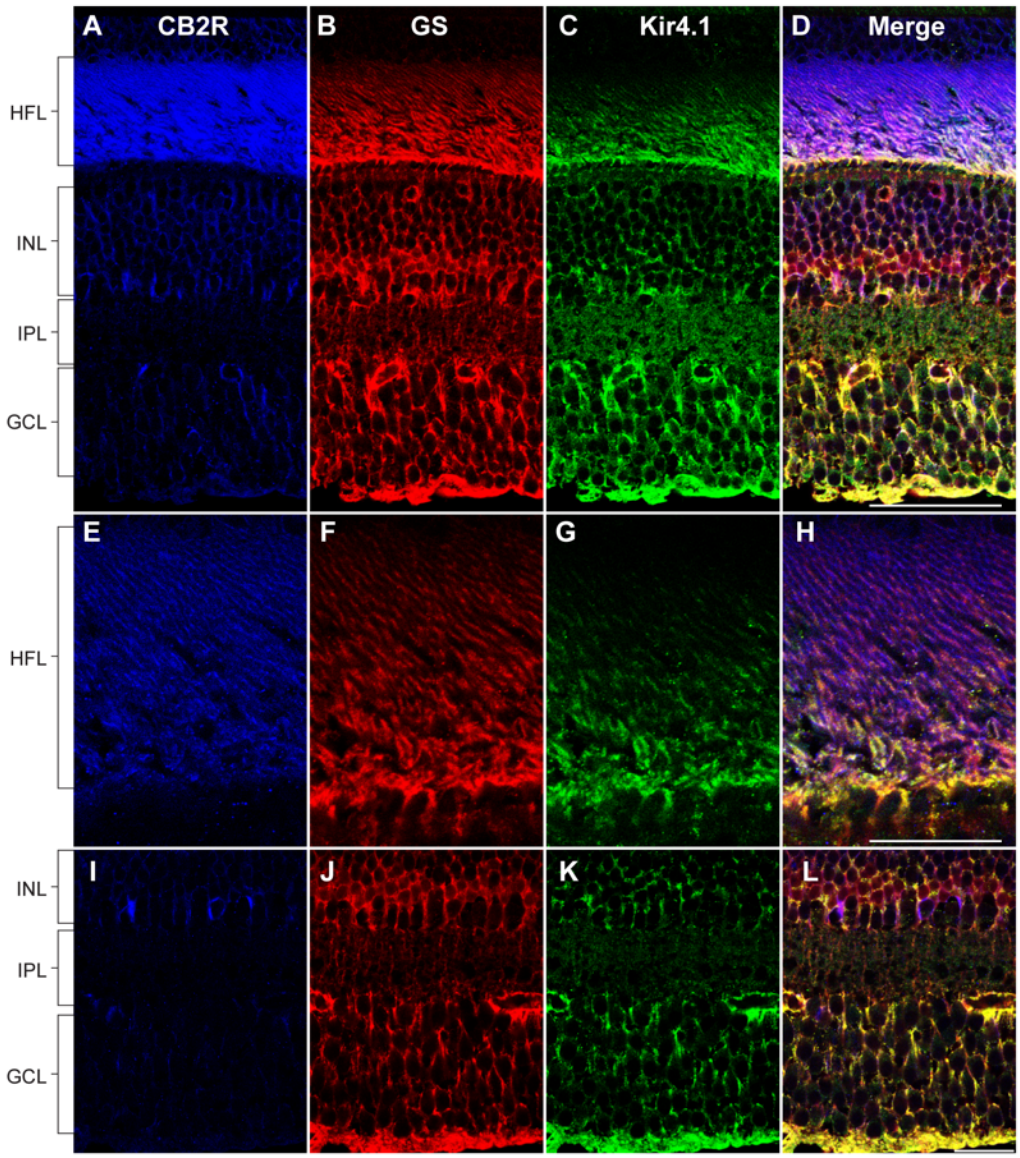

Figure 11. Triple immunofluorescent labeling of CB2R, glutamine synthetase (GS), and the potassium ion channel Kir4.1 in the monkey central retina. Each protein is presented alone in gray scale in the first columns. The merge image is presented in the last column (CB2R in blue, GS in red, and Kir4.1 in green). **A-D**: Low magnification images showing Kir4.1 and CB2R expression in GS positive Müller cells. **E-H**: High magnification images of Kir4.1, CB2R, and GS immunoreactivity in the distal retina showing co-localization of CB2R and Kir4.1 in Müller cell fibers of the Henle fiber layer. **I-L**: High magnification images of Kir4.1 expression in the proximal retina. HFL, Henle fiber layer; INL, inner nuclear layer; IPL, inner plexiform layer; GCL, ganglion cell layer. Scale bar = 75 µm for A-D and 30 µm for E-L.

Discussion

This study reports the presence of cannabinoid CB2 receptor (CB2R) in Müller cells of the vervet monkey retina. These findings are important because, although the presence of CB1R in the monkey retina is well established (Straiker et al., 1999; Bouskila et al., 2012), we are still far from identifying the exact role of eCB signaling in the monkey retina. Furthermore, CB2R has been previously ascribed a critical role in CNS glial function (Cabral et al., 2008) and its visual function remains elusive. Our aim was to characterize further the retinal localization of cannabinoid receptors, especially by comparing CB2R expression profile with CB1R localization. We demonstrate here that CB2R is present in the retina of the vervet monkey and specifically in retinal Müller cells. These data, in agreement with CB2R glial expression in the CNS, suggest that the CB2 receptor plays a role in retinal functions.

There are 3 types of glial cells in the primate retina: Müller cells, astrocytes and microglia. Müller cells are the principal glial cells of the retina and are radially oriented across the thickness of the retina, analogous to CB2R expression profile in the distal retina. Their processes extend from the outer limiting membrane to the inner limiting membrane. Given that the expression of the CB2R followed the same pattern, with a higher polarization towards the outer retina, we suggest that CB2R is localized in these glial cells, verified by the co-localization of CB2R-IR with GS-IR. Müller cell processes surround neuronal cell bodies in the nuclear layers and envelop groups of neural processes in the plexiform layers. A 3D visualization was therefore needed in order to determine whether or not CB2R-IR was present in neurons. The outer limiting membrane, which represents the outer border of CB2R expression, is composed of junctions among Müller cells, and photoreceptor cells. However, CB2R-IR was not detected in the apical villi of Müller cells that extend distally from the OLM. The inner limiting membrane, formed by the conical endfeet of Müller cells, appeared devoid of CB2R-IR. Müller cells also form endfeet on the large retinal blood vessels at the inner surface of the retina. Given the apparent absence of CB2R-IR in the most proximal retina, CB2R may not have a role in the regulation of inner retinal blood vessels.

The presence of CB2R in Müller cells and CB1R in the retinal neuronal cells, points towards a complementary relationship between neurons and glia regarding endocannabinoid function.

CB2R in Müller cells could protect neurons from exposure to excess neurotransmitters such as L-glutamate (Placzek et al., 2008). Generally, CB2R activation leads to sequences of activities of a protective nature (Pacher and Mechoulam, 2011 for review). Stimulation of CB2R increases microglial cell proliferation (Carrier et al., 2004) and reduces the release of harmful factors, including tumor necrosis factor (TNF) and free radicals (Eljaschewitsch et al., 2006; Ramírez et al., 2005; See Stella, 2009 for review). In fact, exposure to eCBs in activated primary human Müller glia inhibited the production of several proinflammatory cytokines (Krishnan and Chatterjee, 2012). CB2R in Müller cells might therefore be an important player in inflammation, neurotoxicity and neuroprotection. The localization of CB1R in the photoreceptor layer already suggested that the transduction of light (Yazulla, 2008) occurring at this stage could also be modulated by the CB2R expressed in distal Müller cells fibers. Perhaps, the whole eCB system participates in the modulation of light transduction, where CB1R is neuronal and CB2R glial. The expression of CB1R in bipolar cells, shown by double-labeling with CHX10 and PKC retinal cell type markers, suggested that the eCB system acts as an autoregulation system that modulates the signal received by the photoreceptors in order to transmit it to ganglion cells (Yazulla et al., 1999; Yazulla, 2008; Bouskila et al., 2012). Similarly, this could also occur in horizontal and amacrine cells that show little expression of CB1R (Bouskila et al., 2012). Finally, it is possible that the results of Lu et al. (2000) who demonstrated the expression of CB2R in the ganglion cell layer of the adult rat retina using *in situ* hybridization and RT-PCR did include CB2R-immunoreactive Müller cell processes. In agreement with the latter study, using immunohistochemistry and cell morphology, López et al. (2011) suggested that CB2R was localized in photoreceptors, horizontal cells, amacrine cells and cells localized in the GCL of the adult rat retina. These studies differ with ours not only regarding the animal model (rat versus monkey) but the choice of the antibody used. While we used an antibody targeted against the 20-33 amino acids of the human CB2R, López et al., (2011) used an antibody against residues 326–342 of the rat CB2R. Moreover, double-labeling of CB2R with a retinal cell marker was not performed and given that Müller cells envelop the cell bodies in the GCL it could be CB2R positive cells. In addition, CB1R-IR in the Henle fiber layer and ganglion cell layer of the monkey retina has the most prominent staining found throughout the retinal layers (Bouskila et al., 2012), as opposed to only the Henle fiber layer that has the highest CB2R signal. Recently, Krishnan and Chatterjee (2012)

showed that CB2R protein was expressed in homogenates of 12-18 days *ex vivo* retinal explants and 18 days *in vitro* primary Müller glia from human retina by Western blotting. We provide here direct evidence for the *in vivo* expression pattern of CB2R in monkey Müller cells by immunohistochemistry.

Hypothetical functional consequences

Activation of photoreceptors by light evokes an increase of K^+ ions in the retinal extracellular space (Newman and Reichenbach, 1996). In order to maintain an electrolytic balance, Müller cell inwardly rectifying K^+ channels (K_{IR}) release the excess K^+ ions into the vitreous. This spatial buffering mechanism is termed K^+ siphoning (Newman et al., 1984). Immunoreactivity to the $K_{IR}4.1$ channel in rat retina was densely distributed around photoreceptor cells in ONL, where the distal ends of Müller cells surround PR cells, and in a scattered manner around ganglion cells in GCL in rat retina (Ishii et al., 1997). Interestingly, $K_{IR}4.1$-IR as reported by Ishii et al., (1997) for the rodent retina is similar to CB2R expression found in Müller cells in the present study in the monkey central retina (Figure 11). The cellular origin of the b-wave component of the ERG is attributed to an interaction between ON-bipolar cells and Müller cells (Stockton and Slaughter, 1989; Wen and Oakley, 1990). The b-wave of the ERG reflects the K^+ mediated spatial buffering currents of Müller cells (Miller and Dowling, 1970; Kline et al., 1985). Moreover, blocking K^+ channels in Müller cells reduces the ERG b-wave (Wen and Oakley, 1990). Given that activation of CB2R leads to a reduction of cAMP and PKA levels due to coupling via $G_{i/o}$ (Howlett et al., 2002 for review Bolognini et al., 2010) and that PKA increases the activity of $K_{IR}4.1$ channels in Müller cells (MacGregor et al., 1998), it is reasonable to propose that CB2R plays a role in the generation of the b-wave. CB2R could act therefore as a negative modulator of K^+ channels. Conversely, blocking CB2R activates K^+ channels (because of the constitutive activity of CB2R) that in turn produce a constant influx of K^+ ions into the Müller cell and an enlarged b-wave (Figure 10B). Further experiments are however still needed in order to verify this retinal CB2R putative function.

Other acknowledgments

We thank Sophie Charron and Florence Dotigny for excellent technical assistance. We are grateful to Dr. Frank Ervin and Dr. Roberta Palmour of the Behavioral Sciences Foundation Laboratories of St Kitts, West Indies, for supplying the vervet monkey tissues.

Conflict of interest statement

The authors declare no conflict of interests.

Role of authors

All authors had full access to all the data in the study and take responsibility for the integrity of the data and the accuracy of the data analysis. Study concept and design: JB. Acquisition of data: JB. Analysis and interpretation of data: JB. Drafting of the manuscript: JB and PJ. Critical revision of the manuscript for important intellectual content: CC. Obtained funding: CC, MP and JFB. Administrative, technical, and material support: CC, MP and JFB. Study supervision: MP and JFB.

Literature cited

Argaw A, Duff G, Cherif H, Cécyre B, Tea N, and Bouchard J-F. 2011. Cannabinoid receptor CB2 modulates axon guidance. Abstract #B045, 8th IBRO World Congress on Neuroscience, Firenze, Italy.

Atwood BK, Mackie K. 2010. CB2: a cannabinoid receptor with an identity crisis. Br J Pharmacol 160(3):467-479.

Barnstable CJ, Hofstein R, Akagawa K. 1985. A marker of early amacrine cell development in rat retina. Brain Res 352(2):286-290.

Bolognini D, Costa B, Maione S, Comelli F, Marini P, Di Marzo V, Parolaro D, Ross RA, Gauson LA, Cascio MG, Pertwee RG. 2010. The plant cannabinoid Delta9-tetrahydrocannabivarin can decrease signs of inflammation and inflammatory pain in mice. Br J Pharmacol 160(3):677-687.

Bordt A, Hoshi H, Yamada E, Perryman Stout W, Marshak D. 2006. Synaptic input to OFF parasol ganglion cells in macaque retina. J Comp Neurol 498(1):46-57.

Bouskila J, Burke MW, Zabouri N, Casanova C, Ptito M, Bouchard JF. 2012. Expression and localization of the cannabinoid receptor type 1 and the enzyme fatty acid amide hydrolase in the retina of vervet monkeys. Neuroscience 202(0):117-130.

Brandon C. 1985. Improved immunocytochemical staining through the use of Fab fragments of primary antibody, Fab-specific second antibody, and Fab-horseradish peroxidase. The journal of histochemistry and cytochemistry 33(7):715-719.

Buckley NE, Hansson S, Harta G, Mezey E. 1998. Expression of the CB1 and CB2 receptor messenger RNAs during embryonic development in the rat. Neuroscience 82(4):1131-1149.

Burke M, Zangenehpour S, Bouskila J, Boire D, Ptito M. 2009. The gateway to the brain: dissecting the primate eye. J Vis Exp(27):e1261.

Cabral GA, Raborn ES, Griffin L, Dennis J, Marciano-Cabral F. 2008. CB2 receptors in the brain: role in central immune function. Br J Pharmacol 153(2):240-251.

Carrier EJ, Kearn CS, Barkmeier AJ, Breese NM, Yang W, Nithipatikom K, Pfister SL, Campbell WB, Hillard CJ. 2004. Cultured rat microglial cells synthesize the endocannabinoid 2-arachidonylglycerol, which increases proliferation via a CB2 receptor-dependent mechanism. Molecular Pharmacology 65(4):999-1007.

Chang ML, Wu CH, Jiang-Shieh YF, Shieh JY, Wen CY. 2007. Reactive changes of retinal astrocytes and Müller glial cells in kainate-induced neuroexcitotoxicity. J Anat 210(1):54-65.

Chen J, Matias I, Dinh T, Lu T, Venezia S, Nieves A, Woodward DF, Di Marzo V. 2005. Finding of endocannabinoids in human eye tissues: implications for glaucoma. Biochem Biophys Res Commun 330(4):1062-1067.

Chiquet C, Dkhissi-Benyahya O, Chounlamountri N, Szel A, Degrip WJ, Cooper HM. 2002. Characterization of calbindin-positive cones in primates. Neuroscience 115(4):1323-1333.

Cravatt BF, Giang DK, Mayfield SP, Boger DL, Lerner RA, Gilula NB. 1996. Molecular characterization of an enzyme that degrades neuromodulatory fatty-acid amides. Nature 384:83–87.

Cuenca N, Herrero MT, Angulo A, de Juan E, Martínez-Navarrete GC, López S, Barcia C, Martín-Nieto J. 2005. Morphological impairments in retinal neurons of the scotopic visual pathway in a monkey model of Parkinson's disease. J Comp Neurol 493(2):261-273.

Devane WA, Hanus L, Breuer A, Pertwee RG, Stevenson LA, Griffin G, Gibson D, Mandelbaum A, Etinger A, Mechoulam R. 1992. Isolation and structure of a brain constituent that binds to the cannabinoid receptor. Science 258(5090):1946-1949.

Di Marzo V, Bisogno T, De Petrocellis L. 2007. Endocannabinoids and related compounds: walking back and forth between plant natural products and animal physiology. Chemistry & Biology 14(7):741-756.

Dinh TP, Carpenter D, Leslie FM, Freund TF, Katona I, Sensi SL, Kathuria S, Piomelli D. 2002. Brain monoglyceride lipase participating in endocannabinoid inactivation. Proc Natl Acad Sci U S A 99:10819–10824.

Distler C, Dreher Z. 1996. Glia cells of the monkey retina—II. Müller cells. Vision Research 36(16):2381-2394.

Eljaschewitsch E, Witting A, Mawrin C, Lee T, Schmidt P, Wolf S, Hoertnagl H, Raine C, Schneider Stock R, Nitsch R, Ullrich O. 2006. The endocannabinoid anandamide protects neurons during CNS inflammation by induction of MKP-1 in microglial cells. Neuron 49(1):67-79.

Ellert-Miklaszewska A, Grajkowska W, Gabrusiewicz K, Kaminska B, Konarska L. 2007. Distinctive pattern of cannabinoid receptor type II (CB2) expression in adult and pediatric brain tumors. Brain Research 1137(0):161-169.

Fischer AJ, Hendrickson A, Reh TA. 2001. Immunocytochemical characterization of cysts in the peripheral retina and pars plana of the adult primate. Invest Ophthalmol Vis Sci 42(13):3256-3263.

Galiègue S, Mary S, Marchand J, Dussossoy D, Carrière D, Carayon P, Bouaboula M, Shire D, Le Fur G, Casellas P. 1995. Expression of central and peripheral cannabinoid receptors in human immune tissues and leukocyte subpopulations. European Journal of Biochemistry 232(1):54-61.

Galve Roperh I, Aguado T, Palazuelos J, Guzmán M. 2008. Mechanisms of control of neuron survival by the endocannabinoid system. Current pharmaceutical design 14(23):2279-2288.

Griffin G, Tao Q, Abood ME. 2000. Cloning and pharmacological characterization of the rat CB(2) cannabinoid receptor. J Pharmacol Exp Ther 292(3):886-894.

Howlett AC, Barth F, Bonner TI, Cabral G, Casellas P, Devane WA, Felder CC, Herkenham M, Mackie K, Martin BR, Mechoulam R, Pertwee RG. 2002. International Union of Pharmacology. XXVII. Classification of cannabinoid receptors. Pharmacol Rev 54(2):161-202.

Inoue A, Obata K, Akagawa K. 1992. Cloning and sequence analysis of cDNA for a neuronal cell membrane antigen, HPC-1. J Biol Chem 267(15):10613-10619.

Ishii M, Horio Y, Tada Y, Hibino H, Inanobe A, Ito M, Yamada M, Gotow T, Uchiyama Y, Kurachi Y. 1997. Expression and clustered distribution of an inwardly rectifying potassium channel, KAB-2/Kir4.1, on mammalian retinal Müller cell membrane: their regulation by insulin and laminin signals. J Neurosci 17(20):7725-7735.

Kline RP, Ripps H, Dowling JE. 1985. Light-induced potassium fluxes in the skate retina. Neuroscience 14(1):225-235.

Kolb H, Zhang L, Dekorver L, Cuenca N. 2002. A new look at calretinin-immunoreactive amacrine cell types in the monkey retina. J Comp Neurol 453(2):168-184.

Kozak KR, Rowlinson SW, Marnett LJ. 2000. Oxygenation of the endocannabinoid, 2-arachidonylglycerol, to glyceryl prostaglandins by cyclooxygenase-2. J Biol Chem 275:33744–33749.

Krishnan G, Chatterjee N. 2012. Endocannabinoids alleviate proinflammatory conditions by modulating innate immune response in Müller glia during inflammation. Glia 60(11):1629-1645.

Li L, Head V, Timpe LC. 2001. Identification of an inward rectifier potassium channel gene expressed in mouse cortical astrocytes. Glia 33(1):57-71.

López EM, Tagliaferro P, Onaivi ES, López-Costa JJ. 2011. Distribution of CB2 cannabinoid receptor in adult rat retina. Synapse 65(5):388-392.

Lu Q, Straiker A, Maguire G. 2000. Expression of CB2 cannabinoid receptor mRNA in adult rat retina. Vis Neurosci 17(1):91-95.

MacGregor GG, Xu JZ, McNicholas CM, Giebisch G, Hebert SC. 1998. Partially active channels produced by PKA site mutation of the cloned renal K+ channel, ROMK2 (kir1.2). Am J Physiol 275(3 Pt 2):F415-422.

Mackie K. 2008. Cannabinoid receptors: where they are and what they do. J Neuroendocrinol 20 Suppl 1:10-14.

Martínez-Navarrete GC, Angulo A, Martín-Nieto J, Cuenca N. 2008. Gradual morphogenesis of retinal neurons in the peripheral retinal margin of adult monkeys and humans. J Comp Neurol 511(4):557-580.

Martínez-Navarrete GC, Martín-Nieto J, Esteve-Rudd J, Angulo A, Cuenca N. 2007. Alpha synuclein gene expression profile in the retina of vertebrates. Mol Vis 13:949-961.

McPartland JM, Norris RW, Kilpatrick CW. 2007. Coevolution between cannabinoid receptors and endocannabinoid ligands. Gene 397(1-2):126-135.

Mechoulam R, Ben Shabat S, Hanus L, Ligumsky M, Kaminski NE, Schatz AR, Gopher A, Almog S, Martin BR, Compton DR. 1995. Identification of an endogenous 2-monoglyceride, present in canine gut, that binds to cannabinoid receptors. Biochemical pharmacology 50(1):83-90.

Miller RF, Dowling JE. 1970. Intracellular responses of the Müller (glial) cells of mudpuppy retina: their relation to b-wave of the electroretinogram. J Neurophysiol 33(3):323-341.

Mills SL, Massey SC. 1999. AII amacrine cells limit scotopic acuity in central macaque retina: a confocal analysis of calretinin labeling. J Comp Neurol 411(1):19-34.

Mukherjee S, Adams M, Whiteaker K, Daza A, Kage K, Cassar S, Meyer M, Yao BB. 2004. Species comparison and pharmacological characterization of rat and human CB2 cannabinoid receptors. Eur J Pharmacol 505(1-3):1-9.

Munro S, Thomas KL, Abu-Shaar M. 1993. Molecular characterization of a peripheral receptor for cannabinoids. Nature 365(6441):61-65.

Nadal-Nicolás FM, Jiménez-López M, Sobrado-Calvo P, Nieto-López L, Cánovas-Martínez I, Salinas-Navarro M, Vidal-Sanz M, Agudo M. 2009. Brn3a as a marker of retinal ganglion cells: qualitative and quantitative time course studies in naïve and optic nerve–injured retinas. Investigative Ophthalmology & Visual Science 50(8):3860-3868.

Nag TC, Wadhwa S. 2001. Differential expression of syntaxin-1 and synaptophysin in the developing and adult human retina. J Biosci 26(2):179-191.

Newman E, Reichenbach A. 1996. The Müller cell: a functional element of the retina. Trends Neurosci 19(8):307-312.

Newman EA, Frambach DA, Odette LL. 1984. Control of extracellular potassium levels by retinal glial cell K+ siphoning. Science 225(4667):1174-1175.

Nishikawa S, Tamai M. 2001. Müller cells in the human foveal region. Curr Eye Res 22(1):34-41.

Onaivi E, Ishiguro H, Gu S, Liu Q-R. 2012. CNS effects of CB2 cannabinoid receptors: beyond neuro-immuno-cannabinoid activity. Journal of psychopharmacology 26(1):92-103.

Pacher P, Mechoulam R. 2011. Is lipid signaling through cannabinoid 2 receptors part of a protective system? Progress in lipid research 50(2):193-211.

Piomelli D. 2003. The molecular logic of endocannabinoid signalling. Nat Rev Neurosci 4(11):873-884.

Placzek EA, Okamoto Y, Ueda N, Barker EL. 2008. Mechanisms for recycling and biosynthesis of endogenous cannabinoids anandamide and 2-arachidonylglycerol. J Neurochem 107(4):987-1000.

Porcella A, Casellas P, Gessa GL, Pani L. 1998. Cannabinoid receptor CB1 mRNA is highly expressed in the rat ciliary body: implications for the antiglaucoma properties of marihuana. Molecular Brain Research 58(1-2):240-245.

Porcella A, Maxia C, Gessa GL, Pani L. 2000. The human eye expresses high levels of CB1 cannabinoid receptor mRNA and protein. European journal of neuroscience 12(3):1123-1127.

Qi H-X, Gharbawie OA, Wong P, Kaas JH. 2011. Cell-poor septa separate representations of digits in the ventroposterior nucleus of the thalamus in monkeys and prosimian galagos. J Comp Neurol 519(4):738-758.

Ramírez BG, Blázquez C, del Pulgar TG, Guzmán M, de Ceballos ML. 2005. Prevention of Alzheimer's disease pathology by cannabinoids: neuroprotection mediated by blockade of microglial activation. J Neurosci 25(8):1904-1913.

Riepe RE, Norenburg MD. 1977. Müller cell localisation of glutamine synthetase in rat retina. Nature 268(5621):654-655.

Röhrenbeck J, Wässle H, Heizmann CW. 1987. Immunocytochemical labelling of horizontal cells in mammalian retina using antibodies against calcium-binding proteins. Neurosci Lett 77(3):255-260.

Shire D, Calandra B, Rinaldi-Carmona M, Oustric D, Pessègue B, Bonnin-Cabanne O, Le Fur G, Caput D, Ferrara P. 1996. Molecular cloning, expression and function of the murine CB2 peripheral cannabinoid receptor. Biochim Biophys Acta 1307(2):132-136.

Stella N. 2009. Endocannabinoid signaling in microglial cells. Neuropharmacology 56 Suppl 1:244-253.

Stockton RA, Slaughter MM. 1989. B-wave of the electroretinogram. A reflection of ON bipolar cell activity. J Gen Physiol 93(1):101-122.

Straiker A, Stella N, Piomelli D, Mackie K, Karten HJ, Maguire G. 1999. Cannabinoid CB1 receptors and ligands in vertebrate retina: localization and function of an endogenous signaling system. Proc Natl Acad Sci U S A 96(25):14565-14570.

Sugiura T, Kondo S, Sukagawa A, Nakane S, Shinoda A, Itoh K, Yamashita A, Waku K. 1995. 2-Arachidonoylglycerol: a possible endogenous cannabinoid receptor ligand in brain. Biochemical and biophysical research communications 215(1):89-97.

Wässle H, Dacey DM, Haun T, Haverkamp S, Grunert U, Boycott BB. 2000. The mosaic of horizontal cells in the macaque monkey retina: with a comment on biplexiform ganglion cells. Vis Neurosci 17(4):591-608.

Wei Y, Wang X, Wang L. 2009. Presence and regulation of cannabinoid receptors in human retinal pigment epithelial cells. Molecular vision 15:1243-1251.

Wen R, Oakley B, 2nd. 1990. K(+)-evoked Müller cell depolarization generates b-wave of electroretinogram in toad retina. Proc Natl Acad Sci U S A 87(6):2117-2121.

Xiang M, Zhou L, Macke JP, Yoshioka T, Hendry SH, Eddy RL, Shows TB, Nathans J. 1995. The Brn-3 family of POU-domain factors: primary structure, binding specificity, and expression in subsets of retinal ganglion cells and somatosensory neurons. J Neurosci 15(7 Pt 1):4762-4785.

Yazulla S. 2008. Endocannabinoids in the retina: from marijuana to neuroprotection. Prog Retin Eye Res 27(5):501-526.

Yazulla S, Studholme KM, McIntosh HH, Deutsch DG. 1999. Immunocytochemical localization of cannabinoid CB1 receptor and fatty acid amide hydrolase in rat retina. J Comp Neurol 415(1):80-90.

Zabouri N, Bouchard JF, Casanova C. 2011a. Cannabinoid receptor type 1 expression during postnatal development of the rat retina. J Comp Neurol 519(7):1258-1280.

Zabouri N, Ptito M, Casanova C, Bouchard JF. 2011b. Fatty acid amide hydrolase expression during retinal postnatal development in rats. Neuroscience 195:145-165.

Zhong L, Geng L, Njie Y, Feng W, Song Z-H. 2005. CB2 cannabinoid receptors in trabecular meshwork cells mediate JWH015-induced enhancement of aqueous humor outflow facility. Investigative Ophthalmology & Visual Science 46(6):1988-1992.

Zurolo E, Iyer AM, Spliet WGM, Van Rijen PC, Troost D, Gorter JA, Aronica E. 2010. CB1 and CB2 cannabinoid receptor expression during development and in epileptogenic developmental pathologies. Neuroscience 170(1):28-41.

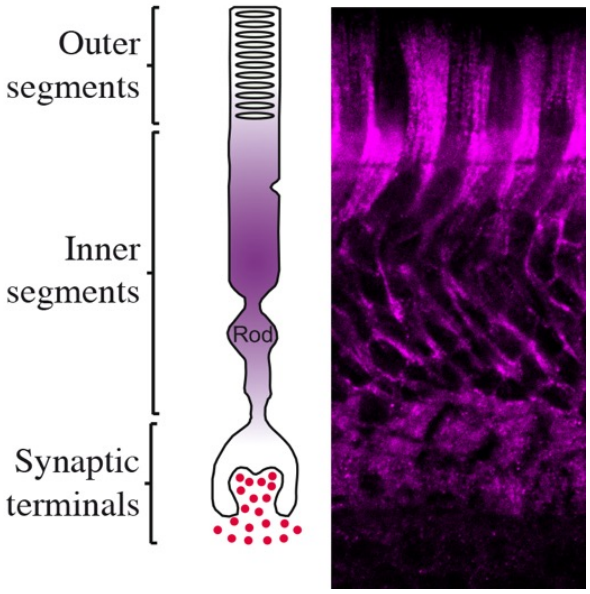

ARTICLE 3: ROD PHOTORECEPTORS EXPRESS GPR55 IN THE ADULT VERVET MONKEY RETINA

Publié dans :

Bouskila J, Javadi P, Casanova C, Ptito M, Bouchard JF (2013) Rod photoreceptors express GPR55 in the adult vervet monkey retina. PLoS One 8:e81080.

Rod photoreceptors express GPR55 in the adult vervet monkey retina

Joseph Bouskila[1, 2], Pasha Javadi[1], Christian Casanova[1], Maurice Ptito[1, 3], Jean-François Bouchard[1]

[1]School of Optometry, University of Montreal, Montreal, QC, Canada

[2]Biomedical Sciences, Faculty of Medicine, University of Montreal, Montreal, QC, Canada

[3]BRAINlab, Department of Neuroscience and Pharmacology, University of Copenhagen, Copenhagen, Denmark

Keywords: GPR55, Cannabinoids, Retina, Monkey, Immunofluorescence, Confocal Microscopy

Correspondence should be addressed to:

Jean-François Bouchard, BPharm, PhD

School of Optometry, room 260-7

3744 Jean-Brillant,

University of Montreal,

Montreal, Quebec, Canada, H3T 1P1

Abstract

Cannabinoids exert their actions mainly through two receptors, the cannabinoid CB1 receptor (CB1R) and cannabinoid CB2 receptor (CB2R). In recent years, the G-protein coupled receptor 55 (GPR55) was suggested as a cannabinoid receptor based on its activation by anandamide and tetrahydrocannabinol. Yet, its formal classification is still a matter of debate. CB1R and CB2R expression patterns are well described for rodent and monkey retinas. In the monkey retina, CB1R has been localized in its neural (cone photoreceptor, horizontal, bipolar, amacrine and ganglion cells) and CB2R in glial components (Müller cells). The aim of this study was to determine the expression pattern of GPR55 in the monkey retina by using confocal microscopy. Our results show that GPR55 is strictly localized in the photoreceptor layer of the extrafoveal portion of the retina. Co-immunolabeling of GPR55 with rhodopsin, the photosensitive pigment in rods, revealed a clear overlap of expression throughout the rod structure with most prominent staining in the inner segments. Additionally, double-label of GPR55 with calbindin, a specific marker for cone photoreceptors in the primate retina, allowed us to exclude expression of GPR55 in cones. The labeling of GPR55 in rods was further assessed with a 3D visualization in the XZ and YZ planes thus confirming its exclusive expression in rods. These results provide data on the distribution of GPR55 in the monkey retina, different than CB1R and CB2R. The presence of GPR55 in rods suggests a function of this receptor in scotopic vision that needs to be demonstrated.

Introduction

The *cannabis sativa* (marijuana) plant contains a group of biologically active substances, termed cannabinoids (CBs), which influence many biological functions [1,2], including vision [3]. The CBs activate mainly two 7-transmembrane G protein-coupled receptors, the cannabinoid CB1 receptor (CB1R) that mediates most of the psychoactive effects of marijuana and the cannabinoid CB2 receptor (CB2R) that mediate the immunological effects. The persistence of cannabinoid effects in CB1R and/or CB2R knockout mice suggested the existence of additional cannabinoid receptors [4]. Following the identification and cloning of a novel human G-protein-coupled receptor 55 (GPR55), several cannabinoid ligands were shown to bind to it, suggesting that it could be a novel cannabinoid receptor [5]. Although some controversy remains, this receptor can be considered a cannabinoid receptor based on its activation by anandamide and THC, the main psychoactive compound of marijuana, at low micromolar concentrations [6-8]. Moreover, the endoCBs anandamide and virodhamine can modulate the activity of GPR55 [9]. However, lysophosphatidylinositol (LPI), an endogenous lipid mediator, has been described as the first ligand that potently and efficaciously activates GPR55 [6,8,10,11]. In fact, the 2-arachidonoyl species of LPI may be the true natural ligand of GPR55 [12]. Agonists and antagonists of GPR55 appear to recognize different domains of the receptor corresponding to their reported pharmacological activities [13]. The atypical cannabinoid O-1602 has also been shown to act upon GPR55 [14]. GPR55 stimulation releases calcium from intracellular stores via phospholipase C [6,8] and, in some cases, activates ERK1/2 MAP kinase [8,11]. Interestingly, GPR55 and CB1R are capable of forming heteromers that exhibit distinct signaling properties in human embryonic kidney (HEK293) cells [15]. Additionally, GPR55 has been shown to associate with lipid rafts thus having an impact on the biological activity of this receptor [16].

GPR55 mRNA is widely distributed from moderate to low levels in the CNS, in both neuron and glia, and is also found in the vasculature and other peripheral tissues [7]. Using real-time PCR, the expression of GPR55 was found in primary microglial cells, suggesting a role for GPR55 in neuroimmunological regulation [17]. Using quantitative PCR, GPR55 mRNA expression was found in the striatum, hippocampus, forebrain, cortex, and cerebellum [18]. Human GPR55 mRNA is also strongly expressed in the basal ganglia (striatum, caudate

nucleus, and putamen), moderately in the nucleus accumbens, hypothalamus, and hippocampus, and weakly in the cerebellum [19]. While the overall human to mouse amino acid sequence similarity is 97% for CB1R, and 79% for CB2R, the human GPR55 protein sequence is only 74% identical to the mouse GPR55. Nevertheless, even though the immunohistochemical localization of GPR55 in the CNS is limited, it has been found in mouse dorsal root ganglia [6]. Interestingly, the GPR55 KO mouse develops normally, no defects in brain structures are detected, and the abundance of endocannabinoids and related lipids are not affected [18]. While GPR55 appears to satisfy the criteria of a cannabinoid receptor, its pharmacology is inconsistent with several of the non-CB1R/non-CB2R effects. Thus, additional cannabinoid receptors clearly remain to be identified.

Expression patterns of CB1R and CB2R have been both localized in the vervet monkey retina [20,21]. There are numerous evidences that show that cannabinoids have many visual effects [3] but no data are available on the expression and role of GPR55. Cannabidiol, a bioactive compound of the plant *cannabis sativa* without psychotropic effects, has been shown to bind to GPR55 with very low binding capacity on CB1R and CB2R. Moreover, cannabidiol seems to have protective effects on retinal neurons [22]. A recent study demonstrated that knocking down the expression of GPR55 with specific shRNAs partially blocked the PEA-induced increase in aqueous humor outflow facility [23]. Although a complicated cannabinoid profile has prevented its classification as a cannabinoid receptor, the therapeutic potential of GPR55 cannot be denied [24]. The present study investigates the presence of GPR55 in the monkey retina, compares the spatial expression of GPR55 to that of CB1R and CB2R, and proposes a putative role for GPR55 in retinal functions.

Materials and Methods

Choice of species. Monkey tissue, the experimental model for the current study, was chosen for several reasons. First, using monkey tissue allows us to infer more easily on what is really present in humans. Additionally, the anatomical similarity between the monkey and human retina is remarkable. Primates are mammals that have a macular/foveal region and multiple cone types responsible for high visual acuity and color vision. Finally, the high cross-reactivity between human and monkey antigens increases chances of success for targeting GPR55 in monkeys using an antibody directed against human GPR55 epitope.

Animal Preparation. Six 42 months-old vervet monkeys (*Chlorocebus sabaeus*) were included in this study: three were used for the immunochemistry protocols, and fresh specimens of retina, visual cortex, and cerebellum were collected from three others for immunoblotting. The animals were born and raised in enriched environments in the laboratories of the Behavioural Sciences Foundation (St-Kitts, West Indies) that is recognized by the Canadian Council on Animal Care (CCAC). The animals were fed with primate chow (Harlan Teklad High Protein Monkey Diet; Harlan Teklad, Madison, WI) and fresh local fruits, with water available ad libitum. Infant vervets are born into an outdoor social group comprising several females, one male and other offspring of the same general age. Infants live with their parents until about 8 months of age, at which time they move to a playpen with 5 other age-mates. The natal cage is equipped with swings, perches, hiding places and jungle gyms. We do put in toys, but the animals are so busy playing with one another that they ignore the toys. In the smaller playpens, there are also swings, perches and climbing spots, as well as puzzle feeders and foraging boards. At about 18 months of age, youngsters graduate to a large, outdoor peer group of about 16 animals (like-ages, both sexes) where there are tunnels, swings, ladders, jungle-gyms and a variety of manipulanda (more complex puzzle feeders; natural forage opportunities, such as brush and vines; foraging boards). Plastic chain and baited balls are popular toys, but vervets of this age are uninterested in most other commercially available toys. The experimental protocol was reviewed and approved by the local Animal Care and Use Committee (Université de Montréal) and the Institutional Review Board of the Behavioural Science Foundation. Each animal was sedated with ketamine (10

mg/kg, i.m.), deeply anaesthetized with sodium pentobarbital (25 mg/kg, i.v.) and perfused transcardially with phosphate buffer saline (PBS pH 7.4), followed by 4% paraformaldehyde.

Antibody characterization. All the primary antibodies used in this work, their sources and working dilutions, are summarized in Table 1. These antibodies were successfully used in previous studies and are well characterized in regards to the specific primate retinal cell type immunostaining, as described below for each antibody.

Table 1. Primary antibodies used in this study.

Antibody[1]	Immunogen	Source[2]	Working dilution
Rhodopsin	Bovine rhodopsin	Abcam, Toronto, ON, ab98887, Mouse monoclonal, Clone Rho 4D2	H: 1:500
CB	Purified bovine kidney calbindin-D28K	Sigma, St. Louis, MO, C9848, Mouse monoclonal, Clone CB-955	H: 1:250
GS	Full protein purified from sheep brain	Chemicon, Temecula, CA, MAB302, Mouse monoclonal, Clone GS-6	H: 1:500
PKCα	Peptide mapping the aa 296-317 of human PKCα	Santa Cruz Biotechnology, Santa Cruz, CA, sc-8393, Mouse monoclonal, Clone H-7	H: 1:500
PV	Full protein purified from frog muscle	Sigma, St. Louis, MO, P3088, Mouse monoclonal, Clone PARV-19	H: 1:250
CB1R	Fusion protein containing aa 1-77 of rat CB1R	Sigma, St. Louis, MO, C1233, Rabbit polyclonal	H: 1:150
CB2R	Synthetic peptide from aa 20-33 of human CB2R	Cayman Chemical, Ann Arbor, MI, 101550, Rabbit polyclonal	H: 1:150
GPR55	Synthetic peptide from aa 207-219 of human GPR55	Cayman Chemical, Ann Arbor, MI, 10224, Rabbit polyclonal	H: 1:200 W: 1:500
GAPDH	The full-length rabbit muscle GAPDH protein	Sigma, St. Louis, MO, G8795, Mouse monoclonal, Clone GAPDH-71.1	W: 1:20,000

[1]Abbreviations: CB, calbindin; GS, glutamine synthetase; PKCα, protein kinase C (α isoform); PV, parvalbumin; CB1R, cannabinoid receptor type 1; CB2R, cannabinoid receptor type 2; GPR55, G-protein coupled receptor 55; GAPDH, glyceraldehyde-3-phosphate dehydrogenase; aa, amino acids; H, immunohistochemistry; W, western blot.

[2]The source column indicates the commercial company, catalog reference and origin. The clone designation is given for monoclonal antibodies.

Rhodopsin. The mouse monoclonal (IgG1) to rhodopsin from Abcam (Cambridge, MA) was obtained by using as immunogen the bovine rhodopsin. This antibody recognizes a 39 kDa band on Western Blots and is predicted to react with human retinal tissues (manufacturer's data sheet). It has been proven effective to specifically label rods in the rodent retina [25].

CB. The mouse monoclonal (IgG1) to calbindin (CB) from Sigma (St. Louis, MO) was obtained by using as immunogen purified bovine kidney Calbindin-D-28K. This antibody recognizes a 28 kDa band on Western Blots. Immunostaining against calbindin is known to label cones outside the foveal region, cone bipolar cells and a subset of horizontal cells on human and monkey retinal sections [20,21,26-30].

GS. The mouse monoclonal to glutamine synthetase (GS) was obtained from Chemicon International (Temecula, CA) by using as immunogen the GS purified from sheep brain. This antibody generates a single 45 kDa band in adult retinal tissue [31]. This antibody labels Müller cells in rat [32-34] and monkey [20,21,35] retinas.

PKCα. The mouse monoclonal (IgG2a) to protein kinase C (PKC) was obtained from Santa Cruz Biotechnology (Santa Cruz, CA) by using as immunogen purified bovine PKC. The epitope is mapped to PKC hinge region (amino acids 296–317). It detects the PKCα isoform, a well-known specific marker for rod bipolar cells [36]. As stated by the manufacturer, this antibody gives a single band of 80 kDa on Western blots of human cell lines, and has been previously used for immunohistochemistry on rodent [33,34] and monkey [20,21,29,37] retinas.

PV. The mouse monoclonal (IgG1) to parvalbumin (PV) was obtained from Sigma (St. Louis, MO) by using as immunogen purified frog muscle PV. It recognizes a 12 kDa band from human, bovine, pig, canine, feline, rabbit, rat, and fish tissues (manufacturer's technical information). The pattern of labeling with this antibody was the same as reported previously [28,38]. This small calcium-binding protein is expressed in the primate retina by horizontal cells [39] and the antiserum has been used to visualize monkey thalamic nuclei [40] and vervet

monkey horizontal cells [21].

GPR55. The rabbit anti-GPR55 was obtained from Cayman Chemical (Ann Arbor, MI) by using as immunogen a synthetic peptide corresponding to the amino acids 207-219 (ILLGRRDHTQDWV) of the human GPR55 sequence. This antibody recognizes a band at 37 kDa (manufacturer's data sheet, 10224). This antibody was characterized and used to detect GPR55 expression in human trabecular meshwork cells [23].

CB1R. The rabbit anti-CB1R was obtained from Sigma (St. Louis, MO) by using a highly purified fusion protein containing the first 77 amino acid residues of the rat CB1R as the immunogen. It recognizes a major band of 60 kDa and less intense bands of 23, 72, and 180 kDa (manufacturer's data sheet, C1233). This antibody targets the rat CB1R but specifically recognizes the CB1R (60 kDa) from many species, including vervet monkey retinal tissue [20,21].

CB2R. The rabbit anti-CB2R was purchased from Cayman Chemical (Ann Arbor, MI) and was developed by using a synthetic peptide corresponding to the amino acids 20-33 (NPMKDYMILSGPQK) of the human CB2R sequence conjugated to KLH as immunogen. This antibody recognizes a band at 45 kDa and a band at 39-40 kDa (manufacturer's data sheet, 101550). This antibody was used in human nervous tissues [41,42] and to detect CB2R from vervet monkey retinal tissue [21].

GAPDH. The mouse monoclonal to GAPDH (clone GAPDH-71.1) was obtained from Sigma (St. Louis, MO) by using as immunogen purified rabbit muscle GAPDH (whole molecule). As stated by the manufacturer, this antibody recognizes monkey GAPDH and gives a single band at about 37 kDa.

GPR55 blocking peptide. The GPR55 blocking peptide containing the human GPR55 amino acid sequence 207-219 (ILLGRRDHTQDWV; Cayman Chemical; catalog number 10225) was used in the present study for immunohistochemistry and western blot analysis. The specificity of the GPR55 antibody was also tested by preincubation with the corresponding

blocking peptide. For preadsorption, 20 µg of primary antibody was mixed with 20 µg of blocking peptide for 2 hours at room temperature with occasional inversion. We then diluted that mixture 1:200 making a final concentration of 10 µg/ml of preadsorbed antibody. The antibody-blocking peptide solution was added to the slices or blots and subsequent immunohistochemistry and western blot analysis followed the protocol as described further.

Tissue preparation. The eyes were extracted and the retina was dissected free from the eyecup in a PBS bath. The retina was laid flat so that the vitreous body could be removed by blotting with filter paper and gentle brushing [43]. Samples of retina (4 mm^2) were taken from the extrafoveal retina (between 1 and 5 degrees of perimetric angle), middle retina (between 6 and 25 degrees of perimetric angle) and periphery (above 25 degrees of perimetric angle). Each sample was then cryoprotected in 30% sucrose overnight and embedded in Shandon embedding media at -65^{0}C. Retinal samples were then sectioned in a cryostat (18 µm) and mounted onto gelatinized glass microscope slides, air-dried and stored at -20^{0}C for further processing.

Western blotting. In order to test the specificity of our antibodies directed against GPR55, Western blots were performed on a piece of monkey tissue. A fresh dissected sample of retina, visual cortex, and cerebellum was homogenized by hand using a sterile pestle in RIPA buffer (150 mM NaCl, 20 mM Tris, pH 8.0, 1% NP-40 (USB Corp., Cleveland, OH, USA), 0.1% SDS, 1 mM EDTA), supplemented with a protease inhibitor mixture (aprotinin (1:1,000), leupeptin (1:1,000), pepstatin (1:1,000) and phenylmethylsulfonyl fluoride (0.2 mg/ml); Roche Applied Science, Laval, QC, Canada). Samples were then centrifuged at 4°C for 10 minutes, and the supernatant was extracted and stored at -20°C until further processing. Protein content was equalized by using a Thermo Scientific Pierce BCA Protein Assay Kit (Fisher Scientific, Ottawa, ON, Canada). Thirty micrograms of protein/sample of the homogenate was resolved with 10% sodium dodecyl sulfate (SDS)-polyacrylamide gel electrophoresis, transferred onto a nitrocellulose membrane filter (BioTrace NT, Life Sciences, Pall, Pensacola, FL), blocked for 1 hour in 5% skim milk (Carnation, Markham, ON, Canada) in TBST (0.15 M NaCl, 25 mM Tris-HCl, 25 mM Tris, 0.5% Tween- 20), and incubated overnight with a primary

antibody, namely, rabbit anti-GPR55 (1:500) in blocking solution. The following day, the blot was exposed to a secondary antibody conjugated to horseradish peroxidase (1:5,000; Jackson ImmunoResearch, West Grove, PA) in blocking solution for 2 hours. Detection was carried out by using homemade ECL Western blotting detection reagents (final concentrations: 2.50 mM luminol, 0.4 mM p-coumaric acid, 0.1 M Tris-HCl pH 8.5, 0.018% H_2O_2). The membrane was then air-stripped, reblocked, and exposed to a second primary antibody, namely mouse anti-GAPDH (1:20,000), until all proteins of interest were tested.

Immunohistochemistry. Single- and double-labeling of the retina were performed according to previously published methods [20,21]. Briefly, sections were postfixed for 5 minutes in 70% ethanol, rinsed 3 x 5 minutes in 0.1 M Tris buffer, pH 7.4/0.03% Triton and blocked for 90 minutes in 10% normal goat serum (NDS) in 0.1 M Tris buffer/0.5% Triton. Sections were incubated overnight at room temperature with primary antibody in blocking solution. The GPR55 antibody was used conjointly with a known specific retinal cell type marker: rhodopsin, calbindin, glutamine synthetase, PKCα, or PV (Table 1). The next day, sections were washed for 10 minutes and 2 x 5 minutes in 0.1 M Tris /0.03% Triton, blocked in 10% NDS, 0.1 M Tris /0.5% Triton for 30 minutes and incubated with secondary antibody for 1 hour: Alexa 488 donkey anti-mouse, and biotinylated donkey anti-rabbit followed by the addition of streptavidin-Alexa 647 (1:200), all in a blocking solution as described above. Sections were washed again in Tris buffer, counterstained with bisbenzimide (Hoechst 33258, Sigma, 2.5 µg/mL), a fluorescent nuclear marker, and coverslipped with Fluoromount-G™ Mounting Medium (SouthernBiotech, Birmingham, AL).

Confocal microscopy. Fluorescence was detected with a Leica TCS SP2 confocal laser-scanning microscope (Leica Microsystems, Exton, PA), using a 40X (n.a: 1.25 – 0.75) or a 100X (n.a: 1.40 – 0.7) objective. Images were obtained sequentially from the green and far-red channels on optical slices of less than 0.9 µm of thickness. When co-expression of GPR55 and retinal cell markers was ambiguous in some retinal layers, co-labeling or its absence was demonstrated by taking z-stacks with optimized steps. This allowed for visualization of the cells in the X-Y, X-Z and Y-Z axes, thereby confirming the presence or absence of GPR55 in specific retinal cells. All photomicrograph adjustments, including size, color, brightness, and

contrast were done with Adobe Photoshop (CS5, Adobe Systems, San Jose, CA) and then exported to Adobe InDesign (CS5, Adobe Systems, San Jose, CA), where the final figure layout was completed. The schematic panels were created using Adobe Illustrator (CS5, Adobe Systems, San Jose, CA).

Results

Expression profile of GPR55 in monkey retina

In order to determine GPR55 antibody specificity in the vervet monkey, we carried out immunoblots on homogenates of fresh vervet monkey retina (Figure 1A – lane 1), visual cortex (Figure 1A – lane 2), and cerebellum (Figure 1A – lane 3). The expected band was noted at 37 kDa for each type of homogenate. Additional protein signals were detected below 37 kDa in the visual cortex homogenate and above 37 kDa in the cerebellum homogenate, but pre-incubation with GPR55 blocking peptide completely abolished antibody signals (Figure 1B). The GAPDH antibody was used in the same blot to ensure the proper equalization and loading of all samples (Figure 1A and 1B, lower panels). As an added control, the GPR55 antibody was preadsorbed against its blocking peptide prior to incubation with retinal sections, resulting in an absence of staining signal in the section (Figure 1D). GPR55-immunoreactivity (IR) is present throughout the monkey retina, extending from the extrafoveal region to the periphery and densely expressed in rods (Figure 1C and Figure 2). GPR55 is absent in cones, and outer Müller glial cell processes (Figure 3 and Figure 4). While cone cell bodies are located in a single row right below the outer limiting membrane, rod cell bodies make up the rest of the ONL below the cone cell bodies. Careful examination of photoreceptors stained with Sytox green, a nuclear stain, and GPR55 indicates an absence of GPR55 expression in the nuclei of rods (Figure 1E-F, arrows).

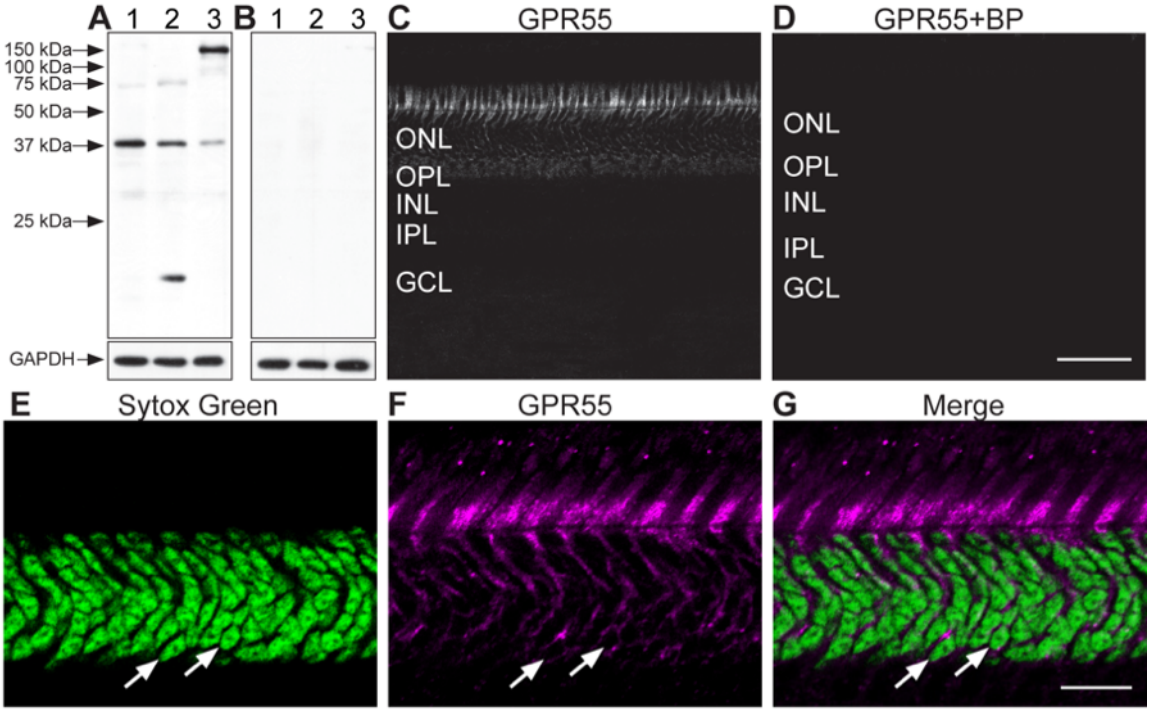

Figure 1. Characterization of GPR55 antibody in the vervet monkey. Western blot analysis of total protein samples from retina (**A – lane 1**), visual cortex (**A – lane 2**) and cerebellum (**A – lane 3**) showing detection of the expected protein band at 37 kDa. The band was not detected when the antibody was pre-incubated with the corresponding GPR55 blocking peptide (BP) (**B – lanes 1-3**). All lanes contained 30 µg of total protein. The lower blots for GPR55 and GPR55-BP show the expression of the protein GAPDH and demonstrates equal loading in all lanes. Immunohistochemistry on vervet retinal tissue with the anti-GPR55 antibody revealed a unique staining profile (**C**). When the GPR55 antibody was pre-incubated with its BP, it revealed an absence of staining (**D**). Double-label of Sytox (green) and GPR55 (magenta) indicated that GPR55 was not present in the nuclei of rods (**E-G**, arrows). ONL, outer nuclear layer; OPL, outer plexiform layer; INL, inner nuclear layer; IPL, inner plexiform layer; GCL, ganglion cell layer. Scale bar = 75 µm for C-D and 15 µm for E-G.

Cellular localization of GPR55 in the retina

The ONL is composed of cone and rod nuclei. There are also Müller cell outer processes that enroll these cell bodies. To distinguish cones and rods, double immunolabeling with cell specific markers was performed. Double-label of GPR55 with rhodopsin, a specific rod

photoreceptor cell marker, allowed us to restrict the labeling to rod photoreceptors (Figure 2). Our results also show that GPR55 was not localized in cone photoreceptors of the monkey extrafoveal and middle retina (Figure 3). Dense GPR55 immunostaining was detected around the cone outer segments (Figure 3). High magnification of the PRL let us identify one cell population immunostained with GPR55 antibody. In the three pairs of retinas used for immunohistochemistry, we found the same staining pattern. No differences in the expression of GPR55 with regard to eccentricity were observed.

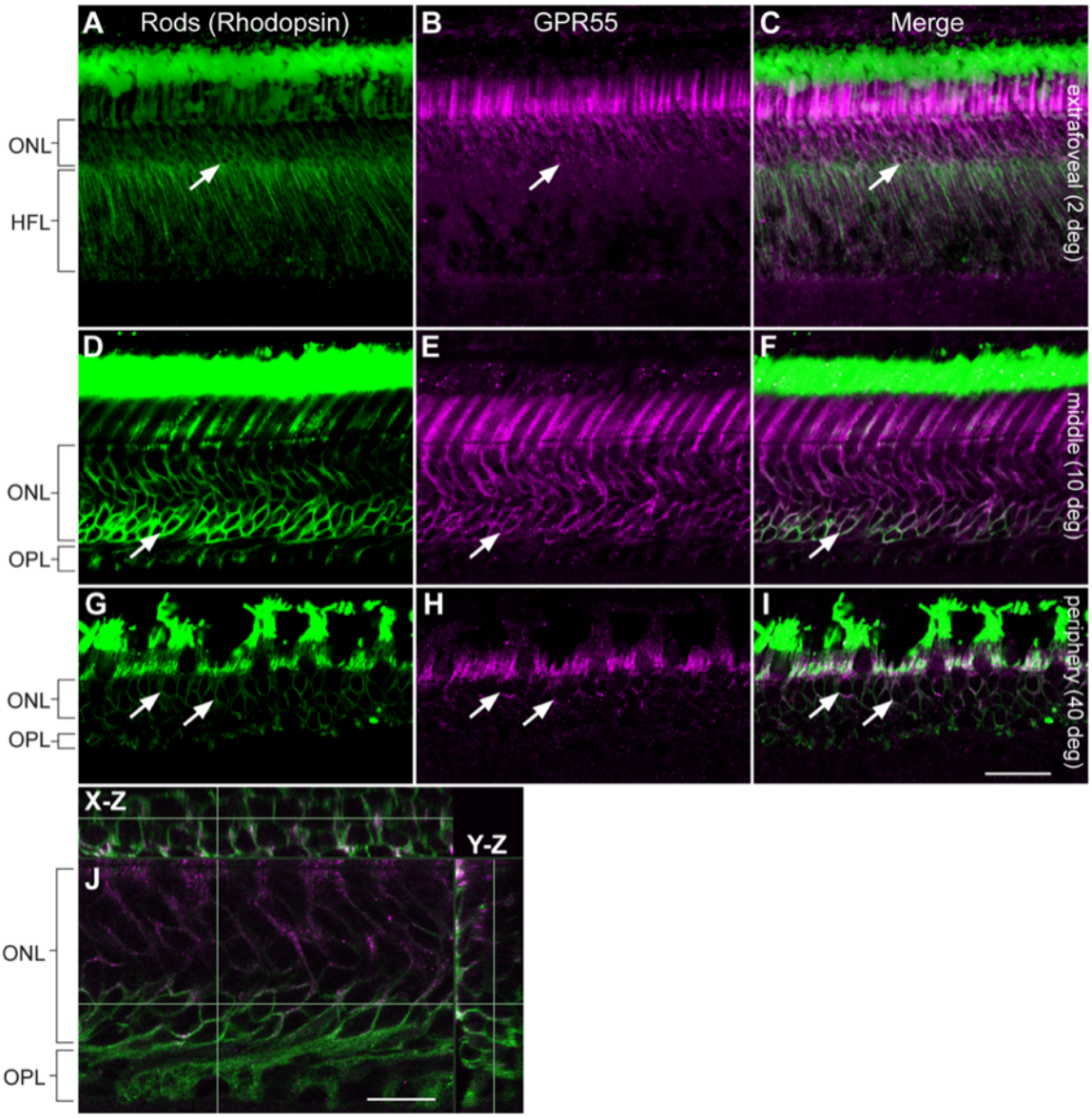

Figure 2. Double-label confocal immunofluorescence illustrating localization of rhodopsin and GPR55 in the monkey extrafoveal, middle, and peripheral retina. Rhodopsin-IR (green)

was not restricted to the rod outer segments; however, this region had the most prominent staining. Note that GPR55-IR (magenta) is present throughout the rods, with the most prominent staining in the inner segments, and very faint staining in the outer segments and spherules. Arrows point to perinuclear staining. Rhodopsin-IR labeled rod photoreceptors in the monkey extrafoveal (**A-C**), middle (**D-F**), and peripheral retina (**G-I**), and these were GPR55 immunoreactive. Note that GPR55-IR is co-localized with rhodopsin-IR, and a 3D reconstruction in the X-Z and Y-Z axes showed no co-localization in rods nuclei (**J**). ONL, outer nuclear layer; HFL, Henle fiber layer; OPL, outer plexiform layer. Scale bar = 75 µm for A-C, 30 µm for D-I, and 15 µm for J.

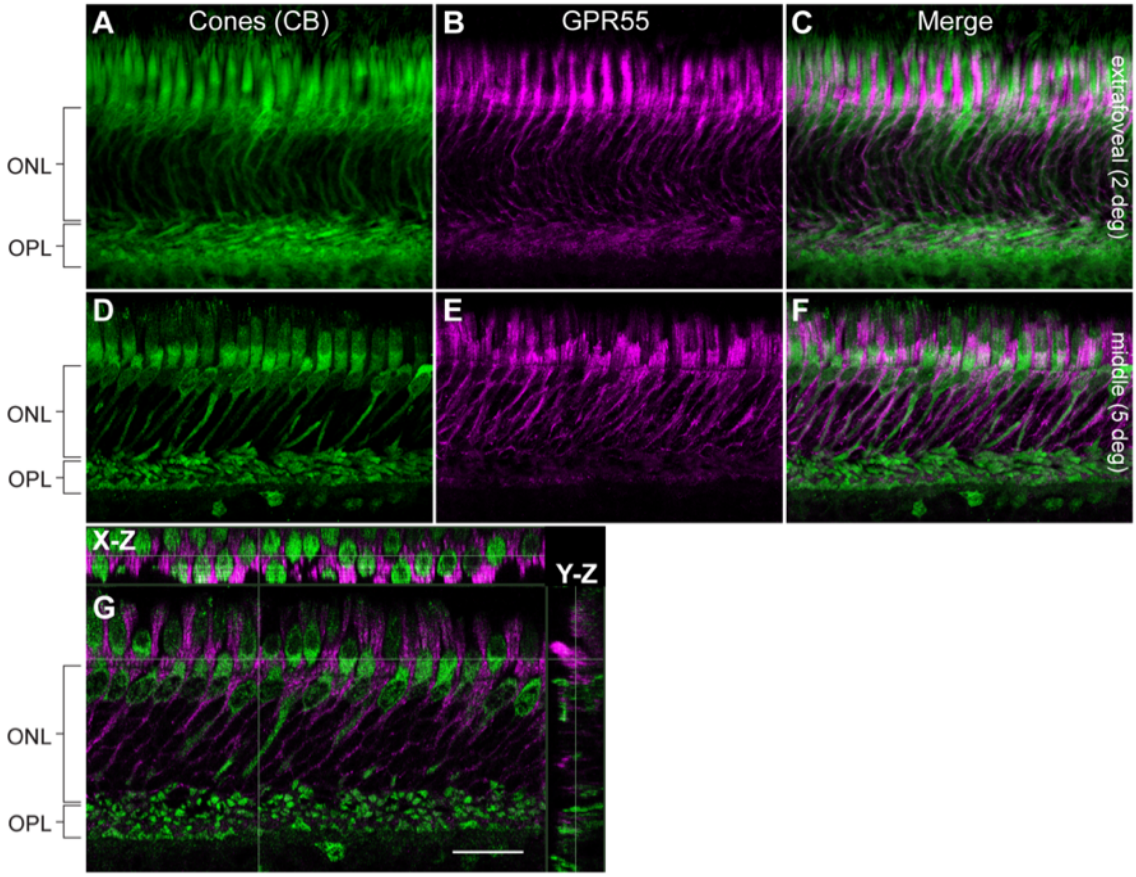

Figure 3. Double-label confocal immunofluorescence illustrating localization of calbindin (CB) and GPR55. Flattened Z-series showing CB-immunoreactive cones photoreceptors (green) in the monkey extrafoveal (**A-C**) and middle (**D-F**) retina, and these were not GPR55-immunoreactive (magenta). Note that GPR55-IR appears co-localized around the cones, but a 3D reconstruction in the X-Z and Y-Z axes showed no co-localization (**G**). This micrograph

shows that the GPR55-immunoreactivity was adjacent to the CB-immunoreactive cone photoreceptors. ONL, outer nuclear layer; OPL, outer plexiform layer. Scale bar = 30 µm.

No GPR55 expression in Müller cells

Double-labeling of GPR55 and GS, a specific marker for labeling both somata and processes of Müller cells [20,21], was performed for assessing the expression of GPR55 in Müller cells. As shown in Figure 4, Müller cells span the entire neural retina and their processes expand in the GCL to form characteristic endfeet. No GPR55 immunoreactivity was detected in GS-positive somata and processes of Müller cells (Figure 4).

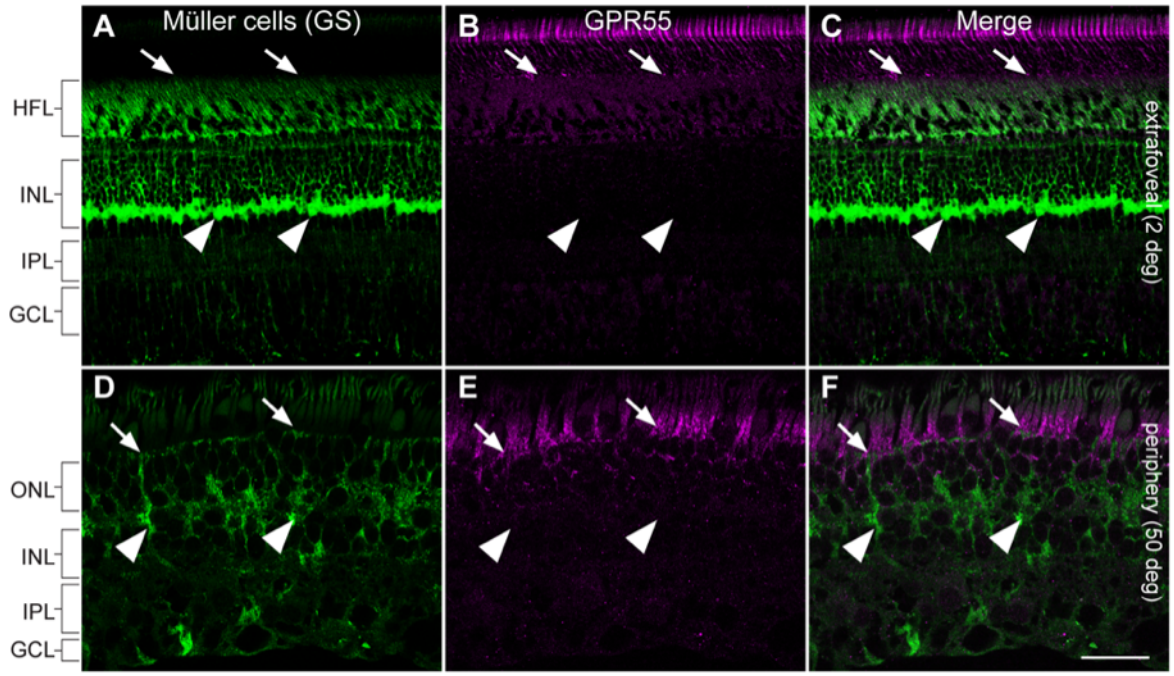

Figure 4. Double-label confocal immunofluorescence illustrating localization of glutamine synthetase (GS) and GPR55. GS-IR (green), labeling Müller cells in the primate retina, did not colocalize with GPR55-IR (magenta) in vertical sections taken from the extrafoveal region (**A-C**). Arrows indicate the projections of the Müller cell membrane in the apical margin known as apical villi that lack GPR55. Arrowheads point at Müller cell bodies that do not express GPR55. The absence of GPR55 and GS colocalization in Müller cells villi and cell bodies is also shown in vertical sections taken from the peripheral retina (**D-F**). HFL, Henle fiber layer; ONL, outer nuclear layer; INL, inner nuclear layer; IPL, inner plexiform layer; GCL, ganglion cell layer. Scale bar = 75 µm for A-C and 30 µm for D-F.

No GPR55 expression in horizontal and bipolar cell extensions in the OPL

We wanted to know if the little GPR55 expression found in rod spherules was also present in horizontal and bipolar cells outer processes. Double label of PKC, a rod bipolar cell marker, and GPR55 allowed us to establish that GPR55 was strictly localized in rods. Dendritic fibers of rod bipolar cells were rather juxtaposed to GRP55 immunoreactive rod spherules (Figure 5A-C). Moreover, GPR55 did not colocalize with parvalbumin, a marker that labels primate horizontal cells including their dendritic invaginations into rod photoreceptor terminals (Figure 5D-F).

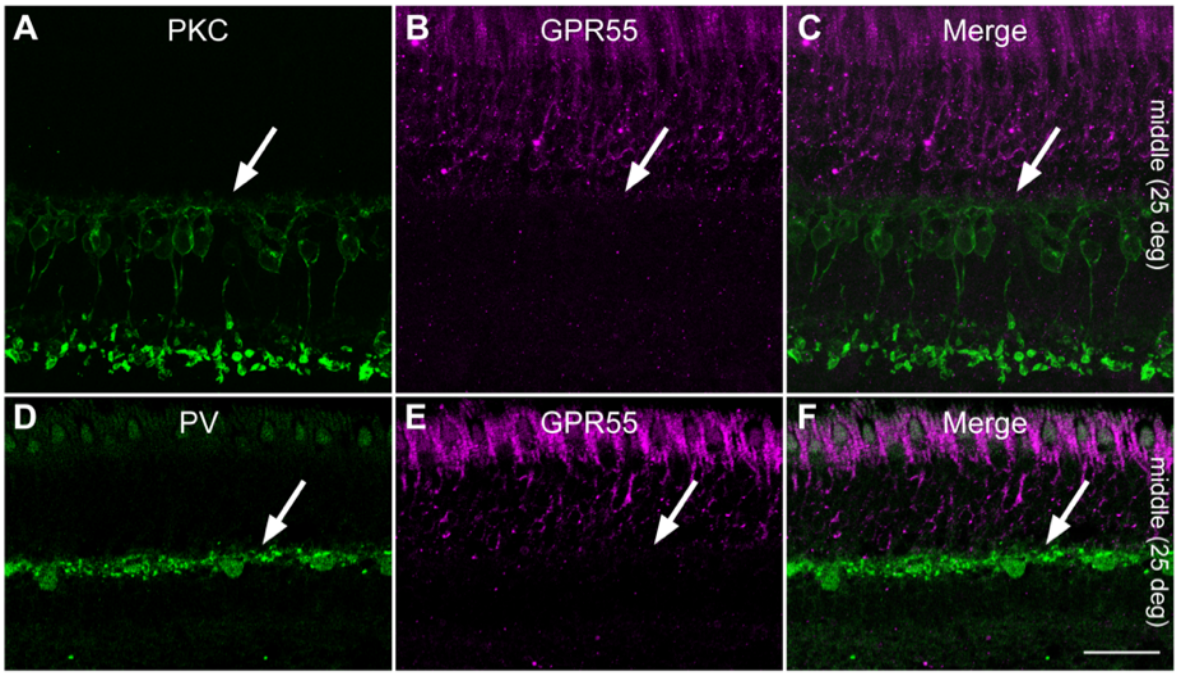

Figure 5. Double-label confocal immunofluorescence illustrating localization of PKC or parvalbumin (PV) and GPR55. PKC-IR (green), labeling specifically rod bipolar cells, did not colocalize with GPR55-IR (magenta) in vertical section taken from the middle retina (**A-C**). Additionally, PV-IR (green), marking horizontal cells in the primate retina, did not colocalize with GPR55-IR (magenta) vertical section taken from the middle retina (**D-F**). Scale bar = 30 µm for A-C and 75 µm for D-F.

Labeling of GPR55, CB1R, and CB2R

The GPR55, CB1R, and CB2R antibodies that we selected came from the same host, making the use of simultaneous double-labeling protocol not adequate. We therefore used serial sections to compare the distribution of CB1R, CB2R, and GPR55 (Figure 6A-C). These 3 receptors are differentially expressed in the retina. CB1R is found in the neural retina, including the photoreceptors (cones with a prominent staining in their outer segments and pedicles, and rods with little staining restricted to their spherules), the horizontal cells, the bipolar cells, amacrine cells, and ganglion cells. CB2R is found in the glial component of the retina, namely Müller cells. GPR55 is exclusively expressed in rods, with a prominent signal in the inner segments. These data are summarized schematically in Figure 6D for all retinal cell types.

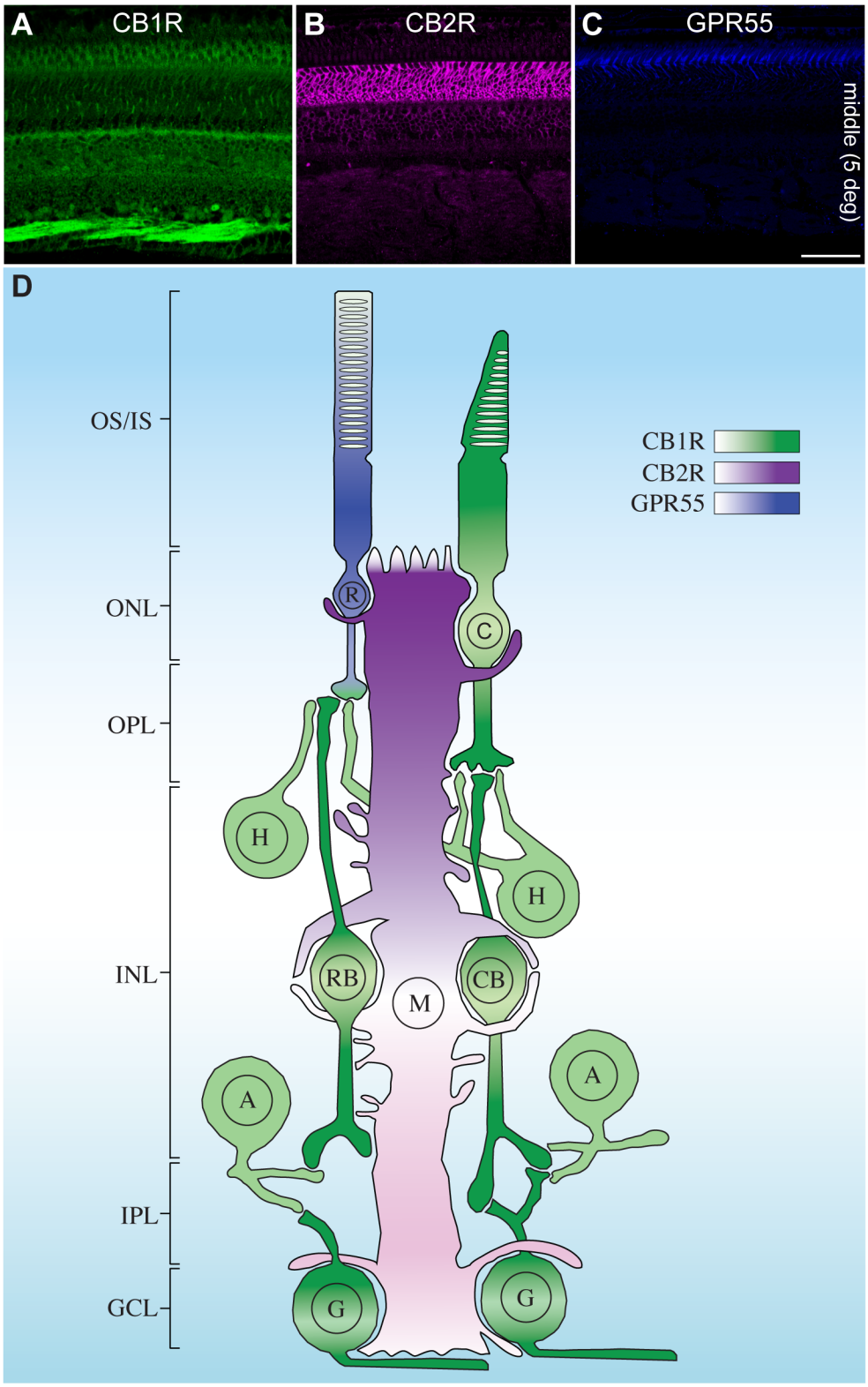

Figure 6. Confocal immunofluorescence images and a schematic illustration representing the localization of CB1R, CB2R, and GPR55 in the monkey retina. CB1R is localized in neural

components, with very weak (albeit absence) of GPR55-IR in rods (**A**). CB2R is strictly expressed in the glial components, the Müller cells (**B**). GPR55 is found exclusively in rods, with the most prominent staining in the inner segments (**C**). Color bars in the schematic illustration (**D**) indicate the intensity of CB1R (green), CB2R (magenta), and GPR55 (blue) expressions. OS/IS, outer and inner segments of rods and cones; ONL, outer nuclear layer; OPL, outer plexiform layer; INL, inner nuclear layer; IPL, inner plexiform layer; GCL, ganglion cell layer; C, cones; R, rods; H, horizontal cells; RB, rod bipolar cells; CB, cone bipolar cells; A, amacrine cells; G, retinal ganglion cells; M, Müller cells. Scale bar = 75 μm.

Discussion

The present results demonstrate the existence of GPR55 in the monkey extrafoveal and peripheral retina. The localization of GPR55 in rods is important because, although the presence of CB1R and CB2R in the monkey retina is well established [20,21,44], we are still far from identifying the exact role of the cannabinoid receptors in primate retinal functions. The data presented here provide new information concerning cannabinoid receptors' expression in the monkey retina, and suggest new directions for uncovering their functions. It is somewhat surprising that protein from CB1R, CB2R, and GPR55 is detectable in distinct cell types of the monkey retina.

CB1R was localized in the neural components of the monkey central and peripheral retina [20]. CB1R immunoreactivity was present in cones, horizontal cells, bipolar cells, amacrine cells and ganglion cells. The most prominent expression of CB1R was found in the cones of the *fovea centralis*. The exact role of this receptor in retinal function is unknown although there is general agreement that cannabinoids suppress dopamine release and reduce neurotransmitter release from cones and bipolar cells [3].

CB2R neuronal expression has been ambiguous and controversial, but nevertheless, the majority agrees on the presence of this receptor in glial components of the CNS. Indeed, CB2R was detected in the glial component of the monkey retina, Müller cells [21]. The role of this receptor has been hypothesized and suggests that it is an important player for the regulation and buffering of potassium following light activation in the retina.

GPR55 expression was found specifically in rod photoreceptors and enriched in the inner segment, although smaller amounts of this protein could be detected essentially throughout the rods of the extrafoveal and peripheral regions of the retina. It is plausible that such an asymmetric distribution of GPR55 reflects its function in phototransduction in relation with transducin.

Given that CB1R is present in the neuroretina, CB2R in the retinal glia, and GPR55 in rods, we can hypothesize that each of these receptors has a unique retinal function.

Furthermore, THC can bind to GPR55 and induce a signal transduction different from that of CB1R and CB2R [6]. Even though GPR55 is phylogenetically distinct from the traditional cannabinoid receptors, in some experimental paradigms, it is also activated by endocannabinoids, phytocannabinoids, and synthetic cannabinoid ligands [45]. While Kumar et al. (2012) using the same antibody reported the presence of GPR55 in human trabecular meshwork cells by Western blot analysis, these authors did not assess the localization of GPR55-positive cells in the retina. By double immunolabeling, we obtained a general picture of GPR55 localization in the monkey retina. A schematic diagram summarizing our results is presented in Figure 6. We report for the first time the presence of GPR55 in rod photoreceptors of the monkey retina. Certainly, immunohistochemistry is extremely sensitive and the presence of a small amount of protein does not guarantee a functionally important protein. It will be worthwhile to verify if CB1R-, CB2R-, or/and GPR55-blockade have an effect on retinal function.

Hypothetical functional implications

In the dark, rods are depolarized and constantly stimulated to allow the release of glutamate. Glutamate then binds to mGluR6 to hyperpolarize rod bipolar cells and to iGluRs to depolarize horizontal cells. It is well documented that LPI is a lysophospholipid-signaling molecule that modulates many cell functions. In fact, the generation of LPI is linked to the metabolism of membrane phospholipids by enzymes like phospholipase A1 and A2 that are activated upon cell stimulation and are located at the inner and outer side of the plasma membrane. Initially, LPI has been discussed to serve as second-messenger lysophospholipid that modulate intracellular signaling events [46]. LPI is a key signaling intermediate that modulates many aspects of cellular function. The identification of this ligand as a novel target for GPR55 suggests a fundamental role for this receptor in physiological processes. It has also been proposed that GPR55 exhibits a constitutive activity [47]. Characterization of the eCB system in other brain areas has shown that GPR55 activation induces intracellular Ca^{++} fluctuations through a RhoA-mediated, and inositol 1,4,5-trisphosphate (IP_3)-sensitive mechanism mobilizing Ca^{++} stores [6,8,10]. In fact, stimulation of GPR55 by LPI evokes an intracellular Ca^{2+} rise in hippocampal slices [48]. We present here a hypothetical model of the role of GPR55 in retina. Given that rods are in a depolarized state and continuously active in

the dark, a high tone of LPI activating GPR55, thereby leaving calcium channels open, maintains the constant release of glutamate. In the presence of light stimulation, rod membranes are hyperpolarized, LPI is in a lower basal tone, and the release of glutamate is reduced (Figure 7). We show here for the first time that GPR55 is exclusively expressed in rods of the vervet monkey, although further experiments are still needed in order to clarify its precise role in scotopic vision. In a companion study, we investigated the effects of intravitreal injections of LPI, a specific endogenous agonist of GPR55, on the scotopic electroretinogram of normal vervet monkeys. We found, in accordance with our hypothesis (illustrated in the model in Figure 7), that the scotopic ERG is modified by the activation of GPR55. Indeed, following the injection of LPI, there is a large increase in the rod response (unpublished data).

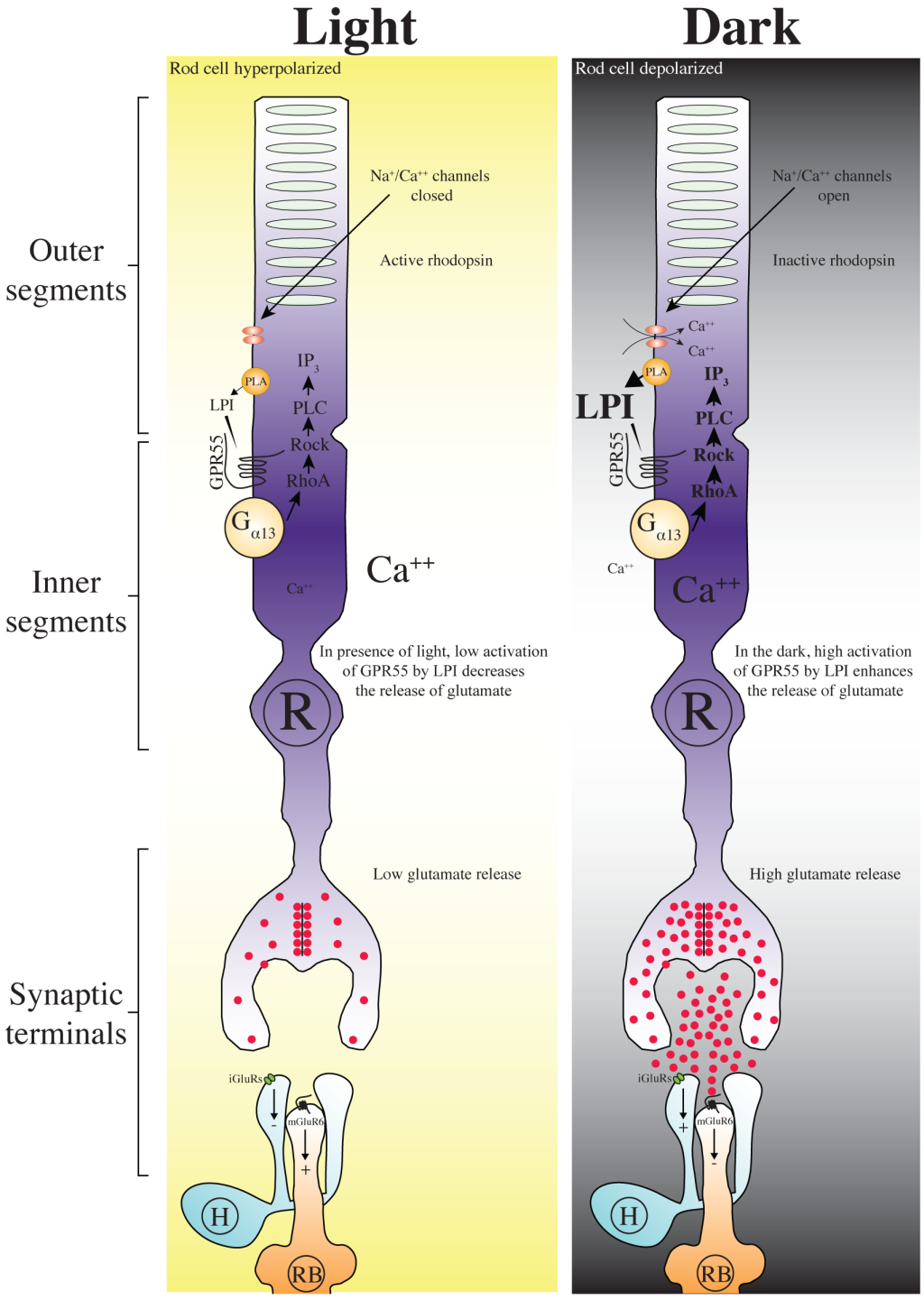

Figure 7. Schematic illustration depicting a hypothetical function for GPR55 in the monkey retina. Activation of GPR55 by LPI could represent a new modulation process in rods thus regulating scotopic vision. In the dark, rods are depolarized and a cytoplasmic isoform of

phospholipase A2 can synthetize LPI and release it in the extracellular media. LPI binds GPR55 and activate distinct intracellular signaling cascades, including RhoA activation, IP_3 release, and Ca^{2+} mobilization, ultimately controlling the release of glutamate. In presence of light, hyperpolarized rods produce low levels of LPI; in the dark, depolarized rods synthesize and accumulate high levels of LPI. R, rods; H, horizontal cells; RB, rod bipolar cells; LPI, lysophosphatidylinositol; iGluR, ionotropic glutamate receptors; mGluR, metabotropic glutamate receptors; cPLA, cytosolic phospholipase A2.

References

1. Di Marzo V, Melck D, Bisogno T, De Petrocellis L (1998) Endocannabinoids: endogenous cannabinoid receptor ligands with neuromodulatory action. Trends Neurosci 21: 521-528.
2. Alger BE, Kim J (2011) Supply and demand for endocannabinoids. Trends Neurosci 34: 304-315.
3. Yazulla S (2008) Endocannabinoids in the retina: from marijuana to neuroprotection. Prog Retin Eye Res 27: 501-526.
4. Begg M, Pacher P, Bátkai S, Osei-Hyiaman D, Offertáler L, et al. (2005) Evidence for novel cannabinoid receptors. Pharmacol Ther 106: 133-145.
5. Zhao P, Abood ME (2013) GPR55 and GPR35 and their relationship to cannabinoid and lysophospholipid receptors. Life Sci 92: 453-457.
6. Lauckner JE, Jensen JB, Chen HY, Lu HC, Hille B, et al. (2008) GPR55 is a cannabinoid receptor that increases intracellular calcium and inhibits M current. Proc Natl Acad Sci U S A 105: 2699-2704.
7. Ryberg E, Larsson N, Sjogren S, Hjorth S, Hermansson NO, et al. (2007) The orphan receptor GPR55 is a novel cannabinoid receptor. Br J Pharmacol 152: 1092-1101.
8. Waldeck-Weiermair M, Zoratti C, Osibow K, Balenga N, Goessnitzer E, et al. (2008) Integrin clustering enables anandamide-induced Ca2+ signaling in endothelial cells via GPR55 by protection against CB1-receptor-triggered repression. J Cell Sci 121: 1704-1717.
9. Sharir H, Console-Bram L, Mundy C, Popoff SN, Kapur A, et al. (2012) The endocannabinoids anandamide and virodhamine modulate the activity of the candidate cannabinoid receptor GPR55. J Neuroimmune Pharmacol 7: 856-865.
10. Henstridge CM, Balenga NA, Ford LA, Ross RA, Waldhoer M, et al. (2009) The GPR55 ligand L-alpha-lysophosphatidylinositol promotes RhoA-dependent Ca2+ signaling and NFAT activation. FASEB J 23: 183-193.
11. Oka S, Nakajima K, Yamashita A, Kishimoto S, Sugiura T (2007) Identification of GPR55 as a lysophosphatidylinositol receptor. Biochem Biophys Res Commun 362: 928-934.

12. Oka S, Toshida T, Maruyama K, Nakajima K, Yamashita A, et al. (2009) 2-Arachidonoyl-sn-glycero-3-phosphoinositol: a possible natural ligand for GPR55. J Biochem 145: 13-20.

13. Elbegdorj O, Westkaemper RB, Zhang Y (2013) A homology modeling study toward the understanding of three-dimensional structure and putative pharmacological profile of the G-protein coupled receptor GPR55. J Mol Graph Model 39: 50-60.

14. Ashton JC (2012) The atypical cannabinoid o-1602: targets, actions, and the central nervous system. Cent Nerv Syst Agents Med Chem 12: 233-239.

15. Kargl J, Balenga N, Parzmair GP, Brown AJ, Heinemann A, et al. (2012) The cannabinoid receptor CB1 modulates the signaling properties of the lysophosphatidylinositol receptor GPR55. J Biol Chem 287: 44234-44248.

16. Gasperi V, Dainese E, Oddi S, Sabatucci A, Maccarrone M (2013) GPR55 and its interaction with membrane lipids: comparison with other endocannabinoid-binding receptors. Curr Med Chem 20: 64-78.

17. Pietr M, Kozela E, Levy R, Rimmerman N, Lin YH, et al. (2009) Differential changes in GPR55 during microglial cell activation. FEBS Lett 583: 2071-2076.

18. Wu CS, Chen H, Sun H, Zhu J, Jew CP, et al. (2013) GPR55, a G-Protein Coupled Receptor for Lysophosphatidylinositol, Plays a Role in Motor Coordination. PLoS One 8: e60314.

19. Henstridge CM, Balenga NA, Kargl J, Andradas C, Brown AJ, et al. (2011) Minireview: recent developments in the physiology and pathology of the lysophosphatidylinositol-sensitive receptor GPR55. Mol Endocrinol 25: 1835-1848.

20. Bouskila J, Burke MW, Zabouri N, Casanova C, Ptito M, et al. (2012) Expression and localization of the cannabinoid receptor type 1 and the enzyme fatty acid amide hydrolase in the retina of vervet monkeys. Neuroscience 202: 117-130.

21. Bouskila J, Javadi P, Casanova C, Ptito M, Bouchard JF (2013) Müller cells express the cannabinoid CB2 receptor in the vervet monkey retina. J Comp Neurol 521: 2399-2415.

22. El-Remessy AB, Khalifa Y, Ola S, Ibrahim AS, Liou GI (2010) Cannabidiol protects retinal neurons by preserving glutamine synthetase activity in diabetes. Mol Vis 16: 1487-1495.

23. Kumar A, Qiao Z, Kumar P, Song ZH (2012) Effects of palmitoylethanolamide on aqueous humor outflow. Invest Ophthalmol Vis Sci 53: 4416-4425.

24. Henstridge CM (2012) Off-target cannabinoid effects mediated by GPR55. Pharmacology 89: 179-187.

25. Ozawa Y, Nakao K, Kurihara T, Shimazaki T, Shimmura S, et al. (2008) Roles of STAT3/SOCS3 pathway in regulating the visual function and ubiquitin-proteasome-dependent degradation of rhodopsin during retinal inflammation. J Biol Chem 283: 24561-24570.

26. Chiquet C, Dkhissi-Benyahya O, Chounlamountri N, Szel A, Degrip WJ, et al. (2002) Characterization of calbindin-positive cones in primates. Neuroscience 115: 1323-1333.

27. Fischer AJ, Hendrickson A, Reh TA (2001) Immunocytochemical characterization of cysts in the peripheral retina and pars plana of the adult primate. Invest Ophthalmol Vis Sci 42: 3256-3263.

28. Kolb H, Zhang L, Dekorver L, Cuenca N (2002) A new look at calretinin-immunoreactive amacrine cell types in the monkey retina. J Comp Neurol 453: 168-184.

29. Martínez-Navarrete GC, Angulo A, Martín-Nieto J, Cuenca N (2008) Gradual morphogenesis of retinal neurons in the peripheral retinal margin of adult monkeys and humans. J Comp Neurol 511: 557-580.

30. Martínez-Navarrete GC, Martín-Nieto J, Esteve-Rudd J, Angulo A, Cuenca N (2007) Alpha synuclein gene expression profile in the retina of vertebrates. Mol Vis 13: 949-961.

31. Chang ML, Wu CH, Jiang-Shieh YF, Shieh JY, Wen CY (2007) Reactive changes of retinal astrocytes and Müller glial cells in kainate-induced neuroexcitotoxicity. J Anat 210: 54-65.

32. Riepe RE, Norenburg MD (1977) Müller cell localisation of glutamine synthetase in rat retina. Nature 268: 654-655.

33. Zabouri N, Bouchard JF, Casanova C (2011a) Cannabinoid receptor type 1 expression during postnatal development of the rat retina. J Comp Neurol 519: 1258-1280.

34. Zabouri N, Ptito M, Casanova C, Bouchard JF (2011b) Fatty acid amide hydrolase expression during retinal postnatal development in rats. Neuroscience 195: 145-165.

35. Nishikawa S, Tamai M (2001) Müller cells in the human foveal region. Curr Eye Res 22: 34-41.

36. Mills SL, Massey SC (1999) AII amacrine cells limit scotopic acuity in central macaque retina: A confocal analysis of calretinin labeling. J Comp Neurol 411: 19-34.

37. Cuenca N, Herrero MT, Angulo A, de Juan E, Martinez-Navarrete GC, et al. (2005) Morphological impairments in retinal neurons of the scotopic visual pathway in a monkey model of Parkinson's disease. J Comp Neurol 493: 261-273.

38. Bordt AS, Hoshi H, Yamada ES, Perryman-Stout WC, Marshak DW (2006) Synaptic input to OFF parasol ganglion cells in macaque retina. J Comp Neurol 498: 46-57.

39. Wässle H, Dacey DM, Haun T, Haverkamp S, Grunert U, et al. (2000) The mosaic of horizontal cells in the macaque monkey retina: with a comment on biplexiform ganglion cells. Vis Neurosci 17: 591-608.

40. Qi H-X, Gharbawie OA, Wong P, Kaas JH (2011) Cell-poor septa separate representations of digits in the ventroposterior nucleus of the thalamus in monkeys and prosimian galagos. J Comp Neurol 519: 738-758.

41. Ellert-Miklaszewska A, Grajkowska W, Gabrusiewicz K, Kaminska B, Konarska L (2007) Distinctive pattern of cannabinoid receptor type II (CB2) expression in adult and pediatric brain tumors. Brain Res 1137: 161-169.

42. Zurolo E, Iyer AM, Spliet WGM, Van Rijen PC, Troost D, et al. (2010) CB1 and CB2 cannabinoid receptor expression during development and in epileptogenic developmental pathologies. Neuroscience 170: 28-41.

43. Burke M, Zangenehpour S, Bouskila J, Boire D, Ptito M (2009) The gateway to the brain: dissecting the primate eye. J Vis Exp: e1261.

44. Straiker A, Stella N, Piomelli D, Mackie K, Karten HJ, et al. (1999) Cannabinoid CB1 receptors and ligands in vertebrate retina: localization and function of an endogenous signaling system. Proc Natl Acad Sci U S A 96: 14565-14570.

45. Balenga NA, Henstridge CM, Kargl J, Waldhoer M (2011) Pharmacology, signaling and physiological relevance of the G protein-coupled receptor 55. Adv Pharmacol 62: 251-277.

46. Corda D, Iurisci C, Berrie CP (2002) Biological activities and metabolism of the lysophosphoinositides and glycerophosphoinositols. Biochim Biophys Acta 1582: 52-69.

47. Brown AJ, Daniels DA, Kassim M, Brown S, Haslam CP, et al. (2011) Pharmacology of GPR55 in yeast and identification of GSK494581A as a mixed-activity glycine transporter subtype 1 inhibitor and GPR55 agonist. J Pharmacol Exp Ther 337: 236-246.

48. Sylantyev S, Jensen TP, Ross RA, Rusakov DA (2013) Cannabinoid- and lysophosphatidylinositol-sensitive receptor GPR55 boosts neurotransmitter release at central synapses. Proc Natl Acad Sci U S A 110: 5193-5198.

Acknowledgements

We sincerely thank Florence Dotigny for excellent technical assistance. We are very grateful to Dr. Frank Ervin and Dr. Roberta Palmour of the Behavioral Sciences Foundation Laboratories of St-Kitts, West Indies, for supplying the vervet monkey tissues.

ARTICLE 4: COMPARATIVE ANALYSIS OF THE ENDOCANNABINOID SYSTEM IN THE RETINA OF MICE, TREE SHREWS AND MONKEYS

Publié dans :

Bouskila J, Javadi P, Elkrief L, Casanova C, Bouchard JF, Ptito M (2016) A comparative analysis of the endocannabinoid system in the retina of mice, tree shrews and monkeys, *Neural Plasticity* 2016 :3127658.

A comparative analysis of the endocannabinoid system in the retina of mice, tree shrews and monkeys

Joseph Bouskila[1, 2], Pasha Javadi[1], Laurent Elkrief[1, 3], Christian Casanova[1], Jean-François Bouchard[1] and Maurice Ptito[1, 4]

[1]School of Optometry, University of Montreal, Montreal, QC, Canada

[2]Biomedical Sciences, Faculty of Medicine, University of Montreal, Montreal, QC, Canada

[3]Faculty of Medicine, University of Montreal, Montreal, QC, Canada

[4]BRAINlab and Neuropsychiatry Laboratory, Department of Neuroscience and Pharmacology, University of Copenhagen, Copenhagen, Denmark

Abbreviated title: The retinal endocannabinoid system

Keywords: CB1R, CB2R, endocannabinoids, mammals, retina, comparative

Correspondence should be addressed to:

Maurice Ptito, PhD

School of Optometry, room 260-7

3744 Jean-Brillant Street,

University of Montreal,

Montreal, Quebec, Canada, H3T 1P1

Abstract

The endocannabinoid (eCB) system is widely expressed in various parts of the central nervous system, including the retina. The localization of the key eCB receptors, particularly CB1R and CB2R, has been recently reported in rodent and primate retinas with striking interspecies differences. Little is known about the enzymes involved in the synthesis and degradation of these eCBs. We therefore examined the expression and localization of the main components of the eCB system in the retina of mice, tree shrews, and monkeys. We found that CB1R and FAAH distributions are well preserved among these species. However, expression of NAPE-PLD is circumscribed to the photoreceptor layer only in monkeys. In contrast, CB2R expression is variable across these species; in mice, CB2R is found in retinal neurons but not in glial cells; in tree shrews, CB2R is expressed in Müller cell processes of the outer retina and in retinal neurons of the inner retina; in monkeys, CB2R is restricted to Müller cells. Finally, the expression patterns of MAGL and DAGLα are differently expressed across species. Overall, these results provide evidence that the eCB system is differently expressed in the retina of these mammals and suggest a distinctive role of eCBs in visual processing.

Introduction

Marijuana contains over 70 cannabinoids that mimic the endogenous ligands called endocannabinoids (eCBs) that cause global psychoactive and physiological effects. The eCB system is mainly composed of the specific G-protein-coupled receptors CB1R and CB2R, the eCBs (anandamide and 2-arachidonoylglycerol), the synthesising enzymes NAPE-PLD (*N*-acyl phosphatidylethanolamine-specific phospholipase D) and DAGLα (diacylglycerol lipase alpha), and the degradation enzymes FAAH (fatty acid amide hydrolase) and MAGL (monoacylglycerol lipase). The cannabinoid receptors are found in many mammals, as well as in various classes of vertebrates and invertebrates, in all major subdivisions of bilaterians, urochordates and cephalochordates, but not in the nonchordate invertebrate phyla like insects [1-3]. The cannabinoid receptors may have evolved in the last common ancestor of the bilaterians with a secondary loss in the insects and other clades [1]. The enzymes responsible for the biosynthesis and the degradation of eCBs are present throughout the animal kingdom [4, 5]. For example, in the rat hippocampus, cerebellum and amygdala, the distribution of the cytosolic enzyme MAGL is complementary to FAAH (presynaptic vs postsynaptic) suggesting different roles for these two eCBs in the central nervous system (CNS) [6]. The eCB system appears widely distributed in the CNS and points to a fundamental modulatory role of eCBs in the control of many central and peripheral biological functions [7]. A number of specific roles have been ascribed to the eCB system in biological functions, such as neuroprotection, neurogenesis, axon guidance, synaptic plasticity, nociception, motor activity, and memory [8-12]. Disturbances of normal eCB activity may therefore be associated with various brain disorders [13-16].

The eCB system is also found in the retina of various species [17] albeit noticeable differences in its anatomical organization. Compared to rodents, the retina of tree shrews is more similar to primates [18]. Mice have a rod-dominated retina that is specialized for scotopic conditions [19] with a low visual resolution [20]. Mouse and tree shrew retinas have no fovea compared to primates. However, tree shrews have a well-developed binocular visual system, with a cone-dominated retina [21].

In the retina, the expression of CB1R is well preserved in many species including mice, rats, chicks, larval tiger salamanders, goldfish, and rhesus monkeys [22]. CB1R and CB2R are also present in various retinal cell types (cones, bipolar, ganglion, horizontal, and amacrine cells) with however some differences [17, 23-27]. For example, CB2R is expressed throughout the mouse retina [25] but it is present exclusively in the Müller cells of the vervet monkey [24]. While DAGLα is widely distributed throughout the IPL in the mouse retina, MAGL is only present in rod spherules, cone pedicles in OPL, but also the IPL [28]. Both MAGL and DAGLα have been found in an overlapping pattern with CB1R and CB2R in the rat retina. In rats, DAGLα is expressed from the early stages of development in photoreceptors, horizontal, amacrine, and ganglion cells and MAGL later during development mainly in amacrine and Müller cells [29]. The expression and distribution of the major components of the eCB system, notably the metabolizing enzymes (NAPE-PLD, DAGLα, FAAH, MAGL), in the retina of different mammals have not been studied in depth. It is therefore our aim to analyze the expression of several components of the eCB system and to characterize their distribution pattern in the distinct retinal layers and cell types of three different mammalian species: mice, tree shrews and monkeys (vervets and macaques).

Materials and Methods

Biological material. Eyes from 3 adult mice (C57BL/6; 3–4 months old), 2 adult tree shrews (*Tupaia belangeri*; 3-4 months old), 3 vervet monkeys (*Chlorocebus sabeus*; 3-4 years of age), and 2 rhesus monkeys (*Macaca mulatta*; 3-4 years of age) were used in this study. The animals were part of ongoing research projects that were approved by the University of Montreal and McGill University Animal Care and Use Committees. For all species, anterior segment of the eye and vitreous were cut away. The eyecups were bathed in 4% paraformaldehyde made in 0.1 M sodium phosphate buffer at pH 7.4, and left overnight in the solution. The retina was dissected free from the eyecup in a phosphate-buffered saline (PBS) medium. It was laid flat so that the vitreous body could be removed by blotting with filter paper and gentle brushing. Samples of the retina were taken at the center and periphery. Each sample was then cryoprotected in 30% sucrose overnight and embedded in Shandon embedding media at -65°C. The blocks were cut in 20 μm sections at -18°C with a Leica CM3050S cryostat and mounted onto gelatinized subbed glass slides, air dried, and stored at -80°C for further processing.

Immunofluorescence. Single-, double-, and triple-labeling of the retina were performed according to previously published methods [23, 24, 30]. Briefly, the sections were post-fixed for 5 minutes in 70% ethanol, rinsed 3 x 5 minutes in 0.1 M Tris buffer, pH 7.4/0.03% Triton and blocked for 90 minutes in 10% normal donkey serum (NDS) in 0.1 M Tris buffer/0.5% Triton. Sections were then incubated with primary antibodies prepared in blocking solution overnight at room temperature. The cannabinoid-related antibodies (CB1R, NAPE-PLD, FAAH, CB2R, DAGLα, MAGL) were also used conjointly with a known specific retinal cell type marker (Table 1). The next day, sections were washed for 10 minutes and 2 x 5 minutes in 0.1 M Tris /0.03% Triton. Then, they were blocked in 10% NDS, 0.1 M Tris /0.5% Triton for 60 minutes and incubated with secondary antibody for one hour (Alexa 488 donkey anti-mouse, and biotinylated donkey anti-rabbit followed by the addition of streptavidin-Alexa 647 (1:200), all prepared in blocking solution). Sections were counterstained with Sytox Green Nucleic Acid Stain (1:50,000; Molecular Probes, Inc., Eugene, OR) washed again in Tris buffer, and coverslipped with Fluoromount-G™ Mounting Medium (SouthernBiotech, Birmingham, AL).

Antibody characterization. In this study, we were confronted with the problem concerning the specificity of some of the antibodies, especially for the tree shrew. Although knockout animals are the best way to test the specificity of antibodies, this model is available only for mice, and not for tree shrews and monkeys. We therefore resorted to the use of conventional alternative methods to circumvent this methodological limitation [23-27]. We have previously published Western blot results for mice and vervet monkeys [23-25]. For tree shrews and macaques, the tissue was not made available to us. Therefore, we resorted to the traditional blocking techniques presented in the manuscript as BP in Figures 1 and 2. Table 1 summarizes the source and the working dilution of all the primary antibodies. The antibodies used in the present study were characterized and published in previous publications: calbindin [23, 31-35], CB1R [23, 26], CB2R [24, 36], DAGLα [26], FAAH [23, 27], GS [23, 37, 38, 39], MAGL, NAPE-PLD [47], rhodopsin [30, 40], and PKCα [23, 26, 27, 34].

Table 1. List of antibodies used in this study.

Antibody[1]	Immunogen	Source[2]	Working dilution
CB	Purified bovine kidney calbindin-D28K	Sigma-Aldrich, St. Louis, MO; C9848, mouse monoclonal, clone CB0955	1:250
CB1R	Fusion protein containing aa 1–77 of rat CB1R	Calbiochem, Gibbstown, NJ; 209550, rabbit polyclonal	1:150
CB2R	Synthetic peptide corresponding to aa 20–33 of human CB2R	Cayman Chemical, Ann Arbour, MI; 101550, rabbit polyclonal	1:150
DAGLα	Peptide with sequence CPAKQDELVISAR, from the C Terminus of the protein sequence	Novus, Littleton, CO; NBP2-31856, rabbit polyclonal	1:100
FAAH	Synthetic peptide aa 561–579 of rat FAAH	Cayman Chemical, Ann Arbour, MI; 101600, rabbit polyclonal	1:150
GS	Full protein purified from sheep brain	Chemicon, Temecula, CA; MAB302, mouse monoclonal, clone GS-6	1:500
MAGL	Human MAGL aa 1-14	Cayman Chemical, Ann Arbour, MI; 100035, rabbit polyclonal	1:150
NAPE-PLD	Purified protein corresponding to aa 159-172 NAPE-PLD human	Cayman Chemical, Ann Arbour, MI; 10305, rabbit polyclonal	1:200
Rhodopsin	Bovine rhodopsin	Abcam, Toronto, ON; ab98887, mouse monoclonal, clone Rho 4D2	1:500
PKCα	Peptide mapping the aa 296–317 of human PKCα	Santa Cruz Biotechnology, Santa Cruz, CA; sc-8393, mouse monoclonal, clone H-7	1:500

[1]Abbreviations: CB, calbindin; CB1R, cannabinoid receptor type 1; CB2R, cannabinoid receptor type 2; DAGLα, diacylglycerol lipase alpha; FAAH, fatty acid amide hydrolase; GS, glutamine synthetase; MAGL, monoacylglycerol lipase; NAPE-PLD, *N*-acyl phosphatidylethanolamine-specific phospholipase D; PKCα, protein kinase C α (alpha isoform); aa, amino acids.

[2]The source column indicates the commercial company, catalog reference and origin. The clone designation is given for monoclonal antibodies.

Confocal microscopy. Immunofluorescence images were taken according to [30]. Using a Leica TCS SP2 confocal laser-scanning microscope (Leica Microsystems, Exton, PA), with a 40X (n.a.: 1.25) or a 100X (n.a: 1.40 - 0.7) objective, images were obtained sequentially from the green, blue or far-red channels on optical slices of less than 0.9 µm of thickness. All photomicrograph adjustments, including size, color, brightness, and contrast were done with Adobe Photoshop (CS5, Adobe Systems, San Jose, CA) and then exported to Adobe InDesign (CS5, Adobe Systems, San Jose, CA), where the final figure layout was completed.

Results

Single-label immunofluorescence

CB1R is present throughout the retina of all three species. A fairly consistent retinal distribution pattern of CB1R across all six retinal layers was observed in mice, tree shrews, vervet and rhesus monkeys, as illustrated in immunolabeled retinal sections (Figure 1**A-D**). The most significant different between species is the low expression of CB1R in the ONL of mice when compared to all other species (arrows Figure 1**A-D**). Furthermore, high expression of CB1R is seen in the GCL and NFL of all species (arrowheads Figure 1**A-D**).

FAAH expression is found throughout the retina of all three species. FAAH, like CB1R, is well expressed in all retinal layers and in the photoreceptor layer of all species (Figure 1**E-H**). In all species, there is a moderate protein expression in the INL (arrows Figure 1**E-H**). Remarkably, there is an important expression of FAAH in the NFL of all species (arrowheads Figure 1**E-H**).

NAPE-PLD distribution is dissimilar between the species. In mice, NAPE-PLD is widely distributed in all layers, but more intensely in the NFL (arrowhead Figure 1**I)**. In tree shrews, NAPE-PLD is found in all six retinal layers, moderately in the INL (arrow Figure 1**J**) and prominently in the OPL and NFL (arrowheads Figure 1**J**). Inversely, in both vervet and macaque monkeys, NAPE-PLD is located in the outer retina, mainly in photoreceptors, ONL and OPL (arrowheads in Figure 1**K,L**), whilst it is undetectable in the inner retinal layers (asterisks Figure 1**K,L**).

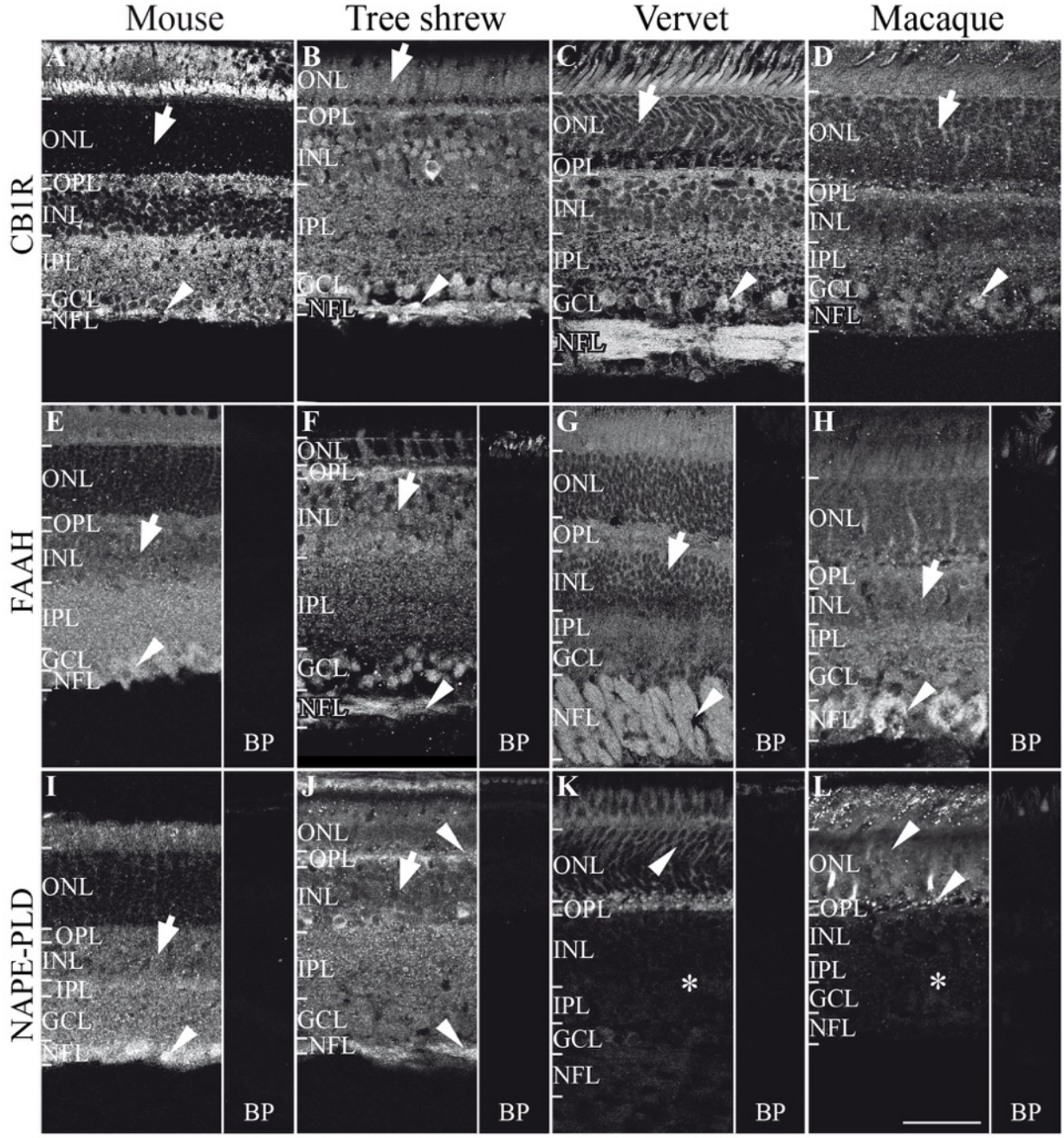

Figure 1. CB1R system immunoreactivity pattern in the retina. Shown are retinal sections immunolabeled for CB1R (**A-D**), FAAH (**E-H**), and NAPE-PLD (**I-L**) in mice, tree shrews, vervet and macaque monkeys. The control staining, preabsoption with the corresponding blocking peptide (BP), is also shown for FAAH and NAPE-PLD in all species. Arrows point to low to moderate expression of CB1R, FAAH, and NAPE-PLD in the retina of all species and arrowheads to high expression of these proteins. The asterisks indicate undetectable

expression of NAPE-PLD in the inner retina of monkeys. ONL, outer nuclear layer; OPL, outer plexiform layer; INL, inner nuclear layer; IPL, inner plexiform layer; GCL, ganglion cell layer; NFL, nerve fiber layer. Scale bar = 75 μm.

CB2R is differently expressed among the species. Unlike CB1R, the immunolabeling pattern of CB2R is not consistent in the 3 species. In mice, CB2R is moderately detectable in ONL and in INL (arrows Figure 2**A**) but strongly expressed in OPL IPL, GCL, and NFL (arrowheads Figure 2**A**). In tree shrews, CB2R is expressed throughout all retinal cell layers with more emphasis (contrary to the mouse) in the external layers (ONL) (upper arrowhead Figure 2**B)** and NFL (lower arrowhead Figure 2**B**). In both vervets and macaques, CB2R expression is more abundant in ONL (arrowheads Figure 2**C,D**), and is very low in the lower layers (INL, IPL, GCL, NFL) (asterisks Figure 2**C,D)**.

Localization of MAGL. In mice, MAGL is expressed in the ONL, OPL, INL, IPL, GCL and NFL (Figure 2**E)**. The most prominent staining is observed in the OPL, in the two laminae of the IPL and in the NFL, as previously described [28] (arrowheads Figure 2**E**). In tree shrews, MAGL is expressed in all layers and most strongly in the INL and GCL (arrowheads Figure 2**F**). In vervets and macaques, MAGL is expressed mainly in the OPL (arrowheads Figure 2**G,H**). It is also found moderately in the IPL and GCL (arrows Figure 2**G, H**).

Expression of the DAGLα. In mice, DAGLα is weakly expressed in the INL, moderately in OPL and ONL (arrows Figure 2**I**), but more strongly in the IPL (arrowhead Figure 2**I**). This result is consistent with that obtained in the mouse retina [28] and in the rat retina [29] that showed expression in the two synaptic layers, the OPL and IPL. DAGLα is also highly expressed in the GCL and NFL in the mouse retina (Figure 2**I**). In tree shrews, the DAGLα is strongly expressed in the GCL and NFL (arrowheads Figure 2**J)**. In vervets and macaques, DAGLα is moderately expressed in the OPL (arrows Figure 2**K,L**), whilst there is a high expression in the NFL (arrowheads Figure 2**K,L**).

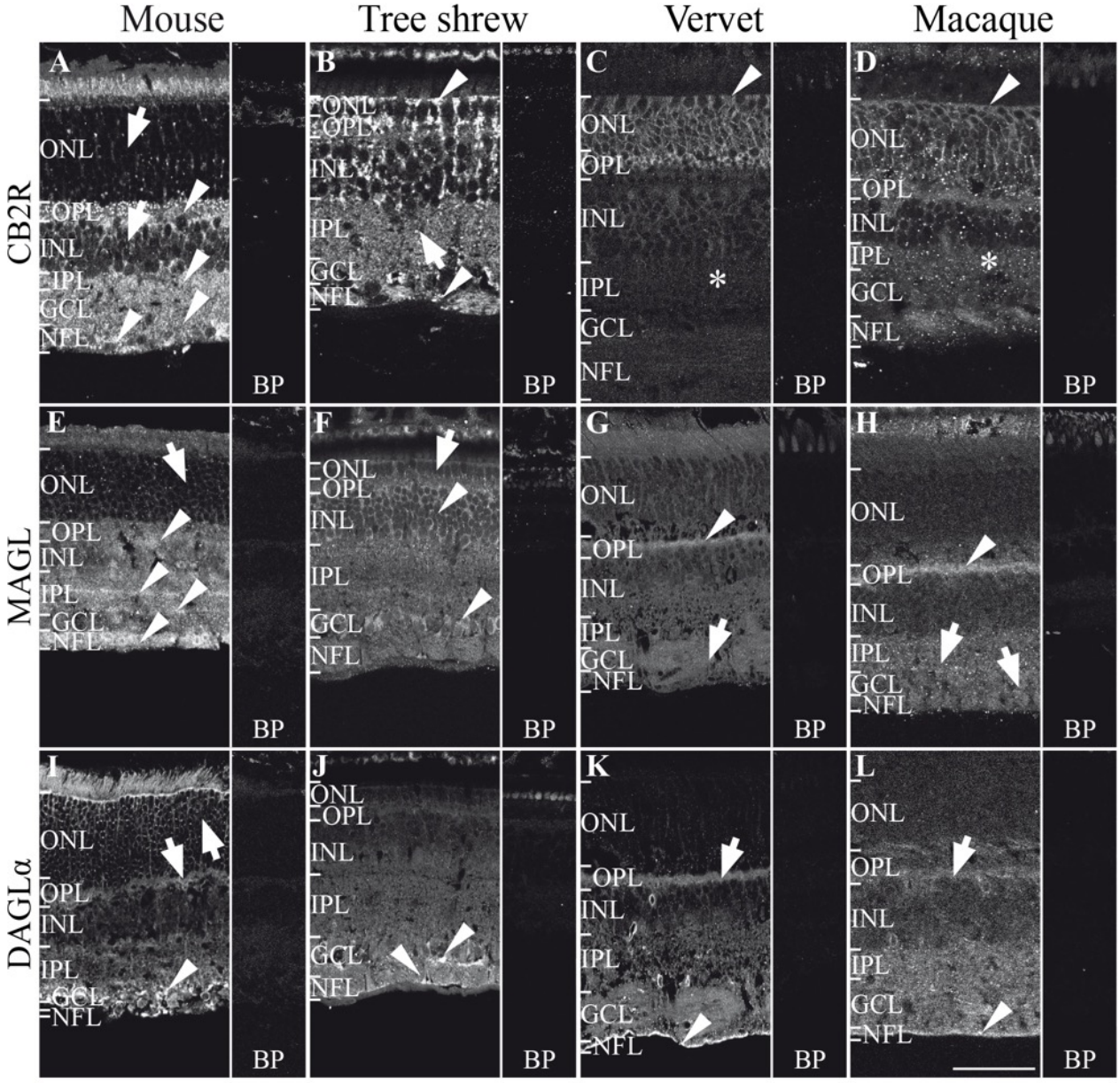

Figure 2. CB2R system immunoreactivity pattern in the retina. Shown are retinal sections immunolabeled for CB2R (**A-D**), MAGL (**E-H**), and DAGLα (**I-L**) in mice, tree shrews, vervet and macaque monkeys. The control staining, preabsoption with the corresponding blocking peptide (BP), is also shown for CB2R, MAGL and DAGLα in all species. Arrows point to low to moderate expression of CB2R, MAGL, and DAGLα in the retina all species and arrowheads to their high expression. The asterisks indicate expression of CB2R under the detection level in the inner retina of monkeys. ONL, outer nuclear layer; OPL, outer plexiform

layer; INL, inner nuclear layer; IPL, inner plexiform layer; GCL, ganglion cell layer; NFL, nerve fiber layer. Scale bar = 75 μm.

Double-label immunofluorescence

To verify the retinal cell type expression, double immuno-staining was carried out with each eCB component and a specific molecular marker for retinal cells.

CB1R and rod bipolar cells. PKCα that labels rod bipolar cells and a subset of amacrine cells is similarly co-expressed with CB1R in the dendrites extending to the OPL (arrows Figure 3) and synaptic terminals in the IPL in all species (arrowheads Figure 3). This is in accordance with previous data reported in rats [26] and vervet monkeys [23]by our group.

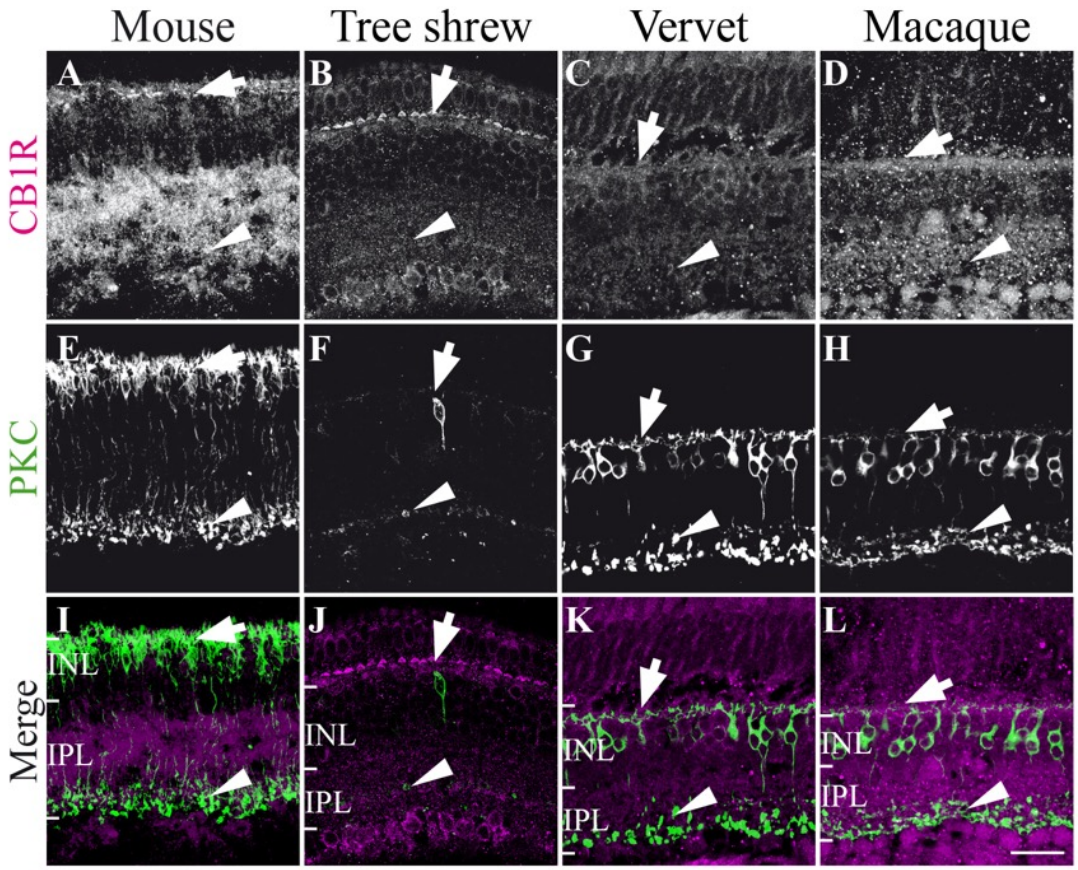

Figure 3. CB1R immunoreactivity in rod bipolar cells. Vertical sections taken from the mouse retina (first column), tree shrew retina (second column), vervet retina (third column), and

macaque retina (fourth column). Confocal micrographs of co-immunolabeling for CB1R and the cell-type-specific marker for rod bipolar cells, protein kinase C alpha (PKCα). Each protein expression is presented alone in grayscale: CB1R in the first line and PKCα in the second line; then the two are presented merged (third line: CB1R in magenta and PKCα in green). Arrows point to dendrites ascending into the OPL, where rod spherules are found, and arrowheads point to synaptic terminals in the IPL. INL, inner nuclear layer; IPL, inner plexiform layer. Scale bar = 30 μm.

CB2R and Müller cells. To label Müller cells, glutamine synthetase (GS) was used. This antibody has proved to be efficient to label Müller cells in the rat [38], mouse [25], and monkey retinas [23, 24, 39]. In mice, CB2R is weakly expressed in the ONL (Figure 4**A,E,I**) although intense expression was found in the inner layers. CB2R was not found in Müller cells in the mouse retina as previously reported [25]. In tree shrews, CB2R and GS were both expressed in the photoreceptor layer and ONL (arrow Figure 4**B,F,J**). Overall, CB2R is co-localized with GS in the outer retina but not in the inner retina (Figure 4**J**). In both vervet and macaque monkeys, double labeling of CB2R and GS shows that CB2R is restricted to Müller cell processes, extending from the internal limiting membrane, with very low staining, to the external limiting membrane, with heavy labeling (arrowheads Figure 4**C,G,K,** and 4**D,H,L)**. These results indicate that the expression of CB2R in Müller cells is a feature of tree shrews and monkeys.

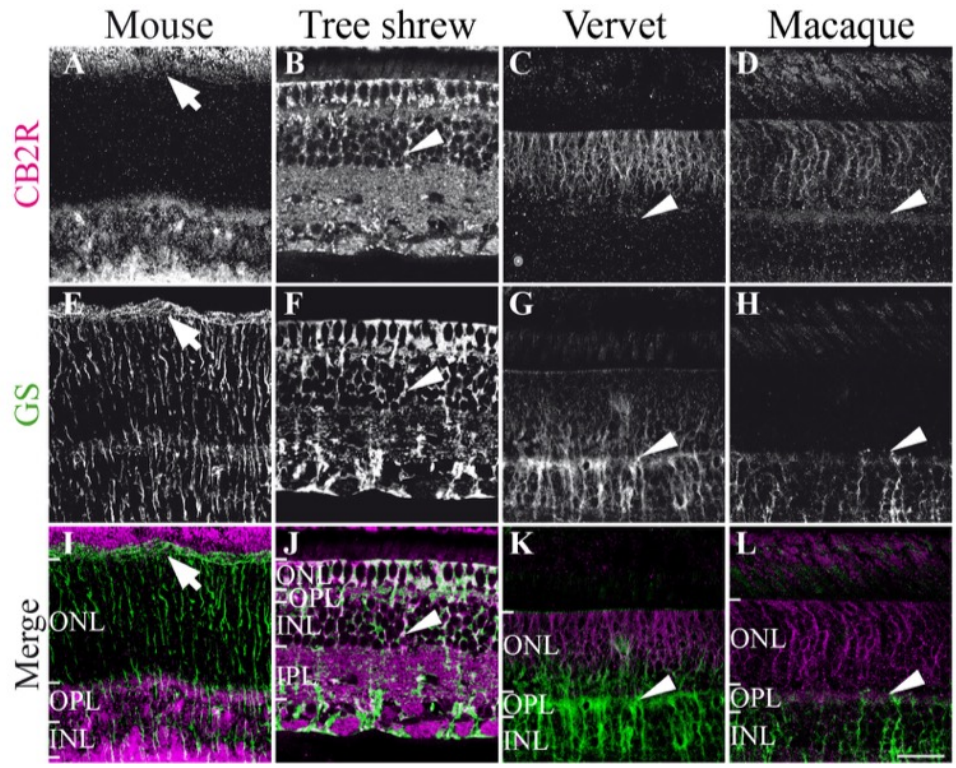

Figure 4. CB2R immunoreactivity in Müller cells. Vertical sections from the mouse retina (first column), tree shrew retina (second column), vervet retina (third column), and macaque retina (fourth column). Confocal micrographs of co-immunolabeling for CB2R and the cell-type-specific marker for glial Müller cells, glutamine synthetase (GS). Each protein immunofluorescent signal is presented alone in grayscale: CB2R in the first line and GS in the second line; then the two are presented merged (third line: CB2R in magenta and GS in green). Arrowheads point to Müller cell processes that all express CB2R, except in mice (arrows). ONL, outer nuclear layer; OPL, outer plexiform layer; INL, inner nuclear layer; IPL, inner plexiform layer. Scale bar = 30 μm.

NAPE-PLD and calbindin-positive retinal cells. Calbindin (CB) is a marker of cones outside the foveal region, cone bipolar cells, and a subset of horizontal cells in tree shrews and monkeys [23, 32]. In contrary, in mice, CB is a marker of horizontal cells and is present in OPL with a weak co-localization of NAPE-PLD (Figure 5**A,E,I**). In both mice and tree shrews CB positive cell bodies found in the INL do not express NAPE-PLD (arrows Figure 5**A,E,I and** 5**B,F,J**). In fact, CB is co-expressed with NAPE-PLD in the OPL of tree shrews (arrowheads Figure 5**B,F,J**). CB is expressed in the ONL of the monkey retina where NAPE-

PLD is abundant (arrowheads Figure 5**C,G,K,** and 5**D,H,L**) and highly co-expressed with NAPE-PLD in the axons of cone photoreceptors (arrowheads Figure 5**C,G,K,** and 5**D,H,L**).

NAPE-PLD and rods. The rhodopsin antibody was used to label rods in the retina. In the mouse, NAPE-PLD is not co-expressed with rods (arrows Figure 6**A,E,I**). Furthermore, in the cone-dominant retina of the tree shrew with only very few rods, NAPE-PLD is also not co-localized with rods (arrows Figure 6**B,F,J**). However, in vervet and macaque monkeys, NAPE-PLD is expressed in rods (arrowheads Figure 6**C,G,K,** and 6**D,H,L**).

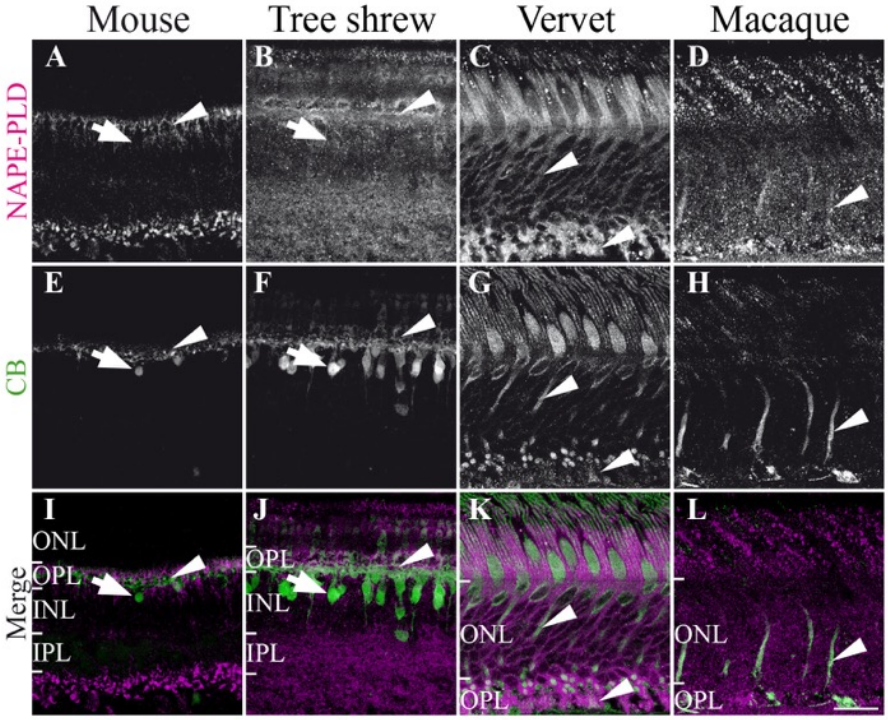

Figure 5. NAPE-PLD immunoreactivity in calbindin-positive retinal cells. Vertical sections from the mouse retina (first column), tree shrew retina (second column), vervet retina (third column), and macaque retina (fourth column). Confocal micrographs of co-immunolabeling for the synthesizing enzyme NAPE-PLD and a cell-type-specific marker for horizontal cells or cones; in mice and tree shrews, calbindin (CB) labels horizontal cells; in monkeys, CB labels cones. Each protein expression is presented alone in grayscale: NAPE-PLD in the first line and the CB in the second line; then the two are presented merged (third line: NAPE-PLD in magenta and the CB in green). Arrowheads point to the processes of CB-positive cells that express the synthetizing enzyme NAPE-PLD and arrows point to CB positive cells bodies,

which do not express NAPE-PLD. ONL, outer nuclear layer; OPL, outer plexiform layer; INL, inner nuclear layer; IPL, inner plexiform layer. Scale bar = 30 µm.

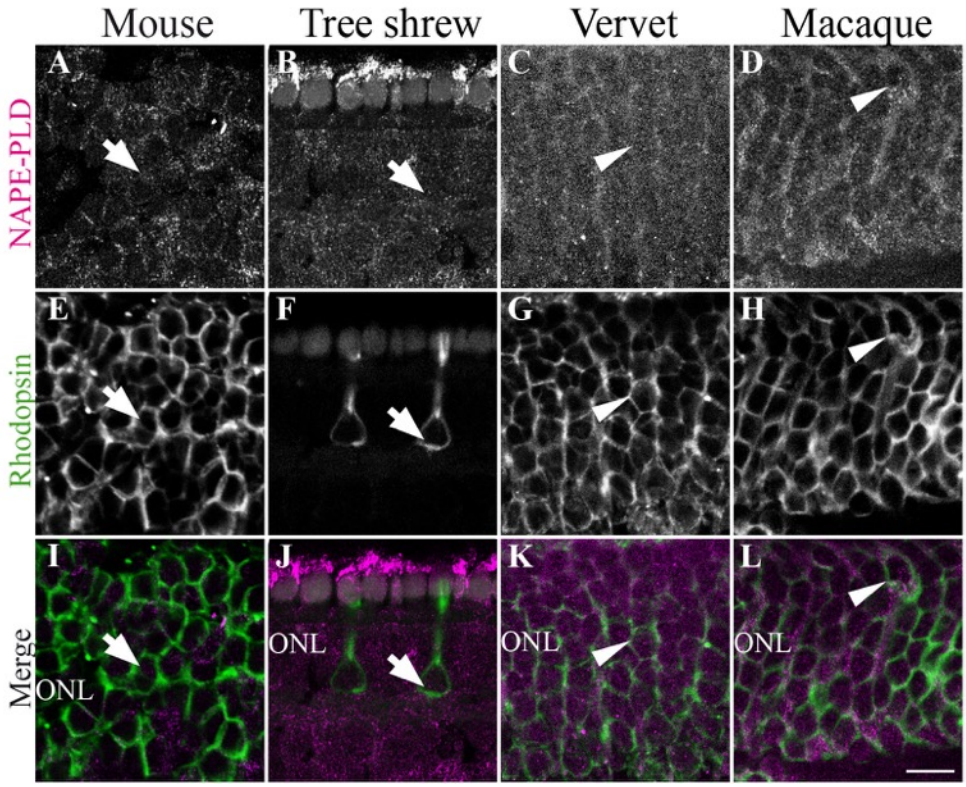

Figure 6. NAPE-PLD immunoreactivity in rod photoreceptors. Vertical sections from the mouse retina (first column), tree shrew retina (second column), vervet retina (third column), and macaque retina (fourth column). Confocal micrographs of co-immunolabeling for the synthesizing enzyme NAPE-PLD and the cell-type-specific marker for rods, rhodopsin. Each immunofluorescent signal is presented alone in grayscale: NAPE-PLD in the first line and rhodopsin in the second line; then the two are presented merged (third line: NAPE-PLD in magenta and rhodopsin in green). Arrowheads point to rhodopsin-positive cell bodies that express NAPE-PLD in vervet and macaque monkeys only, and arrows mark the lack of co-localisation. ONL, outer nuclear layer. Scale bar = 30 µm.

Discussion

In this study, we compared the localization of 2 cannabinoid receptors (CB1R, CB2R), 2 endocannabinoid synthesizing enzymes (NAPE-PLD and DAGLα), and 2 endocannabinoid degrading enzymes (FAAH and MAGL) in the retina of mice, tree shrews, and monkeys. This is the first study that shows the expression pattern of all the above-mentioned eCB components in the tree shrew retina as well as the localization of the NAPE-PLD, MAGL and DAGLα in the monkey retina (Figure 7). These phylogenetically related species were chosen due to the specialization of their visual systems; from the primitive monocular, rod-dominated visual system in mice with a low visual resolution to the well-developed visual system in monkeys [41] that is similar to humans [42]. Tree shrews are a species with binocular cone-dominated vision that is phylogenetically between mice and monkeys [21, 43].

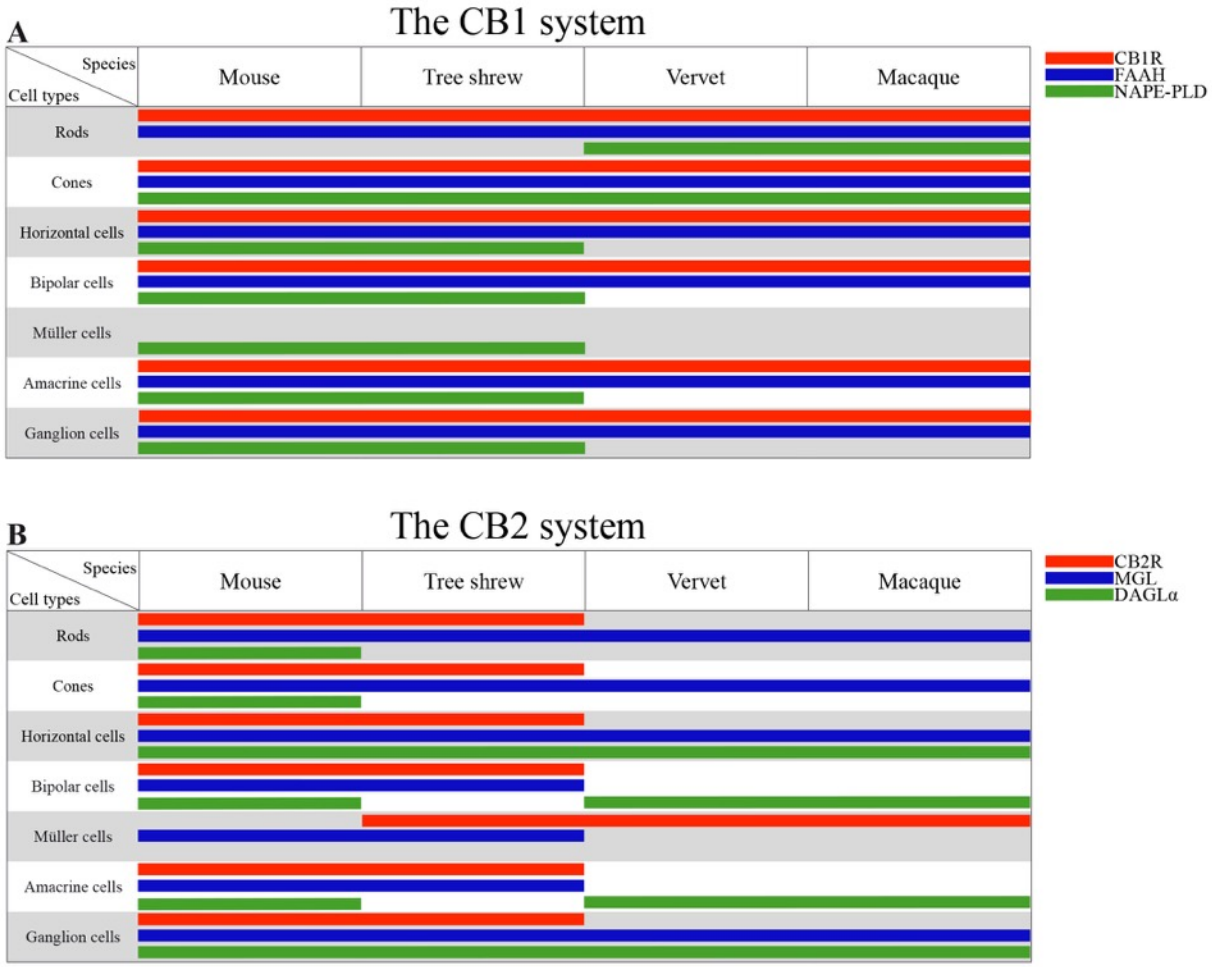

Figure 7. Comparison of the expression patterns of the CB1 system components CB1R, FAAH, and NAPE-PLD (**A**) and of the CB2 system components CB2R, MAGL, and DAGLα (**B**) in the retina of mice, tree shrews, vervets, and macaques. Our results are complemented by data from previously published work [23, 26, 28, 29].

The cannabinoid receptors: localization vs function

We recently reported that the distribution of the CB2R in the primate retina [24] is different than the rodent retina [25]. While the CB2R is expressed in the rodent retinal neuronal cells [25], it is only expressed in the primate retinal glia, the Müller cells [24]. This finding prompted us to look into the retinal eCB system expression profiles across species. Interestingly, we show that only some components of the eCB system are preserved across the three animal species studied here while others are strikingly different. Notably, as reported by Elphick in his thought-provoking review [5], CB1R and CB2R are unique to chordates, but the enzymes involved in the biosynthesis and the inactivation of the eCBs like NAPE-PLD and FAAH are found throughout the animal kingdom [4]. These proteins may have therefore evolved as presynaptic or postsynaptic receptors for eCBs. This is fascinating because the expression and localization of CB1R and FAAH are similar in mice, tree shrews, and primates, while it is not the case for CB2R, NAPE-PLD, MAGL and DAGLα (Figure 7).

There are many controversies on the neuronal and/or peripheral expression of CB2R. Our results show that the expression pattern of the CB2R differs from the mouse to the monkey. Similar to CB1R, CB2R shows a general expression in the neuro-retina: photoreceptors, horizontal cells, amacrine cells, and cells localized in the GCL of rodents [25, 44]. In the mouse, CB2R expressed in the photoreceptor layer, was mostly found in cones and some rods [25]. Similar to its position in the phylogeny tree, the tree shrew has an in-between position showing expressions in all layers, as in rodents, and in Müller cells, as in primates (Figure 2**B**). In agreement with the CB2R glial expression in the CNS, the primate retina expresses CB2R mainly in Müller cells, with a higher polarization towards the outer retina [24]. The Müller cells, with their unique anatomy, span the entire thickness of the retina and contact with the majority of the retinal neurons [45]. This complementary expression pattern of CB1R and CB2R in the primate retina reveals thus a reciprocal relationship between retinal neurons and glia regarding their function via the eCB system. The ubiquitous CB1R system

may play a more general role in the light transduction in all three species, as previously suggested [17].

Significance of the distribution pattern of enzymes and cannabinoid receptors

The expression pattern of CB1R and FAAH has been reported in the CNS as complementary, overlapping or unrelated distributions [17, 46]. Here, we report an overlapping distribution; CB1R expressing neurons also express FAAH. In this case, the degrading enzyme may remotely influence the CB1R [46]. During development of the mouse retina, CB1R and FAAH expression patterns are present in the deepest neuroblast layers at birth, and spread-out throughout the retina in adulthood [26, 27]. In our three species, the FAAH expression overlaps the CB1R distribution pattern not only in the photoreceptor layers but also in the ganglion cells (Figure 1**A-D** and **I-L**). This suggests that cannabinoids act not only on photoreceptors [17] but also directly on ganglion cell. This expression pattern has been reported not only in the retina of the vervet monkey [23], but also in the optic nerve, the dorsal lateral geniculate nucleus [47] and the visual cortex of monkeys [48]. While NAPE-PLD and FAAH are overlapping in different layers of the mouse and tree shrew retinas, they are complementarily expressed in the monkey retina. This unique complementary spatial relationship between NAPE-PLD (exclusively in the photoreceptor layer) and FAAH (in the inner retina), might ensure optimal retinal function in highly-developed retinas. However, further experiments are needed to test this hypothesis.

Anandamide (an endogenous agonist of the CB1R) and other *N*-acylethanolamines (NAEs) are biosynthesized from phospholipids of the cell membrane assisted by NAPE-PLD hydrolysis. In this study, we report a variation in the expression of this membrane associated synthesis enzyme, NAPE-PLD, despite its well-preserved sequence from rodents to humans [49]. In the mouse, NAPE-PLD follows the same pattern of expression as CB1R and FAAH, except that it is not found in rods. Moreover, unlike the mouse but like the primate, the tree shrew has a high expression of NAPE-PLD in ONL and OPL. We show here for the first time that NAPE-PLD expression in monkeys is exclusively restricted to the photoreceptor layer. Unlike CB1R, NAPE-PLD is ubiquitously expressed in the rat brain with the highest level in the thalamus [50]. Besides its role in the eCB biosynthesis, many other physiological roles

have been linked to NAPE-PLD such as, anti-inflammatory effect [51], anorexic effect [52], and pro-apoptotic effect [53]. Moreover, the NAE products in axons suggest a role in the regulation of postsynaptic neuron activity as anterograde synaptic signaling molecules [54]. This pattern of expression also suggests another direct role of NAEs in primate photo-transduction.

Given that the lipophilic eCBs are released and degraded close to their action site, it would be reasonable to assume that the DAGLα and MAGL expressions are in the vicinity of CB2R. In the mouse retina, the DAGLα and MAGL expressions are often near or in the same cell types as CB1R and CB2R. CB1R is present in cones, horizontal, bipolar, amacrine and ganglion cells in the rat retina [26, 27]. CB2R is present in cone and rod photoreceptors, horizontal, bipolar, amacrine and ganglion cells in the adult mouse retina [25]. This distribution pattern may suggest that, in the mouse retina, eCBs such as 2-arachidonoyl glycerol are faithfully expressed adjacent to the cannabinoid receptors and could be involved in their retinal function [25]. But the primates and the tree shrews have followed a complementary distribution pattern, and may have adopted a more complex and specific strategy to regulate their visual activity via the eCB system. The eCB expression pattern in the mouse rod-dominated retina with monocular vision, the tree shrew cone-dominated retina with binocular vision, and the monkey duplex retina with binocular vision proposed that the retinal eCB system plays a fundamental role in the mammal visual processing.

Acknowledgements

The Natural Science and Engineering Research Council of Canada (RGPAS 478115-2015 and RGPIN 2015-06582 JFB; 6362-2012, MP; 194670-2014, CC) and the Canadian Institutes of Health Research (CIHR) (MOP-86495, JFB, MOP-301710, JFB and CC) supported this work. JB received support from a Frederick Banting and Charles Best Canada Graduate Scholarship Doctoral Award from CIHR. MP is Harland Sanders Chair professor in Visual Science. JFB is supported by a "Chercheur-Boursier Senior" from Fonds de Recherche du Québec – Santé (FRQ-S). We are grateful to Dr Frank Ervin and Dr Roberta Palmour of St.-Kitts, West Indies, for supplying the vervet monkey eyes. We would like to thank Dr Amir Shmuel from the Montreal Neurological Institute for donating the macaque eyes. We also would like to thank Reza Abbas Farishta for graciously preparing the tree shrew eyes.

Conflict of interest

The authors declare no conflict of interest.

Role of the authors

All authors had full access to all the data collected in the study and take responsibility for the integrity of these data and the accuracy of the analysis. Study concept and design: JB, PJ, MP, J-FB. Acquisition of data: JB, LE, PJ. Analysis and interpretation of data: JB, LE, PJ, J-FB, MP. Drafting of the manuscript: JB, PJ. Critical revision of the manuscript for important intellectual content: MP, J-FB, CC. Obtained funding: CC, MP, J-FB. Administrative, technical, and material support: CC, MP, J-FB. Study supervision: MP, J-FB.

References

1. J. M. McPartland, J. Agraval, D. Gleeson, K. Heasman and M. Glass, "Cannabinoid receptors in invertebrates," *J Evol Biol*, vol. 19, no. 2, pp. 366-373, 2006.
2. J. M. McPartland, R. W. Norris and C. W. Kilpatrick, "Coevolution between cannabinoid receptors and endocannabinoid ligands," *Gene*, vol. 397, no. 1-2, pp. 126-135, 2007.
3. E. Cottone, V. Pomatto, F. Cerri, E. Campantico, K. Mackie, M. Delpero, A. Guastalla, C. Dati, P. Bovolin and M. F. Franzoni, "Cannabinoid receptors are widely expressed in goldfish: molecular cloning of a CB2-like receptor and evaluation of CB1 and CB2 mRNA expression profiles in different organs," *Fish Physiol Biochem*, vol. 39, no. 5, pp. 1287-1296, 2013.
4. J. M. McPartland, I. Matias, V. Di Marzo and M. Glass, "Evolutionary origins of the endocannabinoid system," *Gene*, vol. 370, pp. 64-74, 2006.
5. M. R. Elphick, "The evolution and comparative neurobiology of endocannabinoid signalling," *Philos Trans R Soc Lond B Biol Sci*, vol. 367, no. 1607, pp. 3201-3215, 2012.
6. T. P. Dinh, D. Carpenter, F. M. Leslie, T. F. Freund, I. Katona, S. L. Sensi, S. Kathuria and D. Piomelli, "Brain monoglyceride lipase participating in endocannabinoid inactivation," *Proc Natl Acad Sci U S A*, vol. 99, no. 16, pp. 10819-10824, 2002.
7. V. Di Marzo, "The endocannabinoid system: its general strategy of action, tools for its pharmacological manipulation and potential therapeutic exploitation," *Pharmacol Res*, vol. 60, no. 2, pp. 77-84, 2009.
8. T. Harkany, M. Guzman, I. Galve-Roperh, P. Berghuis, L. A. Devi and K. Mackie, "The emerging functions of endocannabinoid signaling during CNS development," *Trends Pharmacol Sci*, vol. 28, no. 2, pp. 83-92, 2007.
9. T. Harkany, E. Keimpema, K. Barabas and J. Mulder, "Endocannabinoid functions controlling neuronal specification during brain development," *Mol Cell Endocrinol*, vol. 286, no. 1-2 Suppl 1, pp. S84-90, 2008.
10. A. Argaw, G. Duff, N. Zabouri, B. Cécyre, N. Chaine, H. Cherif, N. Tea, B. Lutz, M. Ptito and J. F. Bouchard, "Concerted action of CB1 cannabinoid receptor and deleted in colorectal cancer in axon guidance," *J Neurosci*, vol. 31, no. 4, pp. 1489-1499, 2011.

11. G. Duff, A. Argaw, B. Cécyre, H. Cherif, N. Tea, N. Zabouri, C. Casanova, M. Ptito and J. F. Bouchard, "Cannabinoid receptor CB2 modulates axon guidance," *PLoS One*, vol. 8, no. 8, pp. e70849, 2013.
12. J. Y. Xu and C. Chen, "Endocannabinoids in synaptic plasticity and neuroprotection," *Neuroscientist*, vol. 21, no. 2, pp. 152-168, 2015.
13. R. Bluett, J. Gamble-George, D. Hermanson, N. Hartley, L. Marnett and S. Patel, "Central anandamide deficiency predicts stress-induced anxiety: behavioral reversal through endocannabinoid augmentation," *Translational psychiatry*, vol. 4, no. 7, pp. e408, 2014.
14. J. M. McPartland, G. W. Guy and V. Di Marzo, "Care and feeding of the endocannabinoid system: a systematic review of potential clinical interventions that upregulate the endocannabinoid system," *PloS one*, vol. 9, no. 3, pp. e89566, 2014.
15. E. B. Russo, "Clinical endocannabinoid deficiency (CECD): can this concept explain therapeutic benefits of cannabis in migraine, fibromyalgia, irritable bowel syndrome and other treatment-resistant conditions?," *Neuro endocrinology letters*, vol. 25, no. 1-2, pp. 31-39, 2003.
16. S. C. Smith and M. S. Wagner, "Clinical endocannabinoid deficiency (CECD) revisited: Can this concept explain the therapeutic benefits of cannabis in migraine, fibromyalgia, irritable bowel syndrome and other treatment-resistant conditions?," *Neuro endocrinology letters*, vol. 35, no. 3, pp. 198-201, 2014.
17. S. Yazulla, "Endocannabinoids in the retina: from marijuana to neuroprotection," *Prog Retin Eye Res*, vol. 27, no. 5, pp. 501-526, 2008.
18. Y. Fan, Z. Y. Huang, C. C. Cao, C. S. Chen, Y. X. Chen, D. D. Fan, J. He, H. L. Hou, L. Hu, X. T. Hu, X. T. Jiang, R. Lai, Y. S. Lang, B. Liang, S. G. Liao, D. Mu, Y. Y. Ma, Y. Y. Niu, X. Q. Sun, J. Q. Xia, J. Xiao, Z. Q. Xiong, L. Xu, L. Yang, Y. Zhang, W. Zhao, X. D. Zhao, Y. T. Zheng, J. M. Zhou, Y. B. Zhu, G. J. Zhang, J. Wang and Y. G. Yao, "Genome of the Chinese tree shrew," *Nat Commun*, vol. 4, pp. 1426, 2013.
19. C. J. Jeon, E. Strettoi and R. H. Masland, "The major cell populations of the mouse retina," *J Neurosci*, vol. 18, no. 21, pp. 8936-8946, 1998.
20. G. T. Prusky and R. M. Douglas, "Characterization of mouse cortical spatial vision," *Vision Res*, vol. 44, no. 28, pp. 3411-3418, 2004.

21. B. Müller and L. Peichl, "Horizontal cells in the cone-dominated tree shrew retina: morphology, photoreceptor contacts, and topographical distribution," *J Neurosci*, vol. 13, no. 8, pp. 3628-3646, 1993.
22. A. Straiker, N. Stella, D. Piomelli, K. Mackie, H. J. Karten and G. Maguire, "Cannabinoid CB1 receptors and ligands in vertebrate retina: localization and function of an endogenous signaling system," *Proc Natl Acad Sci U S A*, vol. 96, no. 25, pp. 14565-14570, 1999.
23. J. Bouskila, M. W. Burke, N. Zabouri, C. Casanova, M. Ptito and J. F. Bouchard, "Expression and localization of the cannabinoid receptor type 1 and the enzyme fatty acid amide hydrolase in the retina of vervet monkeys," *Neuroscience*, vol. 202, pp. 117-130, 2012.
24. J. Bouskila, P. Javadi, C. Casanova, M. Ptito and J. F. Bouchard, "Muller cells express the cannabinoid CB2 receptor in the vervet monkey retina," *J Comp Neurol*, vol. 521, no. 11, pp. 2399-2415, 2013.
25. B. Cécyre, N. Zabouri, F. Huppé-Gourgues, J. F. Bouchard and C. Casanova, "Roles of cannabinoid receptors type 1 and 2 on the retinal function of adult mice," *Invest Ophthalmol Vis Sci*, vol. 54, no. 13, pp. 8079-8090, 2013.
26. N. Zabouri, J. F. Bouchard and C. Casanova, "Cannabinoid receptor type 1 expression during postnatal development of the rat retina," *J Comp Neurol*, vol. 519, no. 7, pp. 1258-1280, 2011a.
27. N. Zabouri, M. Ptito, C. Casanova and J. F. Bouchard, "Fatty acid amide hydrolase expression during retinal postnatal development in rats," *Neuroscience*, vol. 195, pp. 145-165, 2011b.
28. S. S. Hu, A. Arnold, J. M. Hutchens, J. Radicke, B. F. Cravatt, J. Wager-Miller, K. Mackie and A. Straiker, "Architecture of cannabinoid signaling in mouse retina," *J Comp Neurol*, vol. 518, no. 18, pp. 3848-3866, 2010.
29. B. Cécyre, M. Monette, L. Beudjekian, C. Casanova and J. F. Bouchard, "Localization of diacylglycerol lipase alpha and monoacylglycerol lipase during postnatal development of the rat retina," *Front Neuroanat*, vol. 8, pp. 150, 2014.

30. J. Bouskila, P. Javadi, C. Casanova, M. Ptito and J. F. Bouchard, "Rod photoreceptors express GPR55 in the adult vervet monkey retina," *PLoS One*, vol. 8, no. 11, pp. e81080, 2013.
31. C. Chiquet, O. Dkhissi-Benyahya, N. Chounlamountri, A. Szel, W. J. Degrip and H. M. Cooper, "Characterization of calbindin-positive cones in primates," *Neuroscience*, vol. 115, no. 4, pp. 1323-1333, 2002.
32. A. J. Fischer, A. Hendrickson and T. A. Reh, "Immunocytochemical characterization of cysts in the peripheral retina and pars plana of the adult primate," *Invest Ophthalmol Vis Sci*, vol. 42, no. 13, pp. 3256-3263, 2001.
33. H. Kolb, L. Zhang, L. Dekorver and N. Cuenca, "A new look at calretinin-immunoreactive amacrine cell types in the monkey retina," *J Comp Neurol*, vol. 453, no. 2, pp. 168-184, 2002.
34. G. C. Martínez-Navarrete, A. Angulo, J. Martín-Nieto and N. Cuenca, "Gradual morphogenesis of retinal neurons in the peripheral retinal margin of adult monkeys and humans," *J Comp Neurol*, vol. 511, no. 4, pp. 557-580, 2008.
35. G. C. Martínez-Navarrete, J. Martín-Nieto, J. Esteve-Rudd, A. Angulo and N. Cuenca, "Alpha synuclein gene expression profile in the retina of vertebrates," *Mol Vis*, vol. 13, pp. 949-961, 2007.
36. B. Cécyre, S. Thomas, M. Ptito, C. Casanova and J. F. Bouchard, "Evaluation of the specificity of antibodies raised against cannabinoid receptor type 2 in the mouse retina," *Naunyn Schmiedebergs Arch Pharmacol*, vol. 387, no. 2, pp. 175-184, 2014.
37. M. R. Elphick and M. Egertová, "The phylogenetic distribution and evolutionary origins of endocannabinoid signalling," in *Cannabinoids*, Ed., pp. 283-297, Springer, 2005.
38. R. E. Riepe and M. D. Norenburg, "Müller cell localisation of glutamine synthetase in rat retina," *Nature*, vol. 268, no. 5621, pp. 654-655, 1977.
39. S. Nishikawa and M. Tamai, "Müller cells in the human foveal region," *Curr Eye Res*, vol. 22, no. 1, pp. 34-41, 2001.
40. Y. Ozawa, K. Nakao, T. Kurihara, T. Shimazaki, S. Shimmura, S. Ishida, A. Yoshimura, K. Tsubota and H. Okano, "Roles of STAT3/SOCS3 pathway in regulating

the visual function and ubiquitin-proteasome-dependent degradation of rhodopsin during retinal inflammation," *J Biol Chem*, vol. 283, no. 36, pp. 24561-24570, 2008.

41. Y. B. Sirotin and A. Das, "Zooming in on mouse vision," *Nat Neurosci*, vol. 13, no. 9, pp. 1045-1046, 2010.
42. G. H. Jacobs, "Primate color vision: a comparative perspective," *Vis Neurosci*, vol. 25, no. 5-6, pp. 619-633, 2008.
43. B. Müller and L. Peichl, "Topography of cones and rods in the tree shrew retina," *J Comp Neurol*, vol. 282, no. 4, pp. 581-594, 1989.
44. E. M. López, P. Tagliaferro, E. S. Onaivi and J. J. López-Costa, "Distribution of CB2 cannabinoid receptor in adult rat retina," *Synapse*, vol. 65, no. 5, pp. 388-392, 2011.
45. A. Reichenbach, C. Frömter, R. Engelmann, H. Wolburg, M. Kasper and J. Schnitzer, "Müller glial cells of the tree shrew retina," *Journal of Comparative Neurology*, vol. 360, no. 2, pp. 257-270, 1995.
46. M. Egertová, B. F. Cravatt and M. R. Elphick, "Comparative analysis of fatty acid amide hydrolase and cb(1) cannabinoid receptor expression in the mouse brain: evidence of a widespread role for fatty acid amide hydrolase in regulation of endocannabinoid signaling," *Neuroscience*, vol. 119, no. 2, pp. 481-496, 2003.
47. P. Javadi, J. Bouskila, J. F. Bouchard and M. Ptito, "The endocannabinoid system within the dorsal lateral geniculate nucleus of the vervet monkey," *Neuroscience*, vol. 288, pp. 135-144, 2015.
48. S. M. Eggan and D. A. Lewis, "Immunocytochemical distribution of the cannabinoid CB1 receptor in the primate neocortex: a regional and laminar analysis," *Cereb Cortex*, vol. 17, no. 1, pp. 175-191, 2007.
49. Y. Okamoto, J. Morishita, K. Tsuboi, T. Tonai and N. Ueda, "Molecular characterization of a phospholipase D generating anandamide and its congeners," *J Biol Chem*, vol. 279, no. 7, pp. 5298-5305, 2004.
50. J. Morishita, Y. Okamoto, K. Tsuboi, M. Ueno, H. Sakamoto, N. Maekawa and N. Ueda, "Regional distribution and age-dependent expression of *N*-acylphosphatidylethanolamine-hydrolyzing phospholipase D in rat brain," *J Neurochem*, vol. 94, no. 3, pp. 753-762, 2005.

51. D. M. Lambert, S. Vandevoorde, K. O. Jonsson and C. J. Fowler, "The palmitoylethanolamide family: a new class of anti-inflammatory agents?," *Curr Med Chem*, vol. 9, no. 6, pp. 663-674, 2002.
52. F. Rodríguez de Fonseca, M. Navarro, R. Gómez, L. Escuredo, F. Nava, J. Fu, E. Murillo Rodríguez, A. Giuffrida, J. LoVerme, S. Gaetani, S. Kathuria, C. Gall and D. Piomelli, "An anorexic lipid mediator regulated by feeding," *Nature*, vol. 414, no. 6860, pp. 209-212, 2001.
53. M. Maccarrone, R. Pauselli, M. Di Rienzo and A. Finazzi-Agrò, "Binding, degradation and apoptotic activity of stearoylethanolamide in rat C6 glioma cells," *Biochem J*, vol. 366, no. Pt 1, pp. 137-144, 2002.
54. M. Egertová, G. M. Simon, B. F. Cravatt and M. R. Elphick, "Localization of *N*-acyl phosphatidylethanolamine phospholipase D (NAPE-PLD) expression in mouse brain: A new perspective on *N*-acylethanolamines as neural signaling molecules," *J Comp Neurol*, vol. 506, no. 4, pp. 604-615, 2008.

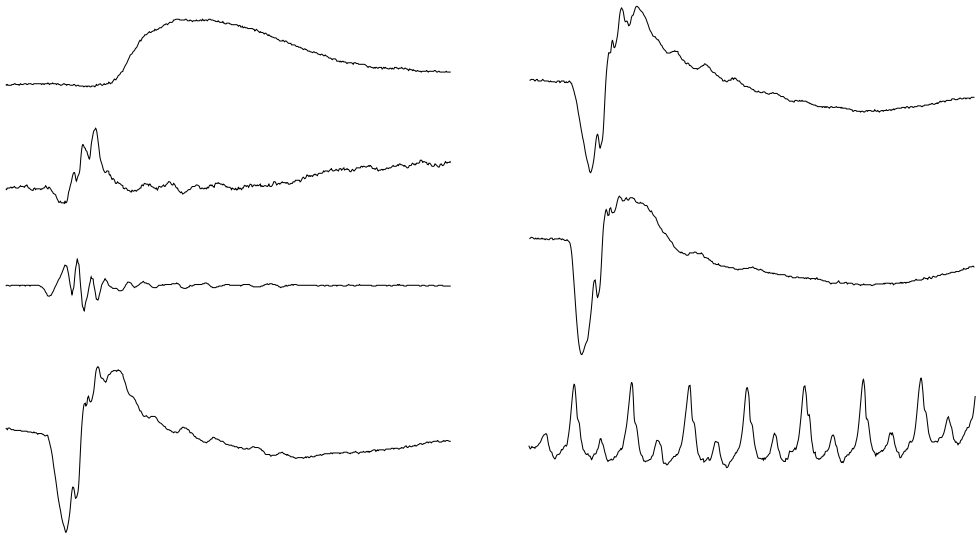

ARTICLE 5: STANDARDIZED FULL-FIELD ELECTRORETINOGRAPHY IN THE GREEN MONKEY

Publié dans :

Bouskila J, Javadi P, Palmour RM, Bouchard JF, Ptito M (2014) Standardized full-field electroretinography in the Green Monkey (Chlorocebus sabaeus). PLoS One 9:e111569.

Standardized full-field electroretinography in the Green Monkey (*Chlorocebus sabaeus*)

Joseph Bouskila[1, 2], Pasha Javadi[1], Roberta M. Palmour[3, 4], Jean-François Bouchard[1] and Maurice Ptito[1, 5]

[1]School of Optometry, University of Montreal, Montreal, Quebec, Canada
[2]Biomedical Sciences, Faculty of Medicine, University of Montreal, Montreal, Quebec, Canada
[3]Behavioral Science Foundation, Basseterre, St. Kitts, West Indies
[4]Departments of Psychiatry and Human Genetics, McGill University, Montreal, Quebec, Canada
[5]BRAINlab and Neuropsychiatry Laboratory, Department of Neuroscience and Pharmacology, University of Copenhagen, Copenhagen, Denmark

Keywords: electroretinogram, dark adaptation, scotopic ERG, photopic ERG, oscillatory potentials, flicker ERG.

Correspondence should be addressed to:
Maurice Ptito, Ph.D.
School of Optometry, room 260-7
3744 Jean-Brillant,
University of Montreal,
Montreal, Quebec, Canada, H3T 1P1

Abstract

Full-field electroretinography is an objective measure of retinal function, serving as an important diagnostic clinical tool in ophthalmology for evaluating the integrity of the retina. Given the similarity between the anatomy and physiology of the human and Green Monkey eyes, this species has increasingly become a favorable non-human primate model for assessing ocular defects in humans. To test this model, we obtained full-field electroretinographic recordings (ERG) and normal values for standard responses required by the International Society for Clinical Electrophysiology of Vision (ISCEV). Photopic and scotopic ERG recordings were obtained by full-field stimulation over a range of 6 log units of intensity in dark-adapted or light-adapted eyes of adult Green Monkeys (*Chlorocebus sabaeus*). Intensity, duration, and interval of light stimuli were varied separately. Reproducible values of amplitude and latency were obtained for the a- and b-waves, under well-controlled adaptation and stimulus conditions; the i-wave was also easily identifiable and separated from the a-b-wave complex in the photopic ERG. The recordings obtained in the healthy Green Monkey matched very well with those in humans and other non-human primate species (*Macaca mulatta* and *Macaca fascicularis*). These results validate the Green Monkey as an excellent non-human primate model, with potential to serve for testing retinal function following various manipulations such as visual deprivation or drug evaluation.

Introduction

The retina is a complex and well-organized neuronal structure that is vulnerable to internal influences such as retinopathies and ocular pathologies, and is furthermore sensitive to external factors such as drugs and alcohol toxicity. Full-field electroretinography represents a useful diagnostic clinical tool in ophthalmology and is widely used as a measure of retinal function. Electroretinogram (ERG) recordings are generated through different summation of currents evoked in distinct populations of retinal cells, including photoreceptors (cones and rods), neurons (horizontal cells, bipolar cells, amacrine cells, and ganglion cells), glial cells (Müller cells), and epithelial cells [1]. Accordingly, the influence of environmental manipulations on the function of retinal cells can be assessed objectively in the ERG. Whereas the full-field ERG reflects the response of the entire retina to stimulus, it is possible to differentiate between responses of various retinal structures to light [2]; in fact, the positive and negative waves of the ERG emerge from different levels of retinal processing, and the response of particular retinal cell populations and circuits is target by the choice of stimulus and recording environment. Research on the origins of pathophysiological conditions displayed in human electroretinography is mostly carried out in animal models, with non-human primates remaining particularly important in visual neuroscience research, due to their superior emulation of human retinal function [3]. Indeed, the non-human primate ERG plays an important role in studies of visual abnormalities and potentially therapeutic pharmacological effects in the retina. The International Society for Clinical Electrophysiology of Vision (ISCEV) proposes a minimum of five types of measurements in order to obtain standardization for investigations in humans [4], all of which can be obtained in non-human primates.

Green Monkeys have become important non-human primate species for visual neuroscience research. The genome of Green Monkeys has 90% parity with the human genome, which lends support to its use to model a range of behavioral and non-behavioral pathologic disorders in human [5], [6]. In fact, Green Monkeys are used as a model organism for the study of diabetes, cardiovascular disease, HIV/AIDS, Parkinson's disease, substance abuse, attention deficit disorder, alcoholism, reproduction, tissue regeneration and other conditions [5], [7], [8], [9]. The Green Monkey has been utilized in visual neuroscience for

many years [7], [10], [11], [12], [13], [14], [15], [16], [17], [18], [19], leading to a thorough anatomical description of the visual pathways and the publication of anatomical brain atlases [20], [21], [22]. Their large brain and ocular size relative to the 3.5 kg bodyweight of adult Green Monkeys is particularly advantageous in the electrophysiological study of visual abnormalities arising in the retina and optic nerve. The organization of the retina of the green monkey is similar to that of other Old World species such as Macaques, for example. The retina contains several layers and different cell populations: photoreceptors, bipolar cells, ganglion cells, amacrines and horizontal cells. There is a monotonic decrease in the number of cones from the fovea centralis (containing mainly cones) to the periphery made out of rods [17], [23]. This developed fovea is well suited for high visual acuity, color vision and photopic sensitivity whereas the peripheral retina is responsible for scotopic vision (nocturnal) [24]. From the study of Herbin et al. (1997), the only one available on the green monkey retina, the retinal ganglion cells (RGCs) number derived from retinal wholemounts was estimated at 1 228 646. The topographical distribution of RGCs shows a strong centro-peripheral gradient, with the majority of small cells (P cells) in the fovea, the larger ones being encountered in the periphery (M cells). The axons of the ganglion cells form the optic nerve and their counts derived from semi-thin sections (1 220 000) are close to the estimated number of RGCs for the vervet monkey and are in the range with those reported for *Macaca Mulatta* (1 468 000 RGCs) [25].

However, little is known about the electrophysiology of the Green Monkey retina, since most of such studies have been conducted in the rhesus monkey, for which a standardized procedure for electroretinographic examination has been published [26]. Due to the lack of corresponding data in Green Monkeys despite their growing importance in visual neuroscience, a standardized electroretinography protocol is needed. We therefore present here full-field ERG data for Green Monkeys, including the five standard responses recommended by the ISCEV.

Materials and Methods

Animals

A total of 15 adult male and female Green Monkeys (*Chlorocebus sabaeus*), aged 3 to 4 years and weighing 3.01 ± 0.35 Kg, were used for this study (Table 1). The animals were born and raised in enriched environments in the laboratories of the Behavioral Science Foundation (St-Kitts, West Indies). As adults, the animals were fed with primate chow (Harlan Teklad High Protein Monkey Diet; Harlan Teklad, Madison, WI) and fresh local fruits, with water available *ad libitum*. Infant Green Monkeys are born into an outdoor social group comprising several females, one male and other offspring of the same general age. Infants live with their parents until about 8 months of age, at which time they move to a playpen with 5 other age-mates. The natal cage is equipped with swings, perches, hiding places and jungle gyms. We do put in toys, but the animals are so busy playing with one another that they ignore the toys. In the smaller playpens, there are also swings, perches and climbing spots, as well as puzzle feeders and foraging boards. At about 18 months of age, youngsters graduate to a large, outdoor peer group of about 16 animals (like-ages, both sexes) where there are tunnels, swings, ladders, jungle-gyms and a variety of manipulanda (more complex puzzle feeders; natural forage opportunities, such as brush and vines; foraging boards). Plastic chain and baited balls are popular toys, but vervets of this age are uninterested in most other commercially available toys. All experiments were performed according to the guidelines of the Canadian Council on Animal Care (CCAC) and the Association for Research in Vision and Ophthalmology (ARVO) Statement for the Use of Animals in Ophthalmic and Vision Research. The experimental protocol was also reviewed and approved by the local Animal Care and Use Committee (University of Montreal, protocol # 14-007) and the Institutional Review Board of the Behavioral Science Foundation that is recognized by the CCAC. None of the animals were sacrificed for this study.

Table 1. Subject profile of animals used in this study.

	Animal ID	Sex	Weight (Kg)	IOP (mm Hg)	Pupil dilatation (mm)
1	05011-5	Male	3.950	OD 10 / OS 9	OD 9 / OS 9
2	05010-6	Male	3.725	OD 7 / OS 7	OD 8 / OS 8
3	09093-1-3-1	Female	3.050	OD 9 / OS 9	OD 9 / OS 9
4	08274	Female	2.800	OD 10 / OS 11	OD 9 / OS 9
5	08275	Female	2.925	OD 8 / OS 6	OD 8.5 / OS 8.5
6	07862	Female	2.875	OD 15 / OS15	OD 8.5 / OS 8.5
7	08297	Female	2.750	OD 6 / OS 6	OD 9 / OS 9
8	07866	Female	2.950	OD 12 / OS 12	OD 9 / OS 9
9	01336-7-1-3	Female	2.950	OD 12 / OS 13	OD 9 / OS 9
10	08315	Female	2.775	OD 10 / OS 11	OD 9 / OS 9
11	07868	Female	2.825	OD 8 / OS8	OD 8.5 / OS 8.5
12	08375	Female	2.900	OD 11 / OS 12	OD 9 / OS 9
13	08376	Female	2.850	OD 6/ OS 6	OD 9 / OS 9
14	08336	Female	2.925	OD 14 / OS 15	OD 9 / OS 9
15	08377	Female	2.852	OD 9 / OS 10	OD 9 / OS 9

Animal preparation for ERG recording

The following procedure describes a typical recording session in Green Monkeys, including successively a 30 minutes of animal preparation, 30 minutes of dark adaptation, 15 minutes of scotopic recordings, 2 minutes of light adaptation, 15 minutes of photopic recordings, and 2 minutes of flicker recordings (Figure 1). The values of dark and light adaptation were chosen based on data obtained in cynomologus monkeys [27]. The animals were sedated with an intramuscular injection of a mixture of ketamine (10 mg/kg; Troy Laboratories, Glendenning, New South Wales, Australia) and xylazine (1 mg/kg; Lloyd Laboratories, Shenandoah, IA). In this condition, the pupils were fully dilated to approximately 9 mm in diameter and the accommodation reflex was paralyzed with topical application of 1% tropicamide (Mydriacyl) and 2.5% phenylephrine hydrochloride (Mydfrin) (Alcon Laboratories, Fort Worth, TX). Intraocular pressures (IOP) were also monitored before and after the recording session by applanation tonometry (TonoPen XL; Mentor, Norwell, MA, USA). There were no significant IOP and pupil size differences noted between the beginning and the end of the ERG

procedure. The eyes were treated with 0.5% proparacaine hydrochloride (Alcaine; Alcon Laboratories, Fort Worth, TX, USA) to anesthetize the cornea and then protected by application of 2.5% methylcellulose (Gonak; Akorn, Inc., Buffalo Grove, IL, USA) to prevent corneal drying. Body temperature was maintained between 36.5°C and 38°C with a heating pad. Recording sessions lasted approximately two hours for each animal, after which they were allowed to recover and returned to their prior naturalistic setting.

Visual Stimulation

Full-field stimulation was produced with an UTAS BigShot Ganzfeld light source (UTAS E-3000 electrophysiology equipment; LKC Technologies, Inc., Gaithersburg, MD, USA) that was placed in front of the animal's face. Both eyes were simultaneously recorded and averaged as detailed below. The ERGs were evoked by white flashes of light of intensities ranging from 0.00025 cd.sec.m^{-2} to 1000 cd.sec.m^{-2} delivered in full-field conditions. During the course of dark adaptation, ERGs were recorded at 3 minutes intervals over 30 minutes of dark adaptation with a constant stimulus of approximately 0.025 cd.s.m^{-2}. LED flash luminance of 0.00025 to 6 cd.sec.m^{-2} (-50 dB to 4 dB in LKC units) was used for scotopic stimulation. Responses were averaged for each of the 14 time-integrated flash luminance levels presented (ranging from -3.6 to 2.9 log cd.s.m^{-2} in approximately 0.3 log-unit steps; flash duration, 20 μs; inter-stimulus interval, 5 sec for -3.6 to 0.4 log cd.s.m^{-2} and 15 sec for 0.6 to 2.9 log cd.s.m^{-2}) and xenon flash luminance of 2.5 to 800 cd.sec.m^{-2} (0 dB to 25 dB in LKC units) for photopic stimulation (ranging from -2.2 to 2.9 log cd.s.m^{-2} in approximately 0.3 log-unit steps; flash duration, 20 μs; inter-stimulus interval, 2 sec for all intensities). For light-adapted ERGs a steady white background-adapting field (30 cd/m^2) was presented inside the Ganzfeld to saturate the rod system. Flash intensities and background luminance were calibrated using a research radiometer (IL1700 Photometer; International Light Inc., Newburyport, MA, USA) with a SED033 detector placed at 36 cm from the source.

ERG recording and analysis

All experimental protocols followed the guidelines of the ISCEV [4], specifying the 5 standard responses: (1) a dark-adapted response (rod response), (2) a dark-adapted maximal response (combined rod–cone response), (3) a dark-adapted oscillatory potentials response, (4) a light-

adapted response (cone response), and (5) a light-adapted response to a rapidly repeated stimulus (30 Hz flicker). ERG recordings and signal processing were recorded with contact lens electrodes lying across the center of the cornea of each eye moistened with 1% carboxymethylcellulose sodium (Refresh Celluvisc, Allergan Inc., Markham, ON, Canada). The corneal contact lens electrode (Jet electrodes; Diagnosys LLC, Lowell, MA, USA) was equipped with four small posts on the convex surface in order to keep the eyelids open. Reference and ground gold disc electrodes (model F-E5GH; Grass Technologies, Astro-Med, Inc., West Warwick, RI, USA) were kept in place with adhesive paste (Ten20 conductive EEG paste; Kappa Medical, Prescott, AZ, USA) at the external canthi and forehead, respectively. Responses were amplified 10,000 times and filtered with a band pass from 1 to 500 Hz except for the oscillatory potentials, which were extracted with the LKC software with a band pass from 75 to 500 Hz. Each tracing included a 20 ms pre-stimulus baseline. Depending on the measured stimulus, up to 10 waveforms were averaged to reduce variability and background noise. Based on literature focusing on the origins of ERG waves in a primate model (macaque monkey) whose retina is very similar to that of humans [2], the origins of the waveforms are described. For the waveform analysis, the amplitude of the a-wave, which mainly reflects the function of photoreceptors, was measured from the baseline to the peak of the a-wave for the combined rod-cone response and the single-flash cone response. The amplitude of the b-wave, which reflects the activity of the inner nuclear layer, was measured from the peak of the a-wave to the peak of the b-wave for all responses. The peak latency was defined from the onset of the flash to the peak. In the case of the oscillatory potentials, the latency to the second peak was usually determined, where the amplitude was defined as peak to trough amplitude from the peak of the second wave to the following trough. The amplitude of the i-wave was measured from the trough of the b-wave to the peak of the i-wave and its respective peak time was also measured from flash onset. The exact origin of the i-wave is still controversial. Some have suggested that this component is generated at the inner retinal level [28], and others that it origins at a more distal location [29]. The latter point is highlighted in ocular pathology studies. For example, the i-wave in glaucoma patients [30] and in glaucoma animal models [29] is increased, suggesting that it does indeed originate in the distal retina. In the 30 Hz flicker ERG, the second peak was evaluated in relation to the preceding trough. Retinal response diagrams were drawn using Adobe Illustrator and processed in Adobe InDesign

(Adobe Systems, software version CS5; San Jose, CA, USA). The ERG procedure is summarized schematically in Figure 1.

Results

The five standard responses

All 15 Green Monkeys displayed very well detectable and easily reproducible ERG recordings, using the protocol described in the Experimental Procedure section (Figure 1). As indicated by the ISCEV, the five standard responses and the recommended additional stronger scotopic flash ERG are illustrated in Figure 2 for a representative Green Monkey. The typical scotopic ERG signal is formed, as expected, by an initial negative wave (the a-wave) and followed by a larger positive wave (the b-wave). Faster components of lower amplitude, known as the oscillatory potentials (OPs), are seen in the ascending limb of the scotopic b-wave. These OPs were as prominent as those obtained in humans. Given uncertainty of how best to quantify OPs, we chose to measure the amplitude from the peak of the second wave to the following trough, as described in the Experimental Procedure section. Thus, the chronological sequence of electrical events in a typical photopic ERG response observed in the Green Monkey, as in humans, is the a-wave, b-wave, and i-wave. During 30 Hz flicker stimulation, double peaks were often detectable in the b-waves. In these cases, both the amplitudes and implicit times were measured at the first peak. The signal-to-noise ratio was high for all categories, and no extra filter such as a notch filter had to be used, even in single sweep curves. Our mean results obtained in 15 Green Monkeys are summarized in Table 2; the mean amplitudes and latencies of the five standard ISCEV responses are specific to a flash intensity and light adaptation status.

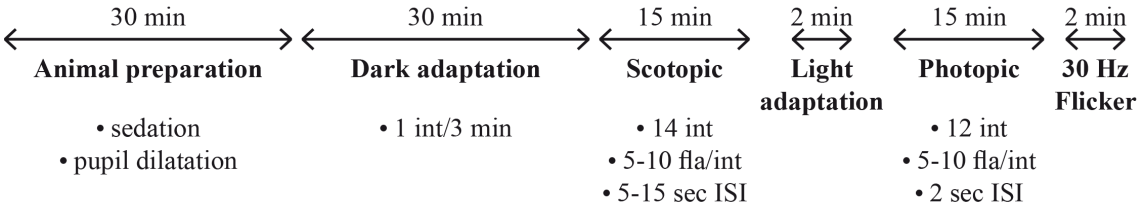

Figure 1. Summarized schematic procedure describing a typical electroretinography recording session in a Green Monkey (*Chlorocebus sabaeus*). Int, intensity; Fla, flashes; ISI, inter stimulus interval.

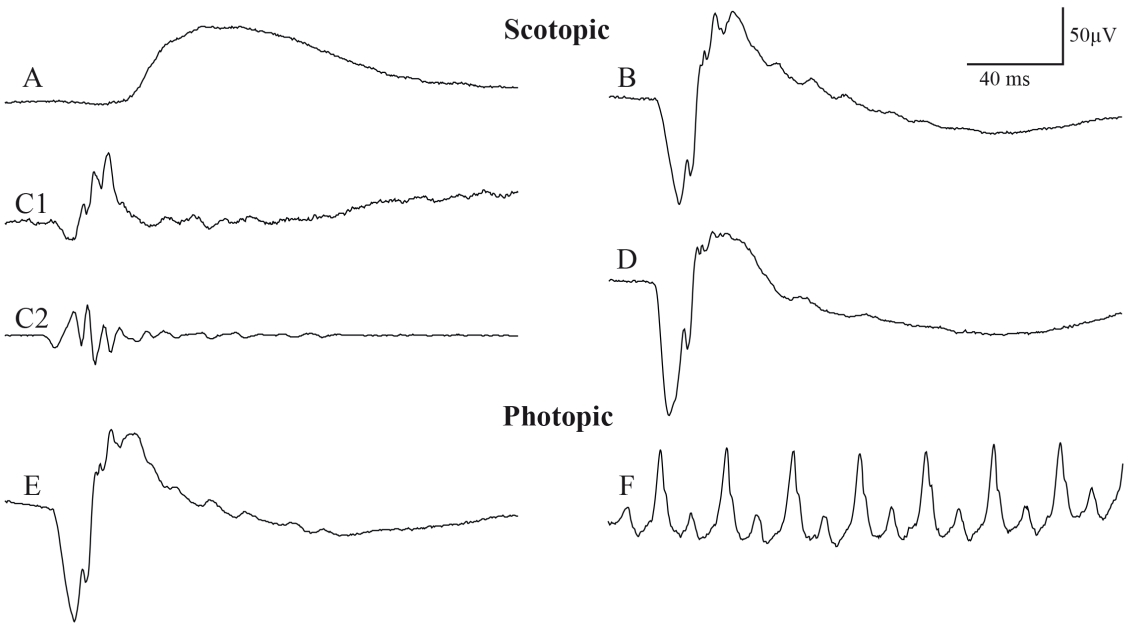

Figure 2. Standard responses for full-field electroretinography in a representative Green Monkey (*Chlorocebus sabaeus*), including the 5 standard responses: a rod response, a combined rod–cone response, oscillatory potentials, a cone response, and a flicker response. (**A**) Rod response elicited at -2.2 log cd.s.m^{-2} (0.0064 cd.s.m^{-2}) after 30 minutes of dark adaptation. (**B**) Maximal response elicited at 0.4 log cd.s.m^{-2} (2.57 cd.s.m^{-2}, standard flash) in the dark-adapted eye. (**C1**) Broadband scotopic ERG waveform and (**C2**) the corresponding software-filtered oscillatory potentials elicited at 0.6 log cd.s.m^{-2} (4.4 cd.s.m^{-2}) in the dark-adapted eye. (**D**) The recommended additional stronger flash ERG elicited at 10.0 cd.s.m^{-2} in the dark-adapted eye. (**E**) White flash cone response elicited at 0.4 log cd.s.m^{-2} in the light adapted eye with a background illumination of 30 cd.m^{-2}. (**F**) Flicker response (30 Hz) elicited at 0.4 log cd.s.m^{-2} after five minutes of light adaptation with a background illumination of 30 cd.m^{-2}. Tracings (**A**, **B**, **C1**, **D**, **E**) included a 20 ms pre-stimulus baseline. Horizontal calibration, 40 ms; vertical calibration, 50 µV.

Table 2. Responses to standardized electroretinography in Green Monkeys. Data are reported as mean ± SEM (standard error of the mean).

Standard response (ISCEV)	a-wave amplitude (μV)	a-wave peak latency (ms)	b-wave amplitude (μV)	b-wave peak latency (ms)	Flash intensity (cd.s.m^{-2})	Adaptation status
Rod response	-	-	88.9 ± 26.6	79.9 ± 6.1	0.0064	Dark
Maximal response	115.1 ± 40.2	14.8 ± 0.7	203.7 ± 52.6	36.7 ± 3.8	2.5	Dark
Oscillatory potential	-	-	60.2 ± 15.5	20.3 ± 0.9	4.4	Dark
Strong flash response	174.9 ± 27.2	9.8 ± 0.4	230.7 ± 40.6	30.8 ± 3.6	10.0	Dark
White flash cone response	22.1 ± 4.5	12.3 ± 1.2	81.5 ± 19.4	27.7 ± 1.5	2.5	Light
30 Hz flicker	-	-	88.9 ± 20.2	24.3 ± 1.0	2.5	Light

ERG responses throughout dark-adaptation

ERGs were recorded during the course of dark-adaptation at 3 min intervals over 30 min with a constant stimulus intensity of approximately 0.006 cd.s.m^{-2} (Figure 3). We have not pursued the recordings over 30 minutes based on the human [4] and monkey literature [27]. For example, Bee (2001) reported that in cynomologus monkeys (*Macaca fascicularis*), plateau was reached around 20 minutes.

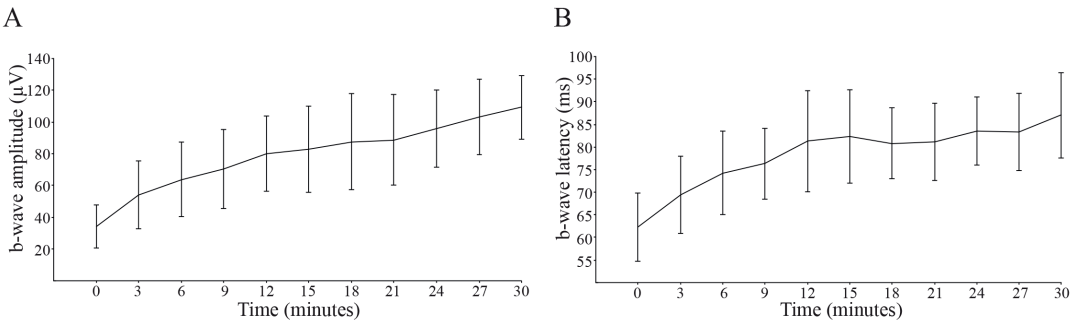

Figure 3. Response versus time functions of b-wave amplitude (**A**) and latency (**B**) throughout dark-adaptation elicited at -2.2 log cd.s.m^{-2} (0.0064 cd.s.m^{-2}). Each data point indicates average (± SEM) of all 15 monkeys.

Intensity–response function of scotopic and photopic ERG

Beyond the ordinary requirements of the ISCEV, ERG responses to stimuli of increasing flash intensity in dark-adapted (Figure 4A) and light-adapted conditions (Figure 4B) were also recorded. Both intensity response series were obtained from the same monkey, and in the same recording session. It can be seen in the figure that the two recording conditions yield ERG responses of different amplitude, timing and morphology. The distribution of full-field ERG amplitudes and implicit times are often asymmetrical, even in large groups of normal monkeys, such that use of statistics based on a normal distribution can be misrepresentative [27]. We used a log transformation of the data to reduce variance. Figure 5 shows the results of the scotopic a-wave and b-wave amplitudes and latency versus log flash intensity (cd.s.m^{-2}) functions. It is worthwhile to note a sigmoid curve characterizes the amplitudes as well as the latencies functions in the Green Monkey. Moreover, the b-wave amplitude decreased at the highest intensity of 2.9 log cd.s.m^{-2} with an inter-stimulus interval of 15 seconds (Figure 5A and 5C). The photopic functions are shown in Figure 6. The values given at 0.4 log cd.s.m^{-2} (standard flash) represent the white flash cone response as recommended by the ISCEV. These results are also known from studies on non-human and human primate retinal functions [27], [31].

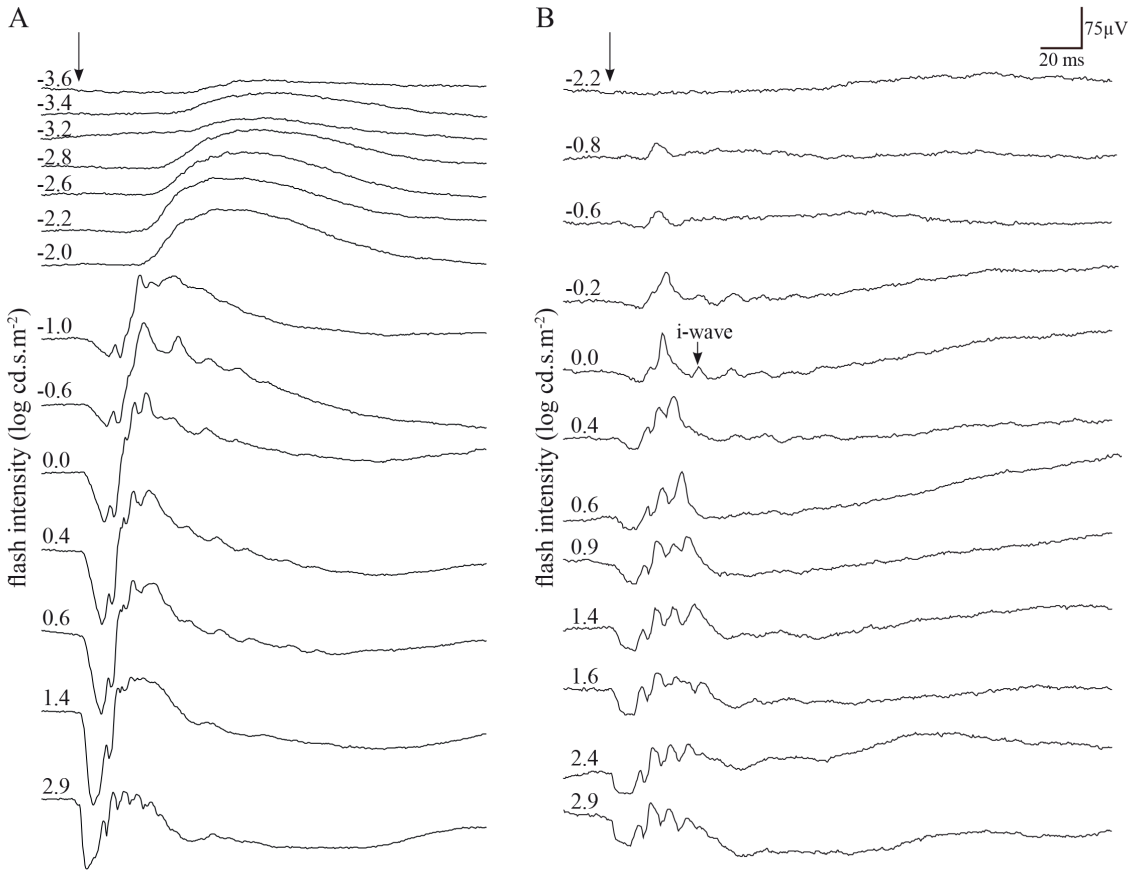

Figure 4. ERG responses to stimuli of increasing flash intensity, from top to bottom, in the dark-adapted eye (**A**) and in the light-adapted eye (**B**) of a representative Green Monkey (*Chlorocebus sabaeus*). Vertical arrow indicates flash onset. Horizontal calibration, 20 ms; vertical calibration, 75 µV.

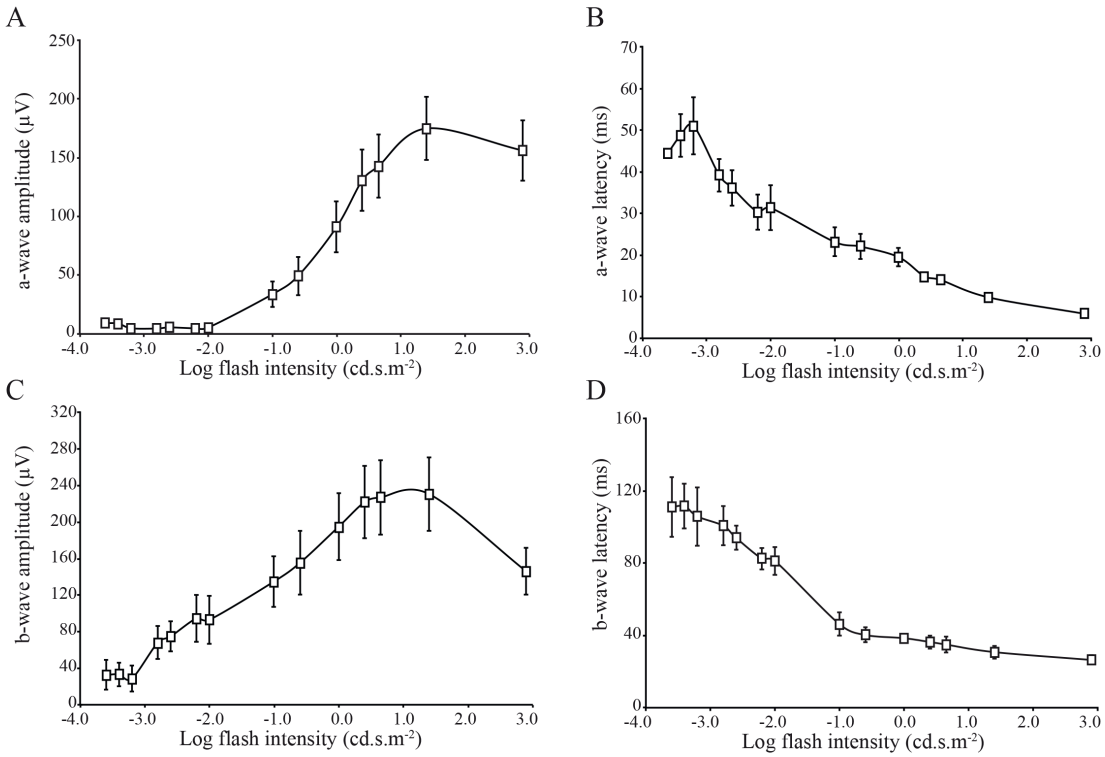

Figure 5. Response versus intensity function for the a-wave amplitude (A), a-wave latency (B), b-wave amplitude (C), and b-wave latency (D) of the scotopic ERG. Each data point indicates average (± SEM) of all 15 monkeys.

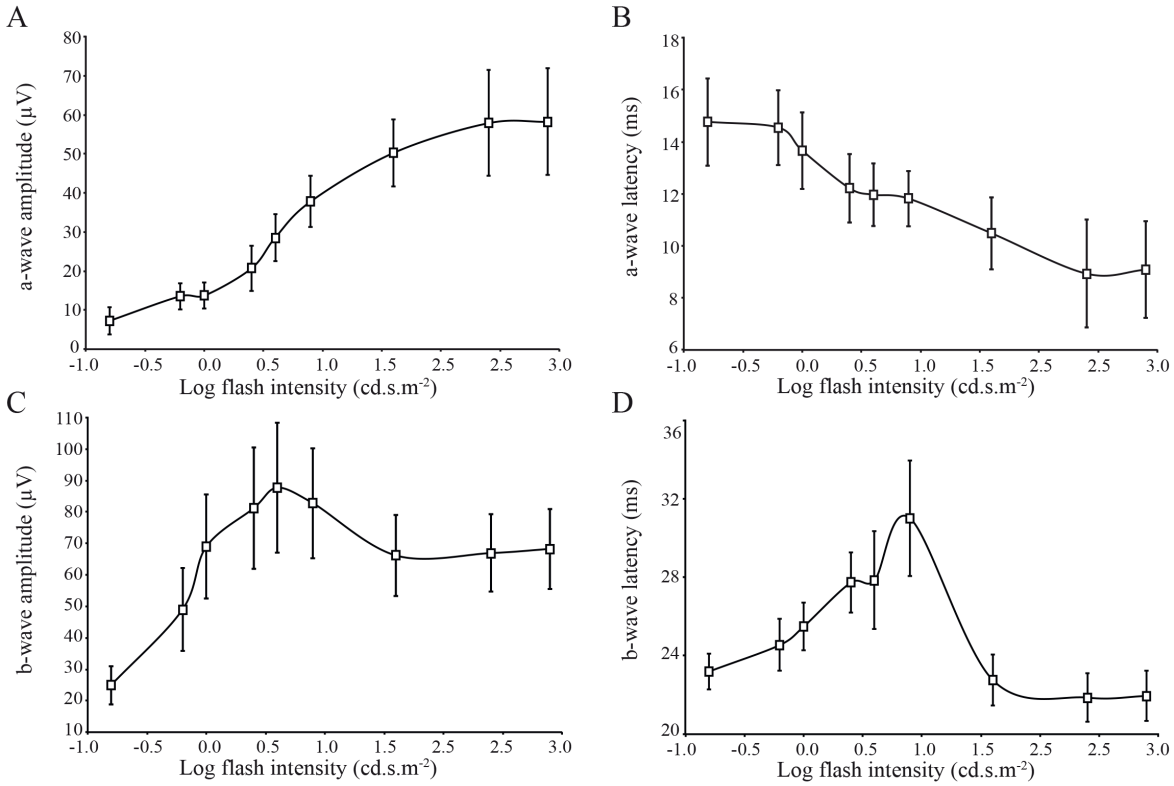

Figure 6. Response versus intensity function for the a-wave amplitude (A), a-wave latency (B), b-wave amplitude (C), and b-wave latency (D) of the photopic ERG under rod-suppressing background illumination (30 cd.m^{-2}). Each data point indicates average (± SEM) of all 15 monkeys.

The photopic hill effect

In the recordings of light-adapted eyes, the amplitude of the a-wave augments regularly with the gradual increase in intensity of the stimulus, while amplitude of the b-wave first increases to a maximum (V_{max}), and finally decreases with presentation of progressively brighter stimuli. This effect has been well demonstrated in humans [32]. The photopic flash ERG of the Green Monkey includes a post b-wave component identified as the i-wave that is best seen using the standard flash (0.0 log cd.s.m^{-2}) after light adaptation (Figure 4).

Discussion

These results provide normative values for the standard ERG protocol in Green Monkeys, with the general finding that full-field flash ERG responses in these monkeys are similar to those in humans. We report the 5 responses in Green Monkeys as recommended by ISCEV, which are the standard protocols for ERG in humans [4] and cynomolgus monkeys [27]. The ISCEV consensus standard provides the basis for stable comparison between research laboratories and clinical ERG recordings. However, information about additional stimuli is often necessary for specific applications, such as in considering the higher retinal illuminances for rod responses in human neonates [33], and dark-adapted flicker in retinitis pigmentosa [34]. Throughout the present study, particular attention was paid to IOP and pupil dilatation, with an aim to reduce variability (Table 1). Human and non-human primates are mammals that share similar vascular anatomy of the eyes, and have a macular/foveal region and multiple cone types that offer them high visual acuity and color vision. It is notable that our values of amplitude and latency in Green Monkeys are closer to those in humans [4], relative to corresponding results in cynomolgus monkeys [27], [35], and it may be that the differences are as much attributable to laboratories they are to species differences.

The ERG responses to the standard tests in Green Monkeys were similar to the responses in humans even though the axial length of Green Monkey eyes is a bit lower than humans, i.e. 18 mm in the Green Monkey and 24 mm in humans [36]. In particular, the shape and latency of the curves are highly comparable. We can safely assume that the higher amplitudes found in man [31] are due to the large diameter and larger retinal surface area of the human eye, which have a direct relation with the net electric field and thus on the measured responses. Accordingly, differences in amplitude but not in latency have been observed in human subjects with high myopia or small refractive error, as expected due to differences in axial length [37]. In the present study, slight differences in amplitude were occasionally noticed in the other eye, but were in every case within the 10% inter-ocular amplitude differences in normal human subjects [38]. Furthermore, the standard amplitude of OPs was a bit larger than the range in cynomolgus monkeys [27], but lower than those of humans [39]. The implicit times of OPs were within the same range for monkeys and humans.

Full-field stimulation, as employed presently, is the most effective way of eliciting an ERG representative of the entire population of cones and rods in the primate retina [40]. Replicable peak amplitudes and implicit times can therefore be obtained with full-field ERG recordings. Recordings of photopic ERGs are used to assess the functioning of the cone system in humans and animals. As defined above, in response to progressively brighter stimuli, the b-wave of the photopic ERG gradually increases in amplitude, attains a plateau (the maximal b-wave amplitude which is reached for a narrow range of intensities, V_{max}), and then rapidly decreases with further increments in the luminance of the flash. This unique luminance–response function was originally termed "the photopic hill" [41]. The photopic hill in the primate ERG results mainly from two factors: the reduction of the ON-component amplitude at higher intensities and the delay in the positive peak of the OFF-component at higher intensities [42]. Scotopic ERGs, on the other hand, are used to evaluate the integrity of the rod system in humans and animals [2], [43].

At about 20 ms after a typical human photopic b-wave, a second positive signal is seen, the i-wave [44]. This feature is common to the photopic ERG of many species except mice and rats [28]. The i-wave amplitudes and latencies in Green Monkeys were similar to those reported previously for most mammals [28]. It is interesting to note that in humans, the amplitude of the i-wave saturates at a dimmer flash intensity than that needed to evoke a b-wave of maximal amplitude [45].

In general, it is important to consider how best to interpret a finding of altered electroretinogram in the clinic and in animal models. Normal scotopic and photopic a-waves indicate normal functioning of rod and cone outer segments. In particular, it has been proposed that the scotopic ERG b-wave is the result of depolarization of ON-bipolar cells [46], [47]. Consequently, a pathological or pharmacological decrease in amplitude of the b-wave of the rod ERG and of the scotopic standard combined ERG might both result from a postsynaptic abnormality in the rod ON-pathway, plausibly due to a postsynaptic abnormality in the cone ON-pathway because it generates this response [46], [48]. The ON-pathway is often considered to influence contrast sensitivity [49], [50]. For instance, impairments of contrast

sensitivity are reported clinically in disorders with ON-pathway dysfunction [51], such as melanoma-associated retinopathy [52], congenital stationary night blindness [53].

Specific values for amplitude and b-wave implicit time will necessarily differ between laboratories due to minor variations in recording electrodes, equipment, and protocol, not to mention species differences. Among the various technical factors potentially impacting the ERG amplitudes include contact lens placement, the structural integrity of the corneal surface, pupil size, and even IOP. It is important to consider these factors when interpreting the results. Nevertheless, in order to control for these technical and biological influences, we collected the physiological relevant data before and after the ERG recordings for each monkey, so as to provide a stable basis for comparison in future studies of pharmacology and disease models in the Green Monkey. The present results entailing recordings performed in accordance with the ISCEV, and with the ERG encompassing 30 minutes of dark adaptation correspond very well with similar results obtained in humans. Thus, the Green Monkey promises to serve as an excellent animal model for retinal function testing, for example in toxicity evaluation.

Acknowledgements

We would like to thank Dr. Pierre Lachapelle (McGill University, Montreal, Quebec) for his constructive comments. We also thank Ms. Anna Polosa, M.Sc. for her assistance in carrying out the calibration of the LKC apparatus and developing the protocol. We are very grateful to Dr. Amy Beierschmitt and Mr. Maurice Matthew, M.Sc. of the Behavioral Science Foundation Laboratories of St-Kitts for their expert technical assistance in handling the monkeys. We acknowledge Inglewood Biomedical Editing (www.inglewoodbiomedediting.com) for expert revision and editing of the manuscript.

References

1. Steinberg RH, Linsenmeier RA, Griff ER (1985) Chapter 2 Retinal pigment epithelial cell contributions to the electroretinogram and electrooculogram. Prog Retin Res 4: 33-66.

2. Frishman LJ (2006) Origins of the electroretinogram. In: Heckenlively JR, Arden GB, editors. Principles and Practice of Clinical Electrophysiology of Vision. The MIT Press: Cambridge, MA, pp 139–183.

3. Curcio C, Sloan K, Packer O, Hendrickson A, Kalina R (1987) Distribution of cones in human and monkey retina: individual variability and radial asymmetry. Science 236: 579-582.

4. Marmor MF, Fulton AB, Holder GE, Miyake Y, Brigell M, et al. (2009) ISCEV Standard for full-field clinical electroretinography (2008 update). Doc Ophthalmol 118: 69-77.

5. Palmour RM, Mulligan J, Howbert JJ, Ervin F (1997) Of monkeys and men: vervets and the genetics of human-like behaviors. Am J Hum Genet 61: 481-488.

6. Jasinska AJ, Service S, Levinson M, Slaten E, Lee O, et al. (2007) A genetic linkage map of the vervet monkey (Chlorocebus aethiops sabaeus). Mamm Genome 18: 347-360.

7. Ptito M, Herbin M, Boire D, Ptito A (1996) Neural bases of residual vision in hemicorticectomized monkeys. Prog Brain Res 112: 385-404.

8. Papia MF, Burke MW, Zangenehpour S, Palmour RM, Ervin FR, et al. (2010) Reduced soma size of the M-neurons in the lateral geniculate nucleus following foetal alcohol exposure in non-human primates. Exp Brain Res 205: 263-271.

9. Burke MW, Kupers R, Ptito M (2012) Adaptive neuroplastic responses in early and late hemispherectomized monkeys. Neural Plast 2012: 852423.

10. Herbin M, Boire D, Ptito M (1997) Size and distribution of retinal ganglion cells in the St. Kitts green monkey (Cercopithecus aethiops sabeus). J Comp Neurol 383: 459-472.

11. Theoret H, Boire D, Ptito M (2000) Retinal projections to the pregeniculate nucleus in the hemispherectomized monkey. Brain Res Bull 53: 239-243.

12. Boire D, Theoret H, Ptito M (2001) Visual pathways following cerebral hemispherectomy. Prog Brain Res 134: 379-397.

13. Theoret H, Boire D, Herbin M, Ptito M (2001) Anatomical sparing in the superior colliculus of hemispherectomized monkeys. Brain Res 894: 274-280.

14. Boire D, Theoret H, Ptito M (2002) Stereological evaluation of neurons and glia in the monkey dorsal lateral geniculate nucleus following an early cerebral hemispherectomy. Exp Brain Res 142: 208-220.

15. Burke MW, Palmour RM, Ervin FR, Ptito M (2009) Neuronal reduction in frontal cortex of primates after prenatal alcohol exposure. Neuroreport 20: 13-17.

16. Burke M, Zangenehpour S, Bouskila J, Boire D, Ptito M (2009) The gateway to the brain: dissecting the primate eye. J Vis Exp: e1261.

17. Bouskila J, Burke MW, Zabouri N, Casanova C, Ptito M, et al. (2012) Expression and localization of the cannabinoid receptor type 1 and the enzyme fatty acid amide hydrolase in the retina of vervet monkeys. Neuroscience 202: 117-130.

18. Bouskila J, Javadi P, Casanova C, Ptito M, Bouchard JF (2013) Muller cells express the cannabinoid CB2 receptor in the vervet monkey retina. J Comp Neurol 521: 2399-2415.

19. Bouskila J, Javadi P, Casanova C, Ptito M, Bouchard JF (2013) Rod photoreceptors express GPR55 in the adult vervet monkey retina. PLoS One 8: e81080.

20. Mikula S, Trotts I, Stone JM, Jones EG (2007) Internet-enabled high-resolution brain mapping and virtual microscopy. NeuroImage 35: 9-15.

21. Mikula S, Stone JM, Jones EG (2008) BrainMaps.org - Interactive High-Resolution Digital Brain Atlases and Virtual Microscopy. Brains Minds Media 3: bmm1426.

22. Woods RP, Fears SC, Jorgensen MJ, Fairbanks LA, Toga AW, et al. (2011) A web-based brain atlas of the vervet monkey, Chlorocebus aethiops. NeuroImage 54: 1872-1880.

23. Osterberg G (1935) Topography of the layer of rods and cones in the human retina. Actaophthal suppi 6: 11-97.

24. Jacobs GH (2008) Primate color vision: a comparative perspective. Vis Neurosci 25: 619-633.

25. Finlay BL, Franco EC, Yamada ES, Crowley JC, Parsons M, et al. (2008) Number and topography of cones, rods and optic nerve axons in New and Old World primates. Vis Neurosci 25: 289-299.

26. Buist DP, Heywood R (1982) A standardized procedure for electroretinographic examination of rhesus monkeys (Macaca mulatta). Lab Anim Sci 32: 91-93.

27. Bee WH (2001) Standardized electroretinography in primates: a non-invasive preclinical tool for predicting ocular side effects in humans. Curr Opin Drug Di De 4: 81-91.

28. Rosolen SG, Rigaudiere F, LeGargasson JF, Chalier C, Rufiange M, et al. (2004) Comparing the photopic ERG i-wave in different species. Vet Ophthalmol 7: 189-192.

29. Rangaswamy N, Frishman L, Dorotheo EU, Schiffman J, Bahrani H, et al. (2004) Photopic ERGs in patients with optic neuropathies: comparison with primate ERGs after pharmacologic blockade of inner retina. Invest Ophthalmol Vis Sci 45: 3827-3837.

30. Viswanathan S, Frishman LJ, Robson JG, Walters JW (2001) The photopic negative response of the flash electroretinogram in primary open angle glaucoma. Invest Ophthalmol Vis Sci 42: 514-522.

31. Jacobi PC, Miliczek KD, Zrenner E (1993) Experiences with the international standard for clinical electroretinography: normative values for clinical practice, interindividual and intraindividual variations and possible extensions. Doc Ophthalmol 85: 95-114.

32. Rufiange M, Dassa J, Dembinska O, Koenekoop RK, Little JM, et al. (2003) The photopic ERG luminance-response function (photopic hill): method of analysis and clinical application. Vision Res 43: 1405-1412.

33. Birch DG, Birch EE, Hoffman DR, Uauy RD (1992) Retinal development in very-low-birth-weight infants fed diets differing in omega-3 fatty acids. Invest Ophthalmol Vis Sci 33: 2365-2376.

34. Berson EL, Gouras P, Hoff M (1969) Temporal aspects of the electroretinogram. Arch Ophthalmol 81: 207-214.

35. Bee WH, Korte R, Vogel F (1995) Electroretinography in the non-human primate as a standardized method in toxicology. In: Weisse I, Hockwin O, Green K, Tripathi R, editors. Ocular Toxicology. Springer US. pp. 53-61.

36. Howland HC, Merola S, Basarab JR (2004) The allometry and scaling of the size of vertebrate eyes. Vision Res 44: 2043-2065.

37. Westall CA, Dhaliwal HS, Panton CM, Sigesmun D, Levin AV, et al. (2001) Values of electroretinogram responses according to axial length. Doc Ophthalmol 102: 115-130.

38. Rotenstreich Y, Fishman GA, Anderson RJ, Birch DG (2003) Interocular amplitude differences of the full-field electroretinogram in normal subjects. Br J Ophthalmol 87: 1268-1271.

39. Birch DG, Anderson JL (1992) Standardized full-field electroretinography. Normal values and their variation with age. Arch Ophthalmol 110: 1571-1576.

40. Weleber RG (1981) The effect of age on human cone and rod ganzfeld electroretinograms. Invest Ophthalmol Vis Sci 20: 392-399.

41. Wali N, Leguire LE (1992) The photopic hill: a new phenomenon of the light adapted electroretinogram. Doc Ophthalmol 80: 335-345.

42. Ueno S, Kondo M, Niwa Y, Terasaki H, Miyake Y (2004) Luminance dependence of neural components that underlies the primate photopic electroretinogram. Invest Ophthalmol Vis Sci 45: 1033-1040.

43. Holopigian K, Seiple W, Greenstein VC, Hood DC, Carr RE (2001) Local cone and rod system function in patients with retinitis pigmentosa. Invest Ophthalmol Vis Sci 42: 779-788.

44. Freund PR, Watson J, Gilmour GS, Gaillard F, Sauve Y (2011) Differential changes in retina function with normal aging in humans. Doc Ophthalmol 122: 177-190.

45. Rufiange M, Rousseau S, Dembinska O, Lachapelle P (2002) Cone-dominated ERG luminance-response function: the Photopic Hill revisited. Doc Ophthalmol 104: 231-248.

46. Tian N, Slaughter MM (1995) Correlation of dynamic responses in the ON bipolar neuron and the b-wave of the electroretinogram. Vision Res 35: 1359-1364.

47. Robson JG, Frishman LJ (1995) Response linearity and kinetics of the cat retina: the bipolar cell component of the dark-adapted electroretinogram. Vis Neurosci 12: 837-850.

48. Stockton RA, Slaughter MM (1989) B-wave of the electroretinogram. A reflection of ON bipolar cell activity. J Gen Physiol 93: 101-122.

49. Knapp AG, Ariel M, Robinson FR (1988) Analysis of vertebrate eye movements following intravitreal drug injections. I. Blockade of retinal ON-cells by 2-amino-4-phosphonobutyrate eliminates optokinetic nystagmus. J Neurophysiol 60: 1010-1021.

50. Sieving PA (1993) Photopic ON- and OFF-pathway abnormalities in retinal dystrophies. Trans Am Ophthalmol Soc 91: 701-773.

51. Iwakabe H, Katsuura G, Ishibashi C, Nakanishi S (1997) Impairment of pupillary responses and optokinetic nystagmus in the mGluR6-deficient mouse. Neuropharmacology 36: 135-143.

52. Wolf JE, Arden GB (1996) Selective magnocellular damage in melanoma-associated retinopathy: comparison with congenital stationary nightblindness. Vision Res 36: 2369-2379.

53. Barnes CS, Alexander KR, Fishman GA (2002) A distinctive form of congenital stationary night blindness with cone ON-pathway dysfunction. Ophthalmology 109: 575-583.

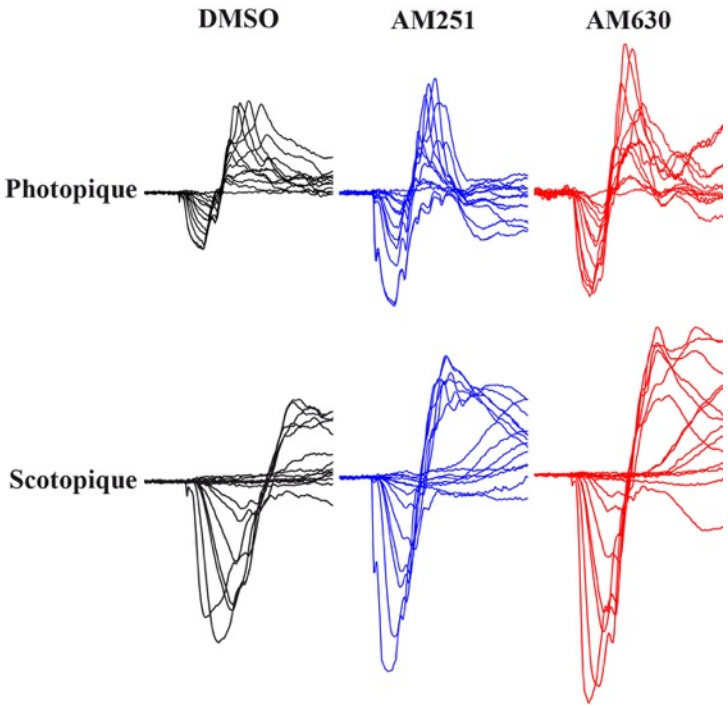

ARTICLE 6: CANNABINOID RECEPTORS CB1 AND CB2 MODULATE THE ELECTRORETINOGRAPHIC WAVES IN VERVET MONKEYS

Publié dans :

Bouskila J, Harrar V, Javadi P, Beierschmitt A, Palmour RM, Casanova C, Bouchard JF, Ptito M (2015) Cannabinoid receptors CB1 and CB2 modulate the electroretinographic waves in vervet monkeys, *Neural Plasticity* 2016:1253245.

Cannabinoid receptors CB1 and CB2 modulate the electroretinographic waves in vervet monkeys

Joseph Bouskila*[1, 2], Vanessa Harrar*[1], Pasha Javadi[1], Amy Beierschmitt[3], Roberta Palmour[3, 4], Christian Casanova[1], Jean-François Bouchard[1] and Maurice Ptito[1, 5]

[1]School of Optometry, University of Montreal, Montreal, QC, Canada
[2]Biomedical Sciences, Faculty of Medicine, University of Montreal, Montreal, QC, Canada
[3]St-Kitts Behavioral Science Foundations, St-Kitts and Nevis, West Indies
[4]Department of Human Genetics, McGill University, Montreal, QC, Canada
[5]BRAINlab and Neuropsychiatry Laboratory, Department of Neuroscience and Pharmacology, University of Copenhagen, Copenhagen, Denmark

Keywords: CB1R, CB2R, electroretinography, a-wave, b-wave, monkey.

*JB and VH contributed equally to the work presented here and should therefore be regarded as equivalent authors.

Correspondence should be addressed to:
Maurice Ptito, PhD
School of Optometry, room 260-7
3744 Jean-Brillant Street,
University of Montreal,
Montreal, Quebec, Canada, H3T 1P1

Running title: Role of CB1R and CB2R in the monkey retina

Acknowledgements: The Natural Science and Engineering Research Council of Canada (6362-2012, MP; RGPAS 478115-2015 and RGPIN 2015-06582, JFB) and the Canadian Institutes of Health Research (MOP-130337, JFB) supported this work. JB received support from a Frederick Banting and Charles Best Canada Graduate Scholarship Doctoral Award from CIHR. A Banting Postdoctoral Fellowship from CIHR was obtained by VH. JFB is supported by a "Chercheur-Boursier Senior" from the Fonds de recherche du Québec - Santé (FRQ-S). MP is Harland Sanders Chair professor in Visual Science. The authors would like to thank Maurice Matthew, M.Sc. for his expert technical assistance in handling the monkeys.

We are very grateful to the late Dr. Frank Ervin for his judicious advice, and to the staff of the Behavioural Sciences Foundation for their continued support.

Abstract

The expression patterns of the cannabinoid receptor type 1 (CB1R) and the cannabinoid receptor type 2 (CB2R) are well documented in rodents and primates. In vervet monkeys, CB1R is present in the retinal neurons (photoreceptors, horizontal cells, bipolar cells, amacrine cells, and ganglion cells) and CB2R is exclusively found in the retinal glia (Müller cells). However, the role of these cannabinoid receptors in normal primate retinal function remains elusive. Using full-field electroretinography in adult vervet monkeys, we recorded changes in neural activity following the blockade of CB1R and CB2R by the intravitreal administration of their antagonists (AM251 and AM630, respectively) in photopic and scotopic conditions. Our results show that AM251 increases the photopic a-wave amplitude at high flash intensities, whereas AM630 increases the amplitude of both the photopic a- and b-waves. In scotopic conditions, both blockers increased the b-wave amplitude, but did not change the a-wave amplitude. These findings suggest an important role of CB1R and CB2R in primate retinal function.

Introduction

The endocannabinoid system is composed of cannabinoid receptor type 1 (CB1R), cannabinoid receptor type 2 (CB2R), their endogenous ligands (endocannabinoids), and their synthetizing and metabolizing enzymes. The physiological and psychological effects of cannabinoids can be detected almost everywhere in the body due to the abundance of cannabinoid receptors. Expression patterns of CB1R and CB2R are well documented in the retina of numerous species, including rodents and primates [1-6]. In rodents, CB1R and CB2R are expressed in many retinal cell types, particularly cone and rod photoreceptors, horizontal cells, amacrine cells, bipolar cells, and ganglion cells [1, 7]. In vervet monkeys, CB1R is mainly found in cones of the central retina, in rod spherules with very low expression, horizontal cells, bipolar cells, amacrine and ganglion cells [5]. CB2R, on the other hand, is strictly expressed in primate glial Müller cells [6]. Beyond the retina, the expression pattern of CB1R has been observed in the dorsal lateral geniculate nucleus [8] and primary visual cortex [9] of primates.

Most of our knowledge on the role of cannabinoids in human vision comes from reports, anecdotes and studies with cannabis consumers (for review see [10]). Besides the well-known “red eye” effect (vasodilation) of marijuana and reduction of intraocular pressure (IOP) [11-13], the functional effects of endocannabinoids on the visual system are not yet well defined [14]. Nevertheless, the administration of cannabinoids produces some known alterations in the human visual system. Indeed, case studies suggested the existence of cannabis-mediated visual effects in humans, particularly an increase in glare recovery at low contrast [15], a reduction in Vernier and Snellen acuities [16, 17], improvement in night vision

[18, 19], blurred vision [20], changes in color discrimination, and an increase in photosensitivity [21]. Most of the latter (psychophysical) effects may have a retinal component, which might be due to neurochemical changes induced by the retinal endocannabinoid system. Indeed, many physiological effects of cannabinoids were reported for every retinal cell type in bovines, guinea pigs, rodents, and fishes (for review see [10, 22]). In the bovine retina, the activation of CB1R increases monoamine oxidase [23]. In the guinea pig retina, stimulation of CB1R results in the inhibition of dopamine release [24], and in the rat retina, the activation of cannabinoid receptors modulates [35S] GTPγ S-binding and voltage-dependent membrane currents in photoreceptors, bipolar cells and ganglion cells [3, 25-28]. In addition, cannabinoid agonists increase the cone response to light offset in the goldfish retina [29].

The electroretinogram (ERG) is a useful tool for assessing retinal function by measuring the electrical responses of all populations of retinal cells, mainly photoreceptors (cones and rods), bipolar cells, amacrine cells, and Müller cells [30, 31, 32]. The ERG waves include two main components: the negative amplitude (a-wave) and the positive one (b-wave). Traditionally, the a-wave reflects the response of rods and cones to light [33-34]. The generation of the b-wave, the second major component of the ERG, is attributed to the inner retina, mainly the depolarization of bipolar and Müller cells [30-32, 35-39]. Specific stimuli and recording environments are selected to isolate the components of the ERG and target particular populations of retinal cells. For instance, rod function is assessed in dark-adapted eyes, under scotopic conditions, while cone responses are better assessed with high intensity flashes, under photopic conditions [38]. In this study, we investigated the changes in normal

retinal function as measured by electroretinography in adult vervet monkeys after blockade of CB1R or CB2R by their antagonists AM251 and AM630, respectively.

Material and Methods

Choice of species. Vervet monkeys are becoming the preferred animal model used in biomedical research second only to the rhesus macaque [40]. Vervets are very similar in physiology and behavior to macaques, and they are more accessible, disease-free with less health and safety risks. Vervet monkeys have a foveal binocular vision with a high cone density that decreases with eccentricity, trichromatic color vision and a six-layered dorsal lateral geniculate nucleus [41, 42]. Recently, we have standardized a non-invasive, painless ERG method for vervet monkeys [43] that showed highly comparable recordings to macaques [44] and humans [45].

Subjects. Sixteen vervet monkeys (*Chlorocebus sabaeus*) were tested in this study. Six of those monkeys were injected with AM251, and another six were injected with AM630. An additional 4 monkeys were injected with the vehicle (DMSO) used for the dilution of our antagonists in order to provide control values. The animals were fed with primate chow (Harlan Teklad High Protein Monkey Diet; Harlan Teklad, Madison, WI, USA) and fresh local fruits, with water available *ad libitum.* All experiments were performed according to the guidelines of the Canadian Council on Animal Care (CCAC) and the Association for Research in Vision and Ophthalmology (ARVO) Statement for the Use of Animals in Ophthalmic and Vision Research. The experimental protocol was also reviewed and approved by the local Animal Care and Use Committee (University of Montreal, protocol # 14-007) and the Institutional Review Board of the Behavioral Science Foundation. None of the animals were sacrificed for this study.

Animal preparation for ERG recordings. All procedures were in accordance with the standard protocol of electroretinography in vervet monkeys [43]. Briefly, all animals received an intramuscular injection of ketamine (10 mg/kg; Troy Laboratories, Glendenning, New South Wales, Australia) and xylazine (1 mg/kg; Lloyd Laboratories, Shenandoah, IA, USA) to maintain an adequate level of sedation that prevents the animals from moving and blinking. This drug mixture has no effect on the ERG recordings [46]. With 1% tropicamide (Mydriacyl) and 2.5% phenylephrine hydrochloride (Mydfrin) (Alcon Laboratories, Fort Worth, TX, USA), the pupils were fully dilated (approximately 9 mm in diameter), and the accommodation paralyzed. The cornea was anesthetized with 0.5% proparacaine hydrochloride (Alcaine; Alcon Laboratories, Fort Worth, TX, USA). To prevent corneal drying, the eyes were moisturized frequently with 2.5% methylcellulose (Gonak; Akorn, Inc., Buffalo Grove, IL, USA). Body temperature was maintained between 36.5°C and 38°C with a heating pad. After a recording session that lasted about 2 hours, the animals were sent back to their prior natural settings after a recovery period in isolation.

Intravitreal Injection. The CB1R antagonist AM251 was purchased from Cayman Chemicals (Ann Arbor, MI, USA). The CB2R antagonist AM630 was purchased from Tocris (Tocris Bioscience, Ellisville, MO, USA). Both antagonists were diluted in DMSO under sterile conditions. Assuming no leakage, the final concentration was 1.5% v/v for DMSO, 0.01 mg/µl for AM251, and 0.003 mg/µl for AM630. To factor out any effects of the vehicle (DMSO), we subtracted the ERG recordings of the DMSO-injected animals from the ERG recordings of the drug-injected animals. In this way, the effects that we report are only those above and beyond effects of the vehicle. After inspection and examination of the eyes, the cornea was cleaned

with 5% povidone-iodine solution for 45 seconds. A drop of the topical anesthetic, pilocarpine proparacaine, was then applied over the injection site. The conjunctival and corneal surfaces were further moistened with methylcellulose (Moisture Eyes, Bausch & Lomb Canada, Vaughan, ON, Canada). The cornea was protected with sterile coatings while placing the Barraquer eye speculum (1.75 inches, 10 mm wide small blades). A total of 50 μL of drug solution was injected 2 mm posterior to the corneal limbus into the vitreous cavity. Upon removal of the needle, the injection site was compressed for about one minute using a sterile cotton swab to avoid reflux. The back of the eye was inspected using an ophthalmoscope before and after the intravitreal injection to verify the integrity of the retina. No substantial differences were observed in intraocular pressure before and after the intravitreal administration. As a follow up, the animals' eyes were checked every day for seven days following injection, and a topical antibiotic ointment was administered (Tobrex, 0.3% Tobramycin ophthalmic ointment, Alcon Canada, Mississauga, Canada).

Visual Stimulation. Full-field stimulation was produced by a Ganzfeld light source (UTAS E-3000 electrophysiology equipment; LKC Technologies, Inc., Gaithersburg, MD, USA) that was placed in front of the animal's face. The ERGs were evoked by <5 ms white flashes delivered in full-field conditions. Xenon flash luminance of 2.5 to 800 $cd.s.m^{-2}$ (0 dB to 20 dB in LKC units) was used for photopic recordings and LED flash luminance of $2.5x10^{-5}$ to 6 $cd.s.m^{-2}$ (-40 dB to 4 dB in LKC units) for scotopic recordings. For light-adapted ERGs a steady background-adapting field (30 $cd.m^{-2}$) was presented inside the Ganzfeld to saturate the rod system. Dark adaptation lasted approximately 20 minutes. Inter-stimulus intervals of at least 20 seconds were used at high intensities in the dark-adapted eyes. Flash intensities and

background luminance were calibrated using a research radiometer (IL1700 Photometer, International Light Inc., Newburyport, MA, USA) with a SED033 detector placed at 36 cm from the source.

ERG recording. All ERG procedures followed the ISCEV guidelines and the recently published standardized ERG protocol of vervet monkeys [43]. ERG responses were recorded differentially between corneal contact lens electrodes (Jet electrodes, Diagnosys LLC, Lowell, MA, USA) lying across the center of the cornea of each eye. The jet electrodes were equipped with four small posts on the convex surface in order to keep the eyelids open. Reference and ground gold disc electrodes (model F-E5GH; Grass Technologies, Astro-Med, Inc., West Warwick, RI, USA) were respectively placed to the external canthi and forehead with adhesive paste (Ten20 conductive EEG paste, Kappa Medical, Prescott, AZ, USA). For the analysis of the waveforms, the a-wave amplitude was measured from the baseline to the trough of the a-wave. The amplitude of the b-wave was measured from the trough of the a-wave to the peak of the b-wave. The peak latency was defined from the onset of the flash to the trough or peak. Baselines and post-injection photopic amplitudes and latencies were calculated as averages to minimize the noise inherent in the ERG signals and improve power, allowing for robust parametric statistical analysis. Since there was only one baseline recording of the injected eye, the baseline value was calculated from an average across both eyes (when available) since ERGs do not vary considerably across eyes [47]. For the post-injection values, we had several recordings from the injected eye (one every 10 minutes for 40 minutes). Visual inspection revealed the peak effect to be present at both the 30 and 40 minutes post-injection recordings. These were therefore averaged to obtain post-injection values for each intensity

flash. Retinal response diagrams were drawn using Adobe Illustrator and processed in Adobe InDesign (Adobe Systems Canada, Ottawa, ON, Canada, software version CS5). The recording protocol for assessing the effect of the drugs is summarized in Figure 1.

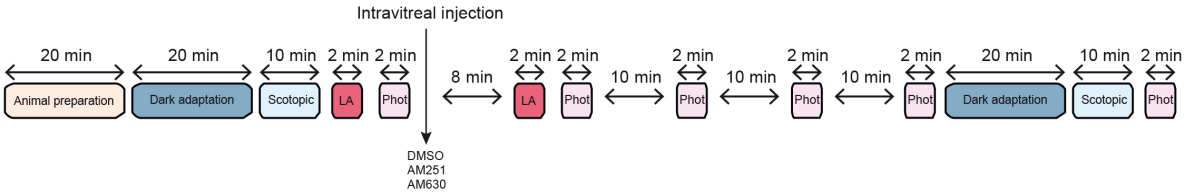

Figure 1. A schematic procedure illustrating a typical ERG recording session for testing ERG changes following an intravitreal injection in vervet monkeys (modified from [43]). LA, light adaptation; Phot, photopic.

Statistical analysis. The absolute trough (a-wave) and peak (b-wave) of the ERG curves were obtained at each light intensity value. When the ERG curve for low light intensities (<-2 log cd.s.m^{-2}) did not return to baseline 350 ms after the stimulus, the amplitudes of the a- and b-wave were corrected to account for the baseline shift. When no a-wave, or no wave at all, was detected, an amplitude of 0 was given and the latency was left blank for that specific stimulus intensity. Outliers (±2.5 STD) were removed (<2% overall). Post-injection amplitudes and latencies were expressed as percent of change from pre-injection amplitudes (post minus pre, divided by pre). The delta change percentages of injecting AM251 and AM630 were then subtracted from the delta change percent for the control injection, the vehicle DMSO. Thus, positive normalized effects indicate an increase as a result of injecting the drug, greater than the change that results from injecting the vehicle alone. To assess the statistical significance of the observed increase, we analyzed the amplitudes of the a- and b- waves using General Estimating Equations (GEE) with flash intensity as a within subject factor, because each

monkey was repeatedly measured (at each flash intensity). These main effects, and their interaction, were used to estimate the normalized effects of retinal injection of AM251 and AM630 on retinal function. Significant effects were followed up, when appropriate, with pairwise comparisons - significant values indicated with stars in the relevant figures.

Results

Retinal function in photopic conditions

Retinal function was evaluated using electroretinography in light-adapted conditions following injection of the vehicle DMSO, the CB1R antagonist AM251, or the CB2R antagonist AM630 (Figure 2).

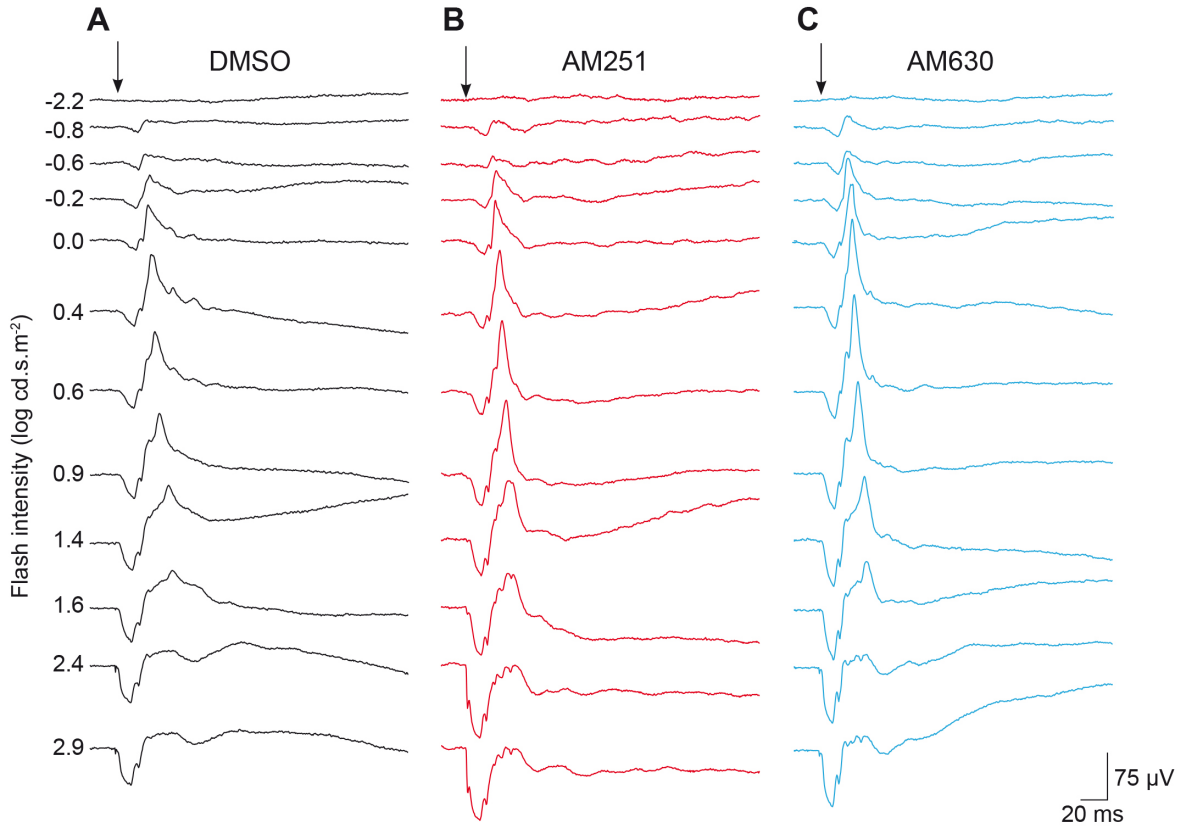

Figure 2. Raw photopic ERGs in the different drug injection groups. Representative ERGs recorded after intravitreal injection of DMSO (black, left column), AM251 (red, middle column) or AM630 (blue, right column). ERG recordings of each treated animal were established by presenting progressively brighter flashes (top to bottom) indicated to the left of the traces as the flash intensity (log cd.s.m^{-2}). Horizontal calibration, 20 ms; vertical calibration, 75 µV.

Photopic b-wave

Our results show that the amplitudes of the b-wave after injection maintained a normal photopic hill shape indicating that the functional integrity of the retina was not impaired (Figure 3A). GEE analysis revealed a significant main effect of flash intensity ($p<.001$), and a significant interaction between the flash intensity and injection group ($p=.001$). The interaction was followed up with pairwise comparisons. AM251 was not significantly different from DMSO at any of the flash intensities (Figure 3B). In contrast, AM630 caused a significant increase in amplitude, relative to the control injection, across several flash intensities, from 0.6 to 1.6 log cd.s.m^{-2} (0.6: 55% increase in amplitude relative to the control, $p=.041$; 0.9: 53% increase, $p=.038$; 1.4: 63% increase, $p=.003$; 1.6: 60% increase, $p=.011$; significant effects indicated with * in Figure 3C). The main effect of AM251 is, on average, a 6% increase, which is not significantly different from the vehicle alone, represented by zero on the y-axis of Figures 3B-D ($p=.713$). Also, the main effect of AM630, averaged across all flash intensities, is a non significant, but trending, 34% increase in responsiveness of the retina compared to the vehicle alone ($p=.067$, Figure 3D). Latencies were also analyzed with the same GEE model and the interaction ($p<.05$) was followed up as above. Pairwise comparisons revealed no significant differences, between the drugs and the vehicle, at any of the flash intensities (not shown).

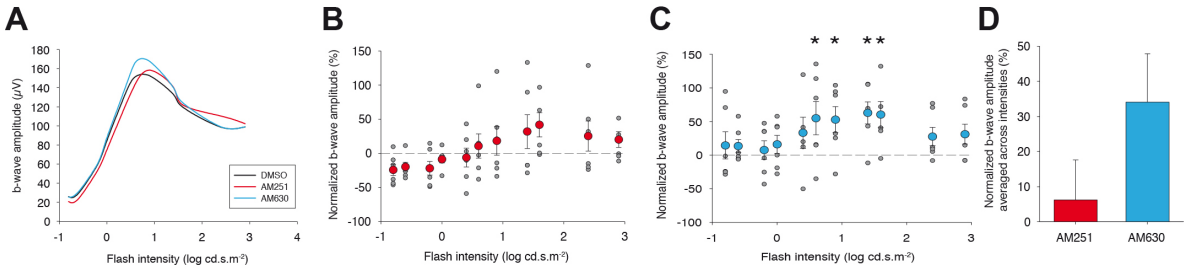

Figure 3. Photopic b-wave amplitudes. (**A**) Amplitudes of photopic ERG b-waves plotted as a

function of flash intensities. (**B**) Scatter plot for normalized b-wave amplitude as a function of flash intensity in AM251-injected monkeys. Grey points indicate raw values, red data points with error bars indicate the mean and standard error of the mean. (**C**) Scatter plot and linear regression for normalized b-wave amplitude as a function of flash intensity in AM630-injected monkeys. Grey points indicate raw values, blue data points with error bars indicate the mean and standard error of the mean. (**D**) Main effect of average amplitudes across intensities in AM251 (red) or AM630 (blue) groups. *p<.05.

Photopic a-wave

Our results show that post-injection, the amplitude of the a-wave followed the normal curve (Figure 4A). The effect of the drugs was, however, quite different from the vehicle. GEE analysis revealed a significant main effect of flash intensity (p<.001), and a significant interaction between the flash intensity and drug group (p<.001). This interaction indicates that the effect of the drugs was not the same across all flash intensities. The interaction was followed up with pairwise comparisons. AM251 caused a significantly higher amplitude than DMSO at the highest flash intensities of 2.4 and 2.9 log cd.s.m^{-2} (2.4: 36% increase in amplitude relative to the vehicle, p=.040; 2.9: 32% increase, p=.038; significant effects indicated with * in Figure 4B). For its part, AM630 caused a significant increase in amplitude, relative to the control injection, across a larger set of flash intensities, from 0.9 to 2.9 log cd.s.m^{-2} (0.9: 30% increase, p<.001; 1.4: 38% increase, p=.002; 1.6: 32% increase, p=.001; 2.4: 39% increase, p=.015; 2.9: 35% increase, p=.006), significant effects indicated with * in Figure 4C). AM251 caused an increase in the a-wave amplitude only at the highest flash intensities, while AM630 increases the a-wave amplitude across a wider set of flash

intensities. The main effect of AM251 is, on average, a 12% increase, which is not significant relative to the vehicle alone (p=.428). Conversely, the main effect of AM630, averaged across all flash intensities, is a non-significant but trending 26% increase in the responsiveness of the retina compared to the vehicle alone (p=.080, Figure 4D). Latencies were also analyzed with the same GEE model and the interaction (p<.05) was followed up as above. Pairwise comparisons at each intensity value revealed no significant differences between the drugs and the vehicle (not shown).

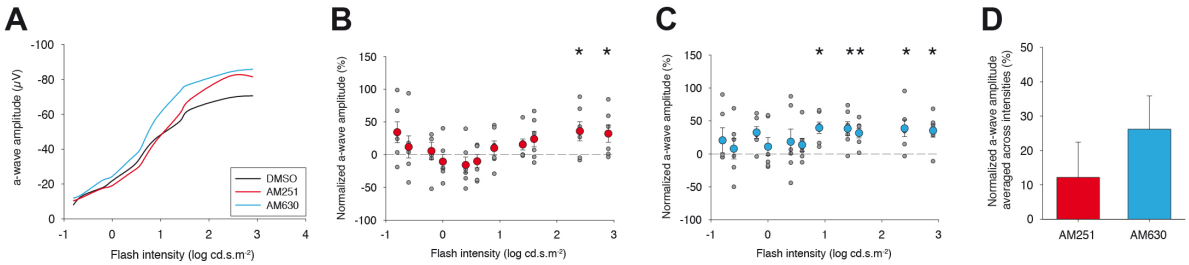

Figure 4. Photopic a-wave amplitudes. (**A**) Amplitudes of photopic ERG a-waves plotted as a function of flash intensities. (**B**) Scatter plot for normalized a-wave amplitude as a function of flash intensity in AM251-injected monkeys. Grey points indicate raw values, red data points with error bars indicate the mean and standard error of the mean. (**C**) Scatter plot and linear regression for normalized a-wave amplitude as a function of flash intensity in AM630-injected monkeys. Grey points indicate raw values, blue data points with error bars indicate the mean and standard error of the mean. (**D**) Main effect of average amplitudes across intensities in AM251 (red) or AM630 (blue) groups. *p<.05.

Retinal function in scotopic condition

To assess the effect of the cannabinoid receptors blockers in scotopic conditions, ERGs responses of the dark-adapted retina were also registered after administration of DMSO,

AM251 or AM630. The ERG tracings maintained their normal shape following injection. However, the amplitudes of the b-wave were increased for both treatment groups, while the drugs did not reliably alter the pattern of the a-waves (Figure 5).

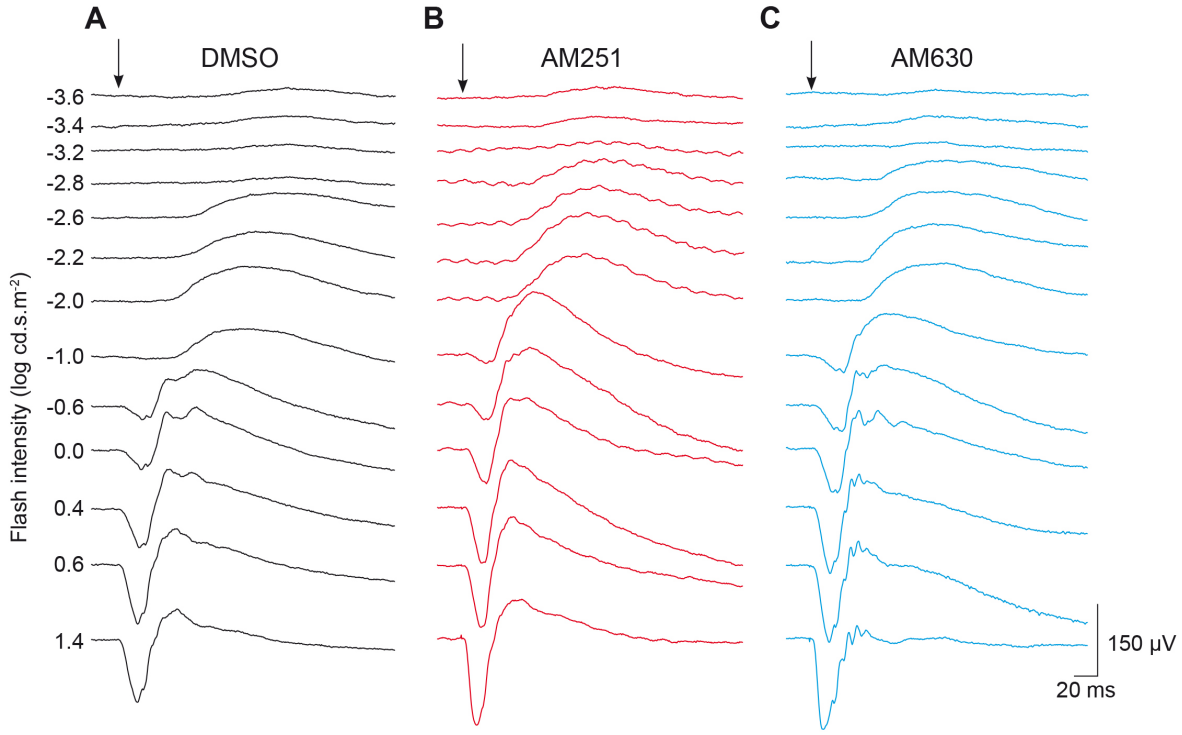

Figure 5. Raw scotopic ERGs in the different drug injection groups. Representative ERGs recorded after intravitreal injection of DMSO (left column), AM251 (middle column) or AM630 (right column). ERG recordings of each treated animal were established by presenting progressively brighter flashes (top to bottom) indicated to the left of the traces as the flash intensity (log cd.s.m^{-2}). Horizontal calibration, 20 ms; vertical calibration, 75 µV.

Scotopic b-wave

Post-injection, the amplitude of the scotopic b-waves had the normal shape: increasing amplitudes for increasing flash intensities (Figure 6A). The effect of the drugs were, however,

quite different from the vehicle. GEE analysis revealed a significant main effect of injection group ($p<.001$). There was no main effect of flash intensity ($p=.842$) nor was there an interaction of group with flash intensity ($p=.953$). Due to a lack of interaction, pairwise comparisons at each flash intensity were not justified, but mean and standard errors are plotted in Figure 6B (AM251) and Figure 6C (AM630). Following up on the main effect of drug, pairwise comparisons between groups revealed significantly higher amplitudes following the injection of AM251 compared to the vehicle alone (20% increase, $p<.001$) and a similar increase in amplitude following injection of AM630 (18% increase, $p=.002$), (Figure 6D). The difference between these two drugs was not significant ($p=.596$). Latencies had the same pattern of effect as the amplitudes. That is, a main effect of drug: both pharmacological agents led to a significant increase in the latency relative to the vehicle (AM251: 8%, $p=.036$; AM630: 12%, $p=.001$). No interactions were present (not shown).

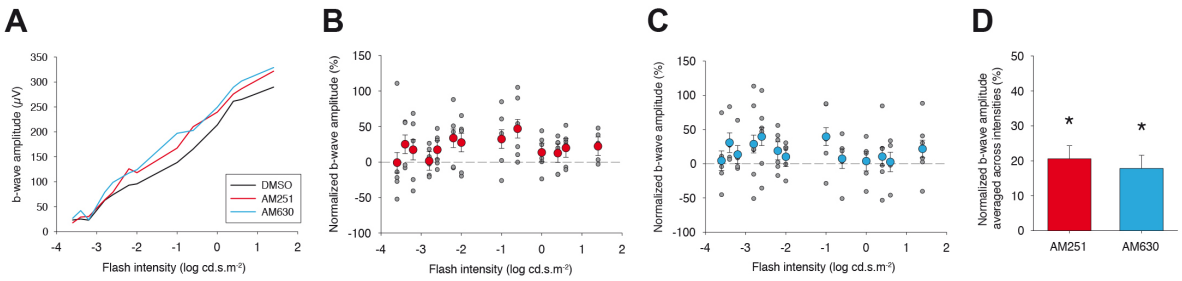

Figure 6. Scotopic b-wave amplitudes. (**A**) Amplitudes of scotopic ERG b-waves plotted as a function of flash intensities. (**B**) Scatter plot for normalized b-wave amplitude as a function of flash intensity in AM251-injected monkeys. Grey points indicate raw values, red data points with error bars indicate the mean and standard error of the mean. (**C**) Scatter plot and linear regression for normalized b-wave amplitude as a function of flash intensity in AM630-injected monkeys. Grey points indicate raw values, blue data points with error bars indicate the mean and standard error of the mean. (**D**) Main effect of average amplitudes across

intensities in AM251 (red) or AM630 (blue) groups. *p<.05.

Scotopic a-wave

Post-injection, the amplitude of the scotopic a-wave had the normal shape: increasing amplitudes for increasing flash intensities, beginning at -1 log cd.s.m^{-2} (Figure 7A.) Therefore, the statistical analysis for the scotopic a-wave only involved the values obtained from the flashes at -1 to 1.4 log cd.s.m^{-2}. GEE analysis revealed a significant main effect of flash intensity (p=.001), and a significant interaction between the intensity of the flash and the drug injected (p<.001). The interaction was followed up with pairwise comparisons, between the drugs and the vehicle alone, at each flash intensity value. This revealed no significant differences, between the drugs and the vehicle, at any of the intensities (Figure 7B and Figure 7C). Thus, while the two agonists cause varied effects at the different flash intensities, the effects of each drug relative to the vehicle alone, at a given flash intensity, were not reliable enough to be significant. The overall effect of AM251 and AM630, averaged across the flash intensities, was not significantly different from the vehicle alone (Figure 7D). Latencies were also analyzed with the same GEE model and the interaction (p<.05) was followed up as above. Pairwise comparisons revealed one significant difference at flash intensity 0.6, following injection of AM251, the latency to peak was 21% slower compared to the injection of the vehicle alone (p=.011, not shown).

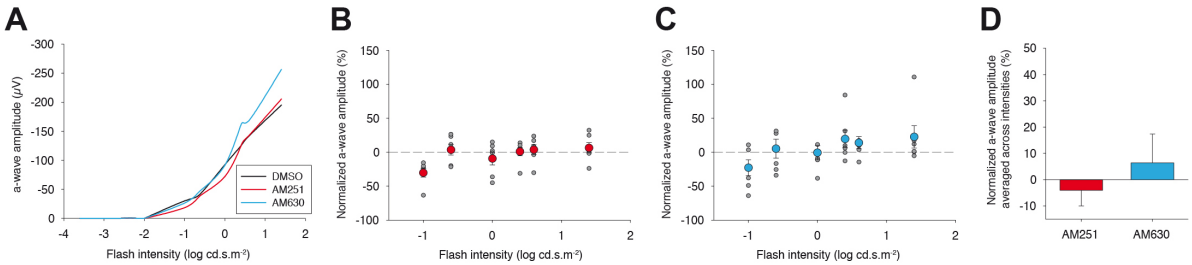

Figure 7. Scotopic a-wave amplitudes. (**A**) Amplitudes of scotopic ERG a-waves plotted as a function of flash intensities. (**B**) Scatter plot for normalized a-wave amplitude as a function of flash intensity in AM251-injected monkeys. Grey points indicate raw values, red data points with error bars indicate the mean and standard error of the mean. (**C**) Scatter plot for normalized a-wave amplitude as a function of flash intensity in AM630-injected monkeys. Grey points indicate raw values, blue data points with error bars indicate the mean and standard error of the mean. (**D**) Main effect of average amplitudes across intensities in AM251 (red) or AM630 (blue) groups. Error bars represent standard error or the mean. *$p<.05$.

Discussion

The purpose of this study was to determine the role of endocannabinoid receptors CB1 and CB2 in the normal monkey retina. The abundance of CB1R and CB2R expression in the retina already pointed to an important role of these receptors in normal vision. We analyzed changes in photopic and scotopic ERG responses after blocking these receptors with their respective antagonists. The experimental design used DMSO as the control, rather than pre-injection values, to control for any effects of the vehicle. We demonstrated that in photopic conditions, only the blockade of CB2R increased the amplitude of the b-wave, above the standard flash intensity value, while blocking CB1R or CB2R increased the amplitude of the a-wave, at high flash intensity values. In scotopic conditions, however, blockade of either CB1R or CB2R increased only the amplitude of the b-wave irrespective of flash intensity.

Photopic condition

The amplitude of the main component of the ERG, the photopic b-wave, represents primarily the activation of depolarization ON-bipolar cells measured as a positive retinal potential on the corneal surface [36, 48-50]. In addition, the b-wave is attributed to the interaction of ON-bipolar cells and Müller glial cells [36, 37]. In the vervet monkey, CB1R is expressed mainly in cones and in the other retinal components, while CB2R is exclusively present in the glial Müller cells, leading to a complementary relationship between neurons and glia regarding endocannabinoid action [6]. The light-induced potassium increase in the outer and inner plexiform layers' cells, which are depolarized by light stimulation, modifies the Müller cell membrane potential thereby generating electrical responses [51]. Müller cells, via KCNJ10 (Kir4.1) channels and potassium siphoning of the excess potassium ions into the

vitreous [52, 53], control the light-mediated potassium increase in retinal extracellular space [54]. The depolarization of the Müller cells contributes to the ERG b-wave through the buffering of potassium channels [35, 55, 56]. Thus, the blockade of these channels should result in a decrease of the ERG b-wave [37]. Our results revealed indeed a significant increase of the photopic b-wave amplitude following the blockade of CB2R, which supports our previously proposed model whereby CB2R in Müller cells activates the potassium channel via $K_{IR}4.1$ [6]. CB2R coupled to $G_{i/o}$ decreases cAMP levels and the PKA activity [57]. PKA is a positive modulator of potassium channels and therefore, the activation of CB2R via a decrease of PKA activity will increase the activity of $K_{IR}4.1$ channels in Müller cells (Figure 8). It may also be possible that AM630 affected the OFF cone pathway, that originates from the dendritic contacts of bipolar cells with cones, which could partially explain the increase of the photopic b-wave amplitude only at the middle intensity flash values [58]. Another potential interpretation is that since CB2R is not expressed on cones [6], AM630 may have modulated other non-CB2 receptors located on cone photoreceptors.

The a-wave measured under photopic conditions represents cone function. Stimulation of cones by light inhibits retinal dark currents through phototransduction signals that take place in the cone outer segments as seen in the a-wave of the ERG. The early portion of the a-wave represents the activity of the cone photoreceptors [59, 60], while the later portion reflects the contribution of hyperpolarizing bipolar cells, proximal amacrine cells, and ganglion cells [61-63]. Stimulation of cones may activate the CB1R in its pedicles [5], which in turn leads to the inhibition of glutamate release in the synaptic cleft. Blocking CB1R will therefore result in the increase in glutamate release. This increase mimics the effect of a bright light that

contributes to larger amplitude of the photopic a-wave. Blocking CB2R on the other hand, has an even larger effect on the amplitude of the a-wave, which can be explained by a similar mechanism that involves additional potassium buffering by Müller cells [6] (Figure 8A). Other receptors that contribute to the photopic b-wave may also explain how AM630 could affect the photopic a-wave. Indeed, the increase of the photopic b-wave might cause a large change in the a-wave (a result of cone modulation), which would be independent of the action of Müller cells.

Scotopic condition

The a-wave measured under scotopic conditions represents rod function. In the dark-adapted retina, blockade of either CB1R or CB2R had no significant affect on the scotopic a-wave. This null effect can be explained by the small quantity of CB1R expressed in the rod spherules in primates [3, 5]. In contrast, the large quantity of putative cannabinoid receptor (GPR55), found exclusively in rods [64], has a significant effect on the scotopic ERG [65]. It has been reported that AM251 could be also a GPR55 agonist [66]. Thus, we cannot rule out that the increase of the scotopic b-wave amplitude following the injection of AM251 might be due to GPR55 activity. However, CB1R is found in large quantities in rod bipolar cells [5], and in conjunction with CB2R in Müller cells [6], likely contributes to the large increase of the scotopic b-wave amplitude. Differential effects between CB1R and CB2R might be explained by the nature of the ions channels involved. The potassium-buffering role of Müller cells leads to the increase of the scotopic b-wave following CB2R blockade. The calcium increase in post-synaptic rod bipolar cells results from CB1R blockade (see Figure 8B). Since CB1R agonists induce a reduction in the amplitude of calcium channel currents in retinal

bipolar cells [3], it is not surprising, as shown here, that the CB1R antagonist AM251 had the opposite effect: mainly, an increase in rod bipolar cells activity.

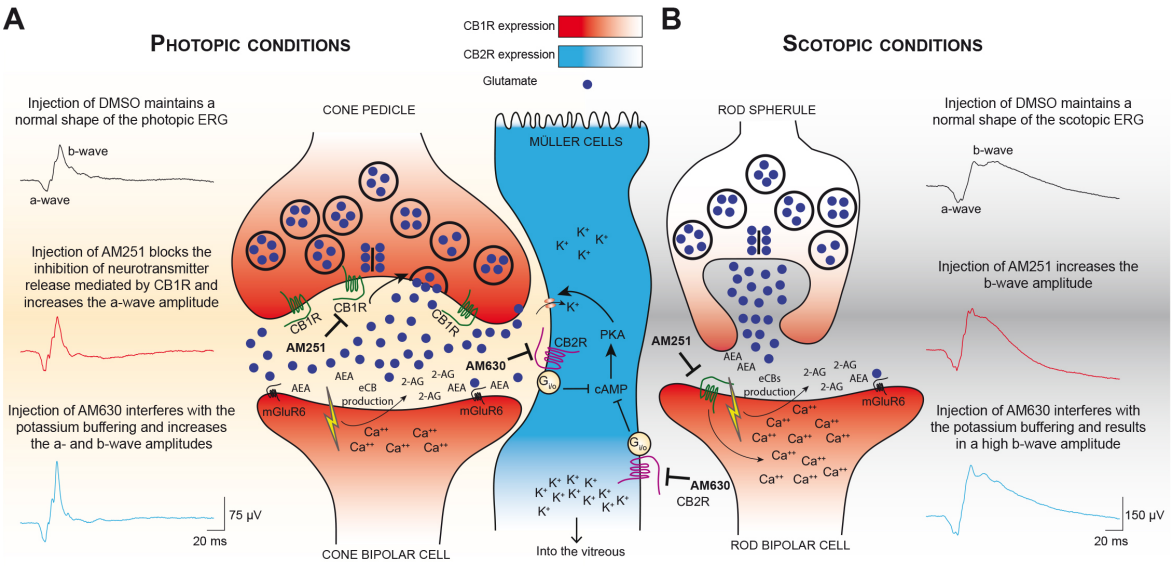

Figure 8. Schematic illustration of the proposed mechanisms underlying the actions of AM251 and AM630 in the monkey retina, as revealed by electroretinography under photopic (**A**) and scotopic (**B**) conditions. (See Discussion for details).

Conclusion

These findings might be helpful for the development of new pharmacological targets for the treatment of retinal intoxications [67, 68] and diseases [69]. These retinal pathologies are generally associated with a decrease in the amplitude of the electroretinographic waves. We show here that pharmacological agents that block the retinal cannabinoid receptors can induce an increase in the amplitude of the ERG response profiles. Manipulating the endocannabinoid system might therefore serve as a therapy to restore normal vision and protect the retina.

References

1. B. Cécyre, N. Zabouri, F. Huppé-Gourgues, J. F. Bouchard and C. Casanova, "Roles of cannabinoid receptors type 1 and 2 on the retinal function of adult mice," *Invest Ophthalmol Vis Sci*, vol. 54, no. 13, pp. 8079-8090, 2013.

2. E. M. López, P. Tagliaferro, E. S. Onaivi and J. J. López-Costa, "Distribution of CB2 cannabinoid receptor in adult rat retina," *Synapse*, vol. 65, no. 5, pp. 388-392, 2011.

3. A. Straiker, N. Stella, D. Piomelli, K. Mackie, H. J. Karten and G. Maguire, "Cannabinoid CB1 receptors and ligands in vertebrate retina: localization and function of an endogenous signaling system," *Proc Natl Acad Sci U S A*, vol. 96, no. 25, pp. 14565-14570, 1999.

4. S. Yazulla, K. M. Studholme, H. H. McIntosh and D. G. Deutsch, "Immunocytochemical localization of cannabinoid CB1 receptor and fatty acid amide hydrolase in rat retina," *J Comp Neurol*, vol. 415, no. 1, pp. 80-90, 1999.

5. J. Bouskila, M. W. Burke, N. Zabouri, C. Casanova, M. Ptito and J. F. Bouchard, "Expression and localization of the cannabinoid receptor type 1 and the enzyme fatty acid amide hydrolase in the retina of vervet monkeys," *Neuroscience*, vol. 202, pp. 117-130, 2012.

6. J. Bouskila, P. Javadi, C. Casanova, M. Ptito and J. F. Bouchard, "Müller cells express the cannabinoid CB2 receptor in the vervet monkey retina," *J Comp Neurol*, vol. 521, no. 11, pp. 2399-2415, 2013.

7. N. Zabouri, J. F. Bouchard and C. Casanova, "Cannabinoid receptor type 1 expression during postnatal development of the rat retina," *J Comp Neurol*, vol. 519, no. 7, pp. 1258-1280, 2011.

8. P. Javadi, J. Bouskila, J. F. Bouchard and M. Ptito, "The endocannabinoid system within the dorsal lateral geniculate nucleus of the vervet monkey," *Neuroscience*, vol. 288, pp. 135-144, 2015.

9. S. M. Eggan and D. A. Lewis, "Immunocytochemical distribution of the cannabinoid CB1 receptor in the primate neocortex: a regional and laminar analysis," *Cereb Cortex*, vol. 17, no. 1, pp. 175-191, 2007.

10. T. Schwitzer, R. Schwan, K. Angioi-Duprez, I. Ingster-Moati, L. Lalanne, A. Giersch and V. Laprevote, "The cannabinoid system and visual processing: a review on experimental findings and clinical presumptions," *Eur Neuropsychopharmacol*, vol. 25, no. 1, pp. 100-112, 2015.

11. M. C. Flom, A. J. Adams and R. T. Jones, "Marijuana smoking and reduced pressure in human eyes: drug action or epiphenomenon?," *Invest Ophthalmol*, vol. 14, no. 1, pp. 52-55, 1975.

12. K. Green, "The ocular effects of cannabinoids," *Curr Top Eye Res*, vol. 1, pp. 175-215, 1979.

13. A. Porcella, P. Casellas, G. L. Gessa and L. Pani, "Cannabinoid receptor CB1 mRNA is highly expressed in the rat ciliary body: implications for the antiglaucoma properties of marihuana," *Molecular Brain Research*, vol. 58, no. 1-2, pp. 240-245, 1998.

14. V. Laprevote, T. Schwitzer, A. Giersch and R. Schwan, "Flash electroretinogram and addictive disorders," *Prog Neuropsychopharmacol Biol Psychiatry*, vol. 56, pp. 264, 2015.

15. A. J. Adams, B. Brown, G. Haegerstrom-Portnoy, M. C. Flom and R. T. Jones, "Marijuana, alcohol, and combined drug effects on the time course of glare recovery," *Psychopharmacology (Berl)*, vol. 56, no. 1, pp. 81-86, 1978.

16. A. J. Adams, B. Brown, M. C. Flom, R. T. Jones and A. Jampolsky, "Alcohol and marijuana effects on static visual acuity," *Am J Optom Physiol Opt*, vol. 52, no. 11, pp. 729-735, 1975.

17. G. F. Kiplinger, J. E. Manno, B. E. Rodda and R. B. Forney, "Dose-response analysis of the effects of tetrahydrocannabinol in man," *Clin Pharmacol Ther*, vol. 12, no. 4, pp. 650-657, 1971.

18. A. Merzouki and J. M. Mesa, "Concerning kif, a Cannabis sativa L. preparation smoked in the Rif mountains of northern Morocco," *J Ethnopharmacol*, vol. 81, no. 3, pp. 403-406, 2002.

19. E. B. Russo, A. Merzouki, J. M. Mesa, K. A. Frey and P. J. Bach, "Cannabis improves night vision: a case study of dark adaptometry and scotopic sensitivity in kif smokers of the Rif mountains of northern Morocco," *J Ethnopharmacol*, vol. 93, no. 1, pp. 99-104, 2004.

20. R. Noyes, Jr., S. F. Brunk, D. A. Avery and A. C. Canter, "The analgesic properties of delta-9-tetrahydrocannabinol and codeine," *Clin Pharmacol Ther*, vol. 18, no. 1, pp. 84-89, 1975.

21. W. W. Dawson, C. F. Jimenez-Antillon, J. M. Perez and J. A. Zeskind, "Marijuana and vision--after ten years' use in Costa Rica," *Invest Ophthalmol Vis Sci*, vol. 16, no. 8, pp. 689-699, 1977.

22. S. Yazulla, "Endocannabinoids in the retina: from marijuana to neuroprotection," *Prog Retin Eye Res*, vol. 27, no. 5, pp. 501-526, 2008.

23. A. M. Gawienowski, D. Chatterjee, P. J. Anderson, D. L. Epstein and W. M. Grant, "Effect of delta 9-tetrahydrocannabinol on monoamine oxidase activity in bovine eye tissues, in vitro," *Invest Ophthalmol Vis Sci*, vol. 22, no. 4, pp. 482-485, 1982.

24. E. Schlicker, J. Timm and M. Gothert, "Cannabinoid receptor-mediated inhibition of dopamine release in the retina," *Naunyn Schmiedebergs Arch Pharmacol*, vol. 354, no. 6, pp. 791-795, 1996.

25. S. F. Fan and S. Yazulla, "Suppression of voltage-dependent K+ currents in retinal bipolar cells by ascorbate," *Vis Neurosci*, vol. 16, no. 1, pp. 141-148, 1999.

26. S. F. Fan and S. Yazulla, "Biphasic modulation of voltage-dependent currents of retinal cones by cannabinoid CB1 receptor agonist WIN 55212-2," *Vis Neurosci*, vol. 20, no. 2, pp. 177-188, 2003.

27. A. Straiker and J. M. Sullivan, "Cannabinoid receptor activation differentially modulates ion channels in photoreceptors of the tiger salamander," *J Neurophysiol*, vol. 89, no. 5, pp. 2647-2654, 2003.

28. S. Yazulla, K. M. Studholme, H. H. McIntosh and S. F. Fan, "Cannabinoid receptors on goldfish retinal bipolar cells: electron-microscope immunocytochemistry and whole-cell recordings," *Vis Neurosci*, vol. 17, no. 3, pp. 391-401, 2000.

29. M. L. Struik, S. Yazulla and M. Kamermans, "Cannabinoid agonist WIN 55212-2 speeds up the cone response to light offset in goldfish retina," *Vis Neurosci*, vol. 23, no. 2, pp. 285-293, 2006.

30. L. J. Frishman, "Chapter 7 - Electrogenesis of the Electroretinogram," in *Retina (Fifth Edition)*, S. J. Ryan, A. P. Schachat, C. P. Wilkinson, D. R. Hinton, S. R. Sadda and P. Wiedemann, Ed., pp. 177-201, W.B. Saunders, London, 2013.

31. L. J. Frishman, "Chapter 12 - Origins of the Electroretinogram," in *Principles and Practice of Clinical Electrophysiology of Vision (2nd Edition)*, J. R. Heckenlively and G. B. Arden, Ed., pp. 139-183, MIT Press, 2006.

32. L. J. Frishman and M. H. Wang, "Chapter 24 - Electroretinogram of Human, Monkey and Mouse," in *Adler's Physiology of the Eye (11th Edition)*, L. A. Levin, S. F. E. Nilsson, J. V. Hoeve, S. Wu, P. L. Kaufman and A. Alm, Ed., pp. 480-501, Elsevier Health Sciences, 2011.

33. J. C. Armington, E. P. Johnson and L. A. Riggs, "The scotopic A-wave in the electrical response of the human retina," *J Physiol*, vol. 118, no. 3, pp. 289-298, 1952.

34. J. G. Robson and L. J. Frishman, "The rod-driven a-wave of the dark-adapted mammalian electroretinogram," *Prog Retin Eye Res*, vol. 39, pp. 1-22, 2014.

35. R. F. Miller and J. E. Dowling, "Intracellular responses of the Müller (glial) cells of mudpuppy retina: their relation to b-wave of the electroretinogram," *J Neurophysiol*, vol. 33, no. 3, pp. 323-341, 1970.

36. R. A. Stockton and M. M. Slaughter, "B-wave of the electroretinogram. A reflection of ON bipolar cell activity," *J Gen Physiol*, vol. 93, no. 1, pp. 101-122, 1989.

37. R. Wen and B. Oakley, 2nd, "K(+)-evoked Müller cell depolarization generates b-wave of electroretinogram in toad retina," *Proc Natl Acad Sci U S A*, vol. 87, no. 6, pp. 2117-2121, 1990.

38. J. G. Robson and L. J. Frishman, "Response linearity and kinetics of the cat retina: the bipolar cell component of the dark-adapted electroretinogram," *Vis Neurosci*, vol. 12, no. 5, pp. 837-850, 1995.

39. R. Hamilton, M. A. Bees, C. A. Chaplin and D. L. McCulloch, "The luminance-response function of the human photopic electroretinogram: a mathematical model," *Vision Res*, vol. 47, no. 23, pp. 2968-2972, 2007.

40. A. J. Jasinska, C. A. Schmitt, S. K. Service, R. M. Cantor, K. Dewar, J. D. Jentsch, J. R. Kaplan, T. R. Turner, W. C. Warren, G. M. Weinstock, R. P. Woods and N. B. Freimer, "Systems biology of the vervet monkey," *ILAR J*, vol. 54, no. 2, pp. 122-143, 2013.

41. D. Boire, H. Theoret and M. Ptito, "Visual pathways following cerebral hemispherectomy," *Prog Brain Res*, vol. 134, pp. 379-397, 2001.

42. M. Herbin, D. Boire and M. Ptito, "Size and distribution of retinal ganglion cells in the St. Kitts green monkey (Cercopithecus aethiops sabeus)," *J Comp Neurol*, vol. 383, no. 4, pp. 459-472, 1997.

43. J. Bouskila, P. Javadi, R. M. Palmour, J. F. Bouchard and M. Ptito, "Standardized full-field electroretinography in the Green Monkey (Chlorocebus sabaeus)," *PLoS One*, vol. 9, no. 10, pp. e111569, 2014.

44. W. H. Bee, "Standardized electroretinography in primates: a non-invasive preclinical tool for predicting ocular side effects in humans," *Curr Opin Drug Discov Devel*, vol. 4, no. 1, pp. 81-91, 2001.

45. D. L. McCulloch, M. F. Marmor, M. G. Brigell, R. Hamilton, G. E. Holder, R. Tzekov and M. Bach, "ISCEV Standard for full-field clinical electroretinography (2015 update)," *Doc Ophthalmol*, vol. 130, no. 1, pp. 1-12, 2015.

46. G. Nair, M. Kim, T. Nagaoka, D. E. Olson, P. M. Thule, M. T. Pardue and T. Q. Duong, "Effects of common anesthetics on eye movement and electroretinogram," *Doc Ophthalmol*, vol. 122, no. 3, pp. 163-176, 2011.

47. Y. Rotenstreich, G. A. Fishman, R. J. Anderson and D. G. Birch, "Interocular amplitude differences of the full field electroretinogram in normal subjects," *Br J Ophthalmol*, vol. 87, no. 10, pp. 1268-1271, 2003.

48. A. G. Knapp and P. H. Schiller, "The Contribution of on-Bipolar Cells to the Electroretinogram of Rabbits and Monkeys - a Study Using 2-Amino-4-Phosphonobutyrate (Apb)," *Vision Res*, vol. 24, no. 12, pp. 1841-1846, 1984.

49. P. A. Sieving, K. Murayama and F. Naarendorp, "Push-pull model of the primate photopic electroretinogram: a role for hyperpolarizing neurons in shaping the b-wave," *Vis Neurosci*, vol. 11, no. 3, pp. 519-532, 1994.

50. N. Tian and M. M. Slaughter, "Correlation of dynamic responses in the ON bipolar neuron and the b-wave of the electroretinogram," *Vision Res*, vol. 35, no. 10, pp. 1359-1364, 1995.

51. E. Dick, R. F. Miller and S. Bloomfield, "Extracellular K+ activity changes related to electroretinogram components. II. Rabbit (E-type) retinas," *J Gen Physiol*, vol. 85, no. 6, pp. 911-931, 1985.

52. E. A. Newman, D. A. Frambach and L. L. Odette, "Control of extracellular potassium levels by retinal glial cell K+ siphoning," *Science*, vol. 225, no. 4667, pp. 1174-1175, 1984.

53. P. Kofuji, P. Ceelen, K. R. Zahs, L. W. Surbeck, H. A. Lester and E. A. Newman, "Genetic inactivation of an inwardly rectifying potassium channel (Kir4.1 subunit) in mice: phenotypic impact in retina," *J Neurosci*, vol. 20, no. 15, pp. 5733-5740, 2000.

54. E. Newman and A. Reichenbach, "The Müller cell: a functional element of the retina," *Trends Neurosci*, vol. 19, no. 8, pp. 307-312, 1996.

55. E. A. Newman, "Distribution of potassium conductance in mammalian Muller (glial) cells: a comparative study," *J Neurosci*, vol. 7, no. 8, pp. 2423-2432, 1987.

56. R. H. Steinberg, L. J. Frishman and P. A. Sieving, "Chapter 6 Negative components of the electroretinogram from proximal retina and photoreceptor," *Progress in Retinal Research*, vol. 10, pp. 121-160, 1991.

57. A. C. Howlett, F. Barth, T. I. Bonner, G. Cabral, P. Casellas, W. A. Devane, C. C. Felder, M. Herkenham, K. Mackie, B. R. Martin, R. Mechoulam and R. G. Pertwee, "International Union of Pharmacology. XXVII. Classification of cannabinoid receptors," *Pharmacol Rev*, vol. 54, no. 2, pp. 161-202, 2002.

58. S. Ueno, M. Kondo, Y. Niwa, H. Terasaki and Y. Miyake, "Luminance dependence of neural components that underlies the primate photopic electroretinogram," *Invest Ophthalmol Vis Sci*, vol. 45, no. 3, pp. 1033-1040, 2004.

59. D. C. Hood and D. G. Birch, "Human cone receptor activity: the leading edge of the a-wave and models of receptor activity," *Vis Neurosci*, vol. 10, no. 5, pp. 857-871, 1993.

60. D. C. Hood and D. G. Birch, "Assessing abnormal rod photoreceptor activity with the a-wave of the electroretinogram: applications and methods," *Doc Ophthalmol*, vol. 92, no. 4, pp. 253-267, 1996.

61. R. A. Bush and P. A. Sieving, "A proximal retinal component in the primate photopic ERG a-wave," *Invest Ophthalmol Vis Sci*, vol. 35, no. 2, pp. 635-645, 1994.

62. C. Friedburg, C. P. Allen, P. J. Mason and T. D. Lamb, "Contribution of cone photoreceptors and post-receptoral mechanisms to the human photopic electroretinogram," *J Physiol*, vol. 556, no. Pt 3, pp. 819-834, 2004.

63. J. G. Robson, S. M. Saszik, J. Ahmed and L. J. Frishman, "Rod and cone contributions to the a-wave of the electroretinogram of the macaque," *J Physiol*, vol. 547, no. Pt 2, pp. 509-530, 2003.

64. J. Bouskila, P. Javadi, C. Casanova, M. Ptito and J. F. Bouchard, "Rod photoreceptors express GPR55 in the adult vervet monkey retina," *PLoS One*, vol. 8, no. 11, pp. e81080, 2013.

65. M. Ptito, J. Bouskila, P. Javadi, C. Casanova, J.F. Bouchard, "Role of retinal cannabinoid receptors CB1 and CB2, and GPR55 defined by electroretinography in vervet monkeys," *FENS Forum Abstr*. FENS-0297, 2014.

66. R. G. Pertwee, "GPR55: a new member of the cannabinoid receptor clan?," Br J Pharmacol, vol. 152, no. 7, pp. 984-986, 2007.

67. R. Hennekes, "Clinical ERG findings in ethambutol intoxication," *Graefes Arch Clin Exp Ophthalmol*, vol. 218, no. 6, pp. 319-321, 1982.

68. G. Duncker and T. Bredehorn, "Chloroquine-induced lipidosis in the rat retina: functional and morphological changes after withdrawal of the drug," *Graefes Arch Clin Exp Ophthalmol*, vol. 234, no. 6, pp. 378-381, 1996.

69. S. E. Nilsson, "Human retinal vascular obstructions. A quantitative correlation of angiographic and electroretinographic findings," *Acta Ophthalmol (Copenh)*, vol. 49, no. 1, pp. 111-133, 1971.

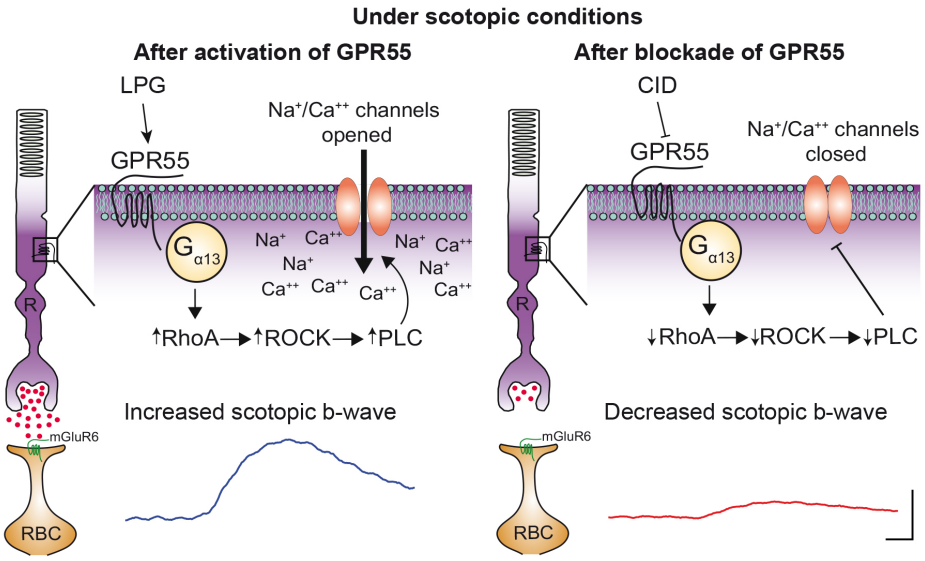

ARTICLE 7: SCOTOPIC VISION IN THE MONKEY IS MODULATED BY THE G PROTEIN-COUPLED RECEPTOR 55

Publié dans :

Bouskila J, Harrar V, Javadi P, Casanova C, Hirabayashi Y, Matsuo I, Ohyama J, Bouchard JF, Ptito M (2015) Scotopic vision in the monkey is modulated by the G protein-coupled receptor 55, *Visual Neuroscience*, In press.

Scotopic vision in the monkey is modulated by the G protein-coupled receptor 55

Running Head: Role of GPR55 in the monkey retinal function

Joseph Bouskila[1, 2], Vanessa Harrar[1], Pasha Javadi[1], Christian Casanova[1], Yoshio Hirabayashi[3], Ichiro Matsuo[4], Jyunpei Ohyama[4], Jean-François Bouchard[1] and Maurice Ptito[1, 5]

[1]School of Optometry, University of Montreal, Montreal, Quebec, Canada
[2]Biomedical Sciences, Faculty of Medicine, University of Montreal, Montreal, Quebec, Canada
[3]Laboratory for Molecular Membrane Neuroscience, RIKEN Brain Science Institute, Wako, Japan
[4]Division of Molecular Science, Gunma University, Maebashi, Japan
[5]Neuropsychiatry Laboratory and BRAINlab, Department of Neuroscience and Pharmacology, University of Copenhagen, Copenhagen, Denmark

Correspondence should be addressed to:
Maurice Ptito and Jean-François Bouchard
School of Optometry, room 260-7
3744 Jean-Brillant,
University of Montreal,
Montreal, Quebec, Canada, H3T 1P1

Number of manuscript pages: **23**

Number of tables: **1**

Number of figures: **5**

Conflict of Interest: The authors declare no competing financial interests.

Keywords: G protein-coupled receptor 55, LPG, CID16020046, retina, electroretinogram, monkey.

Acknowledgements: The Natural Science and Engineering Research Council of Canada (6362-2012, MP; RGPAS 478115-2015 and RGPIN 2015-06582 JFB; 194670-2014, CC) and the Canadian Institutes of Health Research (MOP-130337, CC and JFB) supported this work. JB received support from a Frederick Banting and Charles Best Canada Graduate Scholarship Doctoral Award from CIHR. VH is supported by the Banting Postdoctoral Fellowship from CIHR. JFB is supported by a "Chercheur-Boursier Senior" from the Fonds de recherche du Québec - Santé (FRQ-S). MP is Harland Sanders Chair professor in Visual Science. The authors would like to thank Dr. Amy Beierschmitt and Maurice Matthew, M.Sc. for their expert technical assistance in handling the monkeys. We are very grateful to the late Dr. Frank Ervin, Dr. Roberta Palmour, and the staff of the Behavioural Sciences Foundation Laboratories located in St Kitts, West Indies, for their continued support to our monkey work.

Abstract

The endogenous cannabinoid system plays important roles in the retina of mice and monkeys via their classic CB1 and CB2 receptors (CB1R and CB2R). We have previously reported that the G protein-coupled receptor 55 (GPR55), a putative cannabinoid receptor, is exclusively expressed in rod photoreceptors in the monkey retina, suggesting its possible role in scotopic vision. To test this hypothesis, we recorded full-field electroretinograms (ERGs) after the intravitreal injection of the GPR55 agonist lysophosphatidylglucoside (LPG) or the selective GPR55 antagonist CID16020046 (CID), under light- and dark-adapted conditions. Thirteen vervet monkeys (*Chlorocebus sabaeus*) were used in this study: 4 controls (injected with the vehicle dimethyl sulfoxide, DMSO), 4 injected with LPG and 5 with CID. We analyzed amplitudes and latencies of the a-wave (photoreceptor responses) and the b-wave (rod and cone system responses) of the ERG. Our results showed that after injection of LPG, the amplitude of the scotopic b-wave was significantly higher, whereas after the injection of CID it was significantly decreased, compared to the vehicle (DMSO). On the other hand, the a-wave amplitude, and the a-wave and b-wave latencies, of the scotopic ERG responses were not affected by the injection of either compound. Furthermore, the photopic ERG waveforms were not affected by either drug. These results support the hypothesis that GPR55 plays an instrumental role in mediating scotopic vision.

Introduction

The endocannabinoid system, including endocannabinoids (eCBs), cannabinoid receptors, and enzymes regulating the level of eCBs, is present in the central nervous system of all mammals. In most cases, eCBs act as retrograde messengers binding to the widely distributed CB1R to inhibit the neurotransmitter release at both excitatory and inhibitory synapses (Kreitzer & Regehr, 2001a; Kreitzer & Regehr, 2001b; Ohno-Shosaku et al. 2001; Wilson & Nicoll, 2001; Freund et al., 2003; Yazulla, 2008). In addition to the two main cannabinoid receptors (CB1R and CB2R), GPR55 has been suggested as a cannabinoid receptor since it is activated by anandamide, an endogenous cannabinoid, and tetrahydrocannabinol, an exogenous cannabinoid (Ryberg et al., 2007). In fact, GPR55 is a receptor that is also responsive to other cannabinoids (Oka et al., 2007; Ryberg et al., 2007). While GPR55 is implicated in several physiological and pathophysiological functions (Liu et al., 2014), its role in the retina is as yet unknown. Early case reports in the 1970s suggested the existence of cannabis-mediated visual effects in humans, although the specific mechanisms or activation pathways are still not defined. Cannabis consumption can lead to an increase in glare recovery for low contrast stimuli (Adams et al., 1978), a reduction in Vernier and Snellen acuities (Adams et al., 1975; Kiplinger et al., 1971), blurred vision (Noyes et al., 1975), and changes in color discrimination and photosensitivity (Dawson et al., 1977). Given that most of these effects undoubtedly have a retinal component, recent investigations have focused on examining the endogenous cannabinoid system in the retina.

Cannabinoid receptor expression patterns are well documented in rodent and primate retinas (Straiker et al., 1999a; Straiker et al., 1999b; Yazulla et al., 1999; Lopez et al., 2011; Zabouri et al., 2011; Cécyre et al., 2013), including vervet monkeys (Bouskila et al., 2012; Bouskila et al., 2013a; Bouskila et al., 2013b). The latter species was used as the animal model to study the distribution of cannabinoid receptors in the retina and revealed cell-type specific expression profiles of CB1R, CB2R, and GPR55. While CB1R is present in retinal neurons (Bouskila et al., 2012) and CB2R is strictly expressed in glial Müller cells (Bouskila et al., 2013a), GPR55 is exclusively found in rod photoreceptors (Bouskila et al., 2013b). A variety of anatomical and functional visual effects of cannabinoids have also been reported for every retinal cell types in both rodents and fish (Yazulla, 2008; Cécyre et al., 2013). However, these studies did not investigate GPR55 because of its recent and controversial deorphanization as a

cannabinoid receptor (Henstridge et al., 2009). Despite neuroanatomical and physiological evidence showing that the eCB system can modulate the activity of retinal cells in mammals, very little is known about the specific contribution of GPR55 in retinal functioning. Only one study has reported that palmitoylethanolamide can increase aqueous humor outflow through the trabecular meshwork, which appears to be mediated by GPR55 (Kumar et al., 2012). This finding indirectly suggests that GPR55 plays a role in the eye.

Full-field electroretinography is widely used as a measure of retinal function (McCulloch et al., 2015). Electroretinogram (ERG) recordings represent the sum of electrical current over the entire retina, light-evoked responses in photoreceptors (cones and rods), neurons (horizontal cells, bipolar cells, amacrine cells, and ganglion cells), glial cells (Müller cells), and epithelial cells (Steinberg et al., 1985). Amplitude, latency, and overall shape of the ERG waves depend on the intensity of the flash and its duration, as well as the adaptation state of the retina. While scotopic ERGs represent the contribution of the rod system in dark-adapted conditions, photopic ERGs represent the contribution of the cone system in light-adapted conditions. In the present study, we investigated the effect of the intravitreal injection of lysophosphatidylglucoside (LPG), an agonist of GPR55 (Guy et al., 2015), or CID16020046 (CID), a selective GPR55 antagonist (Kargl et al., 2013), on the dark-adapted and light-adapted full-field ERGs in vervet monkeys. Given that GPR55 is exclusively expressed in rods (Bouskila et al., 2013b), we hypothesized that the modulatory effect of GPR55 would manifest itself only in the ERG curves obtained in scotopic conditions.

Material and methods

Animals. A total of thirteen adult vervet monkeys (*Chlorocebus sabaeus*) were used for this study: four monkeys received an intravitreal injection of DMSO (dimethyl sulfoxide, the vehicle), four monkeys were monocularly injected with LPG (a selective agonist of GPR55), and five monkeys with CID16020046 (a potent and selective antagonist of GPR55) (Table 1). The animals were born and raised in enriched environments in the laboratories of the Behavioural Science Foundation (St-Kitts, West Indies). The animals were fed with primate chow (Harlan Teklad High Protein Monkey Diet; Harlan Teklad, Madison, WI) and fresh local fruits, with water available *ad libitum*. All experiments were performed according to the guidelines of the Canadian Council on Animal Care (CCAC) and the Association for Research in Vision and Ophthalmology (ARVO) Statement for the Use of Animals in Ophthalmic and Vision Research. The experimental protocol was also reviewed and approved by the local Animal Care and Use Committee (University of Montreal, protocol # 14-007) and the Institutional Review Board of the Behavioural Science Foundation. None of the animals were sacrificed for this study.

Table 1. Profile of the animals used in this study.

Monkey ID	Sex	Weight (Kg)	Monocular Injection	Concentration
1	Female	2.925	DMSO	100%
2	Female	2.875	DMSO	100%
3	Female	2.850	DMSO	100%
4	Male	3.555	DMSO	100%
5	Female	2.525	LPG	1 mg in 100% DMSO
6	Female	2.800	LPG	1 mg in 100% DMSO
7	Male	3.225	LPG	1 mg in 100% DMSO
8	Male	2.950	LPG	1 mg in 100% DMSO
9	Male	3.950	CID	1 mg in 100% DMSO
10	Female	2.825	CID	1 mg in 100% DMSO
11	Female	2.900	CID	1 mg in 100% DMSO
12	Female	3.050	CID	1 mg in 100% DMSO
13	Female	2.925	CID	1 mg in 100% DMSO

Animal preparation for ERG recording. The method for ERG recordings in the vervet monkey has been previously described (Bouskila et al., 2014) and is briefly reported here. The

animals were sedated with an intramuscular injection of a mixture of ketamine (10 mg/kg; Troy Laboratories, Glendenning, New South Wales, Australia) and xylazine (1 mg/kg; Lloyd Laboratories, Shenandoah, IA). This mixture has a minimal effect on the ERG (Nair et al. 2011). The depth of sedation was maintained at a sufficient level to prevent the animals from moving, but without causing respiratory depression. In this condition, the pupils were fully dilated to approximately 9 mm in diameter and the accommodation reflex was paralyzed with topical application of 1% tropicamide (Mydriacyl®) and 2.5% phenylephrine hydrochloride (Mydfrin®) (Alcon Laboratories, Fort Worth, TX). Intraocular pressure was monitored before and after the recording session by applanation tonometry (TonoPen XL®, Reichert Technologies, Depew, NY). The eyes were treated with 0.5% proparacaine hydrochloride (Alcaine®; Alcon Laboratories, Fort Worth, TX) to anesthetize the cornea. The eyes were then protected by application of 2.5% methylcellulose (Gonak; Akorn, Inc., Buffalo Grove, IL) to prevent corneal drying. Body temperature was maintained between 36.5°C and 38°C with a heating pad. Recording sessions lasted approximately two hours for each animal, after which they were allowed to recover in their cage, and then returned to their prior naturalistic setting.

Drug administration. Intravitreal injections were performed in one eye only when the animals were in a sedated state. After inspection and examination of the eyes and lids, a topical anesthetic was applied over the injection site. The conjunctival and corneal surfaces were then moistened with methylcellulose (Moisture Eyes, Bausch Lomb, Rochester, NY) for 3 minutes. The eye was covered with sterile coatings and a Barraquer eye speculum (1.75 inches, 10 mm wide small blades; Storz Ophthalmics, St Louis, MO) held the eyes open. The LPG was synthetized using the method described by Guy et al. (2015), where its specificity and selectivity were successfully tested on the spinal cord of mice and chicken. The antagonist CID was purchased from Tocris Bioscience (Cat. No. 4959, Ellisville, MO). With a 30G needle, 50 µL of drug solution (LPG or CID) were injected into the vitreous cavity, 2 mm posterior to the corneal limbus. A similar volume (50 µL) of the vehicle DMSO was injected into the vitreous of one eye in 4 control animals in order to rule out the possibilities that the injection *per se* and/or change in intraocular pressure caused the effects attributed to the drugs. When the needle was removed, the injection site was compressed for a minute using a sterile cotton swab to avoid reflux. Before and after ERGs recordings, the fundi of both eyes were

inspected with a PanOptic ophthalmoscope (Welch Allyn, New York, NY). The following weeks, topical antibiotic ointment was administered to the eye that had been injected, twice daily for four days.

Visual Stimulation. Full-field stimulation was produced with an UTAS BigShot Ganzfeld light source (UTAS E-3000 electrophysiology equipment; LKC Technologies, Inc., Gaithersburg, MD) that was placed in front of the animal's face. The intensity of the flashes ranged from 0.00025 $cd.s.m^{-2}$ to 790 $cd.s.m^{-2}$ delivered in full-field conditions, with a duration of <5 ms. Xenon flash luminance of 2.5 to 790 $cd.s.m^{-2}$ (0 dB to 25 dB in LKC units) was used for photopic conditions and LED flash luminance of $2.5x10^{-4}$ to 6 $cd.s.m^{-2}$ (-40 dB to 4 dB in LKC units) for scotopic conditions. Between stimuli, delay intervals of at least 15 seconds were implemented at high flash intensities when the eyes were dark-adapted. In light-adapted conditions, a steady background-adapting field (30 $cd.m^{-2}$) was maintained inside the Ganzfeld to continually saturate the rod system. Flash intensities and background luminance were calibrated using a research radiometer (IL1700 Photometer, International Light Inc., Newburyport, MA) with a SED033 detector placed at 36 cm from the source (at the same location as the cyclopean eye).

ERG recording. All experimental protocols followed the guidelines of the ISCEV (Marmor et al. 2009; Bouskila et al., 2014; McCulloch et al., 2015). ERG recordings and signal processing ERGs were carried out in the morning. The recorded eye was covered with a corneal contact lens electrode (Jet electrodes, Diagnosys LLC, Lowell, MA) moistened with 1% carboxymethylcellulose sodium (Refresh Celluvisc, Allergan Inc., Markham, ON). The electrode was equipped with four small posts that kept the eyelid open. Reference and ground gold disc electrodes (model F-E5GH; Grass Technologies, Astro-Med, Inc., West Warwick, RI) were kept in place with adhesive paste (Ten20 conductive EEG paste, Kappa Medical, Prescott, AZ) at the external canthi and forehead, respectively. Responses were amplified 10,000 times and filtered with a band pass from 1 to 500 Hz except for the oscillatory potentials, which were extracted with the LKC software with a band pass from 75 to 500 Hz. Each trace included a 20 ms pre-stimulus baseline.

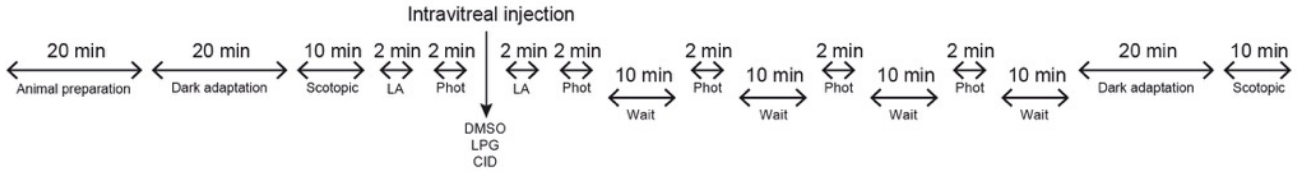

Figure 1. Schematic illustration depicting a typical ERG recording session following monocular intravitreal injections in vervet monkeys (modified from Bouskila et al., 2014). DMSO, dimethyl sulfoxide; LPG, lysophosphatidylglucoside; CID, CID16020046; LA, light adaptation; Phot, photopic.

Statistical analysis. For the waveform analysis, the amplitude of the a-wave was measured from the baseline to the trough of the a-wave. The amplitude of the b-wave was measured from the trough of the a-wave to the peak of the b-wave. The latency was defined from the onset of the flash to the trough (a-wave) or peak (b-wave). If these values fell within the acceptable time window (a-wave: 10-50 ms from flash, b-wave: 50-150 ms from flash), and they were within 3 standard deviations above or below the mean, they were then saved. A repeated measure analysis of variance (ANOVA) was used to determine if the values extracted from the ERG curves in the DMSO-injected group were different from the LPG-injected group or the CID-injected group. Each mixed model ANOVA included one repeated measures factor (intensity of the flash) and one between group factors (drug: DMSO, LPG, or CID).

Results

No changes in the fundus of the eyes were observed after the intravitreal injection in any of the animals. There were also no differences in the intraocular pressure (before: 11±3 mm Hg; after: 11±4 mm Hg) and the pupil size (before: 8.8±0.3 mm; after: 8.8±0.3 mm).

LPG increases the scotopic b-wave amplitude

The effect of LPG on the scotopic ERG was comparable across monkeys. Figure 2A illustrates the average ERG waveform in dark-adapted conditions following the intravitreal injection of DMSO, LPG, or CID at 13 stimulus intensities. Each curve was generated from a simple mean across monkeys. As can be seen in the traces, the intravitreal injection of LPG increases the amplitude of the scotopic ERG. This effect was not significant for the a-wave amplitude (P=0.972, Figure 2B), but was significant for the b-wave amplitude (P=0.050, Figure 2C). On average, LPG caused the scotopic b-wave amplitude to increase by 36% relative to the control (DMSO).

In addition, the effect was significant at several specific flash intensities (-2.6 log cd.s.m^{-2}, P=0.010; -2.2 log cd.s.m^{-2}, P=0.007; -2.0 log cd.s.m^{-2}, P=0.012; -1.0 log cd.s.m^{-2}, P=0.015; -0.6 log cd.s.m^{-2}, P=0.028) and marginally significant at other flash intensities (0 log cd.s.m^{-2}, P=0.077; 1.4 log cd.s.m^{-2}, P=0.074). At the rod standard flash (-2.2 log cd.s.m^{-2}), a flash intensity that corresponds to rod-driven responses, the increase caused by the injection of LPG was 52 ± 18 μV (52% relative to DMSO). At the combined rod-cone standard flash (0.6 log cd.s.m^{-2}), a flash intensity that corresponds to mixed-rod-cone responses, LPG lead to an increase of 56 ± 40 μV (22% relative to DMSO). The latencies for LPG were comparable to DMSO (no significant difference for a-wave latency [P=0.915, Figure 2D] or the b-wave latency [P=0.413, Figure 2E]).

CID decreases the scotopic b-wave amplitude

The effect of CID on the scotopic ERG was comparable across monkeys. Figure 2A illustrates the average ERG waveform in scotopic conditions. The most apparent feature of these curves is that the intravitreal injection of CID decreased the amplitude of the scotopic ERG. This effect was not significant for the a-wave amplitude (P=0.197, Figure 2B), but was

significant for the b-wave amplitude (P=0.004, Figure 2C). CID had no significant effect on the latency for the a-wave (P=0.113, Figure 2D) or the b-wave (P=0.089, Figure 2E). The average decrease of the scotopic b-wave amplitude was 66%.

In addition, the effect of CID on the amplitude of the b-wave was significant at every individual flash intensity (-3.6 log cd.s.m^{-2}, P=0.003; -3.4 log cd.s.m^{-2}, P=0.003; -3.2 log cd.s.m^{-2}, P=0.002; -2.8 log cd.s.m^{-2}, P=0.018; -2.6 log cd.s.m^{-2}, P=0.003; -2.2 log cd.s.m^{-2}, P=0.001; -2.0 log cd.s.m^{-2}, P=0.006; -1.0 log cd.s.m^{-2}, P=0.027; -0.6 log cd.s.m^{-2}, P=0.024; 0 log cd.s.m^{-2}, P=0.016; 0.4 log cd.s.m^{-2}, P=0.007; 0.6 log cd.s.m^{-2}, P=0.002; 1.4 log cd.s.m^{-2}, P=0.004). At the rod standard flash (-2.2 log cd.s.m^{-2}), CID decreased the b-wave amplitude by 66 ± 15 μV (67%) relative to DMSO. At the combined rod-cone standard flash (0.6 log cd.s.m^{-2}), CID decreased the b-wave amplitude by 153 ± 37 μV (59%) relative to DMSO.

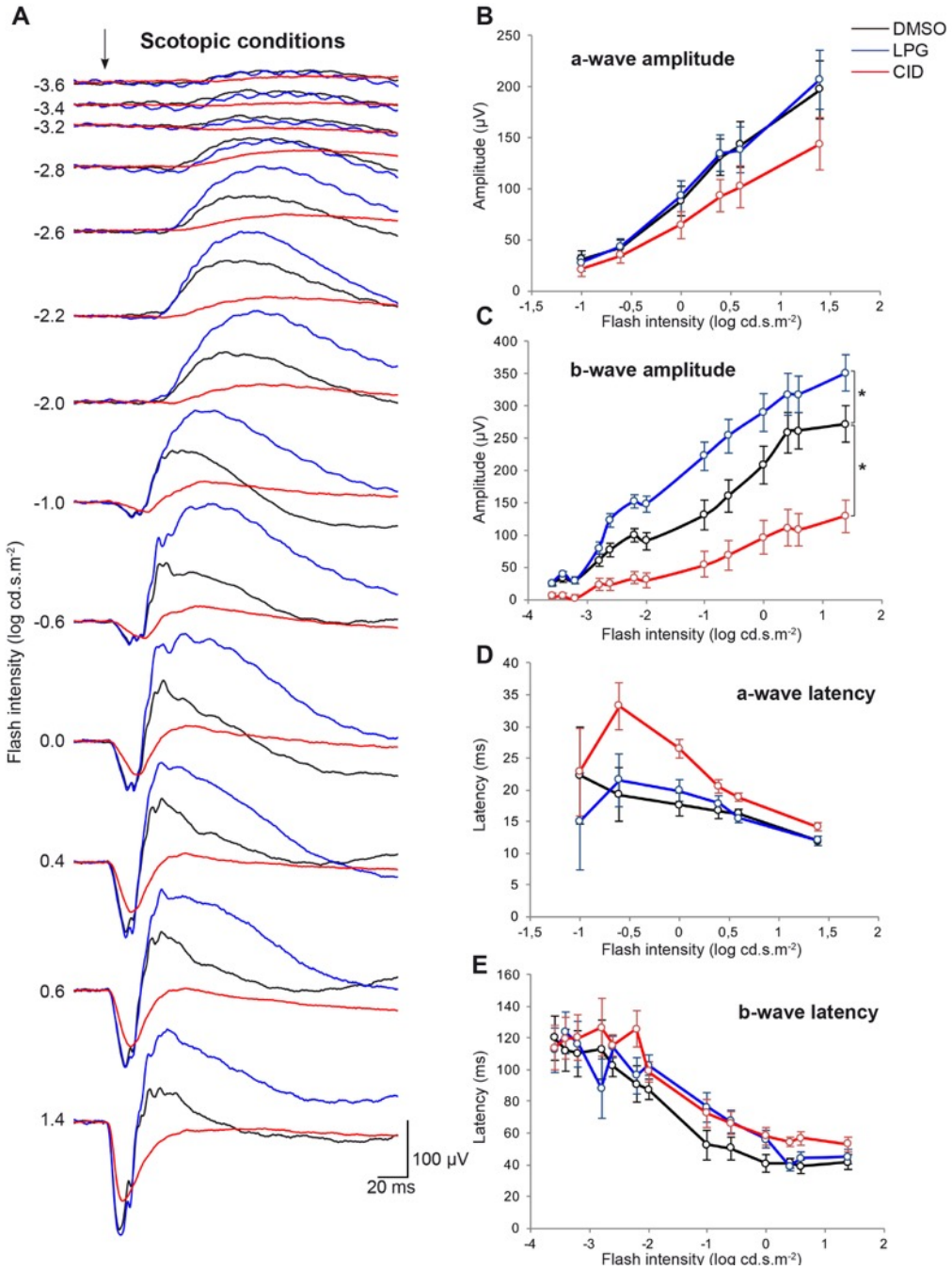

Figure 2. Increase of the scotopic b-wave amplitude after intravitreal injection of LPG and decrease after CID16020046. **(A)** Mean scotopic ERG responses after intravitreal injection of DMSO (black), LPG (blue), or CID (red) are shown for thirteen flash intensities. On the one hand, the intravitreal injection of LPG, a GPR55 agonist, significantly increased the b-wave amplitudes. On the other hand, an overall significant decreased in the b-wave amplitude is observed after CID injection. **(B-E)** Averaged ERG amplitude and latency values are plotted

as a function of flash intensities following injection. Error bars represent ± the standard error of the mean (SEM). The * indicates a significant overall difference ($P < 0.05$) of CID and DMSO, or LPG and DMSO.

The oscillatory potentials are not affected by either compound

A one-way ANOVA was performed on the summed amplitude of the oscillatory potentials at the standard flash (optimal intensity of 0.6 log cd.s.m^{-2}; Bee, 2001; Bouskila et al., 2014). The results show that there was no significant difference between the vehicle and the agonist for the amplitude (DMSO, $\bar{x}$=61.9 ± 14.4 μV; LPG, $\bar{x}$=68.9 ± 11.3 μV; P=0.674) or latency (DMSO, $\bar{x}$=21.0 ± 0.6 ms; LPG, $\bar{x}$=20.5 ± 0.4 ms; P=0.724). A non-significant effect was also found between the vehicle and the antagonist for the amplitude (CID, $\bar{x}$=36.0 ± 7.9 μV; P=0.122) and the latency (CID, $\bar{x}$=18.8 ± 1.2 ms; P=0.123).

LPG has no significant effect on the photopic ERGs

The effects of LPG on the photopic ERG were comparable across monkeys. Figure 3A illustrates the average ERG waveform across monkeys in light-adapted conditions following intravitreal injection of DMSO, LPG or CID for 12 stimulus intensities. There were no significant effects of LPG for a-wave amplitude (P=0.817, Figure 3B), b-wave amplitude (P=0.756, Figure 3C), a-wave latency (P=0.942, Figure 3D), or b-wave latency (P=0.727, Figure 3E).

CID has no significant effect on the photopic ERGs

The effects of CID and DMSO on the photopic ERG were comparable across monkeys, see averages plotted in Figure 3A. There was no statistically significant difference between CID and DMSO: a-wave amplitude (P=0.321, Figure 3B), b-wave amplitude (P=0.067, Figure 3C). CID also had no significant effect on the a-wave latency (P=0.381, Figure 3D) or the b-wave latency (P=0.093, Figure 3E).

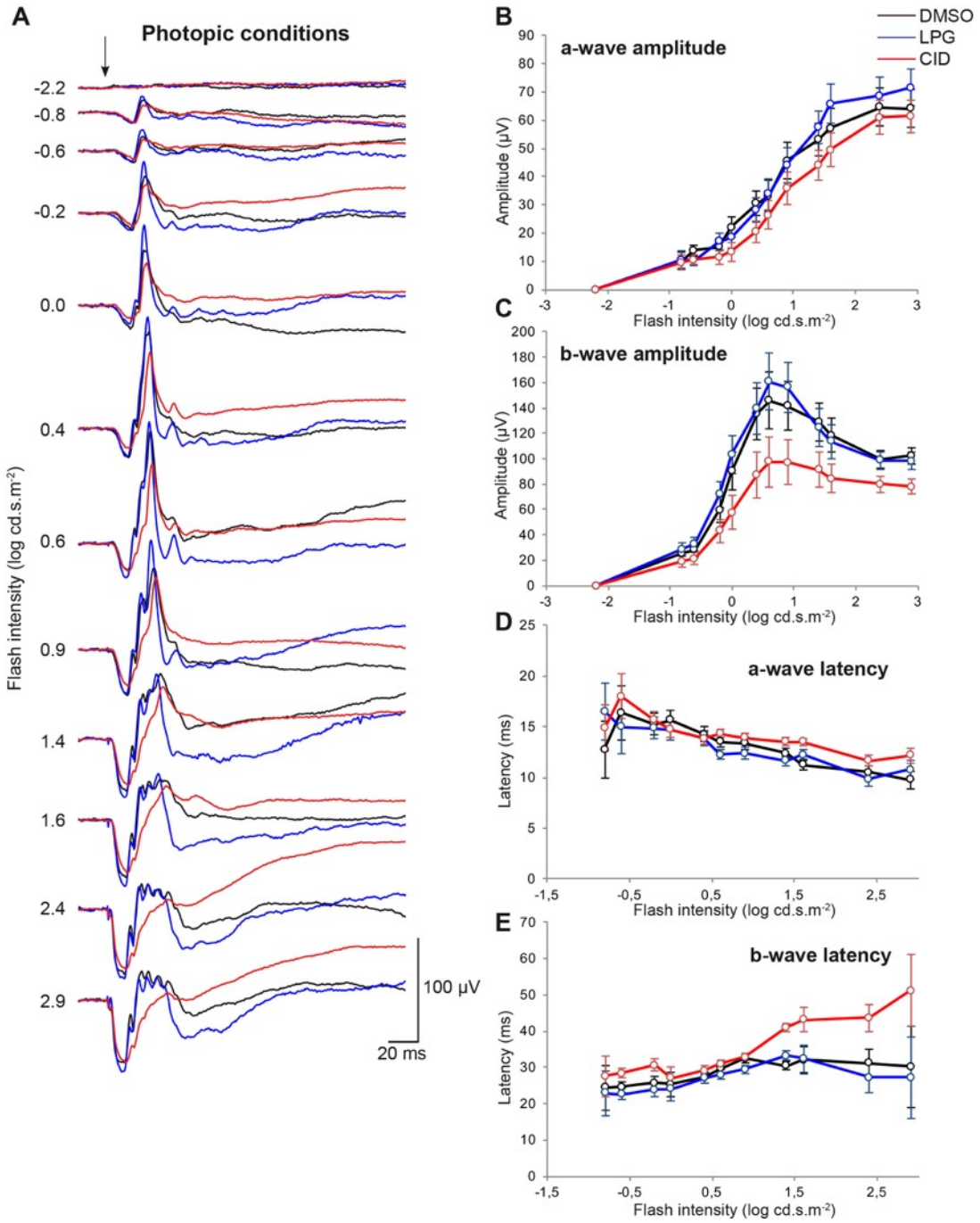

Figure 3. No significant changes in the photopic ERG responses after intravitreal injection of LPG or CID16020046. **(A)** Mean photopic ERG responses after intravitreal injection of DMSO (black), LPG (blue), or CID (red) across twelve flash intensities are shown. **(B-E)** Averaged ERG amplitude and latency values plotted as a function of flash intensities following injection of DMSO (black), LPG (blue), or CID (red). Error bars represent ± SEM.

Discussion

This study investigated the functional consequences of monocular intravitreal injections of potent and selective GPR55 agonist (LPG) or antagonist (CID16020046) in monkeys. Using electroretinographic recordings, we showed that under scotopic conditions, the administration of LPG significantly increased the amplitude of b-wave responses while CID caused them to decrease. The scotopic latencies were not affected by either compound, and neither were the amplitudes or latencies recorded under photopic conditions. This is the first evidence that GPR55 is only involved in scotopic vision since its activation by LPG, and its blockade by CID, modulated the dim-light retinal responses driven by the rod pathway. The strength of this result is visible in Figure 4, which depicts the relationship between the amplitudes of the b- and a-wave (Perlman, 1983). This figure illustrates scotopic retinal function, and its modulation by either blocking GPR55 (impaired retinal function, e.g. nyctalopia) or by activating it (increased retinal function, e.g. hyper-scotopia). The functional effects reported here are in line with the anatomical localization of GPR55 in rod photoreceptors and confirms its purported role in scotopic vision.

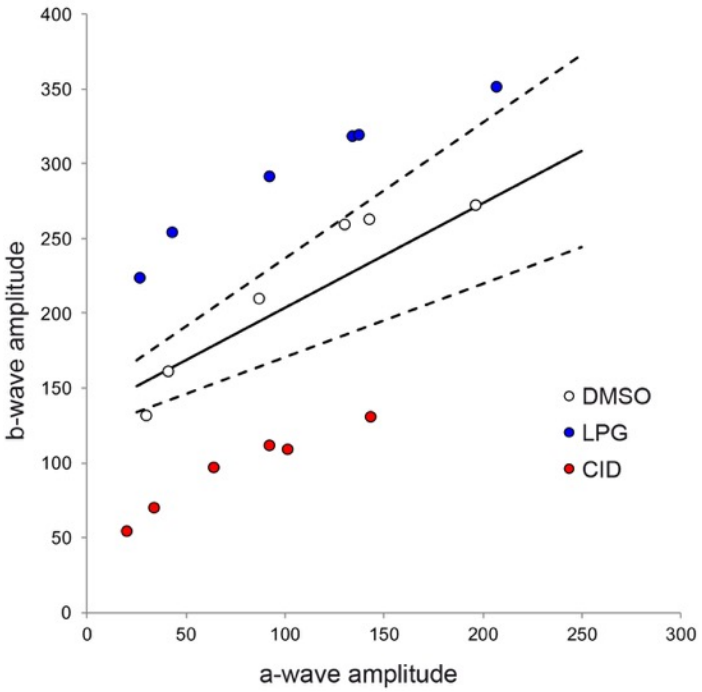

Figure 4. The relationship between the amplitudes of the b- and a-waves obtained in scotopic conditions, as described by Perlman (1983). The continuous line describes the mean relationship while the 2 dashed lines define the normal range (mean ± 2 standard deviations).

White circles represent the amplitudes obtained after the DMSO injection, blue circles after LPG, and red circles after CID. Note that LPG data points are above the normal range (increased retinal function), while those for CID fall below (impaired retinal function).

GPR55 belongs to the Class A rhodopsin-like family of G protein-coupled receptors. Expression of GPR55 in the retina is limited to rod inner segments (Bouskila et al., 2013b), which is implicated in the generation of the scotopic ERG b-wave (Tian & Slaughter, 1995; Robson & Frishman, 1995), although this is somewhat debated (Miller & Dowling, 1970; Wen & Oakley, 1990). Given the expression pattern of GPR55 (Figure 5A), we hypothesized that antagonizing this receptor in the retina would lead to a decrease in the scotopic ERG b-wave. This is indeed what we found, which can be explained by GPR55's influence on the glutamate pathway (Bouskila et al., 2013b; Sylantyev et al., 2013). We speculate that GPR55, located in the rods inner segment and spherules (Bouskila et al., 2013b), acts as the GTPase-Accelerating Protein for $G_{\alpha 13}$, and because rods are directly connected to the ON-rod bipolar cells, GPR55 may also participate in the mGluR6-signaling pathway. In normal conditions of dark adaptation, a large quantity of glutamate is released from rod photoreceptor terminals and binds to the metabotropic glutamate receptor mGluR6 located at the tip of ON-bipolar cell dendrites (Sampath & Rieke, 2004). The activation of GPR55 in rods by LPG coupled to $G_{\alpha 13}$, stimulates RhoA, ROCK, PLC and opens Na^{+}/Ca^{++} channels resulting in membrane depolarization (Bouskila et al., 2013b) and hence an increased scotopic b-wave (Figure 5B). Following the blockade of GPR55 with CID, the hyperpolarization of rods diminishes the release of glutamate (Figure 5C). The putative activation of $G_{\alpha 13}$, RhoA, ROCK and PLC is consequently lowered resulting in the closing of Na^{+}/Ca^{++} channels, and hence a decreased scotopic ERG b-wave. Essentially, blocking GPR55 in the dark-adapted rod is like exposing it to photopic conditions (Bouskila et al. 2013b). It was previously reported that failure to activate mGluR6 on rod ON-bipolar cells abolishes light responses (Sampath & Rieke, 2004). Indeed, the speculation that GPR55 regulates GTP hydrolysis of $G_{\alpha 13}$ is also supported by the notion that phototransduction involves $G_{\alpha 13}$, leading to the release of glutamate (Figure 5). A detailed characterization of other molecules that act as agonists on GPR55 will be informative for treatments of ocular diseases, since activating this protein might be able to increase photosensitivity.

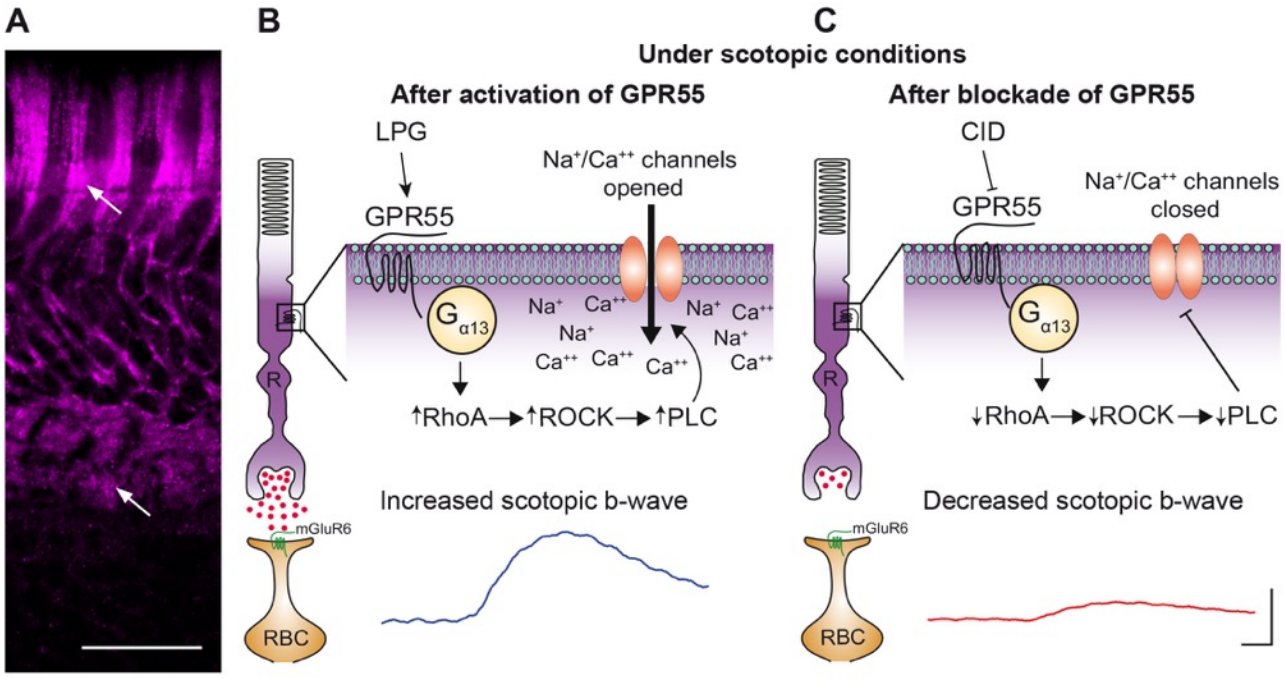

Figure 5. Overview of the putative cannabinoid receptor GPR55 signaling cascade. **(A)** Immunostaining of the vervet monkey retina with a rabbit anti-GPR55 antibody (1:200, magenta) showing that GPR55 is preferentially expressed in the inner segments of rod photoreceptors (upper arrow) and spherules (lower arrow). This observation is identical to the one previously reported (Bouskila et al., 2013b). **(B)** Under scotopic conditions, the activation of GPR55 by LPG on rods coupled to $G_{\alpha 13}$, RhoA, ROCK, and PLC opens Na^{+}/Ca^{++} channels resulting in the membrane depolarization (Bouskila et al., 2013b) and hence an increased scotopic b-wave. (**C**) Following the blockade of GPR55 with CID, the activation of $G_{\alpha 13}$, RhoA, ROCK, and PLC is consequently lowered resulting in the closing of Na^{+}/Ca^{++} channels, and hence a decreased scotopic ERG b-wave in the CID-treated eyes. The scotopic waveforms are taken from Figure 2A at the rod standard flash, (-2.2 log cd.s.m^{-2}). LPG, lysophosphatidylglucoside; R, rods; RBC, rod bipolar cells. Scale bar in (**A**): 30 µm and in (**B**) and (**C**): amplitude (vertical axis), 100 µV; latency (horizontal axis), 20 ms.

Drug delivery directly into the eye in humans is a common treatment for retinal disorders. For example, intravitreal injections are often performed in the treatment of age-related macular degeneration and diabetic retinopathy (see Duvvuri et al., 2003 for review). The effectiveness of treatments for retinal diseases has significantly improved since the

introduction of medications administered directly into the vitreous because of their immediate effects. This procedure is now used on a daily basis in clinics to treat these aforementioned diseases. Night blindness (e.g. nyctalopia), a condition where it is nearly impossible to see in low light, is a symptom of many eye diseases like retinitis pigmentosa, Oguchi disease, and congenital stationary night blindness, which specifically targets the rods (Marc et al., 2003). Given the present findings, GPR55's implication in scotopic vision might therefore be exploited as a pharmacological target in the treatment of retinal diseases that include symptoms of night blindness.

References

ADAMS, A.J., BROWN, B., FLOM, M.C., JONES, R.T. & JAMPOLSKY, A. (1975). Alcohol and marijuana effects on static visual acuity. *American Journal of Optometry and Physiological Optics* **52,** 729-735.

ADAMS, A.J., BROWN, B., HAEGERSTROM-PORTNOY, G., FLOM, M.C. & JONES, R.T. (1978). Marijuana, alcohol, and combined drug effects on the time course of glare recovery. *Psychopharmacology* **56,** 81-86.

BEE, W.H. (2001). Standardized electroretinography in primates: a non-invasive preclinical tool for predicting ocular side effects in humans. *Curr Opin Drug Discov Devel* **4,** 81-91.

BLONDEAU, N., LAURITZEN, I., WIDMANN, C., LAZDUNSKI, M. & HEURTEAUX, C. (2002). A potent protective role of lysophospholipids against global cerebral ischemia and glutamate excitotoxicity in neuronal cultures. *Journal of Cerebral Blood Flow and Metabolism* **22,** 821-834.

BOUSKILA, J., BURKE, M.W., ZABOURI, N., CASANOVA, C., PTITO, M. & BOUCHARD, J.F. (2012). Expression and localization of the cannabinoid receptor type 1 and the enzyme fatty acid amide hydrolase in the retina of vervet monkeys. *Neuroscience* **202,** 117-130.

BOUSKILA, J., JAVADI, P., CASANOVA, C., PTITO, M. & BOUCHARD, J.F. (2013a). Muller cells express the cannabinoid CB2 receptor in the vervet monkey retina. *Journal of Comparative Neurology* **521,** 2399-2415.

BOUSKILA, J., JAVADI, P., CASANOVA, C., PTITO, M. & BOUCHARD, J.F. (2013b). Rod photoreceptors express GPR55 in the adult vervet monkey retina. *PloS One* **8,** e81080.

BOUSKILA, J., JAVADI, P., PALMOUR, R.M., BOUCHARD, J.F. & PTITO, M. (2014). Standardized full-field electroretinography in the Green Monkey (Chlorocebus sabaeus). *PloS One* **9,** e111569.

CÉCYRE, B., ZABOURI, N., HUPPÉ-GOURGUES, F., BOUCHARD, J.F. & CASANOVA, C. (2013). Roles of cannabinoid receptors type 1 and 2 on the retinal function of adult mice. *Investigative Ophthalmology and Visual Science* **54,** 8079-8090.

DAWSON, W.W., JIMENEZ-ANTILLON, C.F., PEREZ, J.M. & ZESKIND, J.A. (1977). Marijuana and vision--after ten years' use in Costa Rica. *Investigative Ophthalmology and Visual Science* **16,** 689-699.

DUVVURI, S., MAJUMDAR, S. & MITRA, A.K. (2003). Drug delivery to the retina: challenges and opportunities. *Expert Opinion on Biological Therapy* **3,** 45-56.

FREUND, T.F., KATONA, I. & PIOMELLI, D. (2003). Role of endogenous cannabinoids in synaptic signaling. *Physiological Reviews* **83,** 1017-1066.

GUY, A.T., NAGATSUKA, Y., OOASHI, N., INOUE, M., NAKATA, A., GREIMEL, P., INOUE, A., NABETANI, T., MURAYAMA, A., OHTA, K., ITO, Y., AOKI, J., HIRABAYASHI, Y. & KAMIGUCHI, H. (2015). Neuronal Development. Glycerophospholipid regulation of modality-specific sensory axon guidance in the spinal cord. *Science* **349,** 974-977.

HENSTRIDGE, C.M., BALENGA, N.A., FORD, L.A., ROSS, R.A., WALDHOER, M. & IRVING, A.J. (2009). The GPR55 ligand L-alpha-lysophosphatidylinositol promotes RhoA-dependent Ca2+ signaling and NFAT activation. *FASEB Journal* **23,** 183-193.

HO, W.S., BARRETT, D. & RANDALL, M. (2008). 'Entourage'effects of N-palmitoylethanolamide and N-oleoylethanolamide on vasorelaxation to anandamide occur through TRPV1 receptors. *British Journal of Pharmacology* **155,** 837-846.

JONSSON, K.O., VANDEVOORDE, S., LAMBERT, D.M., TIGER, G. & FOWLER, C.J. (2001). Effects of homologues and analogues of palmitoylethanolamide upon the inactivation of the endocannabinoid anandamide. *British Journal of Pharmacology* **133,** 1263-1275.

KARGL, J., BALENGA, N., PARZMAIR, G.P., BROWN, A.J., HEINEMANN, A. & WALDHOER, M. (2012). The cannabinoid receptor CB1 modulates the signaling properties of the lysophosphatidylinositol receptor GPR55. *Journal of Biological Chemistry* **287,** 44234-44248.

KIPLINGER, G.F., MANNO, J.E., RODDA, B.E. & FORNEY, R.B. (1971). Dose-response analysis of the effects of tetrahydrocannabinol in man. *Clinical Pharmacology and Therapeutics* **12,** 650-657.

KREITZER, A.C. & REGEHR, W.G. (2001a). Cerebellar depolarization-induced suppression of inhibition is mediated by endogenous cannabinoids. *Journal of Neuroscience* **21,** RC174.

KREITZER, A.C. & REGEHR, W.G. (2001b). Retrograde inhibition of presynaptic calcium influx by endogenous cannabinoids at excitatory synapses onto Purkinje cells. *Neuron* **29,** 717-727.

KUMAR, A., QIAO, Z., KUMAR, P. & SONG, Z.H. (2012). Effects of palmitoylethanolamide on aqueous humor outflow. *Investigative Ophthalmology and Visual Science* **53,** 4416-4425.

LIU, B., SONG, S., JONES, P.M. & PERSAUD, S.J. (2015). GPR55: from orphan to metabolic regulator? *Pharmacology and Therapeutics* **145,** 35-42.

LÓPEZ, E.M., TAGLIAFERRO, P., ONAIVI, E.S. & LÓPEZ-COSTA, J.J. (2011). Distribution of CB2 cannabinoid receptor in adult rat retina. *Synapse* **65,** 388-392.

MACINTYRE, J., DONG, A., STRAIKER, A., ZHU, J., HOWLETT, S.E., BAGHER, A., DENOVAN-WRIGHT, E., YU, D.Y. & KELLY, M.E. (2014). Cannabinoid and lipid-mediated vasorelaxation in retinal microvasculature. *European Journal of Pharmacology* **735,** 105-114.

MARC, R.E., JONES, B.W., WATT, C.B. & STRETTOI, E. (2003). Neural remodeling in retinal degeneration. *Progress in Retinal and Eye Research* **22,** 607-655.

MARMOR, M.F., FULTON, A.B., HOLDER, G.E., MIYAKE, Y., BRIGELL, M., BACH, M. & INTERNATIONAL SOCIETY FOR CLINICAL ELECTROPHYSIOLOGY OF, V. (2009). ISCEV Standard for full-field clinical electroretinography (2008 update). *Documenta Ophthalmologica* **118,** 69-77.

MCCULLOCH, D.L., MARMOR, M.F., BRIGELL, M.G., HAMILTON, R., HOLDER, G.E., TZEKOV, R. & BACH, M. (2015). ISCEV Standard for full-field clinical electroretinography (2015 update). *Documenta Ophthalmologica* **130,** 1-12.

MILLER, R.F. & DOWLING, J.E. (1970). Intracellular responses of the Muller (glial) cells of mudpuppy retina: their relation to b-wave of the electroretinogram. *Journal of Neurophysiology* **33,** 323-341.

NAIR, G., KIM, M., NAGAOKA, T., OLSON, D.E., THULE, P.M., PARDUE, M.T. & DUONG, T.Q. (2011). Effects of common anesthetics on eye movement and electroretinogram. *Documenta Ophthalmologica* **122,** 163-176.

NOYES, R., JR., BRUNK, S.F., AVERY, D.A. & CANTER, A.C. (1975). The analgesic properties of delta-9-tetrahydrocannabinol and codeine. *Clinical Pharmacology and Therapeutics* **18,** 84-89.

OHNO-SHOSAKU, T., MAEJIMA, T. & KANO, M. (2001). Endogenous cannabinoids mediate retrograde signals from depolarized postsynaptic neurons to presynaptic terminals. *Neuron* **29,** 729-738.

OKA, S., NAKAJIMA, K., YAMASHITA, A., KISHIMOTO, S. & SUGIURA, T. (2007). Identification of GPR55 as a lysophosphatidylinositol receptor. *Biochemical and Biophysical Research Communications* **362,** 928-934.

OKUNO, T. & YOKOMIZO, T. (2011). What is the natural ligand of GPR55? *Journal of Biochemistry* **149,** 495-497.

PALMOUR, R.M., MULLIGAN, J., HOWBERT, J.J. & ERVIN, F. (1997). Of monkeys and men: vervets and the genetics of human-like behaviors. *American Journal of Human Genetics* **61,** 481-488.

PEARSON, P.A., JAFFE, G.J., MARTIN, D.F., CORDAHI, G.J., GROSSNIKLAUS, H., SCHMEISSER, E.T. & ASHTON, P. (1996). Evaluation of a delivery system providing long-term release of cyclosporine. *Archives of Ophthalmology* **114,** 311-317.

PERLMAN, I. (1983). Relationship between the amplitudes of the b wave and the a wave as a useful index for evaluating the electroretinogram. *British Journal of Ophthalmology* **67,** 443-448.

REESE, K. (1991). Cannabis seems to improve night vision of fisherman. *Chemical Engineering News* **69,** 44.

ROBSON, J.G. & FRISHMAN, L.J. (1995). Response linearity and kinetics of the cat retina: the bipolar cell component of the dark-adapted electroretinogram. *Visual Neuroscience* **12,** 837-850.

RUSSO, E.B., MERZOUKI, A., MESA, J.M., FREY, K.A. & BACH, P.J. (2004). Cannabis improves night vision: a case study of dark adaptometry and scotopic sensitivity in kif smokers of the Rif mountains of northern Morocco. *Journal of Ethnopharmacology* **93,** 99-104.

RYBERG, E., LARSSON, N., SJOGREN, S., HJORTH, S., HERMANSSON, N.O., LEONOVA, J., ELEBRING, T., NILSSON, K., DRMOTA, T. & GREASLEY, P.J. (2007). The orphan receptor

GPR55 is a novel cannabinoid receptor. *British Journal of Pharmacology* **152,** 1092-1101.

SAMPATH, A.P. & RIEKE, F. (2004). Selective transmission of single photon responses by saturation at the rod-to-rod bipolar synapse. *Neuron* **41,** 431-443.

STEINBERG, R.H., LINSENMEIER, R.A. & GRIFF, E.R. (1985). Chapter 2 Retinal pigment epithelial cell contributions to the electroretinogram and electrooculogram. *Progress in Retinal Research* **4,** 33-66.

STRAIKER, A., STELLA, N., PIOMELLI, D., MACKIE, K., KARTEN, H.J. & MAGUIRE, G. (1999a). Cannabinoid CB1 receptors and ligands in vertebrate retina: localization and function of an endogenous signaling system. *Proceedings of the National Academy of Sciences of the United States of America* **96,** 14565-14570.

STRAIKER, A.J., MAGUIRE, G., MACKIE, K. & LINDSEY, J. (1999b). Localization of cannabinoid CB1 receptors in the human anterior eye and retina. *Investigative Ophthalmology and Visual Science* **40,** 2442-2448.

SYLANTYEV, S., JENSEN, T.P., ROSS, R.A. & RUSAKOV, D.A. (2013). Cannabinoid- and lysophosphatidylinositol-sensitive receptor GPR55 boosts neurotransmitter release at central synapses. *Proceedings of the National Academy of Sciences of the United States of America* **110,** 5193-5198.

TIAN, N. & SLAUGHTER, M.M. (1995). Correlation of dynamic responses in the ON bipolar neuron and the b-wave of the electroretinogram. *Vision Research* **35,** 1359-1364.

TSAI, T.I., BUI, B.V. & VINGRYS, A.J. (2009). Dimethyl sulphoxide dose-response on rat retinal function. *Documenta Ophthalmologica* **119,** 199-207.

WEN, R. & OAKLEY, B., 2ND. (1990). K(+)-evoked Muller cell depolarization generates b-wave of electroretinogram in toad retina. *Proceedings of the National Academy of Sciences of the United States of America* **87,** 2117-2121.

WEST, M.E. (1991). Cannabis and night vision. *Nature* **351,** 703-704.

WILSON, R.I. & NICOLL, R.A. (2001). Endogenous cannabinoids mediate retrograde signalling at hippocampal synapses. *Nature* **410,** 588-592.

YAZULLA, S. (2008). Endocannabinoids in the retina: from marijuana to neuroprotection. *Progress in Retinal and Eye Research* **27,** 501-526.

YAZULLA, S., STUDHOLME, K.M., MCINTOSH, H.H. & DEUTSCH, D.G. (1999). Immunocytochemical localization of cannabinoid CB1 receptor and fatty acid amide hydrolase in rat retina. *Journal of Comparative Neurology* **415,** 80-90.

ZABOURI, N., BOUCHARD, J.F. & CASANOVA, C. (2011a). Cannabinoid receptor type 1 expression during postnatal development of the rat retina. *Journal of Comparative Neurology* **519,** 1258-1280.

ZABOURI, N., PTITO, M., CASANOVA, C. & BOUCHARD, J.F. (2011b). Fatty acid amide hydrolase expression during retinal postnatal development in rats. *Neuroscience* **195,** 145-165.

IV. DISCUSSION GÉNÉRALE

Le but principal de cette thèse était de caractériser l'expression, la localisation et le rôle du système endocannabinoïde (eCB) dans la rétine du singe. Comme il a été évoqué tout au long de cet ouvrage, le système eCB est présent dans la rétine et module la transmission synaptique via le mécanisme de signalisation rétrograde et la régulation de canaux ioniques. Il est évident que ces effets peuvent affecter l'information visuelle déjà au premier niveau de traitement, la rétine. Plusieurs autres études sont par contre nécessaires pour évaluer l'impact que le système eCB rétinien a dans la perception visuelle. D'autant plus, ce système est aussi présent dans des structures visuelles plus centrales, comme le premier relais thalamique, le corps genouillé latéral dorsal (dLGN), et le cortex visuel (au niveau de l'aire visuelle primaire, V1) et les aires visuelles associatives. Ce système eCB module ainsi le signal visuel tout au long de la voie rétinofuge.

La recherche sur le système eCB a pris de plus en plus d'ampleur avec le temps. En effet, après s'être concentrés sur les mécanismes d'action du cannabis et du THC, les chercheurs ont focalisé leurs recherches sur le rôle du système cannabinoïde endogène et son utilité comme cible thérapeutique. Il est clair que le système eCB est un système ubiquitaire qui module de nombreuses fonctions physiologiques. Il est présent dans plusieurs types de cellules dans le règne animal. Ainsi, le projet réalisé dans cette thèse visait à élaborer sur la relation entre le système eCB et la rétine. Nous rapportons pour la première fois que :

1. CB1R et FAAH sont présents dans la rétine centrale et périphérique du singe vervet, mais CB1R est abondamment exprimé dans les cônes de la fovéa. Ces deux composantes sont aussi présentes au niveau des cellules horizontales, cellules bipolaires, cellules amacrines et cellules ganglionnaires (Bouskila et coll., 2012).
2. CB2R est exclusivement présent dans les cellules de Müller, avec une abondante expression du côté de la membrane limitante externe et une très faible expression du côté de la membrane limitante interne. CB1R se retrouve donc dans la neuro-rétine et CB2R dans la glie rétinienne (Bouskila et coll., 2013a).

3. GPR55 est exclusivement exprimé dans les bâtonnets. Plus précisément, ce récepteur se trouve fortement dans les segments internes et faiblement dans les sphérules de bâtonnets. L'activation de GPR55 par son agoniste pourrait donc représenter un processus de modulation des bâtonnets et, probablement, jouer un rôle dans la vision scotopique (Bouskila et coll., 2013b).

4. Le système eCB est exprimé dans la rétine de souris, toupayes et primates, mais avec quelques distinctions notoires. Tandis que l'expression de CB1R, FAAH, MGL et DAGL est similaire à travers ces espèces, CB2R et NAPE-PLD sont exprimés différemment (Bouskila et coll., 2016a).

5. L'ERG du singe vervet est comparable au singe macaque et même à celui de l'humain. Les résultats de cette étude valident le singe vervet comme un excellent modèle de primate non humain pour tester la fonction rétinienne après plusieurs manipulations telles que la privation visuelle ou l'administration de molécules (Bouskila et coll., 2014).

6. CB1R et CB2R sont importants pour l'établissement des ondes de l'ERG. En condition photopique, l'AM251, un antagoniste/agoniste inverse de CB1R, augmente l'amplitude de l'onde a pour des fortes intensités lumineuses, tandis que l'AM630, un antagoniste/agoniste inverse de CB2R, augmente l'amplitude des ondes a et b. En condition scotopique, les deux antagonistes ont augmenté l'amplitude de l'onde b, mais n'ont pas changé l'amplitude de l'onde a. Ces résultats suggèrent un rôle important de CB1R et CB2R dans la fonction rétinienne du primate (Bouskila et coll., 2016b).

7. GPR55 module la vision scotopique. En condition scotopique seulement, l'agoniste de GPR55 (LPG) a augmenté l'amplitude de l'onde b et l'antagoniste de GPR55 (CID) l'a diminué (Bouskila et coll., 2016c).

1. Les différences interespèces sur l'expression et le rôle des récepteurs cannabinoïdes dans la rétine

Nous avons donc démontré qu'il y a une ségrégation anatomique des 3 différents récepteurs, CB1R, CB2R et GPR55 dans la rétine du singe vervet. Plusieurs évidences nous portent à croire que ces récepteurs ne sont pas exprimés dans la rétine de façon similaire à travers les espèces, p. ex. la séquence protéique de CB2R de la souris est différente de celle du primate. La Figure 15 montre la cartographie des récepteurs CB1R, CB2R et GPR55 dans la rétine de la souris, du toupaye et du singe vervet. Il existe donc certaines différences majeures au fur et à mesure qu'on se rapproche de l'homme dans l'arbre phylogénétique. CB1R et CB2R sont uniques aux Chordés (embranchement d'animaux qui possède une notocorde, une lamelle cartilagineuse d'origine mésodermique située sur le côté dorsal de l'animal). Les enzymes de synthèse et de dégradation sont présents dans plusieurs espèces du règne animal (Elphick, 2012). Il est possible que des protéines agissant comme récepteurs soient apparues bien plus tard que les eCBs. Même si les patrons d'expression de certaines composantes eCBs comme CB1R et FAAH sont similaires dans différentes espèces, ce n'est pas le cas pour CB2R et NAPE-PLD (Bouskila et coll., 2016a). Comme l'expression de CB2R dans la rétine de la souris (Cécyre et coll., 2013) est différente du singe (Bouskila et coll., 2013a), nous avons étudié plusieurs composantes du système eCB connues à ce jour dans la rétine de souris, singes et toupayes (une espèce qui se situe entre les souris et les primates dans l'arbre phylogénétique). De plus, l'expression de ce système a été comparée dans la rétine de deux types de singes, les vervets et les macaques.

Chez toutes ces espèces, CB1R et FAAH ont un patron d'expression qui se chevauche ce qui suggère que la dégradation d'eCBs peut se produire dans la même cellule CB1R positive. Dans la rétine dominée par les bâtonnets de la souris, CB2R est exprimé dans la neuro-rétine, dans les photorécepteurs, cellules horizontales, cellules bipolaires, cellules amacrines et cellules ganglionnaires, mais non dans les cellules de Müller (Cécyre et coll., 2013). Dans la rétine dominée par les cônes du toupaye, CB2R est exprimé dans la neuro-rétine et aussi dans les cellules de Müller. Dans la rétine duplex des singes vervet et macaque, CB2R est exclusivement retrouvé dans les cellules de Müller. Une explication possible de

cette transition de CB2R (expression neuronale diffuse vs expression spécifique dans la glie rétinienne) est que ce récepteur a pris une place stratégique pour exercer le rôle de modulateur du potassium au cours de l'évolution de la rétine. L'enzyme de synthèse NAPE-PLD comporte aussi une expression propre à chacune de ces espèces. Chez la souris, NAPE-PLD est exprimé dans la neuro-rétine. Chez le toupaye, NAPE-PLD est exprimé fortement dans la rétine externe et faiblement dans la rétine interne. Chez le singe, NAPE-PLD est uniquement exprimé au niveau des photorécepteurs, cônes et bâtonnets. Le groupe de molécules lipidiques bioactives, les N-acyl éthanolamines (NAE), sont synthétisé par la NAPE-PLD à partir des phospholipides de la membrane cellulaire. Cette différence d'expression rétinienne interespèce est remarquée malgré la séquence protéique conservée de NAPE-PLD, contrairement à CB2R. Cette variation peut être à l'importance des produits de synthèse de NAPE-PLD autre que les eCBs. Cette enzyme synthétise plusieurs molécules comme l'anandamide (un eCB), mais aussi le N-palmitoylethanolamine (un antiinflammatoire ; Lambert et coll., 2002) et le N-oleoylethanolamine (un anorexigène; Rodríguez de Fonseca et coll., 2001). NAPE-PLD peut même avoir des effets proapoptotiques (Maccarrone et coll., 2002). De plus, les produits de cette enzyme, les NAE, sont présents dans les axones et régulent l'activité neuronale postsynaptique en agissant comme des molécules de signalisation synaptique antérograde (Egertová et coll., 2008). Enfin, l'expression de NAPE-PLD dans les photorécepteurs du singe suggère un rôle direct des NAEs dans la phototransduction des primates. Mais ceci reste à être vérifié expérimentalement.

Les patrons d'expression de DAGL et MAGL dans la rétine de souris, toupayes et singes sont similaires, mais comportent différentes intensités de signal. Comme les eCBs sont synthétisés et dégradés autour des leurs récepteurs, l'expression de DAGL et MAGL doit se trouver aux environs de CB2R. Dans la rétine de souris, ces deux enzymes en plus de CB1R et CB2R sont exprimées de manière qu'ils se chevauchent et peuvent donc exercer un rôle d'autorégulation dans chacune des cellules de la rétine. Dans la rétine de toupayes et de singes, l'expression des enzymes du système eCB se retrouve de manière complémentaire. Il se peut que le système eCB se soit spécialisé parallèlement à la complexification du système visuel pour adopter une position stratégique pour la modulation de l'activité visuelle.

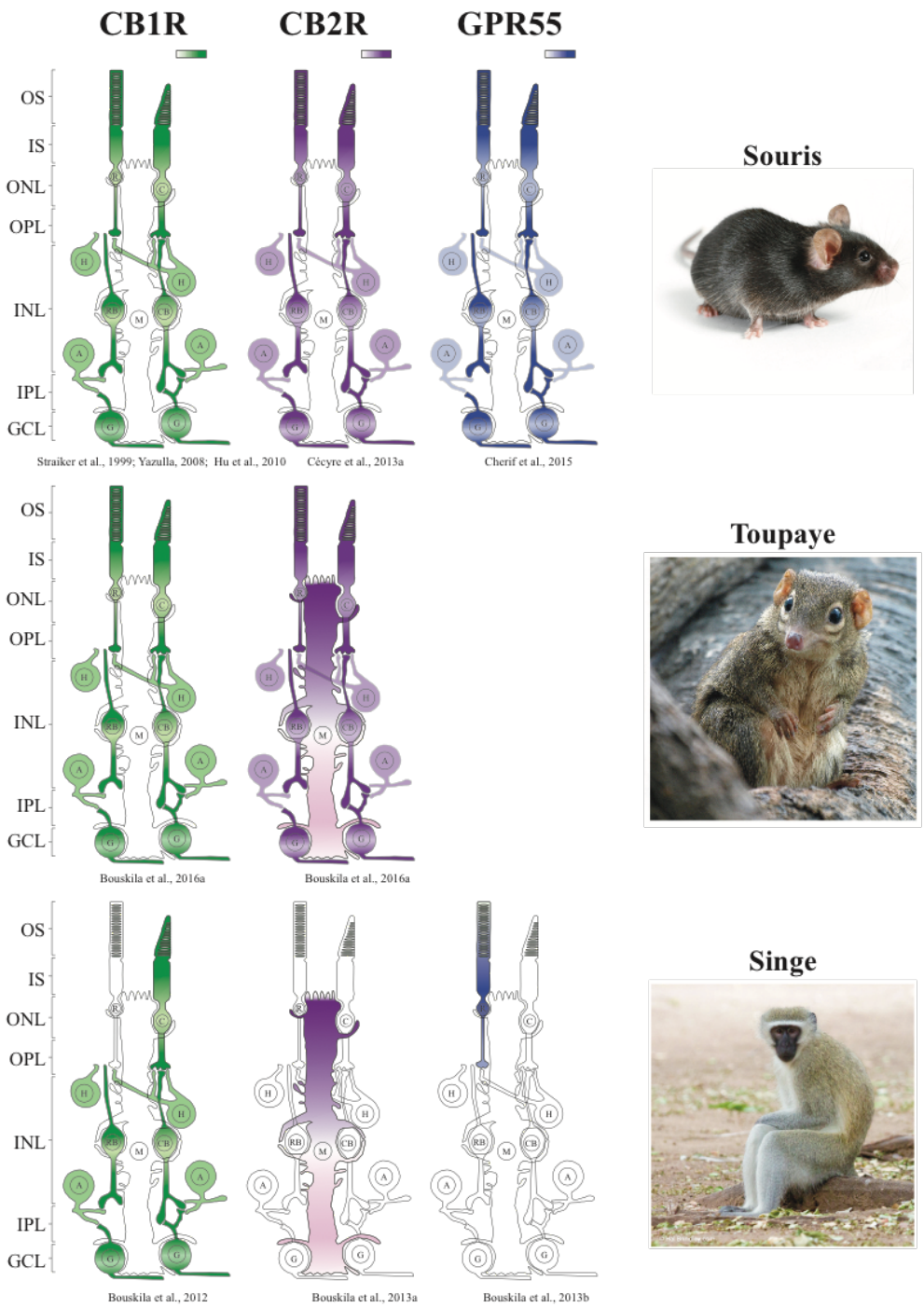

Figure 15. Cartographie des récepteurs CB1R, CB2R et GPR55 dans la rétine de la souris, du toupaye et du singe.

Abréviations : OS, segment externe; IS, segment interne; ONL, couche nucléaire externe; OPL, couche plexiforme externe; INL, couche nucléaire interne; IPL, couche plexiforme interne; GCL, couche des cellules ganglionnaires.

Récemment, les conséquences de la suppression génétique de CB1R ou CB2R sur la fonction rétinienne de la souris ont été mesurées par électrorétinographie (Cécyre et coll., 2013). En condition scotopique, les souris CB2R KO présentent une hausse de l'amplitude de l'onde a, confirmée par l'effet observé qu'un agoniste de CB2R altère la sensibilité du bâtonnet de la salamandre tigrée (Straiker et Sullivan, 2003). En condition photopique, l'amplitude de l'onde b des souris CB2R KO montre un schéma d'adaptation à la lumière différent de la souris de souche sauvage. Aucun effet significatif n'a été observé chez les animaux CB1R KO. Ces données ne correspondent pas du tout aux effets observés chez le singe (Bouskila et coll., 2016b), et ce, pour plusieurs raisons. Tout d'abord, l'anatomie des récepteurs cannabinoïdes dans la rétine est très différente chez ces différentes espèces. Chez la souris, les patrons d'expression de CB1R et CB2R sont similaires (Zabouri et coll., 2011a, Cécyre et coll., 2013). Chez le singe, CB1R est exprimé dans la neuro-rétine (tout comme chez la souris) (Bouskila et coll., 2012), mais CB2R est exclusivement présent dans la glie rétinienne, les cellules de Müller (Bouskila et coll., 2013a). Ensuite, nous comparons des effets aigus (injections intravitréennes chez le singe) avec les effets à long terme d'une délétion du récepteur (souris transgéniques). Il est possible que ces souris KO aient subi des mécanismes de compensation durant leur développement qui entraineraient des différentes réponses physiologiques comparées aux animaux où l'on bloquerait temporairement leurs récepteurs à l'aide d'antagonistes.

2. Les voies de signalisation du système eCB dans la rétine du singe

La présence de CB1R dans la neuro-rétine (surtout dans la voie verticale qui consiste de photorécepteurs, cellules bipolaires et cellules ganglionnaires), de CB2R dans la glie rétinienne (cellules de Müller) et de GPR55 dans les bâtonnets suggère que les ligands endogènes de ces récepteurs sont synthétisés et relâchés par des cellules à proximité, autour du site de production (Gomez-Ruiz et al, 2007). Ceci peut aussi ultimement influencer, directement (par CB1R et GPR55) ou indirectement (par CB2R) la libération de glutamate, le neurotransmetteur principal de la voie verticale de la rétine. Une fois que les ligands sont

produits, plusieurs canaux ioniques comme les canaux K^+ et Ca^{++} sont modulés à la suite de l'activation des récepteurs.

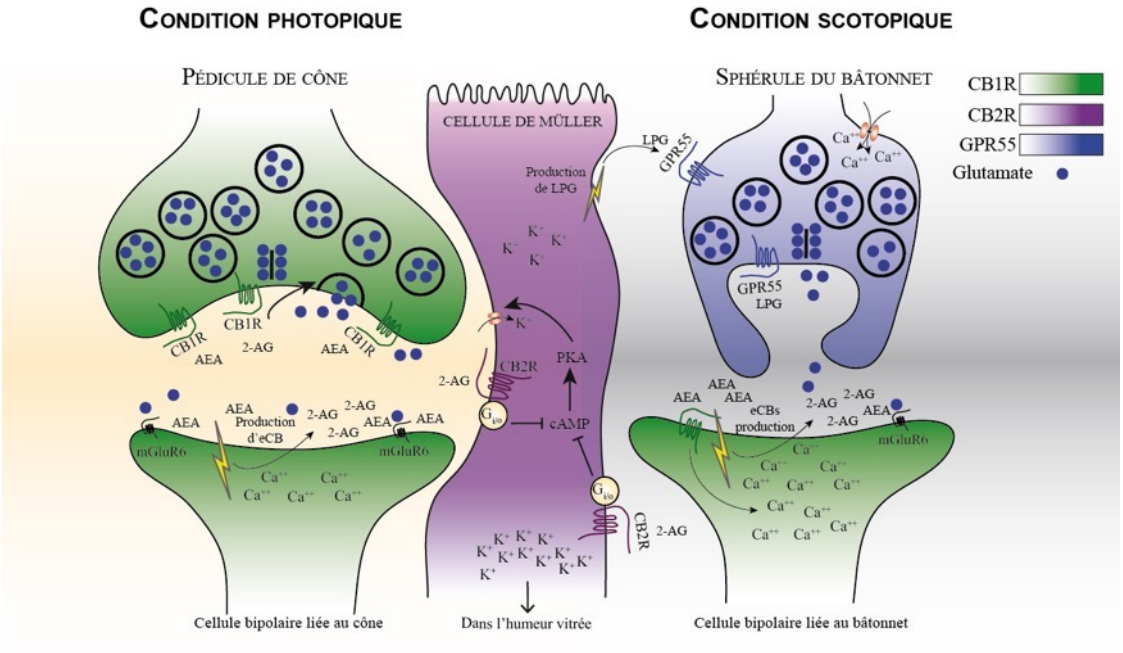

Figure 16. Illustration schématique du rôle hypothétique de CB1R, CB2R et GPR55 dans la rétine du singe.

En condition photopique, lorsque les cônes sont stimulés par la lumière, il se produit une inhibition des courants ioniques, ce qu'on appelle « *inhibition of the retinal dark currents* ». La phototransduction qui en résulte diminue la quantité de glutamate relâchée dans la synapse et propage ainsi un signal vers les cellules bipolaires. Ces cellules bipolaires sont la source de production d'eCBs (notamment l'anandamide) qui va agir de façon rétrograde et activer CB1R dans les pédicules de cônes et ainsi contrôler la libération de glutamate. Cette production d'eCBs va aussi amener la synthèse du 2-AG qui va aller activer CB2R dans les cellules de Müller et ainsi contrôler la circulation de potassium à travers la rétine. L'activation de CB2R couplé à une protéine $G_{i/o}$ mène à une réduction des niveaux d'AMP cyclique et de PKA (Howlett et coll., 2002 pour un article de revue ; Bolognini et coll., 2010). Vu que PKA augmente l'activité des canaux $K_{IR}4.1$ dans les cellules de Müller (MacGregor et coll., 1998), CB2R joue le rôle de modulateur négatif du potassium. Parallèlement, en conditions normales d'adaptation à la noirceur, une large quantité de glutamate est relâchée des terminaisons

synaptiques des bâtonnets. Ce glutamate se lie ensuite aux récepteurs mGluR6 situés dans les dendrites des cellules bipolaires ON liées aux bâtonnets (Sampath & Rieke, 2004). L'activation de GPR55 par son agoniste endogène (le lysophosphatidylglucoside, LPG) va stimuler la cascade $G_{\alpha 13}$, RhoA, ROCK, PLC pour ouvrir les canaux Na^{+}/Ca^{++}, induire la dépolarisation membranaire, et modifier l'ERG scotopique (Bouskila et coll., 2013b; Bouskila et coll., 2016c). Ces mécanismes sont illustrés au niveau de la synapse photorécepteur-cellule bipolaire dans la Figure 16 ci-dessus, mais peuvent exister probablement dans plusieurs autres synapses de la rétine. Cependant, malgré de grands efforts à comprendre la fonction du système eCB rétinien, des études comportementales sont certes nécessaires pour établir son rôle précis dans la vision.

V. CONCLUSION ET PERSPECTIVES D'AVENIR

La rétine comporte donc un système eCB qui permet de moduler l'information visuelle à plusieurs niveaux. Le principe actif du cannabis responsable des effets psychotropes de cette plante, le Δ9-THC, agit au niveau de CB1R présent de façon ubiquitaire dans le corps. CB1R est retrouvé en haute concentration dans certaines régions précises du cerveau notamment, le cervelet, l'hippocampe, la substance noire et les ganglions de la base. La majorité des études portant sur la localisation du système eCB, incluant les récepteurs, les ligands endogènes de ces récepteurs et les enzymes de synthèse et dégradation de ces ligands, font usage de techniques *in vitro*, de modèles animaux, d'électrophysiologie, d'analyse comportementale et de données post-mortem. Comme il existe de grandes différences interespèces, il est très utile de faire des études sur l'humain afin de passer directement aux applications cliniques. De plus, comme certaines études indiquent que le système eCB est exprimé au niveau de plusieurs structures visuelles, il serait intéressant d'aller regarder quelles sont les régions activées du cortex occipital. Ceci nous permettra d'évaluer le rôle neurobiologique et l'impact clinique de ce système en vision.

1. Rôle dans le développement

Comme il a été démontré dans des systèmes autres que la rétine, les eCBs sont des modulateurs de la transmission synaptique et de la plasticité neuronale, principalement via le

mécanisme d'inhibition présynaptique. L'impact du système eCB dans le développement du SNC a bien été documenté durant cette dernière décennie. Ce système régule la prolifération, la migration, la spécification et la survie des cellules progénitrices neuronales (Galve-Roperh et coll., 2006), guide la différenciation neuronale et contrôle l'établissement de connexions synaptiques (Berghuis et coll., 2005; Harkany et coll., 2007). L'importance des eCBs durant le développement du système nerveux est confirmée par le fait que la consommation de cannabis durant la grossesse mène à des déficits cognitifs, moteurs et sociaux (Richardson et coll., 1995; Fried et coll., 2003; Huizink et Mulder, 2006; Calvigioni et coll., 2014). Le niveau de 2-AG augmentent progressivement durant le développement embryonnaire et atteint son pic juste après la naissance (Berrendero et coll., 1999; Fride, 2008). Cependant, les changements des niveaux des composantes du système eCB durant le développement ne sont pas limités aux structures cérébrales de haut niveau, mais peuvent aussi affecter le développement de la rétine. Le système eCB a été démontré comme un élément important au cours du développement du SNC (Fernández-Ruiz et coll., 2000), dans le guidage axonal (Argaw et coll., 2011; Duff et coll., 2013), dans le développement normal de l'embryon de rongeurs (Pagotto et coll., 2006), mais aussi dans le développement de la rétine de rongeurs (Zabouri et coll., 2011a; Zabouri et coll., 2011b).

2. Rôle au niveau du comportement

Il est difficile de développer des tests comportementaux rapides et efficaces chez le singe. Pourtant, les méthodes électrophysiologiques, comme l'ERG et les potentiels évoqués visuels (PEV), sont des avenues de recherches intéressantes puisque nous avons démontré dans la présente thèse que l'ERG peut être modulé par les récepteurs eCBs. Par contre, il serait fort intéressant d'utiliser des tests comportementaux où l'animal doit émettre une réponse relative à un stimulus visuel, ce qui est plus conforme à la réalité, vu que les études électrophysiologiques utilisent des préparations anesthésiées. Étant donné qu'il est difficile et surtout très long d'entrainer des singes à différentes taches visuelles, il est nécessaire de développer des tests visuels qui font appel à des comportements simples comme le regard préférentiel et le nystagmus optocinétique. Justement, ces tests se sont avérés excellents pour

mesurer les fonctions visuelles des enfants en bas âge ou des adultes qui ont perdu les fonctions langagières.

2.1 Le regard préférentiel

La fixation visuelle spontanée survient lorsque le singe est soumis à certains stimuli plus que d'autres (Zangenehpour et coll., 2014). Particulièrement, les singes préfèrent porter leur attention et fixer des patrons de stimuli plutôt que des régions de luminosité uniforme. Ce comportement spontané servant de base dans la mesure quantitative de la vue d'un stimulus porte le nom de *forced-choice preferential looking*. La tâche ne demande aucun entrainement préalable long pour l'animal si ce n'est qu'une familiarisation d'environ deux semaines avec la chaise de contention et la fixation d'une croix présentée au centre de l'écran sur lequel seront projetés les stimuli visuels. La détermination des courbes de sensibilité au contraste peut ensuite nous fournir une mesure de l'acuité visuelle en plus des seuils déterminés par la variation du contraste des différents stimuli. Les stimuli de comparaison et tests sont généralement alternés immédiatement après chaque essai. Si une fréquence spatiale est au-dessus du seuil de détection à un contraste donné, le regard de l'animal devrait s'attarder sur le stimulus contenant la grille. Dans le cas contraire (stimulus en dessous du seuil), l'animal passera autant de temps sur les deux stimuli. De cette façon, il est possible d'établir le niveau de base des aptitudes visuelles.

2.2 Le nystagmus optocinétique

Le nystagmus est un mouvement involontaire des deux globes oculaires. Le nystagmus optocinétique survient lorsque les yeux du sujet se concentrent sur des images qui défilent devant lui. Il est constitué d'une série de saccades de l'œil, qui suit la cible en mouvement, et d'un coup rapide rapporte la fixation vers la cible. Enfants et adultes ont ce réflexe à la suite de la présentation d'une cible en mouvement. Ces mouvements des yeux réflexes sont contrôlés par des mécanismes sous-corticaux (voie rétinotectale), mais aussi corticaux (Leigh et Zee, *The neurology of eye movements*, 1999).

3. Imagerie des récepteurs cannabinoïdes

Jusqu'aujourd'hui, les techniques d'imagerie *in vivo*, particulièrement la tomoscintigraphie par émission de positons (TEP) et la tomographie d'émission monophotonique (TEMP), des récepteurs cannabinoïdes n'ont pas eu beaucoup de succès dû au manque de radioligands hautement sélectifs. Puisque les ligands doivent être hautement lipophiliques comme les eCBs, ils ne sont pas utilisables pour ces techniques d'imagerie donnant beaucoup de liaisons non spécifiques et une basse pénétration cérébrale. Ce n'est que récemment que des ligands hautement spécifiques aux récepteurs cannabinoïdes ont été développé (Burns et coll., 2007). Durant cette dernière décennie, plusieurs études ont démontré que le système eCB est en position parfaite de moduler la vision. En effet, les récepteurs cannabinoïdes se retrouvent dans les structures visuelles (rétine, nerf optique, cortex visuel) de plusieurs espèces. L'activation des récepteurs cannabinoïdes mène à un changement de la fonction visuelle. Ainsi, les techniques d'imagerie avec la liaison des radioligands aux récepteurs cannabinoïdes vont nous permettre d'attribuer un rôle fonctionnel du système eCB en vision.

4. Usage du cannabis pour le traitement des maladies de la rétine

Depuis plusieurs millénaires, le cannabis a été cultivé par l'homme à des fins récréatives et thérapeutiques, mais la recherche scientifique sur cette plante est en pleine émergence. En plus des revendications de ses bienfaits thérapeutiques, la recherche sur les mécanismes par lequel le cannabis produit ces actions gagne de l'intérêt. Malgré les effets bénéfiques de cette plante, l'utilisation du cannabis médical n'est pas répandue à travers le Monde. De nombreux efforts sont encore nécessaires pour que les scientifiques comblent cette lacune. De plus, le fait que le cannabis est une substance illicite pousse les gens à ne pas prendre au sérieux la possibilité d'utiliser le cannabis comme traitement thérapeutique. Les travaux réalisés dans le cadre de cette thèse ont permis d'établir un rôle du système eCB dans la rétine du singe. Si l'on considère que les récepteurs cannabinoïdes sont exprimés de façon similaire chez le singe et l'Homme, la modulation de ce système au niveau rétinien constitue une cible thérapeutique intéressante. Par exemple, plusieurs maladies dégénératives de l'œil ont tendance à diminuer les ondes de l'électrorétinogramme. Comme démontré dans les

Articles 6 et 7, il est possible d'injecter de façon intravitréenne des molécules agissant sur ce système et, ainsi, augmenter et rétablir la fonction rétinienne. Ces résultats sont donc très prometteurs et sont susceptibles d'engendrer de nouvelles méthodes de traitement afin de rétablir la fonction de la rétine et, peut-être même, la vision chez des patients qui souffrent de certaines pathologies rétiniennes.

VI. BIBLIOGRAPHIE

Abbas Farishta, R., Robert, C., Turcot, O., Thomas, S., Vanni, M. P., Bouchard, J. F., & Casanova, C. (2015). Impact of CB1 Receptor Deletion on Visual Responses and Organization of Primary Visual Cortex in Adult Mice. *Invest Ophthalmol Vis Sci, 56*(13), 7697-7707.

Adams, A. J., Brown, B., Haegerstrom-Portnoy, G., Flom, M. C., & Jones, R. T. (1978). Marijuana, alcohol, and combined drug effects on the time course of glare recovery. *Psychopharmacology (Berl), 56*(1), 81-86.

Argaw, A., Duff, G., Zabouri, N., Cécyre, B., Chaine, N., Cherif, H., . . . Bouchard, J. F. (2011). Concerted action of CB1 cannabinoid receptor and deleted in colorectal cancer in axon guidance. *J Neurosci, 31*(4), 1489-1499.

Bari, M., Battista, N., Fezza, F., Gasperi, V., & Maccarrone, M. (2006). New insights into endocannabinoid degradation and its therapeutic potential. *Mini Rev Med Chem, 6*(3), 257-268.

Besharse, J. C., & Bok, D. (2011). *The Retina and Its Disorders*. Academic Press.

Beltramo, M., Stella, N., Calignano, A., Lin, S. Y., Makriyannis, A., & Piomelli, D. (1997). Functional role of high-affinity anandamide transport, as revealed by selective inhibition. *Science, 277*(5329), 1094-1097.

Berghuis, P., Dobszay, M. B., Wang, X., Spano, S., Ledda, F., Sousa, K. M., . . . Harkany, T. (2005). Endocannabinoids regulate interneuron migration and morphogenesis by transactivating the TrkB receptor. *Proc Natl Acad Sci U S A, 102*(52), 19115-19120.

Berrendero, F., Sepe, N., Ramos, J. A., Di Marzo, V., & Fernandez-Ruiz, J. J. (1999). Analysis of cannabinoid receptor binding and mRNA expression and endogenous cannabinoid contents in the developing rat brain during late gestation and early postnatal period. *Synapse, 33*(3), 181-191.

Bisogno, T. (2008). Endogenous cannabinoids: structure and metabolism. *J Neuroendocrinol, 20 Suppl 1*, 1-9.

Bolognini, D., Costa, B., Maione, S., Comelli, F., Marini, P., Di Marzo, V., . . . Pertwee, R. G. (2010). The plant cannabinoid Delta9-tetrahydrocannabivarin can decrease signs of inflammation and inflammatory pain in mice. *Br J Pharmacol, 160*(3), 677-687.

Bouchard, J.-F., Casanova, C., Cécyre, B., & Redmond, W. J. (2015). Expression and Function of the Endocannabinoid System in the Retina and the Visual Brain. *Neural Plast, vol. 501*, 103813.

Bouskila, J., Burke, M. W., Zabouri, N., Casanova, C., Ptito, M., & Bouchard, J. F. (2012). Expression and localization of the cannabinoid receptor type 1 and the enzyme fatty acid amide hydrolase in the retina of vervet monkeys. *Neuroscience, 202*, 117-130.

Bouskila, J., Javadi, P., Casanova, C., Ptito, M., & Bouchard, J. F. (2013a). Muller cells express the cannabinoid CB2 receptor in the vervet monkey retina. *J Comp Neurol, 521*(11), 2399-2415.

Bouskila, J., Javadi, P., Casanova, C., Ptito, M., & Bouchard, J. F. (2013b). Rod photoreceptors express GPR55 in the adult vervet monkey retina. *PLoS One, 8*(11), e81080.

Bouskila, J., Javadi, P., Palmour, R. M., Bouchard, J. F., & Ptito, M. (2014). Standardized full-field electroretinography in the Green Monkey (Chlorocebus sabaeus). *PLoS One, 9*(10), e111569.

Bouskila, J., Javadi, P., Elkrief, L., Casanova, C., Bouchard, J. F., & Ptito, M. (2016a). A comparative analysis of the endocannabinoid system in the retina of mice, tree shrews and monkeys. *Neural Plasticity, vol. 2016*, 3127658.

Bouskila, J., Harrar, V., Javadi, P., Beierschmitt, A., Palmour, R., Casanova, C., . . . Ptito, M. (2016b). Cannabinoid receptors CB1 and CB2 modulate the electroretinographic waves in vervet monkeys. *Neural Plasticity, vol. 2016*, 1253245.

Bouskila, J., Harrar, V., Javadi, P., Casanova, C., Hirabayashi, Y., Matsuo, I., . . . Ptito, M. (2016c). Scotopic vision in the monkey is modulated by the G protein-coupled receptor 55. *Visual Neuroscience*. In press.

Bringmann, A., Pannicke, T., Grosche, J., Francke, M., Wiedemann, P., Skatchkov, S. N., . . . Reichenbach, A. (2006). Muller cells in the healthy and diseased retina. *Prog Retin Eye Res, 25*(4), 397-424.

Buckley, N. E., Hansson, S., Harta, G., & Mezey, E. (1998). Expression of the CB1 and CB2 receptor messenger RNAs during embryonic development in the rat. *Neuroscience, 82*(4), 1131-1149.

Budney, A. J., Moore, B. A., Vandrey, R. G., & Hughes, J. R. (2003). The time course and significance of cannabis withdrawal. *J Abnorm Psychol, 112*(3), 393-402.

Burke, M., Zangenehpour, S., Bouskila, J., Boire, D., & Ptito, M. (2009). The gateway to the brain: dissecting the primate eye. *J Vis Exp*(27), e1261.

Burns, H. D., Van Laere, K., Sanabria-Bohorquez, S., Hamill, T. G., Bormans, G., Eng, W. S., . . . Hargreaves, R. J. (2007). [18F]MK-9470, a positron emission tomography (PET) tracer for in vivo human PET brain imaging of the cannabinoid-1 receptor. *Proc Natl Acad Sci U S A, 104*(23), 9800-9805.

Cairns, E. A., Toguri, J. T., Porter, R. F., Szczesniak, A. M., & Kelly, M. E. (2015). Seeing over the horizon - targeting the endocannabinoid system for the treatment of ocular disease. *J Basic Clin Physiol Pharmacol*. Ahead of print.

Calvigioni, D., Hurd, Y. L., Harkany, T., & Keimpema, E. (2014). Neuronal substrates and functional consequences of prenatal cannabis exposure. *Eur Child Adolesc Psychiatry, 23*(10), 931-941.

Cécyre, B., Zabouri, N., Huppé-Gourgues, F., Bouchard, J. F., & Casanova, C. (2013). Roles of cannabinoid receptors type 1 and 2 on the retinal function of adult mice. *Invest Ophthalmol Vis Sci, 54*(13), 8079-8090.

Cécyre, B., Monette, M., Beudjekian, L., Casanova, C., & Bouchard, J. F. (2014a). Localization of diacylglycerol lipase alpha and monoacylglycerol lipase during postnatal development of the rat retina. *Front Neuroanat, 8*, 150.

Cécyre, B., Thomas, S., Ptito, M., Casanova, C., & Bouchard, J. F. (2014b). Evaluation of the specificity of antibodies raised against cannabinoid receptor type 2 in the mouse retina. *Naunyn Schmiedebergs Arch Pharmacol, 387*(2), 175-184.

Chen, J., Matias, I., Dinh, T., Lu, T., Venezia, S., Nieves, A., . . . Di Marzo, V. (2005). Finding of endocannabinoids in human eye tissues: implications for glaucoma. *Biochem Biophys Res Commun, 330*(4), 1062-1067.

Cottone, E., Pomatto, V., Cerri, F., Campantico, E., Mackie, K., Delpero, M., . . . Franzoni, M. F. (2013). Cannabinoid receptors are widely expressed in goldfish: molecular cloning

of a CB2-like receptor and evaluation of CB1 and CB2 mRNA expression profiles in different organs. *Fish Physiol Biochem, 39*(5), 1287-1296.

Dasilva, M., Grieve, K. L., Cudeiro, J., & Rivadulla, C. (2014). Anandamide activation of CB1 receptors increases spontaneous bursting and oscillatory activity in the thalamus. *Neuroscience, 265*, 72-82.

Dasilva, M. A., Grieve, K. L., Cudeiro, J., & Rivadulla, C. (2012). Endocannabinoid CB1 receptors modulate visual output from the thalamus. *Psychopharmacology (Berl), 219*(3), 835-845.

De Petrocellis, L., Cascio, M. G., & Di Marzo, V. (2004). The endocannabinoid system: a general view and latest additions. *Br J Pharmacol, 141*(5), 765-774.

Di Marzo, V. (2014). *Cannabinoids*. Wiley.

Dowling, John E. (2012) *The Retina: An Approachable Part of the Brain.* Cambridge, MA: Belknap of Harvard UP.

Duff, G., Argaw, A., Cécyre, B., Cherif, H., Tea, N., Zabouri, N., . . . Bouchard, J. F. (2013). Cannabinoid receptor CB2 modulates axon guidance. *PLoS One*, 8(8), e70849.

Egertová, M., Simon, G. M., Cravatt, B. F., & Elphick, M. R. (2008). Localization of N-acyl phosphatidylethanolamine phospholipase D (NAPE-PLD) expression in mouse brain: A new perspective on N-acylethanolamines as neural signaling molecules. *J Comp Neurol, 506*(4), 604-615.

Facci, L., Dal Toso, R., Romanello, S., Buriani, A., Skaper, S. D., & Leon, A. (1995). Mast cells express a peripheral cannabinoid receptor with differential sensitivity to anandamide and palmitoylethanolamide. *Proc Natl Acad Sci U S A, 92*(8), 3376-3380.

Fattore, L. (2015). *Cannabinoids in Neurologic and Mental Disease*. Elsevier Science.

Fattore, L., Fadda, P., Spano, M. S., Pistis, M., & Fratta, W. (2008). Neurobiological mechanisms of cannabinoid addiction. *Mol Cell Endocrinol, 286*(1-2 Suppl 1), S97-S107.

Fegley, D., Kathuria, S., Mercier, R., Li, C., Goutopoulos, A., Makriyannis, A., & Piomelli, D. (2004). Anandamide transport is independent of fatty-acid amide hydrolase activity and is blocked by the hydrolysis-resistant inhibitor AM1172. *Proc Natl Acad Sci U S A, 101*(23), 8756-8761.

Fernández-Ruiz, J., Berrendero, F., Hernández, M. L., & Ramos, J. A. (2000). The endogenous cannabinoid system and brain development. *Trends Neurosci, 23*(1), 14-20.

Finlay, B. L., Franco, E. C., Yamada, E. S., Crowley, J. C., Parsons, M., Muniz, J. A., & Silveira, L. C. (2008). Number and topography of cones, rods and optic nerve axons in New and Old World primates. *Vis Neurosci, 25*(3), 289-299.

Fox, R., Lehmkuhle, S. W., & Westendorf, D. H. (1976). Falcon visual acuity. *Science, 192*(4236), 263-265.

Fraunfelder, F. T., Fraunfelder, F. W., & Chambers, W. A. (2008). *Clinical Ocular Toxicology: Drug-Induced Ocular Side Effects*. Elsevier Health Sciences.

Fride, E. (2008). Multiple roles for the endocannabinoid system during the earliest stages of life: pre- and postnatal development. *J Neuroendocrinol, 20 Suppl 1*(s1), 75-81.

Fried, P. A., Watkinson, B., & Gray, R. (2003). Differential effects on cognitive functioning in 13- to 16-year-olds prenatally exposed to cigarettes and marihuana. *Neurotoxicol Teratol, 25*(4), 427-436.

Galve-Roperh, I., Aguado, T., Rueda, D., Velasco, G., & Guzman, M. (2006). Endocannabinoids: a new family of lipid mediators involved in the regulation of neural cell development. *Curr Pharm Des, 12*(18), 2319-2325.

Garkun, Y., & Maffei, A. (2014). Cannabinoid-dependent potentiation of inhibition at eye opening in mouse V1. *Front Cell Neurosci, 8*, 46.

Giuffrida, A., Parsons, L. H., Kerr, T. M., Rodriguez de Fonseca, F., Navarro, M., & Piomelli, D. (1999). Dopamine activation of endogenous cannabinoid signaling in dorsal striatum. *Nat Neurosci, 2*(4), 358-363.

Green, K. (1979). The ocular effects of cannabinoids. *Curr Top Eye Res, 1*, 175-215.

Harkany, T., Guzman, M., Galve-Roperh, I., Berghuis, P., Devi, L. A., & Mackie, K. (2007). The emerging functions of endocannabinoid signaling during CNS development. *Trends Pharmacol Sci, 28*(2), 83-92.

Hattar, S., Liao, H. W., Takao, M., Berson, D. M., & Yau, K. W. (2002). Melanopsin-containing retinal ganglion cells: architecture, projections, and intrinsic photosensitivity. *Science, 295*(5557), 1065-1070.

Heijl, A., Leske, M. C., Bengtsson, B., Hyman, L., Bengtsson, B., & Hussein, M. (2002). Reduction of intraocular pressure and glaucoma progression: results from the Early Manifest Glaucoma Trial. *Arch Ophthalmol, 120*(10), 1268-1279.

Hepler, R. S., & Frank, I. R. (1971). Marihuana smoking and intraocular pressure. *JAMA, 217*(10), 1392.

Herbin, M., Boire, D., & Ptito, M. (1997). Size and distribution of retinal ganglion cells in the St. Kitts green monkey (Cercopithecus aethiops sabeus). *J Comp Neurol, 383*(4), 459-472.

Hoover, H. S., Blankman, J. L., Niessen, S., & Cravatt, B. F. (2008). Selectivity of inhibitors of endocannabinoid biosynthesis evaluated by activity-based protein profiling. *Bioorg Med Chem Lett, 18*(22), 5838-5841.

Howlett, A. C., Barth, F., Bonner, T. I., Cabral, G., Casellas, P., Devane, W. A., . . . Pertwee, R. G. (2002). International Union of Pharmacology. XXVII. Classification of cannabinoid receptors. *Pharmacol Rev, 54*(2), 161-202.

Howlett, A. C., Breivogel, C. S., Childers, S. R., Deadwyler, S. A., Hampson, R. E., & Porrino, L. J. (2004). Cannabinoid physiology and pharmacology: 30 years of progress. *Neuropharmacology, 47 Suppl 1*, 345-358.

Hu, S. S., Arnold, A., Hutchens, J. M., Radicke, J., Cravatt, B. F., Wager-Miller, J., . . . Straiker, A. (2010). Architecture of cannabinoid signaling in mouse retina. *J Comp Neurol, 518*(18), 3848-3866.

Huizink, A. C., & Mulder, E. J. H. (2006). Maternal smoking, drinking or cannabis use during pregnancy and neurobehavioral and cognitive functioning in human offspring. *Neurosci Biobehav Rev, 30*(1), 24-41.

Jacobs, G. H. (2008). Primate color vision: a comparative perspective. *Vis Neurosci, 25*(5-6), 619-633.

Jarvinen, T., Pate, D. W., & Laine, K. (2002). Cannabinoids in the treatment of glaucoma. *Pharmacol Ther, 95*(2), 203-220.

Jasinska, A. J., Service, S., Levinson, M., Slaten, E., Lee, O., Sobel, E., . . . Ophoff, R. A. (2007). A genetic linkage map of the vervet monkey (Chlorocebus aethiops sabaeus). *Mamm Genome, 18*(5), 347-360.

Javadi, P., Bouskila, J., Bouchard, J. F., & Ptito, M. (2015). The endocannabinoid system within the dorsal lateral geniculate nucleus of the vervet monkey. *Neuroscience, 288*, 135-144.

Jiang, B., Huang, S., de Pasquale, R., Millman, D., Song, L., Lee, H. K., . . . Kirkwood, A. (2010). The maturation of GABAergic transmission in visual cortex requires endocannabinoid-mediated LTD of inhibitory inputs during a critical period. *Neuron, 66*(2), 248-259.

Jiang, B., Sohya, K., Sarihi, A., Yanagawa, Y., & Tsumoto, T. (2010). Laminar-specific maturation of GABAergic transmission and susceptibility to visual deprivation are related to endocannabinoid sensitivity in mouse visual cortex. *J Neurosci, 30*(42), 14261-14272.

Johnson, R. L., Grant, K. B., Zankel, T. C., Boehm, M. F., Merbs, S. L., Nathans, J., & Nakanishi, K. (1993). Cloning and expression of goldfish opsin sequences. *Biochemistry, 32*(1), 208-214.

Kandel, E. R., Schwartz, J. H., Jessell, T. M., Siegelbaum, S. A., & Hudspeth, A. J. (2013). *Principles of Neural Science*. (5^{e} éd.). McGraw-Hill Education.

Kathuria, S., Gaetani, S., Fegley, D., Valino, F., Duranti, A., Tontini, A., . . . Piomelli, D. (2003). Modulation of anxiety through blockade of anandamide hydrolysis. *Nature Medicine, 9*(1), 76-81.

King, A., Azuara-Blanco, A., & Tuulonen, A. (2013). Glaucoma. *BMJ, 346*, f3518.

Kolb, H., Fernandez, E., & Nelson, R. (2011). Webvision: The Organization of the Retina and Visual System. John Moran Eye Center, University of Utah.

Kupers, R., Pietrini, P., Ricciardi, E., & Ptito, M. (2011). The nature of consciousness in the visually deprived brain. *Front Psychol, 2*, 19.

Lachapelle, P. (1987). Analysis of the Photopic Electroretinogram Recorded before and after Dark-Adaptation. *Can J Ophthalmol, 22*(7), 354-361.

Lalonde, M. R., Jollimore, C. A., Stevens, K., Barnes, S., & Kelly, M. E. (2006). Cannabinoid receptor-mediated inhibition of calcium signaling in rat retinal ganglion cells. *Mol Vis, 12*, 1160-1166.

Lambert, D. M., Vandevoorde, S., Jonsson, K. O., & Fowler, C. J. (2002). The palmitoylethanolamide family: a new class of anti-inflammatory agents? *Curr Med Chem, 9*(6), 663-674.

Liu, C. H., Heynen, A. J., Shuler, M. G., & Bear, M. F. (2008). Cannabinoid receptor blockade reveals parallel plasticity mechanisms in different layers of mouse visual cortex. *Neuron, 58*(3), 340-345.

Logothetis, N. K. (1999). Vision: a window on consciousness. *Sci Am, 281*(5), 69-75.

Lograno, M. D., & Romano, M. R. (2004). Cannabinoid agonists induce contractile responses through G(i/o)-dependent activation of phospholipase C in the bovine ciliary muscle. *Eur J Pharmacol, 494*(1), 55-62.

Lopez, E. M., Tagliaferro, P., Onaivi, E. S., & Lopez-Costa, J. J. (2011). Distribution of CB2 cannabinoid receptor in adult rat retina. *Synapse, 65*(5), 388-392.

Lu, Q., Straiker, A., Lu, Q., & Maguire, G. (2000). Expression of CB2 cannabinoid receptor mRNA in adult rat retina. *Vis Neurosci, 17*(1), 91-95.

Maccarrone, M., Pauselli, R., Di Rienzo, M., & Finazzi-Agro, A. (2002). Binding, degradation and apoptotic activity of stearoylethanolamide in rat C6 glioma cells. *Biochem J, 366*(Pt 1), 137-144.

MacGregor, G. G., Xu, J. Z., McNicholas, C. M., Giebisch, G., & Hebert, S. C. (1998). Partially active channels produced by PKA site mutation of the cloned renal K+ channel, ROMK2 (kir1.2). *Am J Physiol, 275*(3 Pt 2), F415-422.

Marshall, J., & Oberwinkler, J. (1999). The colourful world of the mantis shrimp. *Nature, 401*(6756), 873-874.

Matias, I., Wang, J. W., Moriello, A. S., Nieves, A., Woodward, D. F., & Di Marzo, V. (2006). Changes in endocannabinoid and palmitoylethanolamide levels in eye tissues of patients with diabetic retinopathy and age-related macular degeneration. *Prostaglandins Leukot Essent Fatty Acids, 75*(6), 413-418.

Matsuda, L. A., Lolait, S. J., Brownstein, M. J., Young, A. C., & Bonner, T. I. (1990). Structure of a cannabinoid receptor and functional expression of the cloned cDNA. *Nature, 346*(6284), 561-564.

Matteau, I., Boire, D., & Ptito, M. (2003). Retinal projections in the cat: a cholera toxin B subunit study. *Vis Neurosci, 20*(5), 481-493.

Mechoulam, R., Hanus, L. O., Pertwee, R., & Howlett, A. C. (2014). Early phytocannabinoid chemistry to endocannabinoids and beyond. *Nat Rev Neurosci, 15*(11), 757-764.

Mechoulam, R., Panikashvili, D., & Shohami, E. (2002). Cannabinoids and brain injury: therapeutic implications. *Trends Mol Med, 8*(2), 58-61.

Mikula, S., Stone, J. M., & Jones, E. G. (2008). BrainMaps.org - Interactive High-Resolution Digital Brain Atlases and Virtual Microscopy. *Brains Minds Media, 3*, bmm1426.

Mikula, S., Trotts, I., Stone, J. M., & Jones, E. G. (2007). Internet-enabled high-resolution brain mapping and virtual microscopy. *Neuroimage, 35*(1), 9-15.

Munro, S., Thomas, K. L., & Abu-Shaar, M. (1993). Molecular characterization of a peripheral receptor for cannabinoids. *Nature, 365*(6441), 61-65.

Murataeva, N., Li, S., Oehler, O., Miller, S., Dhopeshwarkar, A., Hu, S. S., . . . Straiker, A. (2015). Cannabinoid-induced chemotaxis in bovine corneal epithelial cells. *Invest Ophthalmol Vis Sci, 56*(5), 3304-3313.

Murayama, K., & Sieving, P. (1992). Different rates of growth of monkey and human photopic a-, b-, and d-waves suggest two sites of ERG light adaptation. *Clin Vision Sci, 7*(5), 385-392.

Nagata, M. (1963). Studies on the photopic ERG of the human retina. *Jpn J Ophthalmol, 7*, 96-124.

Nucci, C., Bari, M., Spano, A., Corasaniti, M., Bagetta, G., Maccarrone, M., & Morrone, L. A. (2008). Potential roles of (endo)cannabinoids in the treatment of glaucoma: from intraocular pressure control to neuroprotection. *Prog Brain Res, 173*, 451-464.

Ohiorhenuan, I. E., Mechler, F., Purpura, K. P., Schmid, A. M., Hu, Q., & Victor, J. D. (2014). Cannabinoid neuromodulation in the adult early visual cortex. *PLoS One, 9*(2), e87362.

Okano, T., Kojima, D., Fukada, Y., Shichida, Y., & Yoshizawa, T. (1992). Primary Structures of Chicken Cone Visual Pigments - Vertebrate Rhodopsins Have Evolved out of Cone Visual Pigments. *Proc Natl Acad Sci U S A, 89*(13), 5932-5936.

Osterberg, G. (1935). Topography of the layer of rods and cones in the human retina. *Actaophthal. suppi., 6*, 11-97.

Pagotto, U., Marsicano, G., Cota, D., Lutz, B., & Pasquali, R. (2006). The emerging role of the endocannabinoid system in endocrine regulation and energy balance. *Endocr Rev, 27*(1), 73-100.

Palmour, R. M., Mulligan, J., Howbert, J. J., & Ervin, F. (1997). Of monkeys and men: vervets and the genetics of human-like behaviors. *Am J Hum Genet, 61*(3), 481-488.

Peachey, N. S., Alexander, K. R., Fishman, G. A., & Derlacki, D. J. (1989). Properties of the human cone system electroretinogram during light adaptation. *Appl Opt, 28*(6), 1145-1150.

Perkonigg, A., Goodwin, R. D., Fiedler, A., Behrendt, S., Beesdo, K., Lieb, R., & Wittchen, H. U. (2008). The natural course of cannabis use, abuse and dependence during the first decades of life. *Addiction, 103*(3), 439-449.

Pinar-Sueiro, S., Rodriguez-Puertas, R., & Vecino, E. (2011). [Cannabinoid applications in glaucoma]. *Arch Soc Esp Oftalmol, 86*(1), 16-23.

Piomelli, D. (2003). The molecular logic of endocannabinoid signalling. *Nat Rev Neurosci, 4*(11), 873-884.

Piomelli, D., Beltramo, M., Glasnapp, S., Lin, S. Y., Goutopoulos, A., Xie, X. Q., & Makriyannis, A. (1999). Structural determinants for recognition and translocation by the anandamide transporter. *Proc Natl Acad Sci U S A, 96*(10), 5802-5807.

Porcella, A., Casellas, P., Gessa, G. L., & Pani, L. (1998). Cannabinoid receptor CB1 mRNA is highly expressed in the rat ciliary body: implications for the antiglaucoma properties of marihuana. *Mol Brain Res, 58*(1-2), 240-245.

Purves, D., Augustine, G. J., Fitzpatrick, D., Hall, W. C., Lamantia, A.-S., Mcnamara, J. O., & Williams, S. M. (2005). *Neurosciences*. (Traduit par J.-M. Coquery, 3^{e} éd.). De Boeck Supérieur.

Rafaelsen, O. J., Bech, P., Christiansen, J., Christrup, H., Nyboe, J., & Rafaelsen, L. (1973). Cannabis and Alcohol: Effects on Simulated Car Driving. *Science, 179*(4076), 920-923.

Rangaswamy, N. V., Frishman, L. J., Dorotheo, E. U., Schiffman, J. S., Bahrani, H. M., & Tang, R. A. (2004). Photopic ERGs in patients with optic neuropathies: comparison with primate ERGs after pharmacologic blockade of inner retina. *Invest Ophthalmol Vis Sci, 45*(10), 3827-3837.

Reymond, L. (1987). Spatial visual acuity of the falcon, Falco berigora: a behavioural, optical and anatomical investigation. *Vision Res, 27*(10), 1859-1874.

Richardson, G. A., Day, N. L., & Goldschmidt, L. (1995). Prenatal Alcohol, Marijuana, and Tobacco Use - Infant Mental and Motor Development. *Neurotoxicol Teratol, 17*(4), 479-487.

Rodríguez de Fonseca, F., Carrera, M. R., Navarro, M., Koob, G. F., & Weiss, F. (1997). Activation of corticotropin-releasing factor in the limbic system during cannabinoid withdrawal. *Science, 276*(5321), 2050-2054.

Rodríguez de Fonseca, F., Navarro, M., Gómez, R., Escuredo, L., Nava, F., Fu, J., . . . Piomelli, D. (2001). An anorexic lipid mediator regulated by feeding. *Nature, 414*(6860), 209-212.

Rosolen, S. G., Rigaudiere, F., LeGargasson, J. F., Chalier, C., Rufiange, M., Racine, J., . . . Lachapelle, P. (2004). Comparing the photopic ERG i-wave in different species. *Vet Ophthalmol, 7*(3), 189-192.

Rousseau, S., McKerral, M., & Lachapelle, P. (1996). The i-wave: bridging flash and pattern electroretinography. *Electroencephalogr Clin Neurophysiol Suppl, 46*, 165-171.

Russo, E. B. (2008). Cannabinoids in the management of difficult to treat pain. *Ther Clin Risk Manag, 4*(1), 245-259.

Ryberg, E., Larsson, N., Sjogren, S., Hjorth, S., Hermansson, N. O., Leonova, J., . . . Greasley, P. J. (2007). The orphan receptor GPR55 is a novel cannabinoid receptor. *Br J Pharmacol, 152*(7), 1092-1101.

Sabbah, S., Laria, R. L., Gray, S. M., & Hawryshyn, C. W. (2010). Functional diversity in the color vision of cichlid fishes. *BMC Biol, 8*, 133.

Sampath, A. P., & Rieke, F. (2004). Selective transmission of single photon responses by saturation at the rod-to-rod bipolar synapse. *Neuron, 41*(3), 431-443.

Sarthy, V., & Ripps, H. (2006). *The Retinal Müller Cell: Structure and Function*. Springer US.

Savinainen, J. R., & Laitinen, J. T. (2004). Detection of cannabinoid CB1, adenosine A1, muscarinic acetylcholine, and GABA(B) receptor-dependent G protein activity in transducin-deactivated membranes and autoradiography sections of rat retina. *Cell Mol Neurobiol, 24*(2), 243-256.

Schlicker, E., & Kathmann, M. (2001). Modulation of transmitter release via presynaptic cannabinoid receptors. *Trends Pharmacol Sci, 22*(11), 565-572.

Schlicker, E., Timm, J., & Gothert, M. (1996). Cannabinoid receptor-mediated inhibition of dopamine release in the retina. *Naunyn Schmiedebergs Arch Pharmacol, 354*(6), 791-795.

Schmidl, D., Schmetterer, L., Garhofer, G., & Popa-Cherecheanu, A. (2015). Pharmacotherapy of glaucoma. *J Ocul Pharmacol Ther, 31*(2), 63-77.

Schwitzer, T., Schwan, R., Angioi-Duprez, K., Ingster-Moati, I., Lalanne, L., Giersch, A., & Laprevote, V. (2015). The cannabinoid system and visual processing: a review on experimental findings and clinical presumptions. *Eur Neuropsychopharmacol, 25*(1), 100-112.

Seiple, W., & Holopigian, K. (1994). The 'OFF' response of the human electroretinogram does not contribute to the brief flash 'b-wave'. *Vis Neurosci, 11*(4), 667-673.

Stamer, W. D., Golightly, S. F., Hosohata, Y., Ryan, E. P., Porter, A. C., Varga, E., . . . Yamamura, H. I. (2001). Cannabinoid CB(1) receptor expression, activation and detection of endogenous ligand in trabecular meshwork and ciliary process tissues. *Eur J Pharmacol, 431*(3), 277-286.

Straiker, A., Stella, N., Piomelli, D., Mackie, K., Karten, H. J., & Maguire, G. (1999a). Cannabinoid CB1 receptors and ligands in vertebrate retina: localization and function of an endogenous signaling system. *Proc Natl Acad Sci U S A, 96*(25), 14565-14570.

Straiker, A. J., Maguire, G., Mackie, K., & Lindsey, J. (1999b). Localization of cannabinoid CB1 receptors in the human anterior eye and retina. *Invest Ophthalmol Vis Sci, 40*(10), 2442-2448.

Sun, W., Wang, L., Li, S., Tie, X., & Jiang, B. (2015). Layer-specific endocannabinoid-mediated long-term depression of GABAergic neurotransmission onto principal neurons in mouse visual cortex. *Eur J Neurosci, 42*(3), 1952-1965.

Tamm, E. R., Schmetterer, L., & Grehn, F. (2013). Status and perspectives of neuroprotective therapies in glaucoma: the European Glaucoma Society White Paper. *Cell Tissue Res, 353*(2), 347-354.

Tanda, G., & Goldberg, S. R. (2003). Cannabinoids: reward, dependence, and underlying neurochemical mechanisms--a review of recent preclinical data. *Psychopharmacology (Berl), 169*(2), 115-134.

Vincent, A., Robson, A. G., & Holder, G. E. (2013). Pathognomonic (diagnostic) ERGs. A review and update. *Retina, 33*(1), 5-12.

Viswanathan, S., Frishman, L. J., Robson, J. G., & Walters, J. W. (2001). The photopic negative response of the flash electroretinogram in primary open angle glaucoma. *Invest Ophthalmol Vis Sci, 42*(2), 514-522.

Warrier, A., & Wilson, M. (2007). Endocannabinoid signaling regulates spontaneous transmitter release from embryonic retinal amacrine cells. *Vis Neurosci, 24*(1), 25-35.

Wässle, H. (2004). Parallel processing in the mammalian retina. *Nat Rev Neurosci, 5*(10), 747-757.

Weber, B., & Schlicker, E. (2001). Modulation of dopamine release in the guinea-pig retina by Gi- but not by Gs- or Gq-protein-coupled receptors. *Fundam Clin Pharmacol, 15*(6), 393-400.

Woods, R. P., Fears, S. C., Jorgensen, M. J., Fairbanks, L. A., Toga, A. W., & Freimer, N. B. (2011). A web-based brain atlas of the vervet monkey, Chlorocebus aethiops. *Neuroimage, 54*(3), 1872-1880.

Yazulla, S. (2008). Endocannabinoids in the retina: from marijuana to neuroprotection. *Prog Retin Eye Res, 27*(5), 501-526.

Yazulla, S., Studholme, K. M., McIntosh, H. H., & Deutsch, D. G. (1999). Immunocytochemical localization of cannabinoid CB1 receptor and fatty acid amide hydrolase in rat retina. *J Comp Neurol, 415*(1), 80-90.

Yazulla, S., Studholme, K. M., McIntosh, H. H., & Fan, S. F. (2000). Cannabinoid receptors on goldfish retinal bipolar cells: electron-microscope immunocytochemistry and whole-cell recordings. *Vis Neurosci, 17*(3), 391-401.

Yoneda, T., Kameyama, K., Esumi, K., Daimyo, Y., Watanabe, M., & Hata, Y. (2013). Developmental and visual input-dependent regulation of the CB1 cannabinoid receptor in the mouse visual cortex. *PLoS One, 8*(1), e53082.

Young, B., Eggenberger, E., & Kaufman, D. (2012). Current electrophysiology in ophthalmology: a review. *Curr Opin Ophthalmol, 23*(6), 497-505.

Zabouri, N., Bouchard, J. F., & Casanova, C. (2011a). Cannabinoid receptor type 1 expression during postnatal development of the rat retina. *J Comp Neurol, 519*(7), 1258-1280.

Zabouri, N., Ptito, M., Casanova, C., & Bouchard, J. F. (2011b). Fatty acid amide hydrolase expression during retinal postnatal development in rats. *Neuroscience, 195*, 145-165.

Zangenehpour, S., Javadi, P., Ervin, F. R., Palmour, R. M., & Ptito, M. (2014). A deficit in face-voice integration in developing vervet monkeys exposed to ethanol during gestation. *PLoS One, 9*(12), e114100.

Zhang, K., Zhang, L., & Weinreb, R. N. (2012). Ophthalmic drug discovery: novel targets and mechanisms for retinal diseases and glaucoma. *Nat Rev Drug Discov, 11*(7), 541-559.

ANNEXE I : THE GATEWAY TO THE BRAIN : DISSECTING THE PRIMATE EYE

Publié dans :

Burke M, Zangenehpour S, **Bouskila J**, Boire D, Ptito M (2009) The gateway to the brain: dissecting the primate eye. J Vis Exp e1261

The Gateway to the Brain: Dissecting the Primate Eye

Mark Burke[1], Shahin Zangenehpour[2], Joseph Bouskila[2], Denis Boire[3], Maurice Ptito[2]

[1]Department of Physiology, Universite de Montreal - University of Montreal

[2]School of Optometry, Universite de Montreal - University of Montreal

[3]Departement de chimie-biologie, Universite du Quebec a Trois-Rivieres

Abstract

The visual system in humans is considered the gateway to the world and plays a principal role in the plethora of sensory, perceptual and cognitive processes. It is therefore not surprising that quality of vision is tied to quality of life. Despite widespread clinical and basic research surrounding the causes of visual disorders, many forms of visual impairments, such as retinitis pigmentosa and macular degeneration, lack effective treatments. Non-human primates have the closest general features of eye development to that of humans. Not only do they have a similar vascular anatomy, but amongst other mammals, primates have the unique characteristic of having a region in the temporal retina specialized for high visual acuity, the fovea[1]. Here we describe a general technique for dissecting the primate retina to provide tissue for retinal histology, immunohistochemistry, laser capture microdissection, as well as light and electron microscopy. With the extended use of the non-human primate as a translational model, our hope is that improved understanding of the retina will provide insights into effective approaches towards attenuating or reversing the negative impact of visual disorders on the quality of life of affected individuals.

Protocol

Part 1: Pre-processing of tissue

Tissue should be well perfused with paraformaldehyde, glutaraldehyde, or formalin. This can be achieved through standard transcardial perfusion typically used to harvest other organs. It is recommended that shortly after sacrifice the eyes be injected with fixative just under the lens and stored in fixative.

In the present study the subject was deeply sedated with ketamine hydrochloride (10 mg/kg, i.m.), euthanized with an overdose of sodium pentobarbital (25 mg/kg, i.v.) and perfused transcardially with 0.1 M PBS until completely exsanguinated. This is followed by a 4% paraformaldehyde solution in PBS for 5 min (~1 liter).

Part 2: Removal of the eyeball from the orbital cavity

For easier access to the eyeball it is recommended to first remove the brain. Once the brain has been removed the thin-walled orbit bone is readily apparent. Use the bone rongeurs to slowly chip away the wall of the orbit. Cut away the ocular muscles with a scalpel and remove the connective tissue from the eyeball. Carefully cut the optic nerve, this can be used in electronic microscopy studies. The eyeball should now be released from the orbital cavity.

Part 3: Dissect the retina from the eyecup

Place the eye into a Petri dish with PBS to keep the retina from drying. A dissecting microscope or table mounted magnifying light stand is useful in the dissection, but not a necessity. Remove the cornea by cutting the sclera closely to the perimeter of the cornea at the level of the ora serrata with a pair of spring scissors and remove the lens with the forceps.

Use a paintbrush, forceps, and spring scissors to remove the retina from the sclera. This is done by separating the retina from the sclera and then cutting the sclera away with the scissors. One must carry out this process in small increments so as not to damage or tear the retinal tissue. The sclera is not readily separated from the remnant optic nerve so carefully cut the sclera around the optic nerve.

At this point the retina has retained its curved shape and needs to be flattened for sampling. Before flattening the retina, the vitreous humour, which has the consistency of jelly,

can be removed in a lump. To flatten the retina onto a slide, make several radial cuts with a scalpel blade. The residual vitreous humour can now be removed with ordinary filter paper and a paintbrush. The retinal ganglion cell layer is exposed at this point so it is imperative to be gentle when removing the vitreous humour. If the optic nerve is still attached at the optic disc, remove the optic nerve without ripping the retina using a scalpel blade and a pair of spring scissors. This is now a flat mount retina (Figure 1) and the fovea should be apparent as a dark patch in the temporal/ventral direction from the optic disc.

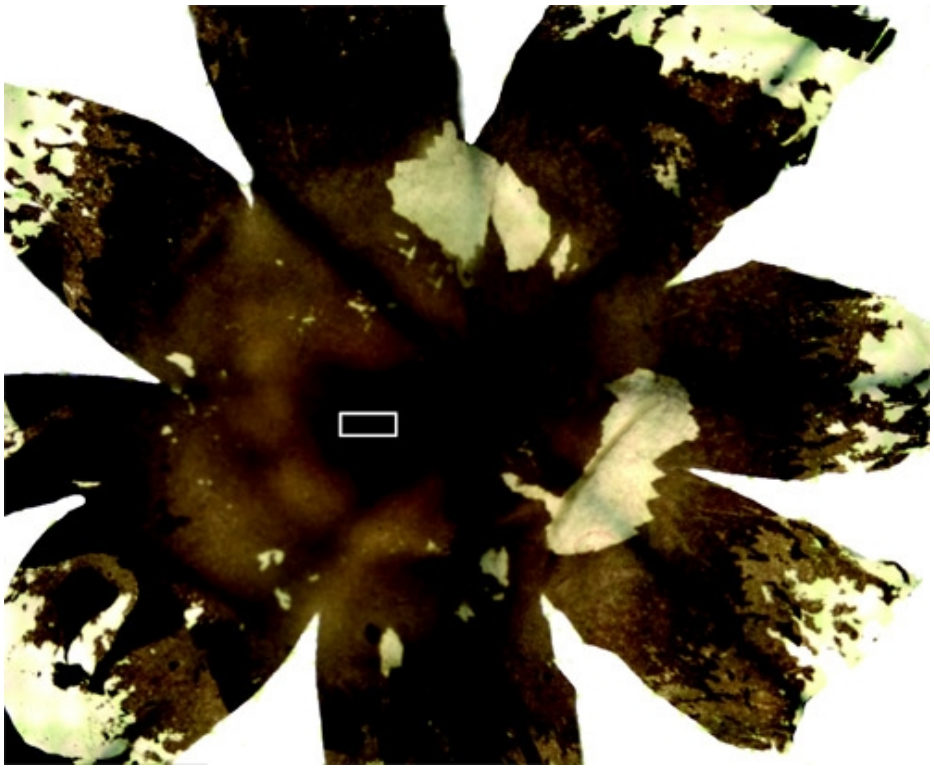

Figure 1. Flatmount Retina. Radial cuts are used to flatten the retina.

Part 4: Sampling

There are a number of options for sampling the retina. Here we will describe the flatmount preparation and isodentric sampling. For both procedures flatmount the retina with the optic fiber layer away from the slide. If the intention is to examine the retinal ganglion cell layer in the flatmount preparation, it is necessary to either remove or bleach the pigmented epithelium. To remove the pigmented epithelium use a paintbrush lightly to remove some of

this layer, this tends to damage the photoreceptor layer. Bleaching involves soaking the retina in potassium permanganate solution (0.25%) for 1 hour, washing in distilled water, and clearing in oxalic acid (5%) for 5 minutes[2].

If the intention is to examine cell distribution and morphology of each layer throughout the retina, then we suggest isometric sampling of the retina. The retina should be flatmounted on a slide and kept moist with PBS. For isometric sampling cut small pieces of tissue equidistant from the optic disc in the nasal, temporal, upper and lower directions (Figure 1). It is not necessary to bleach the pigmented epithelium in this preparation. These pieces can now be sectioned in the coronal plane with a cryostat, vibratome, or ultramicrotome depending on the research question. For cryostat sectioning, the pieces should be cryoprotected in 30% sucrose overnight and frozen in the context of a mounting medium on dry ice. Alternatively, the samples can be embedded in agar and sliced on a vibratome. The cryostat and vibratome preparations will reliably yield sections as thin as 4 μm. If thinner sections are required (e.g. for electron microscope preparation), it is necessary to prepare the samples for the ultramicrotome. To do this, the sections should be post-fixed in osmium tetroxide for 1 hour under the fumehood. This is followed by dehydration in a graded ethanol series (50, 70, 95, 95, 100, 100%) and 100% propylene oxide. The tissue is then embedded in Epon (EMBed-812 embedding kit).

Part 5: Representative Results:

In our laboratory, we routinely perform immunohistochemistry on cryosectioned retinae (Figure 2). In this case we are interested in the isodensity of cannabinoid receptors (CB1) in the primate retina. We also examine the effects of prenatal ethanol exposure on the primate visual system. To this end, we are interested in cell density and layer thickness in the fovea and in the peripheral retina. To accomplish this, we embed pieces of retina in Epon, slice at 700nm on an ultramicrotome, and stain with 1% toluidine blue (Figure 3).

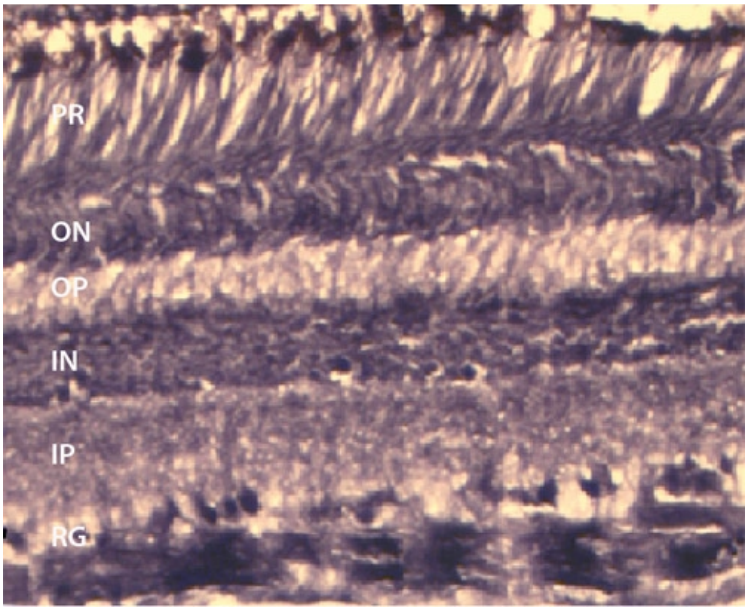

Figure 2. Immunostaining. Cryosection of peripheral retina immunostained for CB1 where the retinal ganglion cells are heavily labeled with some labeling in the inner and outer nuclear layers. The thickness of this section is 14 µm and stained on the slide. RG - retinal ganglion layer; IP - inner plexiform layer; IN - inner nuclear layer; OP - outer plexiform layer; ON - outer nuclear layer.

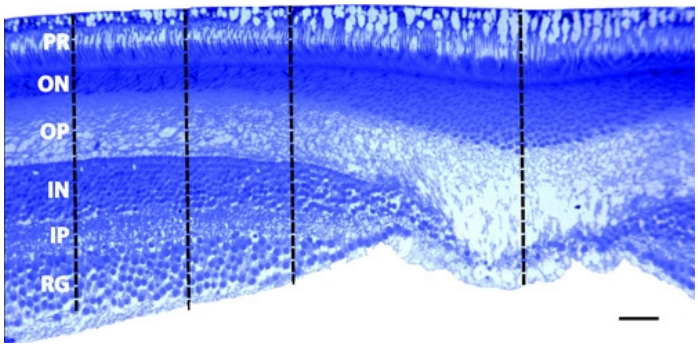

Figure 3. Fovea. Section through the fovea that was embedded in Epon and sliced on an ultramicrotrome at 700 nm. The photoreceptor layer (PR) was used to align the sections. Notice that the entire extent of the photoreceptors can be identified indicating an appropriate angle in the coronal plane. Density measurements were taken at 300 nm, 500 nm, and 800 nm from the center of the foveal pit using the Bioquant Imaging system. RG - retinal ganglion layer; IP - inner plexiform layer; IN - inner nuclear layer; OP - outer plexiform layer; ON - outer nuclear layer; scale bar = 50 µm.

Discussion

The preparation of the retina as a wholemount allows for the analysis of the topography and spatial distribution of either the ganglion cell layer or the endothelial cells of the retinal blood vessels[3]. Quantification of cell density in the periphery of primate retina is readily accomplished. however, in perifoveal and foveal regions, the stacking of multiple layers in the ganglion cell layer obstructs quantification. To circumvent this potential bias, the fovea and perifoveal region can be dissected from the wholemount preparation, embedded in Epon, and serially sectioned using an ultramicrotome to obtain semi-thin sections in the coronal plane[2,4]. There are a number of other disadvantages to the wholemount preparation, which can be overcome with alternative sampling paradigms.

Taking isometric samples from the retina and sectioning in the coronal plane on either a cryostat or vibratome allows for specific examination of the different layers, which cannot be readily performed on a wholemount preparation. Sectioning in this manner also allows for the application of multiple immnohistochemistry protocols[5]. These sections can then be removed from the slide, embedded in Epon and sliced on an ultramicrotome. With an ultramicrotome minor changes in the cutting angle can be made to ensure a standard coronal plane through the photoreceptors. Once a standard plane has been obtained, layer thickness can be measured and compared between retinal regions and subjects. Furthermore, Epon embedded tissue can be used in electron microscopy studies to reveal ultrastructural characteristics of the retina[6].

Acknowledgments

The authors would like to thank Ikiel Ptito for his technical support. We are grateful to Frank Ervin, Roberta Palmour and the staff of Behavioural Sciences Foundation Laboratories located in St Kitts, West Indies, for their continued support of our primate work.

References

1. Hendrickson, A., Kupfer, C. The histogenesis of the fovea in the macaque monkey. Invest Ophthalmol Vis Sci 15, 746-756 (1976).

2. Herbin, M., Boire, D., Ptito, M. Size and distribution of retinal ganglion cells in the St. Kitts green monkey (Cercopithecus aethiops sabeus). J Comp Neurol. 383, 459-472, (1997).

3. Stone, J. The Wholemount Handbook. Maitland Publishing Pty. Ltd., Sydney, (1981).

4. Herbin, M., Boire, D., Theoret, H., Ptito, M. Transneuronal degeneration of retinal ganglion cells in early hemispherectomized monkeys. Neuroreport. 10, 1447-1452, (1999).

5. Krebs, W., Krebs, I. Primate Retina and Choroid Atlas of Fine Structure in Man and Monkey. Springer-Verlag New York, (1991).

6. Pow, D., Sullivan, R. Nuclear kinesis, neurite sprouting and abnormal axonal projections of cone photoreceptors in the aged and AMD-afflicted human retina. Exp Eye Res. 84, 850-857, (2007).

ANNEXE II : THE ENDOCANNABINOID SYSTEM WITHIN THE DORSAL LATERAL GENICULATE NUCLEUS OF THE VERVET MONKEY

Publié dans :

Javadi P, **Bouskila J**, Bouchard JF, Ptito M (2015) The endocannabinoid system within the dorsal lateral geniculate nucleus of the vervet monkey. Neuroscience 288:135-144.

The endocannabinoid system within the dorsal lateral geniculate nucleus of the vervet monkey

Pasha Javadi[1], Joseph Bouskila[1, 2], Jean-François Bouchard[1], and Maurice Ptito[1, 3, 4]

[1]School of Optometry, University of Montreal, Montreal, QC, Canada

[2]Biomedical Sciences, Faculty of Medicine, University of Montreal, Montreal, QC, Canada

[3]BRAINlab, Department of Neuroscience and Pharmacology, University of Copenhagen, Copenhagen, Denmark

[4]Laboratory of Neuropsychiatry, Psychiatric Centre Copenhagen and Department of Neuroscience and Pharmacology, University of Copenhagen, DK-2100 Copenhagen, Denmark

Running title: eCB system expression in the monkey dLGN

Correspondence should be addressed to:

Maurice Ptito, PhD

School of Optometry, room 260-7

3744 Jean-Brillant Street,

University of Montreal,

Montreal, Quebec, Canada, H3T 1P1

Keywords: CB1R, FAAH, NAPE-PLD, dLGN, Monkey, Cannabinoid receptors.

Abbreviation: AEA, anandamide; CB1R, cannabinoid receptor CB1; DAB, 3,3'-Diaminobenzidine; DAGL, diacylglycerol lipase enzyme; dLGN, dorsal lateral geniculate nucleus; eCB, endocannabinoid; ERG, electroretinogram; FAAH, fatty acid amide hydrolase; GABA, GABAergic cell; GFAP, glial fibrillary acidic protein; IR, immunoreactivity; MAGL, monoglycerol lipase; MT, middle temporal; MST, medial superior temporal; NAE, N-acylethanolamines; NAPE, N-acyl-phosphatidylethanolamine; NAPE-PLD, N-acyl-phosphatidylethanolamine phospholipase D; NDS, normal donkey serum ; PBS, phosphate-buffered saline; SEM*, standard error* of the mean; SC, superior colliculus; VGLUT1, vesicular glutamate transporter 1; 2-AG, 2-arachidonoylglycerol.

Abstract

The endocannabinoid system mainly consists of cannabinoid receptors type 1 (CB1R) and type 2 (CB2R), their endogenous ligands termed endocannabinoids (eCBs), and the enzymes responsible for the synthesis and degradation of eCBs. These cannabinoid receptors have been well characterized in rodent and monkey retinae. Here, we investigated the expression and localization of the eCB system beyond the retina, namely the first thalamic relay, the dorsal lateral geniculate nucleus (dLGN), of vervet monkeys using immunohistochemistry methods. Our results show that CB1R is expressed throughout the dLGN with more prominent labeling in the magnocellular layers. The same pattern is observed for the degradation enzyme, fatty acid amide hydrolase (FAAH). However, the synthesizing enzyme N-acyl-phosphatidylethanolamine phospholipase D (NAPEPLD) is expressed homogenously throughout the dLGN with no preference for any of the layers. These proteins are weakly expressed in the koniocellular layers. These results suggest that the presence of the eCB system throughout the layers of the dLGN may represent a novel site of neuromodulatory action in normal vision. The larger amount of CB1R in the dLGN magnocellular layers may explain some of the behavioral effects of cannabinoids associated with the integrity of the dorsal visual pathway that plays a role in visual-spatial localization and motion perception.

Introduction

The physiological and psychological effects of phytocannabinoids, the active components of the cannabis plant, can be detected almost everywhere in the body due to their actions on specific receptors: mainly the cannabinoid receptors type 1 (CB1R) and type 2 (CB2R). Cannabinoid receptors are membrane receptors principally coupled to inhibitory G-proteins that modulate the release of neurotransmitters (Piomelli, 2003 and Gómez-Ruiz et al., 2007). They mediate biological functions not only via the exogenous cannabinoids, but also via eCBs such as N-arachidonoylethanolamide (anandamide or AEA) and 2-arachidonoylglycerol (2-AG). Unlike the classical neurotransmitters, eCBs are synthesized "on demand" by catalyzing the release of N-acylethanolamines (NAEs) from N-acyl-phosphatidylethanolamine (NAPE) by specific enzyme, like N-acyl-phosphatidylethanolamine phospholipase D (NAPE-PLD) or from arachidonic acid via diacylglycerol lipase enzyme (DAGL). The eCBs are not accumulated into synaptic vesicles and are rather degraded rapidly by specific enzymes like fatty acid amid hydrolase (FAAH) and monoglycerol lipase (MAGL) (for review, see Deutsch and Chin, 1993).

The localization and function of the molecular components of the eCB system in the central nervous system have been the subject of recent research. In fact, the role of the eCB system in learning, memory, neuroprotection and visual processing is essentially due to the modulation of neurotransmitter release by the presynaptic location of CB1R (Di Marzo et al., 1998 and Straiker et al., 1999a). CB1R expression is found in the hippocampus, prefrontal cortex, cerebellum and basal ganglia of rodents (Herkenham et al., 1991) and primates (Eggan and Lewis, 2007). It is expressed in glutamatergic and GABAergic neurons throughout the central and peripheral nervous systems (Egertová and Elphick, 2000). In the visual system, CB1R and FAAH have been localized in cone photoreceptors, horizontal, amacrine, bipolar, and retinal ganglion cells in the central and peripheral retina of vervet monkeys (Bouskila et al., 2012). CB1R is also found in the human retina (Straiker et al., 1999b).

Earlier studies reported that cannabis could affect several visual functions, such as photosensitivity (Adams et al., 1978), visual acuity (Moskowitz et al., 1972 and Adams and Brown, 1975), color vision (Dawson et al., 1977), ocular tracking (Flom et al., 1976), binocular depth inversion, and stereoscopic vision (Emrich et al., 1991, Leweke et al., 1999

and Semple et al., 2003). Some case studies later claimed other visual effects of cannabis such as visual distortions, altered perception of distance, illusions of movement in stationary and moving objects, color intensification of objects, dimensional distortion and blending of patterns and objects (Levi and Miller, 1990 and Lerner et al., 2011). Given the localization of CB1R in the central retina, from cones to ganglion cells, it is reasonable to assume its implication in these visual manifestations.

In homogenates of rodent thalamus, high levels of AEA (Felder et al., 1996) and FAAH (Egertová et al., 2003), as well as an elevated cannabinoid receptor/G-protein amplification ratio (Breivogel et al., 1997) have been found. Also, using immunohistochemistry, moderate to low levels of CB1R expressions have been found in the thalamus of rats (Egertová et al., 1998, Tsou et al., 1998 and Moldrich and Wenger, 2000), non-human primates (Ong and Mackie, 1999) and humans (Glass et al., 1997) without focusing on dorsal lateral geniculate nucleus (dLGN). However, there is no study, to our knowledge, that has thoroughly studied the expression of the eCB system in this retino-recipient primary thalamic relay of the primate. Similar to apes and humans, the dLGN of vervet monkeys consists of six layers. The first two ventral layers, the magnocellular layers, receive input from large ganglion cells (rod signals) and are necessary for the perception of movement, depth and small difference in brightness. The four dorsal layers, parvocellular layers, receive input from small ganglion cells of the retina (cone signals) and play a role in color and form perception. These layers are well separated by an inter-laminar zone called koniocellular layers that contribute to short-wavelength “blue” cones (Xu et al., 2001). Given the expression and localization of CB1R in the retinal mosaic, we expect to find this receptor in the optic nerve and the dLGN layers.

Experimental procedures

Animals. Monkey tissues were obtained from four adult vervet monkeys (*Chlorocebus sabaeus*). The monkeys were part of Dr. Ptito's and Dr. Palmour's research project that was approved by McGill University Animal Care and Use Committee. The animals were born and raised under an enriched natural environment in the laboratories of the Behavioral Sciences Foundation (St-Kitts, West Indies), a facility recognized by the Canadian Council on Animal Care (CCAC). The experimental protocol was reviewed and approved by the local Animal Care and Use Committee (University of Montreal) and the Institutional Review Board of the Behavioral Science Foundation.

Tissue preparation. Each animal was sedated with ketamine hydrochloride (10 mg/kg, i.m.) and euthanized by an overdose of intravenously administered sodium pentobarbital (25 mg/kg), followed by transcardial perfusion of 0.1 M phosphate-buffered saline (PBS) (pH 7.4). The brains were then removed, blocked and flash-frozen in an isopentane bath cooled in a dry ice chamber and maintained at −80 °C. The blocks were cut along the coronal plane in 20-µm sections at −18 °C on a Leica CM3050S cryostat and mounted onto gelatinized subbed glass slides. The slide-mounted tissue sections were stored at −80 °C until further histological processing.

Immunohistochemistry (DAB). At least one slide-mounted 20-µm fresh-frozen tissue section per animal was selected from A6 to A9, at a level where the lamination of the dLGN is the clearest and thawed at room temperature. A hydrophobic barrier was created surrounding the slides, using PAP pen (Vector, Burlingame, CA, USA) to keep staining reagents localized on the tissue section. Sections were fixed with 70% ethanol solution for 15 min, followed by two 5-min rinses with 0.1 M Tris buffer, pH 7.4/0.03% Triton X-100. To block the endogenous peroxidase activity, sections were washed with 0.3% hydrogen peroxide in PBS for 15 min. Following three times 5-min PBS-triton rinse, sections were blocked for 60 min with a solution of 10% normal donkey serum (NDS) and 0.1 M Tris buffer/0.5% Triton. Each section was incubated overnight at room temperature with primary antibodies (Table 1) diluted in the blocking solution. The next day, sections underwent three 10-min PBS-triton washes, followed by incubation in a secondary antibody solution (biotinylated donkey anti-rabbit antibody diluted 1:200 in blocking solution) for 2 h. After three consecutive 10-min washes

with PBS-triton, the sections were incubated for 1 h in an avidin–biotin-conjugated horseradish peroxidase (Vectastain ABC kit, Burlingame, CA, USA) solution (1:500). Following three subsequent 10-min washes in PBS-triton, the sections were treated with a 3,3′-diaminobenzidine (DAB) substrate. After rinsing in PBS-triton three times for 5 min each, sections underwent dehydration in graded ethanol steps, cleared in xylene, and cover-slipped with Permount mounting media (Fisher Scientific; Pittsburgh, PA, USA). Sections were examined on a Leica DMRB under bright field illumination.

Immunofluorescence. Double and triple labeling of the brain tissues were performed according to previously published methods on the vervet monkey retina (Bouskila et al., 2012, Bouskila et al., 2013a and Bouskila et al., 2013b). Briefly, sections were post-fixed for 15 min in 70% ethanol, rinsed two times for 5 min in 0.1 M Tris buffer, pH 7.4/0.03% Triton and blocked for 90 min in 10% NDS and 0.1 M Tris buffer/0.5% Triton. Sections were incubated overnight at room temperature with primary antibodies in blocking solution. The antibodies directed against molecular eCB components all raised in rabbit were used conjointly with a known cell marker: glial fibrillary acidic protein (GFAP) (astrocytes marker), vesicular glutamate transporter 1 (VGLUT1) (glutamatergic cell marker) and GABA (GABAergic cell marker) (Table 1). The next day, sections were washed for 10-min and two times for 5 min in 0.1 M Tris/0.03% Triton and incubated with biotinylated donkey anti-rabbit diluted 1:200 in blocking solution for 2 h for the eCB targets to amplify the signals. Sections were then incubated for another 2 h with streptavidin 647 in order to amplify the signal and alexa 555 or 488 secondary antibodies when necessary. Sections were cover-slipped with Fluoromount-G™ Mounting Medium (SouthernBiotech, Birmingham, AL, USA) after 3 × 10 min washes with 0.1 M Tris buffer. In the case of the GABA antibody, the sections had to be fixed in PFA 4% and glutaraldehyde 1%. The GABA signals were amplified with biotinylated donkey anti-mouse and the cannabinoid signals with donkey anti rabbit HRP and alexa fluor tyramide (Invitrogen, Eugene, Oregon).

Antibody characterization

The source and working dilution of all primary antibodies used in this study are summarized in Table 1. The antibodies with the exception of NAPE-PLD were successfully used in previous studies and were well characterized in the vervet monkey (Bouskila et al., 2012).

Antibody	Immunogen	Source	Working dilution
CB1R	Fusion protein containing aa 1–77 of rat CB1R	Sigma, St. Louis, MO C1233, Rabbit polyclonal	H: 1:200
FAAH	Synthetic peptide aa 561–579 of rat FAAH	Cayman Chemical, Ann Arbor, MI, 101600, rabbit polyclonal	H: 1:200
NAPE-PLD	Synthetic peptide aa 159–172 of human NAPE-PLD	Cayman Chemical, Ann Arbor, MI, 10305, rabbit, polyclonal	H: 1:200
GFAP	Purified protein isolated from pig spinal cord	Sigma-Aldrich, St. Louis, MO, G3893, mouse, G-A-5, monoclonal	H: 1:200
VGLUT1	Fusion protein containing aa 456–560 of rat VGLUT1	Synaptic System, Goettingen, Germany,135 311, mouse, 317D5 monoclonal	H: 1:200
GABA	Fusion Protein coupling to BSA with glutaraldehyde	Millipore, MA, MAB316, Monoclonal	H: 1:200

Table 1. Primary antibodies used in this study.

CB1R. The rabbit anti-CB1R (Calbiochem, Gibbstown, NJ, USA) was developed using a highly purified fusion protein with the first 77 amino acid residues of rat CB1R. According to the manufacturer's data sheet, it recognizes a major band of 60 kDa with also less intense bands of 23, 72, and 180 kDa. This antibody was shown to be specific using CB1R knockout mouse retinal tissue (Zabouri et al., 2011). It recognizes the CB1R (60 kDa) from many species, including the vervet monkey tissues (Bouskila et al., 2012).

GFAP. The mouse anti-glial fibrillary acidic protein (GFAP, Clone G-A-5, Sigma–Aldrich, St. Louis, MO, USA) was produced using purified GFAP isolated from the pig spinal cord. This antibody recognizes the GFAP protein of 50 kDa in Western blots (manufacturer's data sheet). GFAP stains cells with the morphology and distribution expected for astrocytes in monkey dLGN (Takahata et al., 2010).

FAAH. The rabbit anti-fatty acid amide hydrolase (FAAH, Cayman Chemical, Ann Arbor, MI, USA) was developed using a synthetic peptide from rat FAAH amino acids 561–

579 (CLRFMREVEQLMTPQKQPS) conjugated to KLH. As expected, it recognizes a dense band at about 66 kDa and a very light one below 37 kDa. The specificity of this antibody has been demonstrated in rat (Suárez et al., 2008 and Zabouri et al., 2011) and vervet monkey (Bouskila et al., 2012) tissues.

NAPE-PLD. The rabbit anti-N-acyl phosphatidylethanolamine-specific phospholipase D (NAPE-PLD, Cayman Chemical, Ann Arbor, MI, USA) was developed using a synthetic peptide from human NAPE-PLD amino acids 159–172 (YMGPKRFRRSPCTI). Its cross reactivity has been tested in many species, and it recognizes an intense band at 46 kDa on Western blot of the human cerebellum (manufacturer's data sheet).

NAPE-PLD blocking peptide. The NAPE-PLD blocking peptide containing the human NAPE-PLD amino acid sequence 159–172 (YMGPKRFRRSPCTI; Cayman Chemical, Ann Arbor, MI, USA) was used in the present study for Western blot analysis. The specificity of the NAPE-PLD antibody was tested by pre-incubation with the corresponding blocking peptide. For pre-adsorption, the primary antibody was diluted in PBS and incubated with a ratio 1:5 for 2 h at room temperature, with occasional inversion. Thereafter, the antibody-blocking peptide solution was added to the blot and subsequent Western blotting followed the protocol as described further.

VGLUT1. The mouse anti-vesicular glutamate transporter 1 (VGLUT1, Synaptic System, Goettingen, Germany) was raised against the aa 456–560 of the rat VGLUT1 protein. It is used as a glutamatergic neuron marker and its specificity has been verified in vglut1 KO mouse tissue (Wojcik et al., 2004) as well as using the corresponding blocking peptide (Zhou et al., 2007).

GABA. The mouse anti-gamma aminobutyric acid antibody (GABA, Millipore, MA, USA) was synthesized coupling to BSA with glutaraldehyde. It is used as a marker of GABAergic neurons. Thus, for the GABA antibody, sections were fixed for 20 min in 1% glutaraldehyde, 4% PFA in PBS. The antibody has been frequently used in different animals, and its specificity has been verified in monkey (Jongen-Relo et al., 1999).

Microscopy. To detect the fluorescence signals, a Leica TCS SP2 confocal laser-scanning microscope (Leica Microsystems, Exton, PA, USA) with 40× (n.a. 1.25–0.75) and

100x (n.a. 1.40–0.7) objectives was used. Subsequently, images were acquired from the green and far-red channels on optical slices of less than 0.9 μm. Adobe Photoshop (CS5; Adobe Systems, San Jose, CA, USA) was used for all photomicrographic adjustments on size, color and shape before exporting them to Adobe InDesign (CS5; Adobe Systems), where the final figure layout was completed. For DAB staining, all photomicrographs were captured with a Leica DMR photomicroscope equipped with a Retiga 1300 video camera system (Q Imaging) using the QCapture software with a Leica 2.5× (n.a. 0.07) objective.

Quantification. In order to enhance the visualization of CB1R spatial distribution throughout the dLGN layers, photomicrographs demonstrating the entire structure were generated in an 8-bit gray scale. Using a MatLab code, the minimum and maximum thresholds of the gray values in the image were measured. The gray spectrum values were then eventually distributed within the RGB spectral subdivision in which the maximum threshold gray values were presented in red and the minimum in blue. Moreover, the average contrast intensity of each layer was calculated using the FIJI program (v. 1.48t, Wayn Rasband, NIH, USA). The program was calibrated using a calibration grid slide. The RGB images were inverted to 8-bit with a linear gray scaling from a minimum to a maximum pixel intensity (arbitrary value 0–255). The mean intensity of four sections (per condition) in their whole magno-, parvo- and koniocellular layers (±SEM) was reported after subtracting the average background intensity.

Results

Spatial expression of the endocannabinoid system in dLGN. To examine the laminar expression of the endocannabinoid system profile in dLGN, tissues were labeled with specific antibodies against CB1R, FAAH, and NAPE-PLD. Their expression pattern in the brain was quantified using heatmap analysis. Immunolabeled sections for CB1R were found throughout the magnocellular and parvocellular layers of the dLGN with a higher intensity in the magnocellular layers (Fig. 1a, d, g). The koniocellular layers had the lowest expression of CB1R (Fig. 1a, d, g). Similar patterns of expression were observed for FAAH (Fig. 1b, e, g). NAPE-PLD was expressed homogenously with no preferences for the magnocellular or parvocellular layers. The koniocellular layers still showed very low expression of the synthesizing enzyme (Fig. 1c, f, g). A consistent staining pattern across all four monkeys dLGN was found. Interestingly, all these three proteins were also highly expressed in the optic nerve (data not shown).

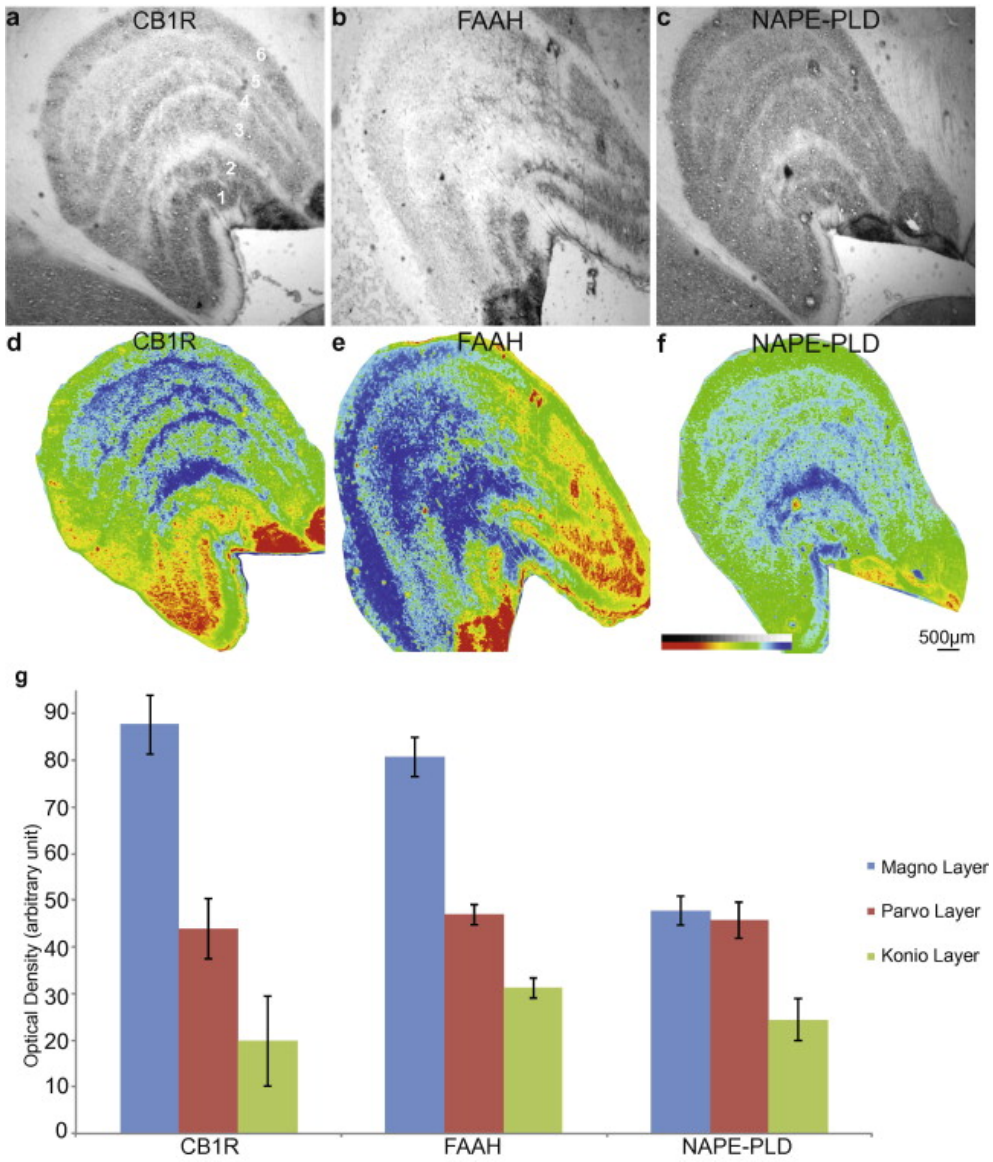

Fig. 1. Spatial distribution of CB1R, FAAH, and NAPE-PLD throughout the dLGN (a–c) of vervet monkeys. The RGB heat map was used to enhance the display of the abundance of the CB1R (d), FAAH (e) and NAPE-PLD (f) in the dLGN. The gray spectrum was distributed within the RGB spectral subdivision in which the maximum threshold gray values were expressed as red and the minimum as blue. CB1R is more expressed within the first two layers of dLGN. FAAH expression pattern is similar to CB1R. The NAPE-PLD expression is similarly distributed throughout the magno and parvo cellular layers. Scale bars = 500 µm. (g) Quantification of the mean contrast intensity of CB1R, FAAH and NAPE-PLD-IR in magno-, parvo- and koniocellular layer. The bars indicate the standard error.

CB1R, FAAH and NAPE-PLD are not present in LGN astrocytes. The double immunostaining was carried out with molecular markers to examine the eCB system expression at the cellular level. Cytosolic spread expression of CB1R is not co-localized with GFAP-positive glial cells (Fig. 2a–f). There is an apparent higher expression of CB1R in the magnocellular layers (Fig. 2a–c) compared to the parvocellular layers (Fig. 2d–f). The very weak expression of this receptor in the koniocellular layers is also evident (Fig. 1g, h). Similarly, FAAH-IR is not detected in astrocytes of magnocellular layer (Fig. 2j–l).

Triple-label immunofluorescence of the CB1R (magenta) and GFAP (green) ... In contrast to the difference in the pattern of expression of NAPE-PLD, the cellular expression of this synthesizing enzyme is similar to that of CB1R and FAAH. NAPE-PLD is also absent in astrocytes; however, it is abundant in the cytosol of the both magnocellular (Fig. 2m–o) and parvocellular (data not shown) dLGN neurons.

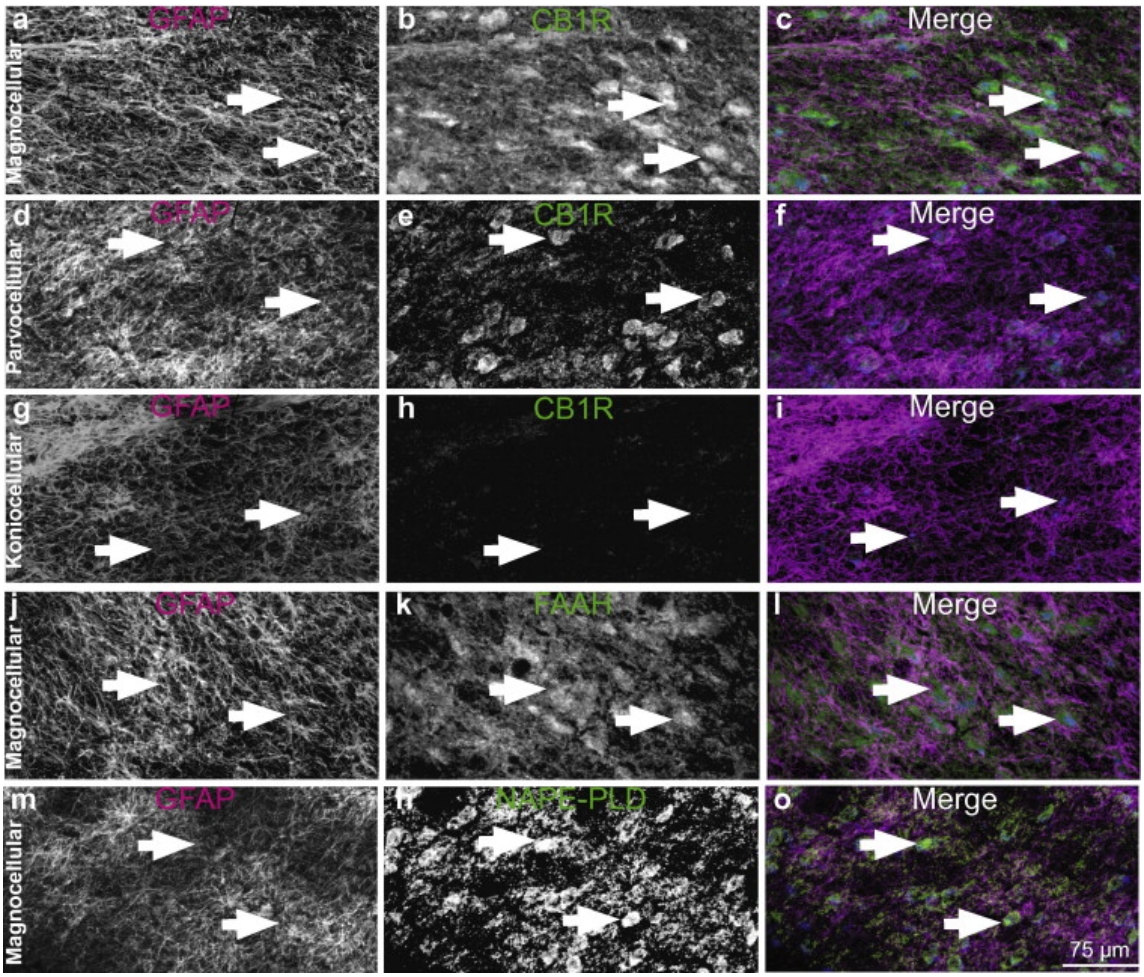

Fig. 2. Triple-label immunofluorescence of the CB1R (magenta) and GFAP (green) expression with nucleic acid stain Sytox (blue), respectively in magnocellular (a–c), parvocellular (d–f) and koniocellular layers (g–i). The absence of GFAP with FAAH (j–l) and NAPE-PLD (m–o) co-localizations in the magnocellular layers of the monkey dLGN are shown. Each immunostaining is presented alone in gray scale in the first two columns (1st column: GFAP and 2nd column: CB) following their merged image in the third column. Arrows point at GFAP cell bodies with no expression of CB. Scale bars = 75 µm.

CB1R, FAAH and NAPE-PLD are expressed in glutamatergic and GABAergic neurons. As previously reported in the rat brain, CB1R is expressed in both GABAergic and glutamatergic cells (Egertová and Elphick, 2000). Our results validate the expression of CB1R within the GABAergic (Fig. 3a–c) and glutamatergic cells in the magnocellular layers (Fig.

3d–f). Furthermore, we report the same pattern of expression for FAAH and NAPE-PLD in both GABAergic (Fig. 3g–i and m–o) and glutamatergic neurons (Fig. 3j–l and p–r) without any preferences for any of them.

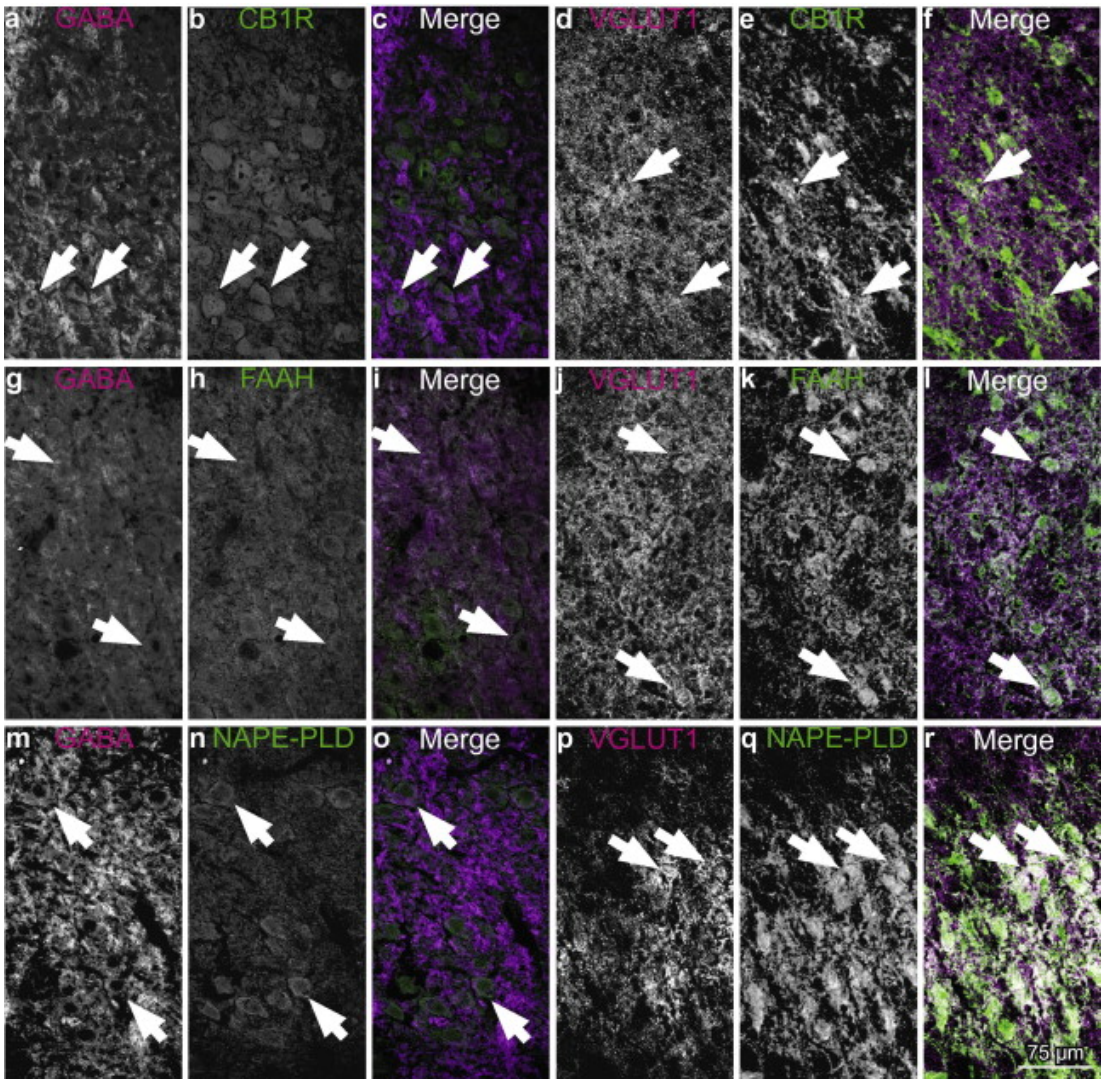

Fig. 3. Immunofluorescence labeling illustrating the co-localization of CB1R (a–f), FAAH (g–l) and NAPE-PLD (m–r) with GABAergic (three left columns) and glutamatergic (three right columns) neurons in the magnocellular layer 1 of the dLGN. Each immunostaining is presented alone in gray scale in the first two columns following their merged image in the third column. Arrows point to the co-localization of eCB components with GABA and VGLUT1. Scale bar = 75 µm.

Discussion

To our knowledge, this is the first study reporting the spatial distribution of CB1R and the enzymes regulating the levels of its ligands, namely FAAH and NAPE-PLD in the dLGN of primates. Given that CB1R, FAAH and NAPE-PLD are expressed in an overlapping pattern in the dLGN (Fig. 1), it might play a role in the auto-feedback control of neurotransmitter release, as proposed for the retina of the same species (Bouskila et al., 2012). This means that the same neurons that produce eCBs may also respond to their ligands in order to control the release of neurotransmitters.

CB1R: from the retina to the dLGN. There are studies that assessed CB1R expression in the whole brain and reported its expression in the thalamus. The dorsal thalamus was found to slightly express CB1Rs in rats (Tsou et al., 1998), not at all (Eggan and Lewis, 2007) or moderately (Ong and Mackie, 1999) in primates and humans (Glass et al., 1997), without any focus on the dLGN. To date, we have found only one study looking specifically at the rodent dLGN and reporting CB1R expression (Argaw et al., 2011). These results are however difficult to generalize to the monkey and human dLGN given the major anatomical differences in its organization as well as its cortical projections. Moreover, while the vast majority of retinal inputs projects to the dLGN in primates, only a limited number of retinal ganglion cells axons converge to the basic dLGN of rodents (Dacey et al., 2003 and Huberman and Niell, 2011).

Retinal ganglion cells receive their input from rods and cones and transfer the visual information via parasol and midget cells to the magnocellular layers and the parvocellular layers of dLGN, respectively. Magnocellular and parvocellular layers target layer four of area V1 (4Cα and 4Cβ respectively). Both the M and P pathways also project to layer six of the primary visual cortex and receive a robust corticogeniculate feedback from the same layer that is mainly excitatory and glutamatergic (McCormick and von Krosigk, 1992 and Fitzpatrick et al., 1994). The LGN is not just a passive relay; about 90% of its inputs are coming from sites other than retina, and about 30% of them are feedback inputs from V1 (Van Horn et al., 2000). Recent studies revealed that a close relationship in feedforward and feedback parallel streams instigates the functional influence of the LGN in visual processing. The magnocellular pathway is more sensitive to low spatial frequencies, low luminance contrasts, and responsible

for the perception of motion and luminance, but it is chromatically non-opponent. On the other hand, parvocellular neurons (eight times more numerous than magno cells) convey chromatic and form information and are less sensitive to luminance contrasts (Briggs and Usrey, 2011). Additionally, the middle temporal visual area (MT) and medial superior temporal area (MST), motion detection centers, mainly receive the magnocellular layers' primary inputs (Maunsell et al., 1990 and Merigan et al., 1991). In human and non-human primates, low to moderate density of CB1R has been reported in several cortical areas like the primary visual cortex (V1), specially layer five and six, in higher-order visual areas (V2, V3, V4) with more density in MT and MST (Eggan and Lewis, 2007). In V1, layers five and six contained the highest expression of CB1R (Eggan and Lewis, 2007). Interestingly, the higher density of CB1R in magnocellular layers of LGN in our study concurs with well-defined thalamo-recipient cortical areas. Thus, expression of eCB components in the visual cortex of rodent and primate brains (Eggan and Lewis, 2007 and Jiang et al., 2010) indicates that the whole visual pathway, from the retina to cortex, can be influenced by cannabinoids.

CB1R and FAAH are highly co-expressed throughout the retinal layers of the same species (Bouskila et al., 2012). Here, we show that both CB1R and FAAH are present in the dLGN mainly in the magnocellular layers. Previous studies showed a similar overlapping distribution of FAAH and CB1R in pyramidal cells of the mouse hippocampus, amygdala and entorhinal cortex (Marsicano and Lutz, 1999) and the rat cortex (Hill et al., 2007).

NAPE-PLD: a dissimilar pattern of expression. NAPE-PLD is widely expressed in the mouse thalamus (Egertová et al., 2008). Furthermore, the presence of NAPE-PLD in the rat brain has been reported, with an increased expression in the thalamus (Morishita et al., 2005). Unlike CB1R and FAAH, the synthesizing enzyme, NAPE-PLD, is expressed homogenously throughout the magnocellular and parvocellular layers of the dLGN without any laminar preference (Fig. 1c, f, g). Besides synthesizing the endocannabinoid AEA, NAPE-PLD also generates NAEs that are major substrates for mediating various motivational functions (Viveros et al., 2008). Interestingly, the degrading enzyme FAAH can metabolize NAEs into cellular membrane components (Cravatt et al., 1996 and Cravatt et al., 2001). Even though both FAAH and NAPE-PLD are expressed in rodent thalamic nuclei neuronal cells, FAAH is only present in neuronal somata (Egertová et al., 2003). Given that these proteins are

targeted to the axons, axon terminals and cytosol of neurons suggest a putative role of the eCB system as a mediator of anterograde signaling at thalamic synapses. Our results show that FAAH and NAPE-PLD are also co-expressed in the monkey dLGN (Fig. 1b, c). They support previously reported results that NAE could serve as an autocrine synaptic signaling molecules regulating the release of neurotransmitters (Egertová et al., 2008).

CB1R, FAAH and NAPE-PLD are not present in LGN astrocytes. The presence of CB1R in astrocytes is controversial. While some studies have failed to show any expression of CB1R in astrocytes (reviewed in Stella, 2004), others have detected it in the caudate, putamen (Rodriguez et al., 2001) and hippocampal astrocytes (Navarrete and Araque, 2008). In the hippocampus, astrocyte activation of CB1R leads to phospholipase C-dependent Ca2+ mobilization from the store and mediation of the eCBs communication with the neurons. This intermediation might play a role in the physiology of CB addiction (Navarrete and Araque, 2008). Our results show no co-expression between CB1R, FAAH and NAPE-PLD with GFAP in the LGN.

Functional significance

The geniculo-cortical distribution of CB1R (Fig. 1) sheds light into the putative functions of the eCB system in vision. Indeed, cannabis at the retinal level could affect the upstream visual pathways namely the ventral and dorsal visual streams. The higher expression of CB1R and FAAH in the magnocellular layers could have a functional value for the dorsal visual system involved in motion processing and object location ("how/where" pathway) (Goodale and Milner, 1992 and Kupers and Ptito, 2014). The abundance of the CB1R in the magnocellular layers of dLGN, areas MT and MST supports a role of eCB system in motion perception. In agreement with our findings, case studies on high-potency heavy cannabis smokers reported visual disturbances and impairment in motion perception (Levi and Miller, 1990). Likewise, cannabis causes impaired performance in tests that require fine psychomotor control such as tracking a moving point of light on a screen (Adams et al., 1975 and Adams et al., 1978). Magnocellular neurons are also more sensitive to low luminance contrasts (Tootell et al., 1988) and relatively unresponsive to chromatic contrasts (Croner and Kaplan, 1995).

Higher expression of CB1R in the magnocellular pathway prompts a role of the endocannabinoid system in the night vision. In agreement with this speculation, numerous reports claim that smoking marijuana improves dim light vision and photosensitivity (Dawson et al., 1977, Merzouki and Mesa, 2002 and Russo et al., 2004). Besides, the neurons in the magnocellular pathway are also sensitive to flickering stimuli (Lee et al., 1989) and lesions to the magnocellular layers of the dLGN can cause deficits in critical flicker fusion (Merigan and Maunsell, 1990) and flicker detection (Schiller et al., 1990).

Even though the expression of the CB1R and FAAH is more abundant in magnocellular layers, they are nonetheless present in the parvocellular layers of the dLGN. If the eCB system plays any role in color perception, it should be through chromatic properties of parvo cells and retinal cones. Both of these components of the visual system express CB1R. Conjointly, one of the most frequently reported effects of cannabis is more intense and brighter colors (Green et al., 2003 and Lerner et al., 2011). Although the eCB system is considered as a good candidate for modulation of the dynamics of the cortical networks (Robbe et al., 2006), there are few electrophysiological studies on the role of cannabinoids in the visual system. Recently, it has been reported that the CB1R and CB2R full agonist, CP55940, decreases electroencephalogram and local field potential power in V1 and V2 in macaque monkeys (Ohiorhenuan et al., 2014). To the best of our knowledge, there is only one study that has characterized the physiological effects of CB1R-mediated activity in the rat visual thalamus (Dasilva et al., 2012). Using single-unit extracellular recordings, the authors showed that, at the level of thalamus, CB1R activation revealed two cellular populations, one exhibiting excitatory effects (28%) and the other inhibitory ones (72%). These actions were blocked using AM251, a specific inverse agonist of CB1R. This suggests that CB1R in the rat thalamus acts as a dynamic modulator of visual information funneled to the cortex. The modulatory role of CB1R in the thalamus of monkeys and especially the dLGN could have a higher impact on visual processing due to its complex laminar structure and increased retinal inputs. Our results are in accordance with these electrophysiological findings and revealed that this neuromodulation of CB1R receptors may be due to their expression in the dLGN.

The expression pattern of these eCB components has been also well characterized in the primate retinal cells (Bouskila et al., 2012, Bouskila et al., 2013a and Bouskila et al.,

2013b) that project to the dLGN through the optic nerve. The importance of CB1R has been highlighted in a recent electroretinographic study (ERG) that showed the implication of this cannabinoid receptor in the generation of the ERG responses (Ptito et al., 2014). Indeed, blocking CB1R induces an increase in the b-wave component of the ERG. This increase is possibly reflecting the gating of calcium (Ca2+) and potassium (K+) ionic channels (Bouskila et al., 2013a). The change in neuronal membrane permeability to Ca2+ ions and activity of adenylyl cyclase may affect neurotransmitter release and action (Di Marzo et al., 1998) not only at the retinal level, but also probably at the dLGN level.

The data presented here provide the first insight into the neuroanatomy of CB1R, FAAH, and NAPE-PLD expression in the primate dLGN and a new perspective of the neural function of this system. In other words, the presence of the endocannabinoid system in the dLGN and especially in the magnocellular pathway suggests a putative neuromodulatory action that affects the functions of the dorsal visual pathway involved in motion perception, object localization and action-oriented behaviors that depend on the perception of space.

Acknowledgments

The Natural Science and Engineering Research Council of Canada (6362-2012, MP; 311892-2010, JFB) and the Canadian Institutes of Health Research (MOP-86495, JFB) supported this project financially. J.F.B. holds a Chercheur Boursier Senior from the Fonds de Recherche du Québec-Santé (FRQ-S). M.P is Harland Sanders Char Professor in Visual Science. We are also grateful to Dr. Frank Ervin and Dr. Roberta Palmour of St.-Kitts, West Indies, for supplying the vervet monkey tissues. We would like to thank Dr. Mohammad Jabbari Hagh for writing the MATLAB codes for heat map.

Conflict of interest

The authors declare that they have no conflict of interest.

References

Adams AJ, Brown B (1975) Alcohol prolongs time course of glare recovery. Nature 257 (5526):481-483

Adams AJ, Brown B, Flom MC, Jones RT, Jampolsky A (1975) Alcohol and marijuana effects on static visual acuity. Am J Optom Physiol Opt 52 (11):729-735

Adams AJ, Brown B, Haegerstrom-Portnoy G, Flom MC, Jones RT (1978) Marijuana, alcohol, and combined drug effects on the time course of glare recovery. Psychopharmacology (Berl) 56 (1):81-86

Argaw A, Duff G, Zabouri N, Cécyre B, Chaine N, Cherif H, Tea N, Lutz B, Ptito M, Bouchard JF (2011) Concerted action of CB1 cannabinoid receptor and deleted in colorectal cancer in axon guidance. J Neurosci 31 (4):1489-1499

Bouskila J, Burke MW, Zabouri N, Casanova C, Ptito M, Bouchard JF (2012) Expression and localization of the cannabinoid receptor type 1 and the enzyme fatty acid amide hydrolase in the retina of vervet monkeys. Neuroscience 202:117-130.

Bouskila J, Javadi P, Casanova C, Ptito M, Bouchard JF (2013a) Muller cells express the cannabinoid CB2 receptor in the vervet monkey retina. J Comp Neurol.

Bouskila J, Javadi P, Casanova C, Ptito M, Bouchard JF (2013b) Rod photoreceptors express GPR55 in the adult vervet monkey retina. PLoS One 8 (11):e81080.

Breivogel CS, Sim LJ, Childers SR (1997) Regional differences in cannabinoid receptor/G-protein coupling in rat brain. J Pharmacol Exp Ther 282 (3):1632-1642

Briggs F, Usrey WM (2011) Corticogeniculate feedback and visual processing in the primate. J Physiol 589 (Pt 1):33-40.

Casagrande VA (1994) A third parallel visual pathway to primate area V1. Trends Neurosci 17 (7):305-310

Casagrande VA (1999) The mystery of the visual system K pathway. J Physiol 517 (Pt 3):630

Cécyre B, Thomas S, Ptito M, Casanova C, Bouchard JF (2014) Evaluation of the specificity of antibodies raised against cannabinoid receptor type 2 in the mouse retina. Naunyn-Schmiedeberg's archives of pharmacology 387 (2):175-184.

Cravatt BF, Demarest K, Patricelli MP, Bracey MH, Giang DK, Martin BR, Lichtman AH (2001) Supersensitivity to anandamide and enhanced endogenous cannabinoid signaling in mice lacking fatty acid amide hydrolase. Proc Natl Acad Sci U S A 98 (16):9371-9376

Cravatt BF, Giang DK, Mayfield SP, Boger DL, Lerner RA, Gilula NB (1996) Molecular characterization of an enzyme that degrades neuromodulatory fatty-acid amides. Nature 384 (6604):83-87.

Croner LJ, Kaplan E (1995) Receptive fields of P and M ganglion cells across the primate retina. Vision Res 35 (1):7-24

Dacey DM, Peterson BB, Robinson FR, Gamlin PD (2003) Fireworks in the primate retina: in vitro photodynamics reveals diverse LGN-projecting ganglion cell types. Neuron 37 (1):15-27

Dasilva MA, Grieve KL, Cudeiro J, Rivadulla C (2012) Endocannabinoid CB1 receptors modulate visual output from the thalamus. Psychopharmacology (Berl) 219 (3):835-845.

Dawson WW, Jimenez-Antillon CF, Perez JM, Zeskind JA (1977) Marijuana and vision--after ten years' use in Costa Rica. Invest Ophthalmol Vis Sci 16 (8):689-699

Dell'Osso LF (2000) Suppression of pendular nystagmus by smoking cannabis in a patient with multiple sclerosis. Neurology 54 (11):2190-2191

Deutsch DG, Chin SA (1993) Enzymatic synthesis and degradation of anandamide, a cannabinoid receptor agonist. Biochem Pharmacol 46 (5):791-796.

Di Marzo V, Melck D, Bisogno T, De Petrocellis L (1998) Endocannabinoids: endogenous cannabinoid receptor ligands with neuromodulatory action. Trends Neurosci 21 (12):521-528

Egertová M, Cravatt BF, Elphick MR (2003) Comparative analysis of fatty acid amide hydrolase and cb(1) cannabinoid receptor expression in the mouse brain: evidence of a

widespread role for fatty acid amide hydrolase in regulation of endocannabinoid signaling. Neuroscience 119 (2):481-496

Egertová M, Elphick MR (2000) Localisation of cannabinoid receptors in the rat brain using antibodies to the intracellular C-terminal tail of CB. J Comp Neurol 422 (2):159-171.

Egertová M, Giang DK, Cravatt BF, Elphick MR (1998) A new perspective on cannabinoid signalling: complementary localization of fatty acid amide hydrolase and the CB1 receptor in rat brain. Proc Biol Sci 265 (1410):2081-2085

Egertová M, Simon GM, Cravatt BF, Elphick MR (2008) Localization of N-acyl phosphatidylethanolamine phospholipase D (NAPE-PLD) expression in mouse brain: A new perspective on N-acylethanolamines as neural signaling molecules. J Comp Neurol 506 (4):604-615.

Eggan SM, Lewis DA (2007) Immunocytochemical distribution of the cannabinoid CB1 receptor in the primate neocortex: a regional and laminar analysis. Cereb Cortex 17 (1):175-191.

Emrich HM, Weber MM, Wendl A, Zihl J, von Meyer L, Hanisch W (1991) Reduced binocular depth inversion as an indicator of cannabis-induced censorship impairment. Pharmacol Biochem Behav 40 (3):689-690

Felder CC, Nielsen A, Briley EM, Palkovits M, Priller J, Axelrod J, Nguyen DN, Richardson JM, Riggin RM, Koppel GA, Paul SM, Becker GW (1996) Isolation and measurement of the endogenous cannabinoid receptor agonist, anandamide, in brain and peripheral tissues of human and rat. FEBS Lett 393 (2-3):231-235

Fitzpatrick D, Usrey WM, Schofield BR, Einstein G (1994) The sublaminar organization of corticogeniculate neurons in layer 6 of macaque striate cortex. Vis Neurosci 11 (2):307-315

Flom MC, Brown B, Adams AJ, Jones RT (1976) Alcohol and marijuana effects on ocular tracking. Am J Optom Physiol Opt 53 (12):764-773

Glass M, Dragunow M, Faull RL (1997) Cannabinoid receptors in the human brain: a detailed anatomical and quantitative autoradiographic study in the fetal, neonatal and adult human brain. Neuroscience 77 (2):299-318

Gómez-Ruiz M, Hernández M, de Miguel R, Ramos JA (2007) An overview on the biochemistry of the cannabinoid system. Mol Neurobiol 36 (1):3-14

Goodale MA, Milner AD (1992) Separate visual pathways for perception and action. Trends Neurosci 15 (1):20-25

Green B, Kavanagh D, Young R (2003) Being stoned: a review of self-reported cannabis effects. Drug and alcohol review 22 (4):453-460.

Hendry SH, Reid RC (2000) The koniocellular pathway in primate vision. Annual review of neuroscience 23:127-153.

Hendry SH, Yoshioka T (1994) A neurochemically distinct third channel in the macaque dorsal lateral geniculate nucleus. Science 264 (5158):575-577

Hepp K, Van Opstal AJ, Straumann D, Hess BJ, Henn V (1993) Monkey superior colliculus represents rapid eye movements in a two-dimensional motor map. J Neurophysiol 69 (3):965-979

Herkenham M, Lynn AB, Johnson MR, Melvin LS, de Costa BR, Rice KC (1991) Characterization and localization of cannabinoid receptors in rat brain: a quantitative in vitro autoradiographic study. J Neurosci 11 (2):563-583

Hill EL, Gallopin T, Ferezou I, Cauli B, Rossier J, Schweitzer P, Lambolez B (2007) Functional CB1 receptors are broadly expressed in neocortical GABAergic and glutamatergic neurons. J Neurophysiol 97 (4):2580-2589.

Huberman AD, Niell CM (2011) What can mice tell us about how vision works? Trends Neurosci 34 (9):464-473.

Jiang B, Sohya K, Sarihi A, Yanagawa Y, Tsumoto T (2010) Laminar-specific maturation of GABAergic transmission and susceptibility to visual deprivation are related to endocannabinoid sensitivity in mouse visual cortex. J Neurosci 30 (42):14261-14272.

Jongen-Relo AL, Pitkanen A, Amaral DG (1999) Distribution of GABAergic cells and fibers in the hippocampal formation of the macaque monkey: an immunohistochemical and in situ hybridization study. J Comp Neurol 408 (2):237-271

Kupers R, Ptito M (2013) Compensatory plasticity and cross-modal reorganization following early visual deprivation. Neuroscience and biobehavioral reviews.

Lee BB, Martin PR, Valberg A (1989) Sensitivity of macaque retinal ganglion cells to chromatic and luminance flicker. J Physiol 414:223-243

Leigh RJ, Das VE, Seidman SH (2002) A neurobiological approach to acquired nystagmus. Annals of the New York Academy of Sciences 956:380-390

Lerner AG, Goodman C, Rudinski D, Bleich A (2011) Benign and time-limited visual disturbances (flashbacks) in recent abstinent high-potency heavy cannabis smokers: a case series study. The Israel journal of psychiatry and related sciences 48 (1):25-29

Levi L, Miller NR (1990) Visual illusions associated with previous drug abuse. Journal of clinical neuro-ophthalmology 10 (2):103-110

Leweke FM, Schneider U, Thies M, Munte TF, Emrich HM (1999) Effects of synthetic delta9-tetrahydrocannabinol on binocular depth inversion of natural and artificial objects in man. Psychopharmacology (Berl) 142 (3):230-235

Marsicano G, Lutz B (1999) Expression of the cannabinoid receptor CB1 in distinct neuronal subpopulations in the adult mouse forebrain. Eur J Neurosci 11 (12):4213-4225.

Martin PR, White AJ, Goodchild AK, Wilder HD, Sefton AE (1997) Evidence that blue-on cells are part of the third geniculocortical pathway in primates. Eur J Neurosci 9 (7):1536-1541

Maunsell JH, Nealey TA, DePriest DD (1990) Magnocellular and parvocellular contributions to responses in the middle temporal visual area (MT) of the macaque monkey. J Neurosci 10 (10):3323-3334

McCormick DA, von Krosigk M (1992) Corticothalamic activation modulates thalamic firing through glutamate "metabotropic" receptors. Proc Natl Acad Sci U S A 89 (7):2774-2778

Merigan WH, Byrne CE, Maunsell JH (1991) Does primate motion perception depend on the magnocellular pathway? J Neurosci 11 (11):3422-3429

Merigan WH, Maunsell JH (1990) Macaque vision after magnocellular lateral geniculate lesions. Vis Neurosci 5 (4):347-352

Merzouki A, Mesa JM (2002) Concerning kif, a Cannabis sativa L. preparation smoked in the Rif mountains of northern Morocco. Journal of ethnopharmacology 81 (3):403-406

Moldrich G, Wenger T (2000) Localization of the CB1 cannabinoid receptor in the rat brain. An immunohistochemical study. Peptides 21 (11):1735-1742

Morishita J, Okamoto Y, Tsuboi K, Ueno M, Sakamoto H, Maekawa N, Ueda N (2005) Regional distribution and age-dependent expression of N-acylphosphatidylethanolamine-hydrolyzing phospholipase D in rat brain. J Neurochem 94 (3):753-762.

Moskowitz H, Sharma S, McGlothlin W (1972) Effect of marihuana upon peripheral vision as a function of the information processing demands in central vision. Percept Mot Skills 35 (3):875-882

Navarrete M, Araque A (2008) Endocannabinoids mediate neuron-astrocyte communication. Neuron 57 (6):883-893.

Ohiorhenuan IE, Mechler F, Purpura KP, Schmid AM, Hu Q, Victor JD (2014) Cannabinoid neuromodulation in the adult early visual cortex. PLoS One 9 (2):e87362.

Ong WY, Mackie K (1999) A light and electron microscopic study of the CB1 cannabinoid receptor in primate brain. Neuroscience 92 (4):1177-1191

Piomelli D (2003) The molecular logic of endocannabinoid signalling. Nat Rev Neurosci 4 (11):873-884.

Pradeep A, Thomas S, Roberts EO, Proudlock FA, Gottlob I (2008) Reduction of congenital nystagmus in a patient after smoking cannabis. Strabismus 16 (1):29-32.

Ptito M, Javadi, P, Bouskila J, Casanova C, Bouchard JF (2014), Role of retinal cannabinoid receptors cb1 and cb2, and gpr55 defined by electroretinography in vervet monkeys. FENS -0297-D021

Robbe D, Montgomery SM, Thome A, Rueda-Orozco PE, McNaughton BL, Buzsaki G (2006) Cannabinoids reveal importance of spike timing coordination in hippocampal function. Nat Neurosci 9 (12):1526-1533.

Rodriguez JJ, Mackie K, Pickel VM (2001) Ultrastructural localization of the CB1 cannabinoid receptor in mu-opioid receptor patches of the rat Caudate putamen nucleus. J Neurosci 21 (3):823-833

Russo EB, Merzouki A, Mesa JM, Frey KA, Bach PJ (2004) Cannabis improves night vision: a case study of dark adaptometry and scotopic sensitivity in kif smokers of the Rif mountains of northern Morocco. Journal of ethnopharmacology 93 (1):99-104.

Schiller PH, Logothetis NK, Charles ER (1990) Role of the color-opponent and broad-band channels in vision. Vis Neurosci 5 (4):321-346

Schiller PH, Malpeli JG, Schein SJ (1979) Composition of geniculostriate input ot superior colliculus of the rhesus monkey. J Neurophysiol 42 (4):1124-1133

Schon F, Hart PE, Hodgson TL, Pambakian AL, Ruprah M, Williamson EM, Kennard C (1999) Suppression of pendular nystagmus by smoking cannabis in a patient with multiple sclerosis. Neurology 53 (9):2209-2210

Semple DM, Ramsden F, McIntosh AM (2003) Reduced binocular depth inversion in regular cannabis users. Pharmacol Biochem Behav 75 (4):789-793.

Stella N (2004) Cannabinoid signaling in glial cells. Glia 48 (4):267-277.

Straiker A, Stella N, Piomelli D, Mackie K, Karten HJ, Maguire G (1999a) Cannabinoid CB1 receptors and ligands in vertebrate retina: localization and function of an endogenous signaling system. Proc Natl Acad Sci U S A 96 (25):14565-14570

Straiker AJ, Maguire G, Mackie K, Lindsey J (1999b) Localization of cannabinoid CB1 receptors in the human anterior eye and retina. Invest Ophthalmol Vis Sci 40 (10):2442-2448

Suárez J, Bermudez-Silva FJ, Mackie K, Ledent C, Zimmer A, Cravatt BF, de Fonseca FR (2008) Immunohistochemical description of the endogenous cannabinoid system in the rat cerebellum and functionally related nuclei. J Comp Neurol 509 (4):400-421.

Tootell RB, Hamilton SL, Switkes E (1988) Functional anatomy of macaque striate cortex. IV. Contrast and magno-parvo streams. J Neurosci 8 (5):1594-1609

Tsou K, Brown S, Sanudo-Pena MC, Mackie K, Walker JM (1998) Immunohistochemical distribution of cannabinoid CB1 receptors in the rat central nervous system. Neuroscience 83 (2):393-411

Van Horn SC, Erisir A, Sherman SM (2000) Relative distribution of synapses in the A-laminae of the lateral geniculate nucleus of the cat. J Comp Neurol 416 (4):509-520

Viveros MP, de Fonseca FR, Bermudez-Silva FJ, McPartland JM (2008) Critical role of the endocannabinoid system in the regulation of food intake and energy metabolism, with phylogenetic, developmental, and pathophysiological implications. Endocrine, metabolic & immune disorders drug targets 8 (3):220-230

Xu X, Ichida JM, Allison JD, Boyd JD, Bonds AB, Casagrande VA (2001) A comparison of koniocellular, magnocellular and parvocellular receptive field properties in the lateral geniculate nucleus of the owl monkey (Aotus trivirgatus). J Physiol 531 (Pt 1):203-218

Zabouri N, Bouchard JF, Casanova C (2011) Cannabinoid receptor type 1 expression during postnatal development of the rat retina. J Comp Neurol 519 (7):1258-1280.

ANNEXE III : LISTE DES BOURSES ET PRIX QUE CES ARTICLES ONT PERMIS DE GAGNER.

- Prix Bundesverband Auge e. V., Berlin, Germany, Octobre 2016
- Bourse d'excellence de la FESP « J.A. DeSève », Novembre 2015
- Bourse d'excellence de la FESP, Décembre 2014
- Bourses d'études supérieures du Canada - Suppléments pour études à l'étranger Michael-Smith, Avril 2014
- Trente-deuxième concours du prix Réseau de recherche en Santé de la vision (RRSV)/FRQ-S pour meilleur article (Article 2), 2013
- Bouse d'études supérieures du Canada Banting et Best des IRSC - Bourse au doctorat, 2013
- Bourse de recherche au doctorat du FRQ-S, 2012
- Bourse du département des sciences biomédicales, 2012
- Bourse d'excellence de l'École d'optométrie (ÉOUM/FESP), 2010
- Bourse d'études supérieures du Canada Banting et Best des IRSC - Bourse à la maitrise, 2009
- Bourse de doctorat du Groupe de recherche universitaire sur le médicament (GRUM), 2009
- Bourse d'excellence de l'ÉOUM/FESP, 2009